

AD-A279 919



PL-TR-94-2135

Environmental Research Papers, No. 1149

**PROCEEDINGS OF THE 15TH ANNUAL CONFERENCE
ON ATMOSPHERIC TRANSMISSION MODELS,
2-3 JUNE 1992**

Editors:

**Michael L. Hoke
Leonard W. Abreu**

18 May 1994

DTIC
ELECTE
JUN 01 1994
S G D

3778 **94-16212**

APPROVED FOR PUBLIC RELEASE; DISTRIBUTION UNLIMITED




**PHILLIPS LABORATORY
Directorate of Geophysics
AIR FORCE MATERIEL COMMAND
HANSCOM AIR FORCE BASE, MA 01731-3010**

DTIC QUALITY INSPECTED

94 5 31 022

"This technical report has been reviewed and is approved for publication"


WILLIAM A.M. BLUMBERG, Chief
Simulation Branch
Optical Environment Division


ROGER A. VAN TASSEL, Director
Optical Environment Division

This report has been reviewed by the ESC Public Affairs Office (PA) and is releasable to the National Technical Information Service (NTIS).

Qualified requestors may obtain additional copies from the Defense Technical Information Center. All others should apply to the National Technical Information Service.

If your address has changed, or if you wish to be removed from the mailing list, or if the addressee is no longer employed by your organization, please notify PL/TSI, Hanscom AFB, MA 01731-3010. This will assist us in maintaining a current mailing list.

Do not return copies of this report unless contractual obligations or notices on a specific document requires that it be returned.

REPORT DOCUMENTATION PAGE			Form Approved OMB No. 0704-0188	
Public reporting burden for this collection of information is estimated to average 1 hour per response, including the time for reviewing instructions, searching existing data sources, gathering and maintaining the data needed, and completing and reviewing the collection of information. Send comments regarding this burden estimate or any other aspect of this collection of information, including suggestions for reducing this burden, to Washington Headquarters Services, Directorate for Information Operations and Reports, 1215 Jefferson Davis Highway, Suite 1204, Arlington, VA 22202-4302, and to the Office of Management and Budget, Paperwork Reduction Project (0704-0188), Washington, DC 20503.				
1. AGENCY USE ONLY (Leave blank)	2. REPORT DATE 18 May 1994	3. REPORT TYPE AND DATES COVERED Scientific		
4. TITLE AND SUBTITLE PROCEEDINGS OF THE 15th ANNUAL CONFERENCE ON ATMOSPHERIC TRANSMISSION MODELS, 2-3 JUNE 1992.		5. FUNDING NUMBERS PE 62101F PR 3054 TA GD WU 01		
6. AUTHOR(S) EDITORS: MICHAEL L. HOKE LEONARD W. ABREU				
7. PERFORMING ORGANIZATION NAME(S) AND ADDRESS(ES) Phillips Laboratory/GPOS 29 Randolph Road Hanscom AFB, MA 01731-3010		8. PERFORMING ORGANIZATION REPORT NUMBER PL-TR-94-2135 ERP, No. 1149		
9. SPONSORING / MONITORING AGENCY NAME(S) AND ADDRESS(ES)		10. SPONSORING / MONITORING AGENCY REPORT NUMBER		
11. SUPPLEMENTARY NOTES				
12a. DISTRIBUTION / AVAILABILITY STATEMENT Approved for public release; distribution unlimited		12b. DISTRIBUTION CODE		
13. ABSTRACT (Maximum 200 words) CONTAINS THE VIEWGRAPHS AND OTHER MATERIALS FOR THE 26 PAPERS PRESENTED AT THE 15th ANNUAL REVIEW CONFERENCE ON ATMOSPHERIC TRANSMISSION MODELS HELD AT THE GEOPHYSICS DIRECTORATE, PHILLIPS LABORATORY (AFMC), HANSCOM AFB, MA ON: 2-3 JUNE 1992.				
14. SUBJECT TERMS Atmospheric transmittance Aerosols Atmospheric propagation		Clouds Radiative transfer Optical turbulence		15. NUMBER OF PAGES 382
				16. PRICE CODE
17. SECURITY CLASSIFICATION OF REPORT Unclassified	18. SECURITY CLASSIFICATION OF THIS PAGE Unclassified	19. SECURITY CLASSIFICATION OF ABSTRACT Unclassified	20. LIMITATION OF ABSTRACT SAR	

Table of Contents

	Page
INTRODUCTION	vii
Session on Code Enhancements	
"Improvement of MODTRAN and FASCOD to Full Solar Capability Including Multiple Scattering and Spherical Geometry" M. Yeh, K. Stamnes, S. Tsay	2
"Upgraded Line-of-Sight Geometry Package for MODTRAN" P.K. Acharya, D.C. Robertson, A. Berk	3
"IR Visibility" C.N. Touart	26
"A MODTRAN Algorithm for Predicting Directional Skyshine Irradiance" D.C. Robertson, J.A. Kristl, B.P. Sandford	41
Session on Atmospheric Propagation Models	
"Status of PL/GP High Resolution Radiance-Transmittance Model: FASCODE" F.X. Kneizys, G.P. Anderson, J.H. Chetwynd, L.W. Abreu, M.L. Hoke, S.A. Clough, R.D. Worsham, E.P. Shettle	57
"HITRAN 1992: M ³ (Multi-Media Milieu)" L.S. Rothman	58
"Status of PL/GP Moderate Resolution Radiance/Transmittance Models: MODTRAN and Derivatives" F.X. Kneizys, L.W. Abreu, G.P. Anderson, J.H. Chetwynd	75
"The Atmospheric Ultraviolet Radiance Integrated Code (AURIC)" C.C. Betchley, J.A. Conant, G.P. Anderson, L.A. Hall	82
"SAM: SHARC And MODTRAN Merged" A. Berk, D.C. Robertson, L.S. Bernstein, R. Sharma	98
"Smart Model for Atmospheric and Astronomical Radiance and Transmittance (SMAART)" S.B. Downer, J.P. Kennealy, P.C.F. Ip, F.O. Clark	115

Table of Contents (continued)

	<u>Page</u>
"Oncore: The ONTAR Implementation of LOWTRAN 7" J. Schroeder	128
"Microwave Refractive Path Calculations for the Phillips Laboratory (PL) RADTRAN Attenuation/Transmittance/Brightness Temperature Computer Code" R.G. Isaacs, W.O. Gallery, R.D. Worsham, V.J. Falcone	140
"Atmospheric Transmission Models for Passive Millimeter Wave Target Signature Simulation" W.T. Kreiss, R.S. Dummer	149
Session on Measurements and Models	
"Absorption Cross Section Measurements of Schumann-Runge Continuum of O ₂ at 78 K and 295 K" K. Yoshino, J.R. Esmond, W.H. Parkinson	189
"The SPECTral Radiation Experiment (SPECTRE): An Overview - Clear-Sky Observations and Their Use in ICRCCM" R.G. Ellingson, W.J. Wiscombe, J. DeLuisi, V. Kunde, H. Melfi, D. Murcray, W. Smith	203
"On the Use of Ground-Based Remote Sensing to Provide Temperature and Moisture Soundings for Atmospheric Transmission Models" J.C. Liljegren, R.O. Knuteson	204
"Model Climatologies of Trace Species in the Atmosphere" M.E. Summers, W.J. Sawchuck, G.P. Anderson	221
"Far-wing Line Shape Contribution to the Water Continuum: Recent Results and Future Directions" R.H. Tipping, Q. Ma	245
"Toward an Improved Water Vapor Continuum Model" S.A. Clough	266
"A Correlated K-Distribution Model of the Heating Rates for CH ₄ and N ₂ O in the Atmosphere Between 0 and 60km*" K. Grant, A. Grossman	267

Table of Contents (continued)

	<u>Page</u>
"Line by Line Calculation of Atmospheric Fluxes and Cooling Rates: Application to Water Vapor, Ozone, Carbon Dioxide and the Fluorocarbons" S.A. Clough, M.J. Iacono, J.-L. Moncet	286
Session on Aerosols and Clouds	
"BACKSCAT Lidar Simulation: Version 3.0" J.R. Hummel, D.R. Longtin, N.L. DePiero, R.J. Grasso	288
"Development of a Raman Lidar Simulation Option Within BACKSCAT Version 3.0" R.J. Grasso, J.R. Hummel	307
"Calculation of the Angular Radiance Distribution For a Coupled System of Atmosphere and Canopy Media Using an Improved Gauss-Seidel Algorithm" S. Liang, A. Strahler	325
"A Physically Reasonable Analytic Expression for the Single Scattering Phase Function" W.M. Cornette, J.G. Shanks	338
"Analysis of Solar Transmission Data Over the South Atlantic Ocean During SABLE 89" D. Longtin, J. Hummel, G.G. Koenig	353

ATTENDANCE LIST

AUTHOR INDEX

Accession For	
NTIS CRA&I	<input checked="" type="checkbox"/>
DTIC TAB	<input type="checkbox"/>
Unannounced	<input type="checkbox"/>
Justification	
By	
Distribution /	
Availability Codes	
Dist	Avail and/or Special
A-1	

367

373

INTRODUCTION

The Fifteenth DoD Tri-Service Review Conference on Atmospheric Transmission Models was held at the Geophysics Directorate, Hanscom AFB, Massachusetts on 2-3 June 1992. The purpose of the meeting was to review progress in the modeling of radiation propagating through the earth's atmosphere, identify deficiencies in these models, and make recommendations for improvements.

Approximately 120 scientists and engineers, representing DoD, other government agencies, industry, and the academic community were in attendance. The agenda consisted of twenty six papers distributed into sessions on: Code Enhancements, Atmospheric Propagation Models, Measurements and Models, and Aerosols and Clouds.

This proceedings volume summarizes the technical presentations at the conference. The main part of the report consists of abstracts and copies of the viewgraphs or slides and other material as provided by the authors of the presentations. The Appendix includes the original call for papers, the invitation, and a copy of the final agenda. An author index is at the end of the proceedings.

On a personal note, this 15th Annual Conference was the first not organized, run, and attended by Francis X. Kneizys. The "default" organizers wish to acknowledge the impact of his absence. While Frank took great care to train his apprentices, his skills in organization, maintenance of rich historic friendships (including instant name-recall), and constant flexibility, edged with an intellectually exciting (though subtle) sense of humor, cannot be transmitted through any traditional approaches. The current organizers, along with past and present attendees, hereby extend to Frank and his family a heartfelt THANK YOU and BEST WISHES for continued happiness and good health in their retirement.



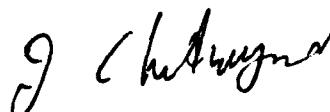
Leonard W. Abreu
Simulation Branch
Optical Environment Division



Michael L. Hoke
Simulation Branch
Optical Environment Division



Gail P. Anderson
Simulation Branch
Optical Environment Division



James H. Chetwynd
Simulation Branch
Optical Environment Division

**CODE
ENHANCEMENTS**

IMPROVEMENT OF MODTRAN AND FASCOD TO FULL SOLAR CAPABILITY INCLUDING MULTIPLE SCATTERING AND SPHERICAL GEOMETRY

M. Yeh

Caelum Research Corporation, 11229 Lockwood Drive, Silver Spring, MD 20901

K. Stamnes, S. Tsay

Geophysical Institute, University of Alaska, Fairbanks, AK 99775-0800

We have started a significant upgrade of MODTRAN and FASCOD to encompass full solar capability, including rigorous multiple scattering and spherical geometry. As part of this project we are attempting to modularize and restructure the existing codes to enhance the flexibility and readability and thus facilitate their use as well as the inclusion of future improvements. We plan to unify the structure of these codes to provide a framework within which the atmospheric conditions and optical properties other than gaseous absorption are a common feature. Thus, the desired spectral resolution, which dictates the treatment of gaseous absorption by atmospheric constituents, is the key feature distinguishing the codes. To solve the ensuing radiative transfer problem we will utilize existing state-of-the-art multiple scattering algorithms. The end product of this effort will be modern, well-documented and tested software tools that can easily and safely be used by others in a variety of applications.

UPGRADED LINE-OF-SIGHT GEOMETRY PACKAGE FOR MODTRAN

P.K. Acharya, D.C. Robertson, A. Berk

Spectral Sciences, Inc., 99 South Bedford Street, #7, Burlington, MA 01803-5169

The geometry package in MODTRAN was modified so that the actual line-of-sight (LOS) parameters used for the transmittance/radiance calculations always closely match the user's requested input values. For example, the case specified by (H1, ZENITH ANGLE, RANGE) would sometimes result in an output range that differed from the input by 20% or more. The geometry routines incurred round-off problems on 32-bit machines due to subtraction of large numbers, each of which includes the square of the earth-radius. The new routines replace numerically unstable algebraic expressions by more stable identities and occasionally resort to double precision arithmetic. Furthermore, the geometry routines can now deal with very short paths down to 0.001 km. This new geometry package will be part of the next release of MODTRAN.



*UPGRADED
LINE-OF-SIGHT GEOMETRY PACKAGE
FOR
LOWTRAN 7 AND MODTRAN*

*P. K. ACHARYA
D. C. ROBERTSON
A. BERK*

*Spectral Sciences, Inc.
99 South Bedford Street, Suite 7
Burlington, MA 01803*

JUNE 2, 1992



OUTLINE

- GENERAL PROBLEM AND OVERALL OBJECTIVE
- PROBLEMS WITH SPECIFIC PATH TYPES
- SOLUTION
 - GENERAL CHANGES
 - SPECIFIC CHANGES FOR VARIOUS SLANT PATHS
 - SHORT SLANT PATHS OF ALL TYPES
- SUMMARY



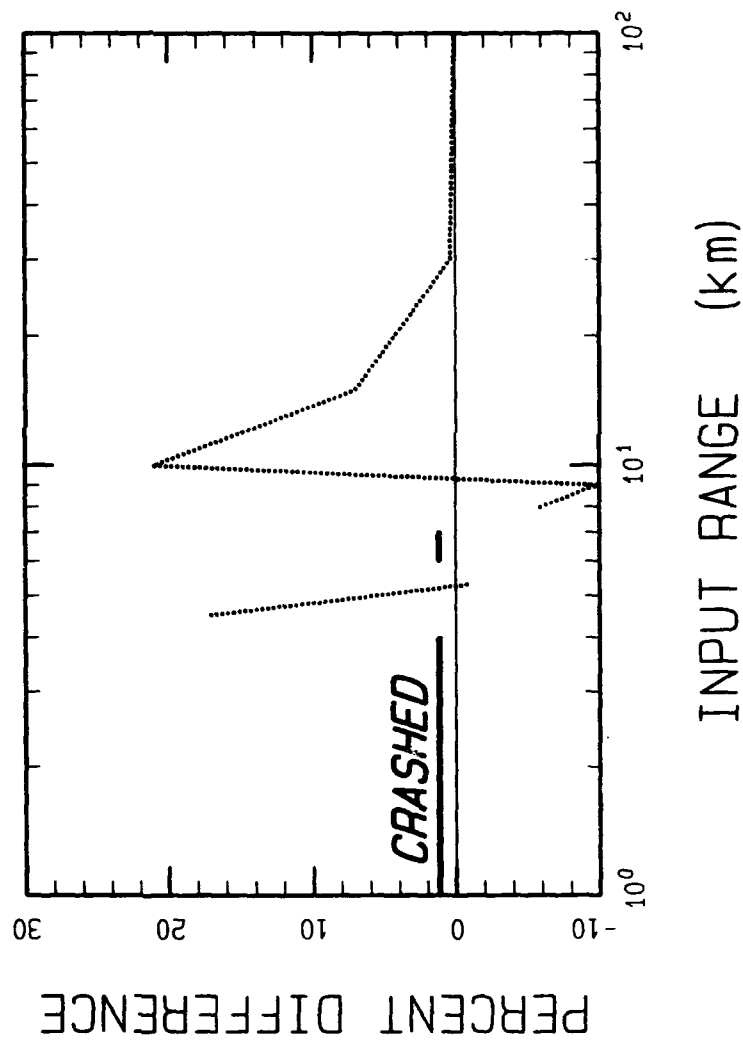
GENERAL PROBLEM

- LOWTRAN 7 GEOMETRY ROUTINES SOMETIMES RETURN LOS PARAMETERS SIGNIFICANTLY DIFFERENT FROM WHAT THE USER REQUESTED
- SOMETIMES THEY CRASH OR GET STUCK IN AN INFINITE LOOP
- THIS PROBLEM EXTENDS TO MODTRAN



CHANGE IN OUTPUT RANGE

$H1 = H2 = 5 \text{ km}$





OVERALL OBJECTIVE

- UPGRADE LOWTRAN 7/MODTRAN ROUTINES SO THAT THE USER OBTAINS CALCULATIONS FOR THE LOS PARAMETERS THAT AGREE WITH THE INPUTS
 - EFFECT UPGRADES WITH "MINIMAL" CHANGES TO PRESENT ROUTINES



NOMENCLATURE

- MODTRAN 2: REFERS TO UPGRADED GEOMETRY
- MODTRAN: REFERS TO PRESENT GEOMETRY OF LOWTRAN 7 AND MODTRAN

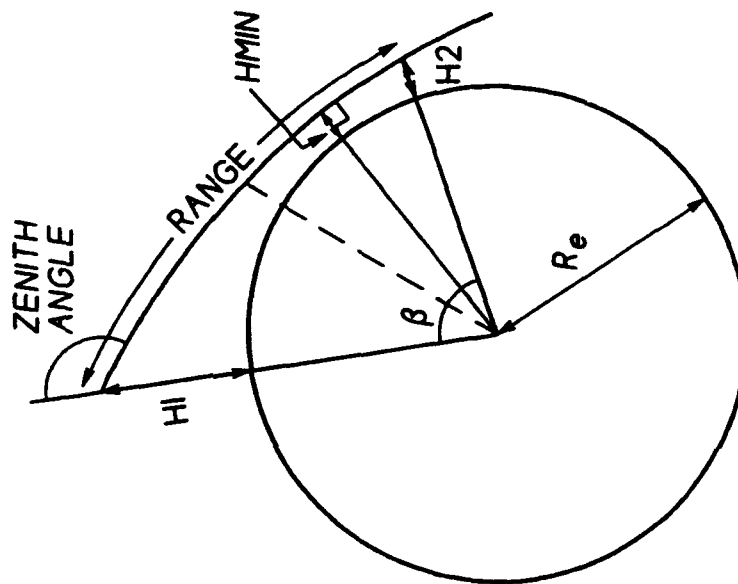


PATH TYPES IN MODTRAN

- *ITYPE = 1 HORIZ. CONSTANT TEMPERATURE, PRESSURE, CONCENTRATION (HOMOGENEOUS) PATH*
 - NO PROBLEMS, NO CHANGES MADE
- *ITYPE = 2 VERTICAL OR GENERAL SLANT PATH BETWEEN TWO ALTITUDES H1 AND H2*
 - MAJOR PROBLEMS, SIGNIFICANT CHANGES MADE
- *ITYPE = 3 VERTICAL OR SLANT PATH TO SPACE*
 - SOME PROBLEMS, USES CHANGES FOR ITYPE = 2



A GENERAL SLANT PATH



- H₁ (SENSOR)
- H₂ (SOURCE)
- RANGE
- ZENITH ANGLE
- BETA
- H_{MIN} (TANGENT HEIGHT)
- R_e



APPROACH TO SOLUTION

- GENERAL CHANGES TO IMPROVE NUMERICAL ACCURACY
- SLANT-PATH-SPECIFIC CHANGES AS REQUIRED
- SPECIAL TREATMENT FOR ALL SHORT PATHS



GENERAL CHANGES

- NUMERICAL ACCURACY IMPROVED BY REARRANGING ALGEBRAIC EXPRESSIONS
- SOME GEOMETRY VARIABLES CHANGED TO DOUBLE PRECISION



EXAMPLE

$$R_1^2 + R_2^2 - 2R_1R_2\cos(\beta), \quad R_i = R_e + H_i$$

REPLACED BY

$$(H_1 - H_2)^2 + 4R_1R_2\sin^2\frac{\beta}{2}$$

OR

$$(H_1 - H_2)^2 - R_1R_2\left(-\frac{\beta^6}{135} + \frac{\beta^4}{12} - \beta^2\right), \quad \text{FOR SMALL } \beta$$



SPECIFIC CHANGES

- GENERAL CHANGES DID NOT ELIMINATE ALL PROBLEMS
- ALL PROBLEMS ELIMINATED BY SPECIFIC CHANGES TO CERTAIN SLANT PATH AND ALL SHORT PATH INPUT SCHEMES



SLANT PATH (ITYPE = 2) OPTIONS

- ALL PARAMETERS TAKEN TOGETHER OVERSPECIFY LOS
- H1 (SENSOR) PLUS TWO OTHER PARAMETERS SUFFICE.
FOUR WAYS MODTRAN SPECIFIES LOS:

2A: H1, H2, ZENITH ANGLE

2B: H1, ZENITH ANGLE, RANGE

2C: H1, H2, RANGE

2D: H1, H2, BETA



PATH 2A: H1, H2, ZENITH ANGLE

- *NO FURTHER CHANGES OTHER THAN THE GENERAL
ONES NEEDED*



PATH 2B: H1, ZENITH ANGLE, RANGE

- MODTRAN
 - RECASTS AS 2A (H1, H2, ZENITH ANGLE), THEN PROCEEDS WITH REFRACTION
 - H2 CALCULATED W/O REFRACTION
 - INPUT AND OUTPUT RANGES DIFFER; MAY CRASH
- MODTRAN 2
 - SUBROUTINE NEWH2 COMPUTES $H2_{NEW}$ W/ REFRACTION
 - $H2_{NEW}$ CALCULATION QUICK AND ACCURATE (A NON-ITERATIVE METHOD)
 - PROCEEDS AS USUAL W/CASE 2A BUT USES $H2_{NEW}$
 - INPUT AND OUTPUT MATCH; CRASHES ELIMINATED



ILLUSTRATIVE CALCULATIONS: PATH 2B

H1 = 5 km. ZENITH ANGLE = 92 degrees

INPUT <u>RANGE</u>	OUTPUTS		<u>MODTRAN 2</u> <u>RANGE</u>	<u>MODTRAN</u> <u>H2</u>		<u>MODTRAN 2</u> <u>H2</u>	
	<u>MODTRAN</u> <u>RANGE</u>						
10	10 (0 %)		10	4.66		4.66	
50	49 (-2 %)		50	3.45		3.43	
100	96 (-4 %)		100	2.29		2.20	
150	136 (-9 %)		150	1.53		1.32	
200	162 (-19 %)		201	1.16		0.77	
250	358 (+63 %)		250	1.18		0.54	
300	385 (+28 %)		300	1.59		0.68	
350	427 (+22 %)		350	2.39		0.59	



PATH 2D: H1, H2, BETA

- MODTRAN

- ZENITH ANGLE, INCLUDING REFRACTION EFFECTS,
FOUND BY ITERATION
- ITERATION CONVERGES WHEN COMPUTED BETA AGREES W/INPUT
- CONVERGENCE DOES NOT ALWAYS OCCUR

- MODTRAN 2

- IMPLEMENTED A ROBUST AND EFFICIENT ITERATIVE SCHEME
 - A NEWTON-RAPHSON METHOD
 - "NEXT INCREMENT" OF ZENITH ANGLE
BASED ON ITS DERIVATIVE W.R.T BETA



PATH 2C: H1, H2, RANGE

- *MAPPED TO CASE 2D (H1, H2, BETA)*
- *ONLY THE GENERAL CHANGES NEEDED*



SHORT SLANT PATHS

- MODTRAN

- OFTEN GIVES ZEROS FOR SHORT SEGMENTS
- OFTEN CRASHES

- MODTRAN 2

- ACTIVATED FOR RANGES < 2 KM
- VALID FOR PATHS AS SHORT AS 0.001 KM
- ALL CALCULATIONS DONE AS CASE 2A (H1, H2, ZENITH ANGLE)
- REFRACTION IGNORED
- FLAT EARTH APPROX. USED TO COMPUTE SEGMENT LENGTHS
- ABSORBER AMOUNTS CALCULATED AS BEFORE



ILLUSTRATIVE CALCULATIONS: CASE 2C

H1 = H2 = 5 km

<u>INPUT</u> <u>RANGE</u>	<u>MODTRAN</u> <u>RANGE</u>	<u>MODTRAN 2</u> <u>RANGE</u>	
0.01	5.28	0.01	
1.0	5.29	1.00	
4.7	5.28	4.72	
6.0	-----*	6.01	
8.0	7.46	8.01	* CRASH, PROBABLY COMPUTER-DEPENDENT
9.0	-----*	9.01	
20.0	20.69	20.01	
100.0	100.23	100.00	
300.0	300.00	300.01	



NEW AND CHANGED ROUTINES

- **NEW:**

NEWH2, TANHT, RTBIS, IAFXN, FNDPTH, SMPREP,
SMGEO

- **CHANGED:**

ANDEX, DRIVER, EXPINT, FDBETA, FILL,
FNDHMN, FNDHMN, GEOINP, GEO, LAYER,
RADREF, REDUCE, RFPATH, SCALHT



SUMMARY

- OUTPUT LOS PARAMETERS NOW MATCH INPUT
- ITERATIVE SCHEME TO DETERMINE ZENITH ANGLE MORE ROBUST AND EFFICIENT
- SHORT SLANT PATHS DOWN TO 1 METER NOW POSSIBLE
- ALL CHANGES EQUALLY APPLICABLE TO LOWTRAN 7 AND MODTRAN
- ROUTINES BEING CHECKED BY PL

IR VISIBILITY

C.N. Touart

Hughes STX Corporation, 109 Massachusetts Avenue, Lexington, MA 02173

In response to demand from field users, the current release of the Phillips Lab EOTDA (EO Tactical Decision Aid) outputs values of an 8-12 μm "visibility" that is denoted IRVIS. It is defined as the MRT detection range for an "average" FLIR viewing a target of "standard" size and inherent contrast. The rationale for this definition and how IRVIS behaves in various weather conditions will be presented.

ATMOSPHERIC TRANSMISSION MODELS
ANNUAL REVIEW CONFERENCE, JUNE 1992
GEOPHYSICS DIRECTORATE, PHILLIPS LABORATORY

IR VISIBILITY

CHAN TOUART
HUGHES STX CORP

IR VISIBILITY OUTLINE

- **BACKGROUND**
- **ALGORITHM**
- **EXAMPLES**

**IR VISIBILITY
BACKGROUND**

- **E-O TACTICAL DECISION AIDS:
TV, LLLTV, NVG
1.06 μm LASER
8-12 μm IIR**
- **PERFORMANCE PREDICTION FOR
HIGHLY SPECIFIC SCENARIOS**
- **CLAMOR FROM FIELD FOR A
GENERIC INDEX -- IR VISIBILITY**

IR VISIBILITY ALGORITHM

- FLIR DETECTION RANGE AS BASIS
FOR QUANTIFYING IRVIS
- AVERAGE MRT = 0.153K at 1 cy/mr
- FIXED INHERENT CONTRAST = 2K
(normalized)

IR VISIBILITY
ALGORITHM

$$\Delta T(R) = \Delta T(0) e^{-\beta(IR) R}$$

When $\Delta T(R) = MRT$,
R = DR, the max detection range

Define IRVIS = DR for $\Delta T(0) = 2K$
MRT = 0.153K

$$IRVIS = 2.570 / \beta(IR)$$

IRVIS in an Urban Aerosol	
VIS (km)	IRVIS (km)
1	7
2	14
5	37
10	70
15	111

IRVIS in Advection Fog	
VIS (km)	IRVIS (km)
0.1	0.1
0.2	0.1
0.4	0.2
0.6	0.3
0.8	0.5
1.0	0.6

IRVIS in Snow	
VIS (km)	IRVIS (km)
0.2	0.1
0.5	0.3
1.0	0.5
2.0	1.1
5.0	2.6
10.0	5.3

IRVIS in Rain	
Rainrate (in/hr)	IRVIS (km)
0.01	48
0.1	3.9
0.2	2.5
0.5	1.4
1.0	0.9

IRVIS in Water Vapor	
Dew Point Temp (deg C)	IRVIS (km)
-10	48
0	28
10	15
20	7
30	3

Sensitivity of IRVIS to $\Delta T(0)$				
	IRVIS (km)			
$\Delta T(0)$ (K) =	1	2	3	
TRANS4				
0.9	91	98	113	
0.7	21	29	33	
0.5	11	15	17	
0.3	6	9	10	
0.1	3	4	5	

Sensitivity of IRVIS to MRT				
	IRVIS (km)			
MRT (K) =	0.1	0.15	0.2	
TRANS4				
0.9	114	98	88	
0.7	34	29	26	
0.5	17	15	13	
0.3	10	9	8	
0.1	5	5	4	

IR VISIBILITY
COMPARISON WITH METEOROLOGICAL RANGE

IRVIS = 2.570 / β (IR)

METRNG = 3.912 / β (0.55 μm)

**IR VISIBILITY
SUMMARY**

Version 3.0 of the Mark 3 EOTDA computes an index of 8-12 μ m transmissivity called IRVIS.

IRVIS is the MRT detection range of an average EOTDA FLIR in NFOV mode under the following conditions:

- Target inherent contrast is 2K.
- Clutter in the target scene is moderate.
- Target height subtends 1 mr.

A MODTRAN ALGORITHM FOR PREDICTING DIRECTIONAL SKYSHINE IRRADIANCE

D.C. Robertson
Spectral Sciences, Inc., 111 S. Bedford Street, Burlington, MA 01803

J.A. Kristl
Stewart Radiance Laboratory, 139 Great Road, Bedford, MA 01730

B.P. Sandford
Phillips Laboratory/GPOA, Hanscom AFB, MA 01731-5000

A set of empirical algorithms has been developed to predict the directional dependence of skyshine irradiance calculated with MODTRAN. They provide a spectral/directional skyshine function that allows skyshine to be predicted for arbitrary directions from just a few (four) MODTRAN calculations. The algorithms include the thermally emitted and multiply-scattered skyshine radiance components, which are not uniform in azimuth and elevation. This approach is applicable to many background and target signature models which often approximate the incident skyshine by a contrast. Illustrative calculations are presented to show its impact on calculations of the reflected skyshine signature components.

A MODTRAN ALGORITHM
FOR PREDICTING DIRECTIONAL
SKYSHINE IRRADIANCE

42

BY
DAVID ROBERTSON JOE KRISTL BRIAN SANDFORD
SPECTRAL SCIENCES, INC. STEWART RADIANCE LAB PHILLIPS LABORATORY
BURLINGTON, MA BEDFORD, MA HANSCOM AFB, MA

PRESENTED TO
ANNUAL REVIEW CONFERENCE ON
ATMOSPHERIC TRANSMISSION MODELS
GEOPHYSICS DIRECTORATE, PHILLIPS LABORATORY
HANSCOM AIR FORCE BASE, MA

2 JUNE 1992



ACKNOWLEDGEMENTS

- SPONSORSHIP:

AIR FORCE ELECTRONIC WARFARE CENTER
SAN ANTONIO, TX

SSI INTERNAL RESEARCH FUNDS

- TECHNICAL DISCUSSIONS:

DR. JOHN SCHUMMERS
GEOPHYSICS DIRECTORATE, PHILLIPS LABORATORY



OUTLINE

- INTRODUCTION
- DIRECTIONAL ALGORITHMS
- COMPARISONS TO DIRECT CALCULATIONS
- ILLUSTRATIVE SIGNATURE CALCULATIONS
- CONCLUSION



INTRODUCTION

- **GOAL:**

DEVELOP AN ALGORITHM TO PREDICT SKYSHINE RADIATION

- BASED ON MODTRAN CALCULATIONS
- REASONABLY FAST
- INCLUDES SPECTRAL AND DIRECTIONAL DEPENDENCE

- **MOTIVATION:**

MANY IR SIGNATURE MODELS (e.g., SSTARS, SPIRITS, etc.) ASSUME THAT INCIDENT SKYSHINE IS ISOTROPIC

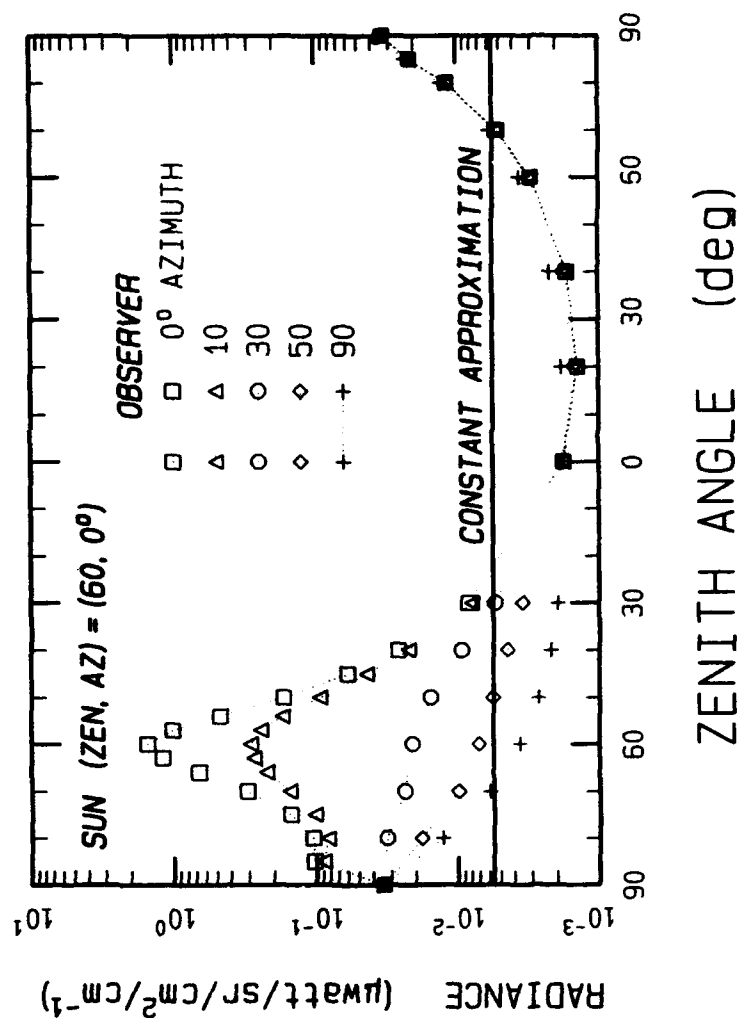
SKYSHINE IS USUALLY APPROXIMATED BY A SINGLE CALCULATION AT AN ARBITRARY ANGLE (~50° Zenith)

SKYSHINE IS MOST DECIDEDLY NON-ISOTROPIC



SKYSHINE ANGULAR VARIATION

- MODTRAN CALCULATIONS AT $4.0 \mu\text{m}$ (2500cm^{-1})





APPROACH

- CHARACTERIZE ESSENTIAL FEATURES AT EACH WAVELENGTH WITH A FEW (4) MODTRAN CALCULATIONS
- USE SCALING ALGORITHMS TO PROVIDE ESTIMATES FOR OTHER ANGLES
- COMPARE TO MODTRAN CALCULATIONS AT DIFFERENT ANGLES
- INTEGRATE INTO SIGNATURE CODES



DIRECTIONAL ALGORITHMS

- THERMAL EMISSIONS

MODTRAN
CALCULATIONS

$$E(\lambda, \theta) = \frac{E_\lambda}{\Delta_\lambda + \cos\theta}$$

70, 90° Zenith

- SCATTERED SOLAR RADIATION

$$E_1(\lambda, \theta) = \frac{\tau_\lambda E_{\lambda\tau} + E_\lambda}{\Delta_\lambda + \cos\theta}$$

70, 90° Zenith

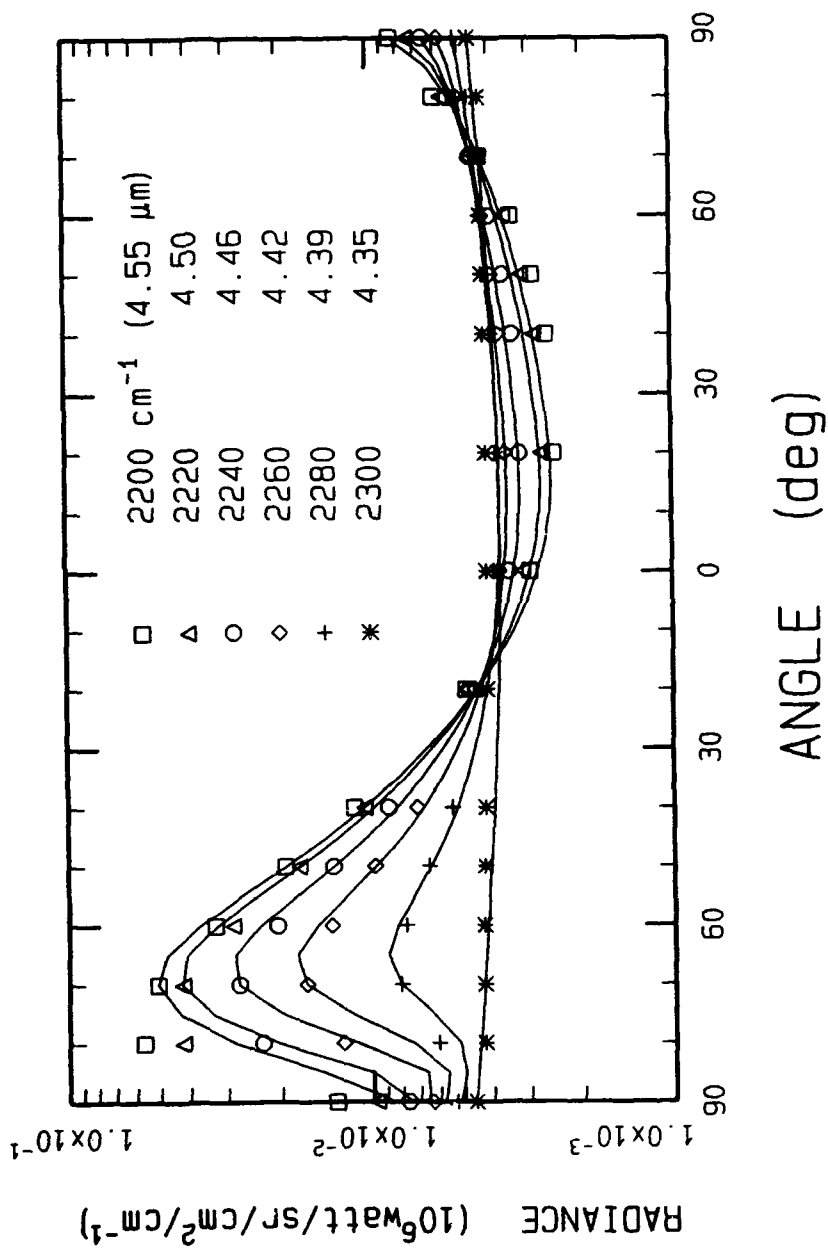
$$E_2(\lambda, \theta) = \frac{E_{sol} - E_1}{e_\lambda \cos^2\theta_{sct} + \sin^2\theta_{sct}}$$

$\theta_{sol}, \theta_{sol} - 20^\circ$



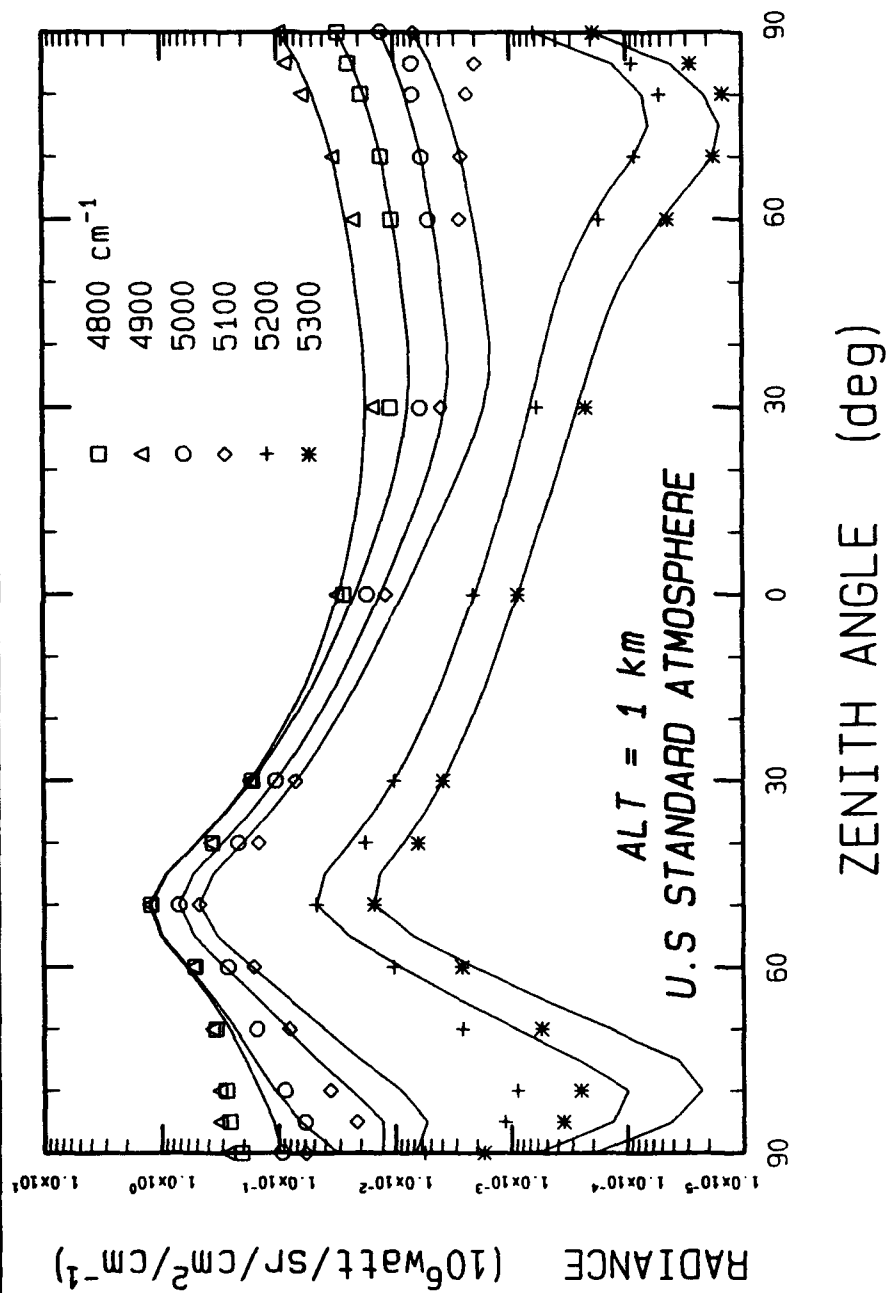
SKYSHINE - 4.3 μm CO_2 REGION

● ALT = 10km - SUN AT (ZN, AZ) = 70, 0°



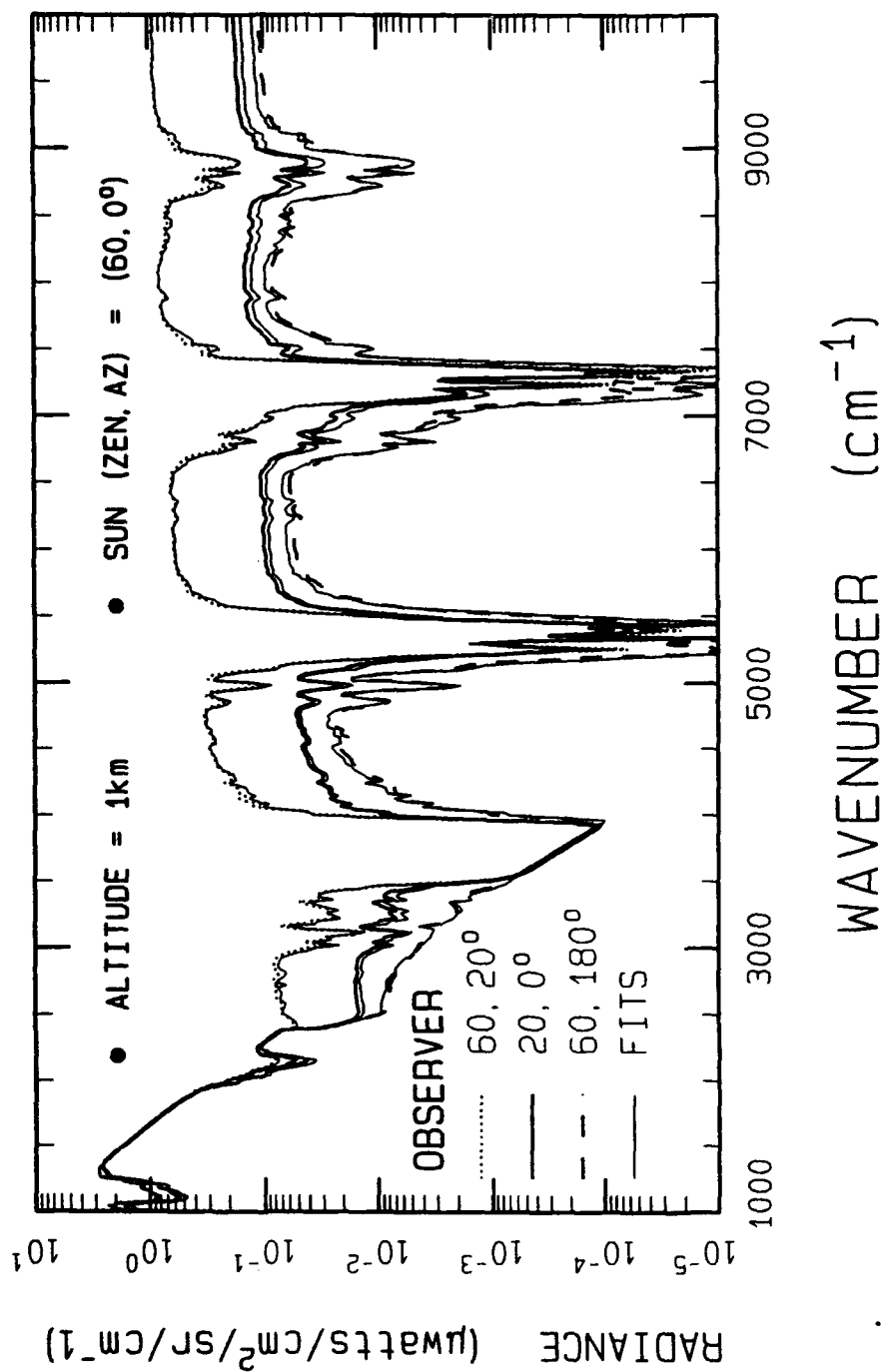


SKYSHINE - SOLAR DOMINATED



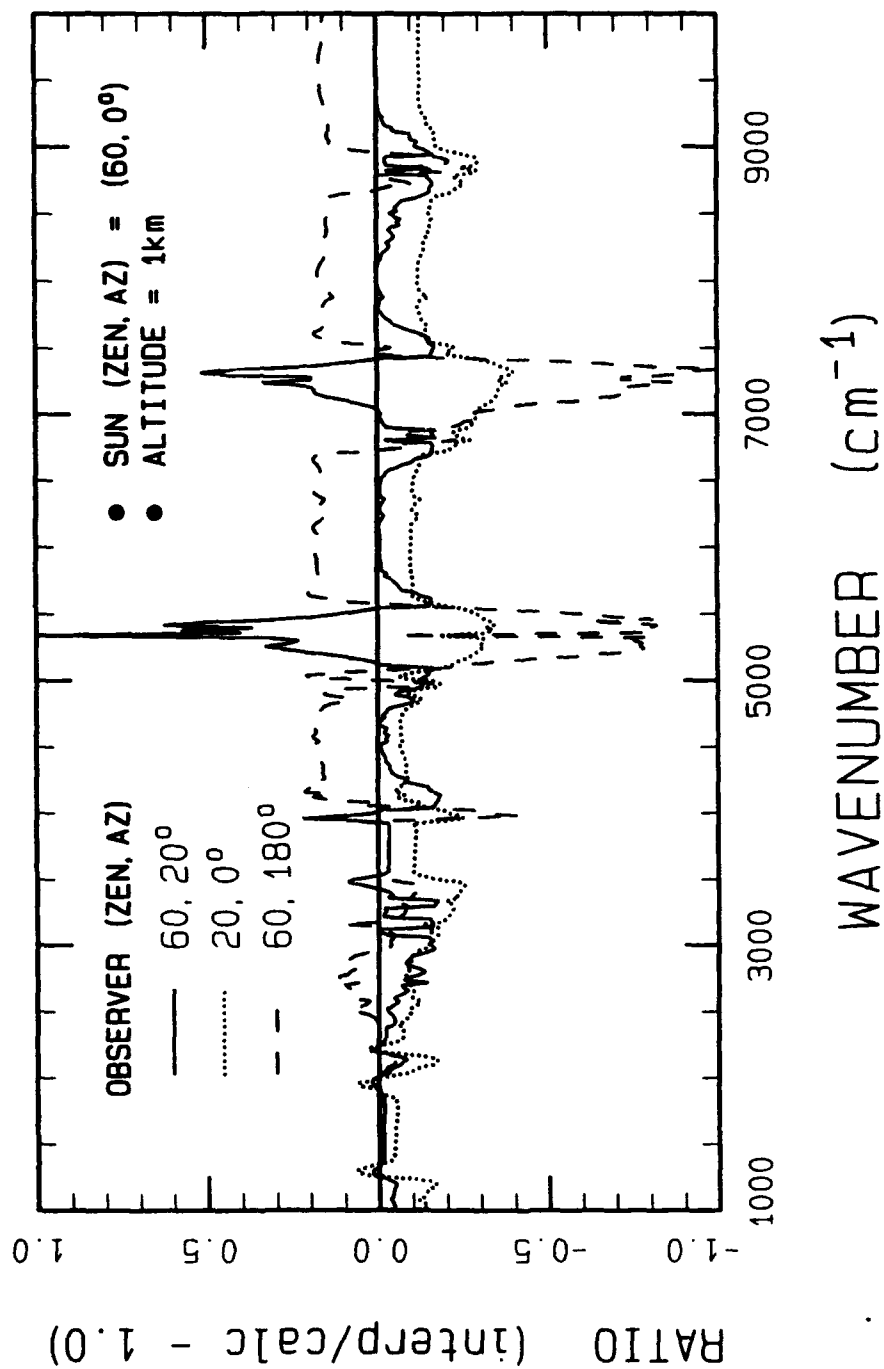


SKYSHINE - SPECTRAL RADIANCE



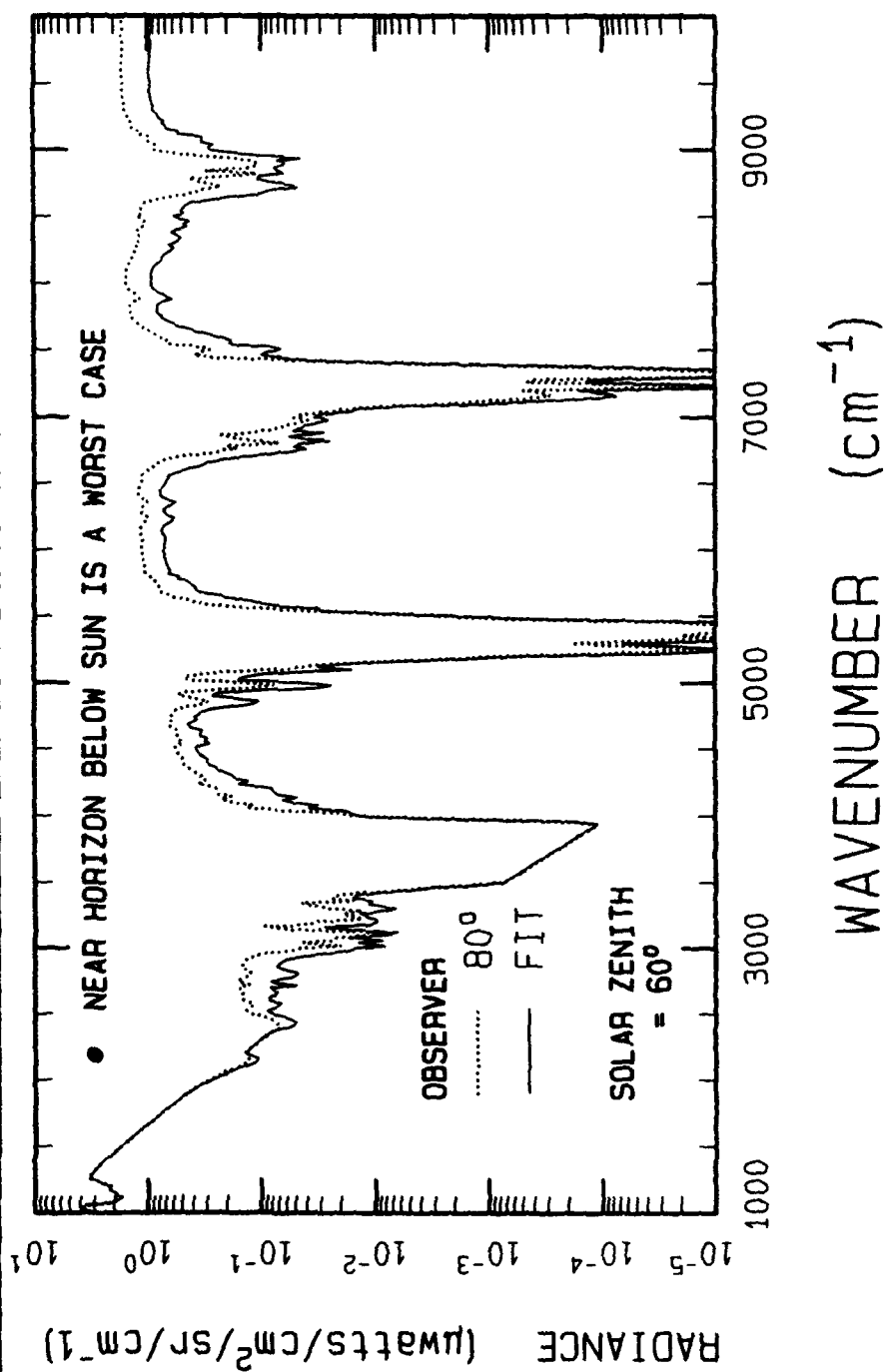


RATIO - INTERPOLATED/MODTRAN





SKYSHINE - NEAR HORIZON





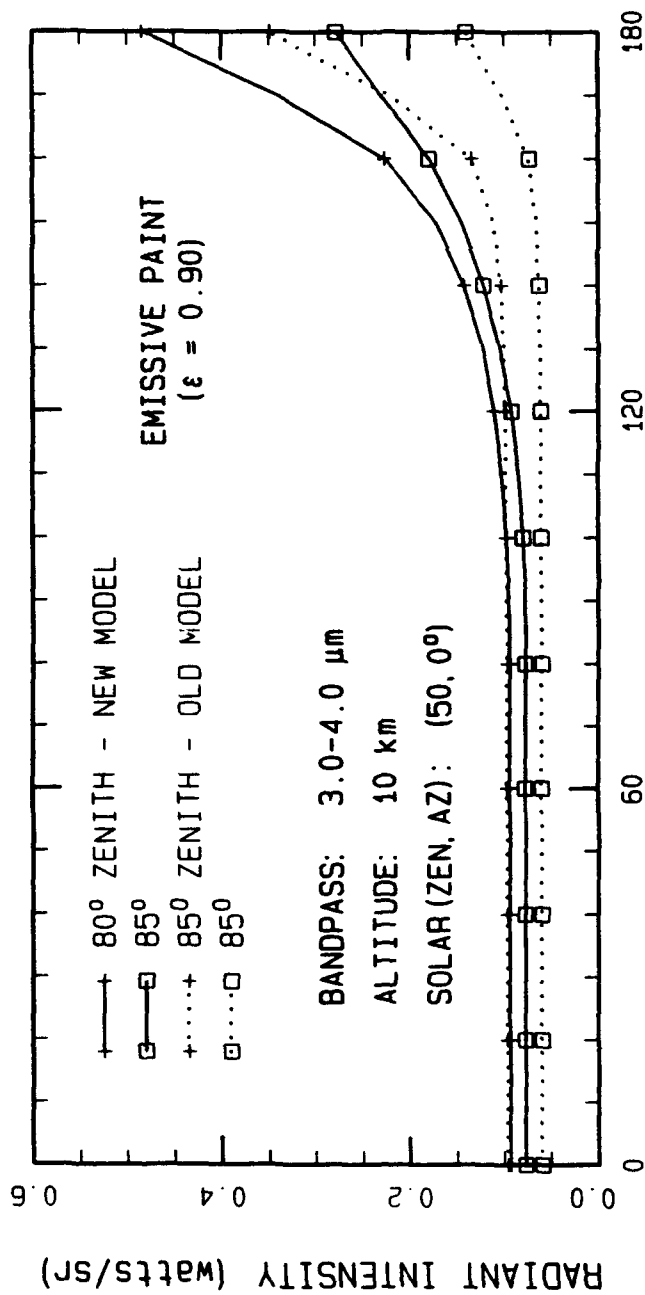
SIGNATURE CALCULATIONS

- AN INITIAL VERSION OF THIS SKYSHINE ALGORITHM HAS BEEN INTEGRATED INTO BOTH SSTIRS & SPIRITS
- BOTH CODES CALCULATE AIRCRAFT IR SIGNATURES FOR DIFFERENT VIEWING SCENARIOS
- SSTIRS: SCENARIO CALCULATIONS FOR UNRESOLVED TARGETS
SPECTRAL SCIENCES TARGET IR SIGNATURE CODE
- SPIRITS: SCENARIO CALCULATIONS FOR IMAGED TARGETS
SPECTRAL AND IN-BAND RADIOMETRIC IMAGING OF
TARGETS AND SCENES MODEL



ILLUSTRATIVE SIGNATURE - SSTIRS

● FLAT PLANAR SURFACE (WING) VIEWED FROM ABOVE





CONCLUSION

- DEVELOPED A NEW SKYSHINE ALGORITHM
 - BASED ON MODTRAN RADIANCE CALCULATIONS
 - EFFICIENTLY USES A FEW MODTRAN RUNS
 - INTERPOLATES TO OTHER DIRECTIONS SPANNING ONE TO THREE ORDERS OF MAGNITUDE
 - RELATIVELY FAST
- ACCURACY
 - COMPARED TO VARIOUS MODTRAN CALCULATIONS FOR DIFFERENT: SUN LOCATIONS, LOOK DIRECTIONS AND WAVELENGTHS
 - GENERALLY GOOD TO WITHIN 30%
 - WEAKEST AT HORIZON BELOW SETTING SUN
- APPLICATION
 - INITIAL INTEGRATION INTO SIGNATURE CODES

**STATUS OF PL/GP HIGH RESOLUTION
RADIANCE-TRANSMITTANCE MODEL: FASCODE**

**F.X. Kneizys, G.P. Anderson, J.H. Chetwynd, L.W. Abreu, M.L. Hoke
Geophysics Directorate, Phillips Laboratory, Hanscom AFB, MA 01731**

**S.A. Clough, R.D. Worsham
Atmospheric and Environmental Research, Inc., 840 Memorial Drive, Cambridge, MA 02139**

**E.P. Shettle
Naval Research Laboratory, Code 6522, Washington, DC 20375**

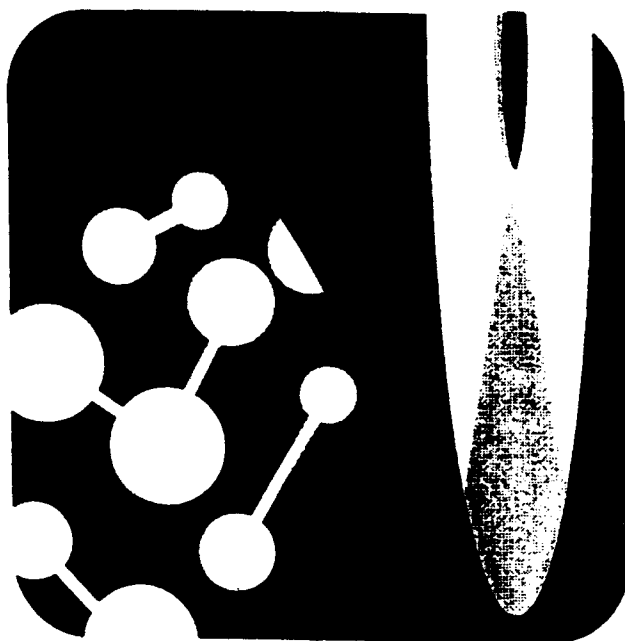
FASCODE, a line-by-line atmospheric radiance-transmittance code, has been released in a preliminary version, FASCOD3P (March 1992). As with previous versions, FASCOD3P is applicable to spectral regions from the microwave to the middle ultraviolet, employing standard spectroscopic parameters supplied from external line atlases. FASCOD3P is the only DoD code currently implementing all HITRAN92 data, including the temperature-dependent CFC absorption cross sections. Other important upgrades include: weighted radiance algorithms, multiple line coupling options, efficient weighting functions, LTE/NLTE line shape compatibility, and enhanced output options.

HITRAN 1992: M³ (MULTI-MEDIA MILIEU)

L.S. Rothman

**Geophysics Directorate, Phillips Laboratory/Optical Environment Division Simulation Branch
(OPS), Hanscom AFB, MA 01731-5000**

A new edition of the spectroscopic molecular database, HITRAN, became available in March 1992. This current edition contains over 70 Megabytes of high resolution data of transitions for 31 species and their atmospherically-significant isotopic variants. In addition, there is a file of cross-sections for heavy molecular species, with bands at several representative temperatures that can be used for atmospheric retrievals with some codes such as FASCODE3P. HITRAN is now available on alternative media: floppy diskettes and optical CD-ROM. Unlike the mainframe-standby nine-track magnetic tape, these media permit rapid access and new user features. This talk will summarize some of the major updates, improvements, and modifications to HITRAN as well as the new PC-oriented media options.



HITRAN 1992

Laurence S. Rothman
PL/GPOS



**HITRAN 1992:
M³ (Multi-Media Milieu)**

**Laurence S. Rothman
Geophysics Directorate
Optical Environment Division
Simulation Branch (OPS)
Hanscom AFB, MA 01731-5000 USA**

Abstract

A new edition of the spectroscopic molecular database, HITRAN, became available in March 1992. This current edition contains over 70 Megabytes of high resolution data of transitions for 31 species and their atmospherically-significant isotopic variants. In addition, there is the file of cross-sections for heavy molecular species, with bands at several representative temperatures that can be used for atmospheric retrievals with some codes such as FASCODE3P. HITRAN is now available on alternative media: floppy diskettes and optical CD-ROM. Unlike the mainframe-standby nine-track magnetic tape, these media permit rapid access and new user features. This talk will summarize some of the major updates, improvements, and modifications to HITRAN as well as the new PC-oriented media options.

HITRAN'92

Details (of both 1991 and 1992 issues) to appear in
Journal of Quantitative Spectroscopy and Radiative
Transfer, Volume 48, 1992

Media options:

- Magnetic Tape (9-track, 6250 CPI)
- CD-ROM
- Floppy diskettes

HAWKS →

- Faster publication
- Supplemental files (CFC's; High-vib bands)

Next HITRAN Conference → June 1993

THE HITRAN MOLECULAR DATABASE:
EDITIONS OF 1991 AND 1992

L.S. ROTHMAN[†]

Phillips Laboratory, Geophysics Directorate
Hanscom AFB, MA 01731, U.S.A.

R.R. GAMACHE

University of Massachusetts Lowell, Center for Atmospheric Research
450 Aiken Street, Lowell, MA 01854, U.S.A.

R. H. TIPPING

Department of Physics & Astronomy, University of Alabama
Tuscaloosa, AL 35487, U.S.A.

C.P. RINSLAND and M.A.H. SMITH

Chemistry & Dynamics Branch, NASA Langley Research Center
Hampton, VA 23665, U.S.A.

D.CHRIS BENNER and V.MALATHY DEVI

Department of Physics
College of William and Mary
Williamsburg, VA 23187, U.S.A.

J.-M. FLAUD, C. CAMY-PEYRET, and A. PERRIN

LPMA, CNRS, Université P. et M. Curie
4 Place Jussieu, 75252 Paris, France

A. GOLDMAN

Department of Physics, University of Denver
Denver, CO 80208, U.S.A.

S.T. MASSIE

National Center for Atmospheric Research
P.O. Box 3000, Boulder, CO 80307, U.S.A.

L.R. BROWN and R.A. TOTH

Jet Propulsion Laboratory
4800 Oak Grove Drive, Pasadena, CA 91109, U.S.A.

[†]To whom all correspondence should be addressed.

New or Modified Parameters by Edition

	<u>1991</u>	<u>1992</u>
H ₂ O	★	
CO ₂	★	★
O ₃	★	
CO	★	
CH ₄	★	★
NO	★	
SO ₂		★
NO ₂		★
HNO ₃	★	
HF	★	★
HCl	★	
HBr	★	
HI	★	
OCS	★	
N ₂		★
H ₂ O ₂	★	★
C ₂ H ₂	★	
C ₂ H ₆	★	
COF ₂	★	★
SF ₆	★	
H ₂ S		★

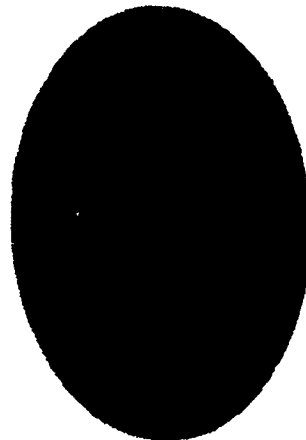
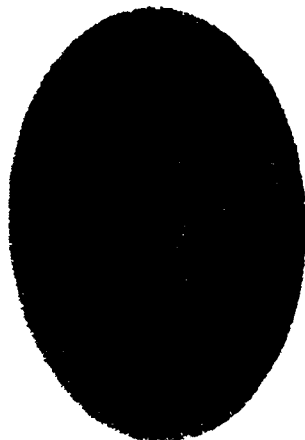
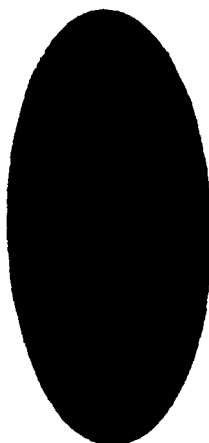
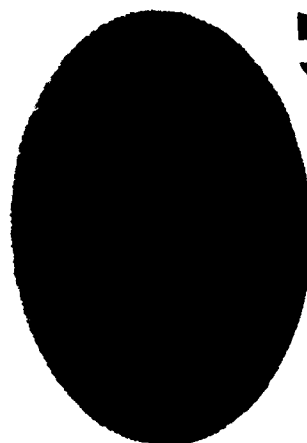
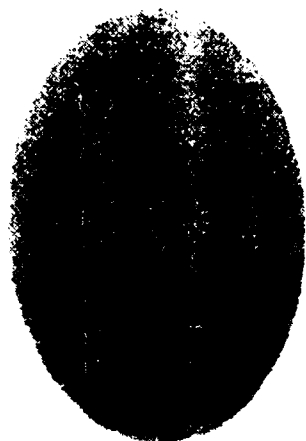
Molecule	Isotopes	# of Bands	# of Lines
H ₂ O	4	134	48 523
CO ₂	8	592	60 790
O ₃	3	76	168 881
N ₂ O	5	140	24 125
CO	5	31	3 600
CH ₄	3	48	47 415
O ₂	3	18	2 254
NO	3	13	7 385
SO ₂	2	7	26 225
NO ₂	1	9	55 468
NH ₃	2	9	5 817
HNO ₃	1	13	143 021
OH	3	27	8 676
HF	1	6	107
HCl	2	17	371
HBr	2	16	398
HI	1	9	237
ClO	2	8	6 020
OCS	4	6	737
H ₂ CO	3	10	2 702
HOCl	2	6	15 565
N ₂	1	1	120
HCN	3	8	772
CH ₃ Cl	2	6	6 687
H ₂ O ₂	1	2	5 444
C ₂ H ₂	2	9	1 258
C ₂ H ₆	1	2	4 749
PH ₃	1	2	2 886
COF ₂	1	7	46 894
SF ₆	1	1	11 520
H ₂ S	1	1	661

Molecule	Spectral Range (cm ⁻¹)	No. of Temps	Number of points per T
CCl ₃ F (CFC-11)	830-860	6	2 023
	1060-1107	6	3 168
CCl ₂ F ₂ (CFC-12)	867-937	6	4 718
	1080-1177	6	6 539
CClF ₃ (CFC-13)	765-805	6	2 696
	1065-1140	6	5 056
	1170-1235	6	4 382
C ₂ Cl ₃ F ₃ (CFC-113)	780.5-995	6	430
	1005.5-1232	6	454
C ₂ Cl ₂ F ₄ (CFC-114)	815-860	6	3 034
	870-960	6	6 067
	1030-1067	6	2 494
	1095-1285	6	12 808
C ₂ ClF ₅ (CFC-115)	955-1015	6	4 044
	1110-1145	6	2 360
	1167-1259	6	6 269
N ₂ O ₅	555.4-599.8	4	93
	720.3-764.7	4	93
	1210.1-1274.8	4	135
	1680.2-1764.6	4	176
ClONO ₂	740-840	2	10 371
	1240-1340	2	1 400
	1680-1790	2	1 540
HNO ₄	770-830	1	5 476
CHCl ₂ (CFC-21)	785-840	1	5 020
CCl ₄	786-806	1	1 826
CF ₄ (CFC-14) †	1255-1290	6	2 359
CHClF ₂ (CFC-22) †	780-1335	6	11 798
HNO ₃ ‡	1270-1350	1	7 301

† Omitted from HITRAN'91, added to HITRAN'92.

‡ Removed from HITRAN'92 (already on high resolution portion).

1992 CD-ROM



HITRAN 92 CD-ROM

- Available June 1992
- High Sierra Format
Compatible with All IBM PC's
Compatible with most Workstations and minicomputers
- Available at no charge from PL/GP

Contact: Dr. Laurence Rothman
Telephone: 617-377-2336
FAX: 617-377-4451
E-Mail: PL 9000.PLH.AF.MIL



Future Version 1993

- HITRAN 1993
- Management Software
 - data editing, searching, sorting, etc.
 - output on tape, disk, hard copy
 - simple mathematical and statistical functions
- Graphical Display
 - stick plots of line strength
 - color coded for molecules, bands, etc.
- Additional Databases
 - hot gas
 - supplemental data files.



USF HITRAN-PC (SEARCH Program)

Random Access
HITRAN '91
Database

ASCII Data File
(For Later Use)

Smaller Random
Access Data File

Quit Output Param <Forward> Back Restart Range Mol Temp S min

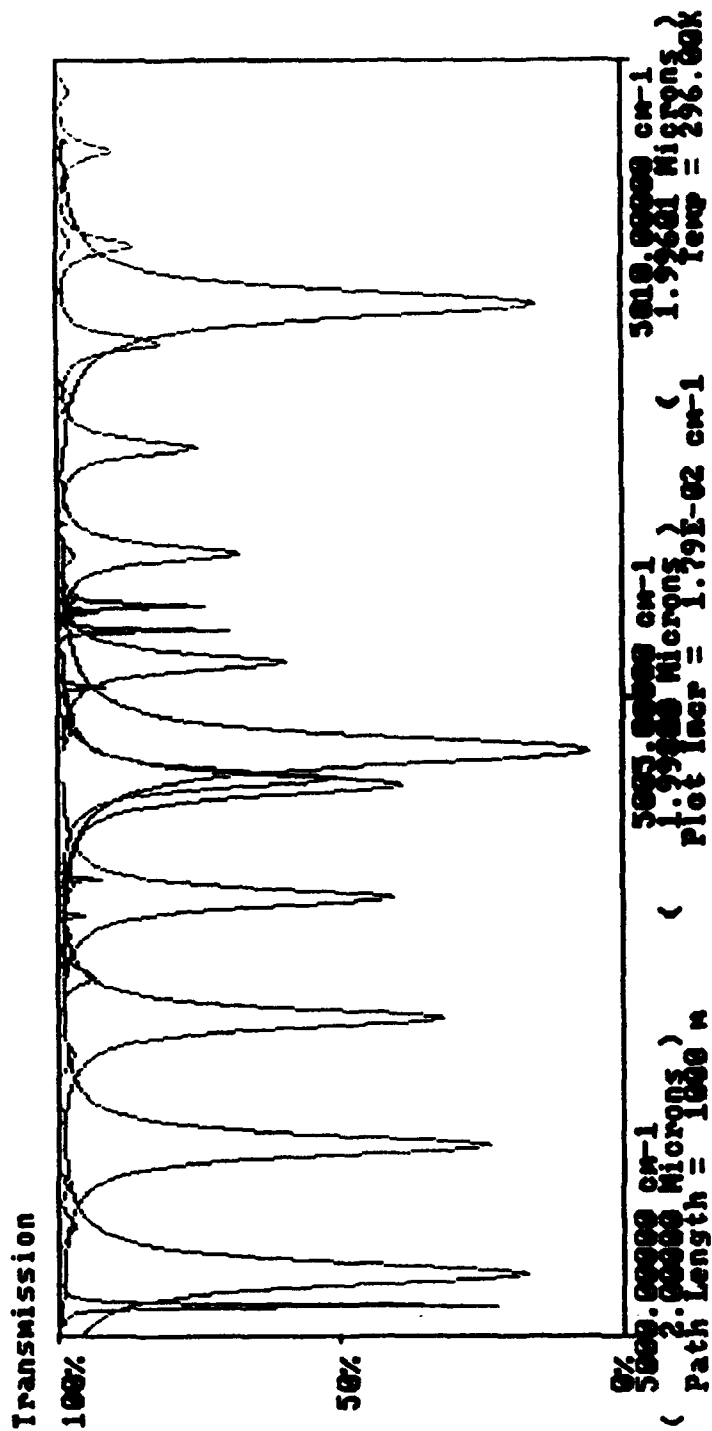
Searching Wavenumber : 5000.8578 cm-1

N	J	Wavenumber	S	R	Q	E"	Q'	Q''
CO2	1	5000.8587	3.963E-27	6.206E	-6.0720	2703.34014		P 33
CO2	3	5000.8593	1.814E-26	1.495E	-6.0703	975.59039		P 51
CO2	1	5000.22347	1.477E-25	0.707E	-6.0674	2240.23755		R 68
CO2	2	5000.22500	2.160E-24	1.068E	-4.0000	2350.30356	14 814	15 815
H2O	1	5000.33473	1.649E-26	1.004E	-5.0094	1390.12122		R 0
CO2	1	5000.35100	4.203E-25	0.710E	-6.0606	2004.66040		R 58
CO2	2	5000.47617	3.192E-25	6.004E	-7.0720	316.67001		P 27
H2O	1	5000.42000	2.990E-23	4.751E	-6.0016	754.00672		P 16
CO2	1	5000.40003	4.319E-22	9.496E	-6.0719	404.17169		P 32
CO2	2	5000.40453	5.953E-27	4.607E	-6.0720	1710.65910		P 32
H2O	1	5000.54070	6.959E-27	1.096E	-8.0557	1411.61206	9 5 4	0 6 3
H2O	4	5000.75000	4.620E-27	3.108E	-6.0057	809.39502	0 3 5	0 4 4
CO2	1	5000.83037	9.316E-26	0.702E	-6.0669	2340.73210		R 65
H2O	4	5000.83600	4.469E-26	3.439E	-6.0323	300.61700	5 0 5	6 1 6
CO2	2	5000.85697	2.214E-24	5.195E	-6.0056	60.07300		R 12
CO2	3	5000.99115	2.146E-26	1.502E	-6.0764	930.00057		P 50

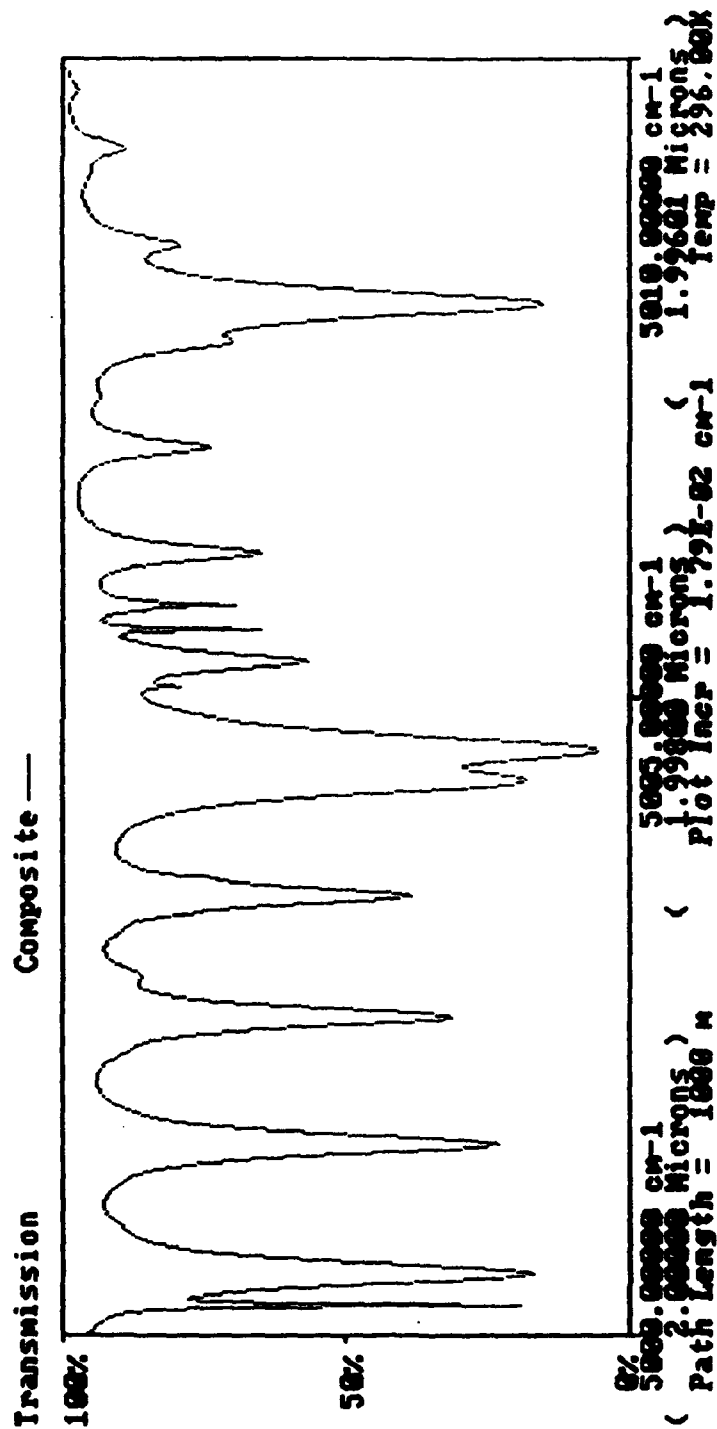
T = 296 K Int Lim = 1E-00 Wm2 = 5000 cm-1 Wm2 = 5020 cm-1

Run Mol Temp MN/ML Range Incr ~~LineShop~~ PatLen Press Sor File Quit
 Stick (Lorentz Peak)
 Pressure (Lorentzian)
 Stick (Doppler Peak)
 Doppler (Gaussian)

Molec Sel P(atm)
 CO2 — 3.30E-04
 H2O — 7.75E-03
 N2O — 3.20E-07
 OH — 4.40E-14
 HBr — 1.70E-12



<Run> Mol Temp Wavenumber Range Increment LineShape PathLength Press Scan File Quit
 Standard Plot
 Laser Line Overlay
 Composite of Previous Plot



AFGL Memorial BBS

- Established to provide a support alternative for Geophysics Directorate codes and to broaden the user base.
- Exact level of support depends on program manager; options include bulletins, message base, and files available for download.
- Access is by dial-up modem at (617) 377-7373. BBS operates at 300/1200/2400 baud, 8N1, no MNP. BBS is available 24hrs per day, 7 days a week beginning 1 June 1992.
- Problem reports should be directed to the System Operators
Dale Sinclair, 377-3694 Bob Hawkins, 377-3614

**ATMOSPHERIC
PROPAGATION
MODELS**

STATUS OF PL/GP MODERATE RESOLUTION RADIANCE/ TRANSMITTANCE MODELS: MODTRAN AND DERIVATIVES

**F.X. Kneizys, L.W. Abreu, G.P. Anderson, J.H. Chetwynd
Geophysic Directorate, Phillips Laboratory/GPOS, Hanscom AFB, MA 01731**

MODTRAN (public release: November 1990) is a 2 parameter (pressure and temperature) band model code with moderate spectral resolution (2cm^{-1} full width-half maximum). The MODTRAN band model parameters were calculated by directly utilizing the HITRAN-86 data base. The resultant code is fully compatible with LOWTRAN 7 capabilities and has been successfully validated against FASCODE.

Because of its relative accuracy and ease of use, MODTRAN is undergoing an applications revolution. For instance, it serves as a primary foundation for:

AURIC-E, the Atmospheric Ultraviolet Radiance Integrated Code (Extension), describing solar scattering and transmittance to 0.15 microns.

SAM, SHARC and MODTRAN, a newly envisioned rapid combined algorithm for surface to space NLTE calculations.

MOSART, Moderate Spectral Atmospheric Radiance and Transmittance Code, a combination of the MODTRAN band model and the APART scene and cloud formulations.

FAUST, Fast Atmospheric Unified Synthesis Technique, a pragmatic limb viewing algorithm, combining MODTRAN and SHARC path segments.

1992 Annual Review Conference on
Atmospheric Transmission Models

STATUS OF PL/GP MODERATE RESOLUTION
RADIANCE/TRANSMITTANCE MODELS:

MODTRAN AND DERIVATIVES

F.X. Kneizys, L.W. Abreu, G.P. Anderson, and J.H. Chetwynd
Geophysics Directorate, PL/GPOS, Hanscom AFB

MODTRAN (public release: November 1990) is a 2 parameter (pressure and temperature) band model code with moderate spectral resolution (2cm⁻¹ full width-half maximum). The MODTRAN band model parameters were calculated by directly utilizing the HITRAN-86 data base. The resultant code is fully compatible with LOWTRAN 7 capabilities and has been successfully validated against FASCODE.

Because of its relative accuracy and ease of use, MODTRAN is undergoing an applications revolution. For instance, it serves as a primary foundation for:

AURIC-E, the Atmospheric Ultraviolet Radiance Integrated Code (Extension), describing solar scattering and transmittance to 0.15 microns.

SAM, SHARC and MODTRAN, a newly envisioned rapid combined algorithm for surface to space VLTE calculations.

MOSART, Moderate Spectral Atmospheric Radiance and Transmittance Code, a combination of the MODTRAN band model and the PRA/APART scene and cloud formulations.

FAUST, Fast Atmospheric Unified Synthesis Technique, a pragmatic limb viewing algorithm, combining MODTRAN and SHARC path segments.

GPOS RADIATIVE TRANSFER CODES:

LOWTRAN
MODTRAN
FASCODE

Low Spectral Resolution Transmission and Radiance (LOWTRAN) Code:

LOWTRAN (LOWTRAN7, 1989) is a low spectral resolution (20cm^{-1}) code for predicting the atmospheric transmittance and background radiance for line-of-sight paths at altitudes below 50 km over the spectral range from 0 to $50,000\text{ cm}^{-1}$. The radiance includes, in addition to emission from 13 atmospheric gases, contributions from single scattered solar and lunar radiance and multiple scattered solar and thermal radiation. Direct solar irradiance is also an option. A single parameter band model is used for molecular line absorption (based on spectrally degraded "exact" line-by-line calculations using FASCOD2 (see below), and the HITRAN86 data base). Molecular continuum-type absorption spectra (for H_2O , CO_2 , O_2 , N_2 , and O_3) have been developed separately and subsequently incorporated into LOWTRAN. Molecular scattering, aerosol and hydrometeor absorption and scattering, and surface emittance/reflectance properties are also included, as well as a self-contained spherical viewing geometry algorithm that includes the effects of refraction and earth curvature. Representative atmospheric gas, aerosol, cloud and rain models are provided with options to replace them with user-defined values. This fast-running code has long been the standard for broad-band electro/optical systems design in the ultraviolet through infrared frequencies. With the extension to the microwave, the code can also be employed as a primitive energy balance (climate) code. Future options will center on maintaining parallelism with MODTRAN; see below.

Moderate Resolution Transmission and Radiance Code: (MODTRAN)
MODTRAN (MODTRAN, 1990) is a moderate resolution (2 cm^{-1}) code for predicting the atmospheric transmittance and background radiance, appropriate for altitude regions not effected by non-local thermodynamic equilibrium (non-LTE) signatures, generally below 60km. A two-parameter (temperature and pressure) band model is used for molecular line absorption, based directly on the HITRAN86 data base, employing FASCODE exact calculations as validation only. MODTRAN contains all the options and spectral coverage (0 to $50,000\text{ cm}^{-1}$) of LOWTRAN 7, including default gases, aerosol, cloud and rain profiles, surface properties, continua contributions, viewing geometry, and solar/lunar and/or thermal direct or multiply scattered radiance. User-defined input can replace default options. Because of its improved spectral resolution and accuracy, MODTRAN is recommended as the appropriate replacement for LOWTRAN 7 for systems evaluation,

including transmission of aircraft and plume signatures. Suitable scanning and filter options are available to match E/O systems resolution. Note that MODTRAN explicitly contains LOWTRAN 7 as an operational mode to facilitate comparisons. Future options will include addition of: enhanced UV capability (AURIC), man-made contaminant signatures (CFC's), suitable modifications for climate simulations, and improved surface and cloud properties (MOSART).

Fast Atmospheric Signature Code (FASCODE)

FASCODE, most recently released as FASCOD3P, a preliminary version of FASCOD3 (1992), is a state-of-the-art line-by-line transmittance and radiance simulation code. For atmospheric cases, it has all the flexibility and default options (UV to mm-wave, clouds, rain, surface properties, etc.) of LOWTRAN and MODTRAN, with the exception of solar/lunar irradiances. The altitude range is essentially unlimited (0-300km) but default constituent profiles are currently specified only to 120km. Because it explicitly calculates the exact line shape for the set of species specified by the HITRAN spectroscopic parameters adjusted for local temperature and pressure, FASCODE can accurately follow arbitrarily configured lines of sight, including those that cross from Doppler to Voigt regimes and/or intersect the surface. The code also has a non-LTE capability, incorporating contributions from non-thermal emission sources, given appropriate populations (as precalculated by SHARC, below). FASCOD3P is the only DoD code that has fully implemented the fluorocarbon cross sections in conjunction with local heating/cooling rate estimates, enhancing its role as validation standard, climate code, and "forward" radiance algorithm for remote sensing. Operational speed of FASCODE can be prohibitive for real time analyses, but the accuracy is essential for evaluating more pragmatic algorithms. Future endeavors include additions of: full vectorization, improved line shape for remote sensing, solar capability with new multiple scattering algorithm, and optimized feedback to radiative/photochemical/dynamical programs.

Moderate Spectral Atmospheric Radiance and Transmittance: MOSART MOSART is a "spatially extended" version of MODTRAN, providing much enhanced descriptions of constituent, aerosol, cloud and surface properties. The new data bases and implementation algorithms for the complex scene descriptors will be derived from the APART Code (Photon Research Associates) but the spectroscopic foundation will remain MODTRAN. All ongoing MODTRAN enhancements will be maintained. This new code is expected to readily into SSGM.

MODTRAN Authorship

**F.X. Kneizys, L.W. Abreu, E.P. Shettle¹,
J.H. Chetwynd, G.P. Anderson, W.O. Gallery²,
J.E.A. Selby³, S.A. Clough²
(PL/Geophysics Directorate)**

and

**A. Berk, L.S. Bernstein, D.C. Robertson
(Spectral Sciences, Inc.)**

POC/LOWTRAN and MODTRAN

**Gail P. Anderson
PL/GPOS
Hanscom AFB, MA 01731**

**617-377-2335
617-377-2337
FAX 617-377-8780**

AVAILABILITY

**NATIONAL CLIMATIC DATA CENTER (NOAA)
CLIMATE SERVICE SECTION
FEDERAL BUILDING
ASHEVILLE, NC 28801**

704-259-0272

or

**DoD Requests to G.P. Anderson
as, above**

1992 PLANS

MODTRAN: Evolution, Documentation, Mutations

MODTRAN

MODTRANn AURIC MOSART SAM etc.

NEAR TERM -

Geometry/Precision	*SSI
O3 9.6 micron band	*SSI
1992 HITRAN database	*SSI

IR CFC's	?
----------	---

UV:

O2 S/R	Aerodyne
CFC's	?
SO2, NO2	?

Vis:

O3 Chappuis	?	?
-------------	---	---

Multiple Scattering	Caelum
Very Low Sun Solution	AER?

PHOTOCHEMISTRY-related -

Heating/Cooling Rates
FSC3 Validation

Photodissociation Rates	?	?
-------------------------	---	---

Climate Change Scenarios	?
--------------------------	---

INVERSION ALGORITHM DEVELOPMENT -

Inversion Algorithm:

Feasibility	?
FSC3 Validation	?

SENTRAN Extensions	SPARTA
A-matrix or wgt.fun.	?

PATH DESCRIPTORS -

Climatologies:

Cloud, Aerosol	?
CFC's	NRL

Image Properties: APART

Surface	SSI/PRA
Clouds	" / "
Backgrounds	" / "

OTHER -

Compatibility

SHARC	SSI
SSGM	PRA/?
SMAART	MRC/?
FAUST	MRC/?

Cooperative Efforts

NASA	
Model Comparisons	Harvard
Ozone Depletion	APL
ITRA/ICRCCM	DOE/WMO

THE ATMOSPHERIC ULTRAVIOLET RADIANCE INTEGRATED CODE (AURIC)

C.C. Betchley, J.A. Conant
Aerodyne Research, Inc., 45 Manning Road, Billerica, MA 01821

G.P. Anderson, L.A. Hall
Geophysics Directorate, Phillips Laboratory, Hanscom AFB, MA 01731

This project is a multi-year effort to develop new capabilities for simulating background radiance and transmission throughout the atmosphere, as viewed by ultraviolet sensors. The recent focus has been to develop an initial version, built upon the existing MODTRAN model. This version extends the altitude range from 120km up to 1000km, and the wavelength range from 200nm down to 120nm.

The routines in AURIC were generalized to handle more atmospheric layers than with MODTRAN. The current dimensioning is for 100 layers, but can be changed by editing one file and then re-compiling the software. The profile data in MODTRAN were then extended to 1000km altitude, using data from the SHARC code from 120 km to 300 km and from the US 1976 Standard Atmosphere from 300 km to 1000 km. The Schumann-Runge O₂ continuum and band system model was upgraded using the model developed by K. Minschwaner of Harvard University. Coefficients for a set of quadratic expressions in temperature were derived to generate appropriate cross-sections at a resolution of 1.0 cm⁻¹. Recent SUSIM solar data were added in the 120 to 400 nm wavelength region.

SYSTEMS

ARI File No. 1579
VGS/233



THE ATMOSPHERIC ULTRAVIOLET RADIANCE INTEGRATED CODE (AURIC)

PRESENTED TO:

**THE ANNUAL REVIEW CONFERENCE ON
ATMOSPHERIC TRANSMISSION MODELS**

PRESENTED BY:

**C. C. BETCHLEY, J. A. CONANT (AERODYNE RESEARCH, INC.)
G. P. ANDERSON, L. A. HALL (PHILLIPS LABORATORY)**

JUNE 1992

**WORK SPONSORED BY
THE STRATEGIC DEFENSE INITIATIVE OFFICE
UNDER CONTRACT NO. F19628-89-C-0091**

45 Manning Road
Billerica, Ma 01821-3976
(508) 663-9500 Fax: (508) 663-4918





AURIC EXTENSIONS TO MODTRAN

- NEW O₂ SCHUMANN-RUNGE BAND AND CONTINUUM MODELS
 - SPECTRAL REGION 49,000 - 66,000 cm⁻¹ (152 - 204nm)
- ATMOSPHERIC MODEL EXTENDED TO HIGHER ALTITUDES
 - CURRENTLY 1000 KM
- INCREASED NUMBER OF LAYERS FOR THE CALCULATIONS
 - 87 OR MORE
 - EASILY INCREASED BY CHANGING A SINGLE NUMBER AND RE-COMPILING
- SOLAR IRRADIANCE EXTENDED IN THE ULTRAVIOLET TO 83,000 cm⁻¹ (120nm)
- NEW UV NO₂ AND SO₂ DATA PLANNED FOR INCLUSION

SYSTEMS



USER OPERATION OF AURIC

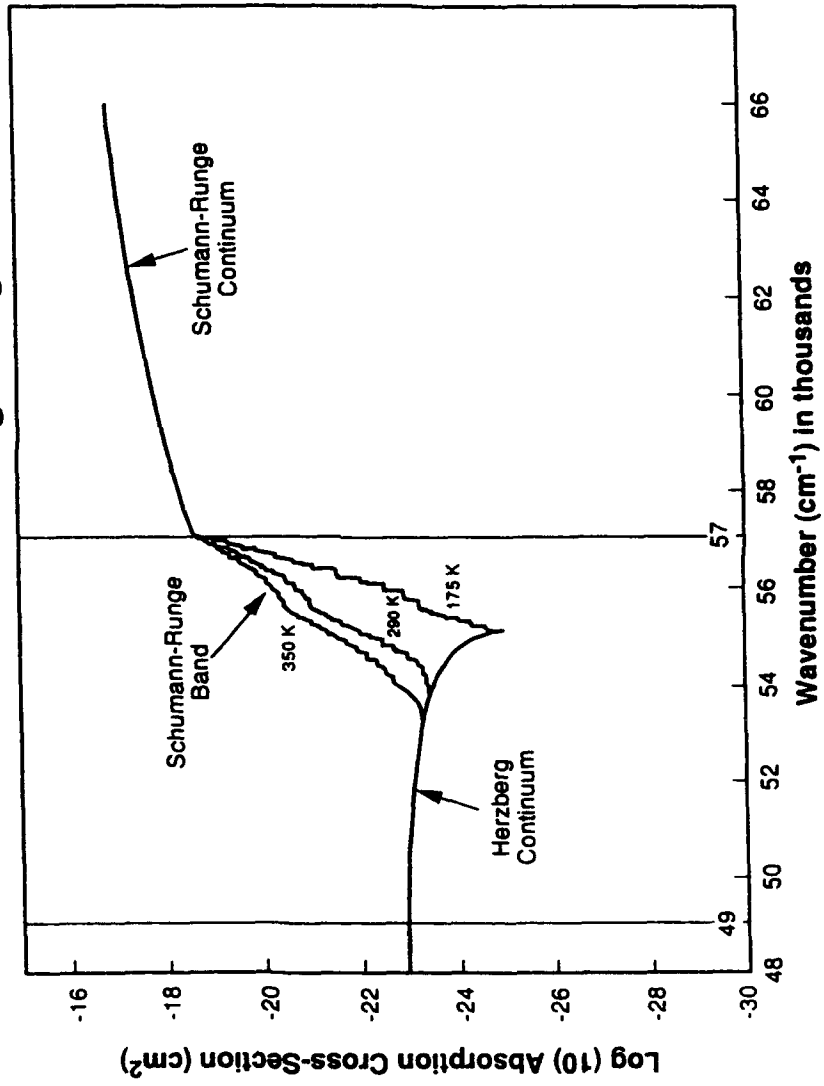
- AURIC IS A DIRECT EXTENSION OF MODTRAN
- ALL INPUTS ARE THE SAME AS MODTRAN, EXCEPT THE FIRST THREE SPACES ON CARD 1, WHICH IS NOW A CHARACTER VARIABLE
- THE CODE WILL RUN AS MODTRAN/LOWTRAN7 IF MODTRAN INPUT FILES ARE USED
- THE CODE WILL RUN AS AURIC IF AN "A" IS PLACED IN ANY ONE OF THE FIRST THREE SPACES
- WHEN RUN AS AURIC, THE MODTRAN/LOWTRAN7 SWITCH REMAINS AVAILABLE, ALLOWING SELECTION OF BAND MODEL TYPE AND RESOLUTION





SYSTEMS

Schumann-Runge Region



MP92-153/C.B.



OXYGEN SCHUMANN-RUNGE BAND MODEL

- SPECTRAL BAND FROM $49,000 \text{ cm}^{-1}$ TO $57,000 \text{ cm}^{-1}$ (175 TO 204 nm)
- ABSORPTION CROSS SECTIONS ($\text{cm}^2/\text{molecule}$) GIVEN EVERY $1/2 \text{ cm}^{-1}$
- KEN MINSCHWANER (HARVARD) FIT 144,000 COEFFICIENTS IN 3 TEMPERATURE REGIONS TO RECENT HIGH RESOLUTION LABORATORY DATA:

$$\sigma = [Ax^2 + Bx + C] \cdot 10^{-20}, \text{ WHERE}$$

$$x = [(T-100)/10]^2$$

- SEPARATE FITS IN THREE TEMPERATURE REGIONS:

$$130^\circ \leq T \leq 190^\circ, \quad 190^\circ < T \leq 280^\circ, \quad 280^\circ < T \leq 500^\circ$$





OXYGEN SCHUMANN-RUNGE CONTINUUM MODEL

- SPECTRAL BAND FROM 57,000 TO 66,000 cm^{-1} (175 TO 152 nm)
- KEN MINSCHWANER (HARVARD) FIT CONTINUUM ABSORPTION CROSS SECTIONS WITH SINGLE TEMPERATURE-INDEPENDENT EXPRESSION:

$$\sigma = [Ay^2 + By + C] \cdot 10^{-19} \quad , \quad \text{WHERE}$$

$$y = (\omega - 57000) / 10 \quad ,$$

$$A = 1.1538 \cdot 10^{-4} \quad , \quad B = 1.8083 \cdot 10^{-2} \quad , \quad C = 1.5062 \quad , \quad \text{AND}$$

$$\omega = \text{WAVENUMBER (cm}^{-1}\text{)}$$

SYSTEMS



SCHUMANN-RUNGE IMPLEMENTATION

- BAND DATA STORED IN THREE FILES (ONE PER TEMPERATURE RANGE)
- EACH FILE STORES THREE QUADRATIC COEFFICIENTS AT EACH WAVENUMBER
- COLUMN DENSITIES AND TEMPERATURE-WEIGHTED COLUMN DENSITIES COMPUTED IN SUBROUTINES STDMDL AND GEO FOR THE NINE COEFFICIENTS TO CALCULATE PATH OPTICAL DEPTH
- BEER'S LAW USED IN SUBROUTINE TRANS TO COMPUTE TRANSMITTANCE



SYSTEMS



ATMOSPHERE PROFILE EXTENSION TO 1000 KM

- MODTRAN ATMOSPHERIC DATA CONTAIN 50 LAYERS WHICH EXTEND TO AN ALTITUDE OF 120km, ONLY 100km OF WHICH ARE USED BY MODELS 1 THROUGH 6
- THE MODTRAN/LOWTRAN7 MODEL ATMOSPHERES 1 THROUGH 6 HAVE BEEN KEPT AS IS TO RUN WITH AURIC "OFF"; THEY ARE STILL STORED IN BLOCK DATA MLATMB
- TWO ADDITIONAL BLOCK DATA HAVE BEEN ADDED TO HOLD AURIC MODEL ATMOSPHERES 1 THROUGH 6, ONE FOR DAYTIME (ALATMB) AND ONE FOR NIGHTTIME (NLATMB)

21



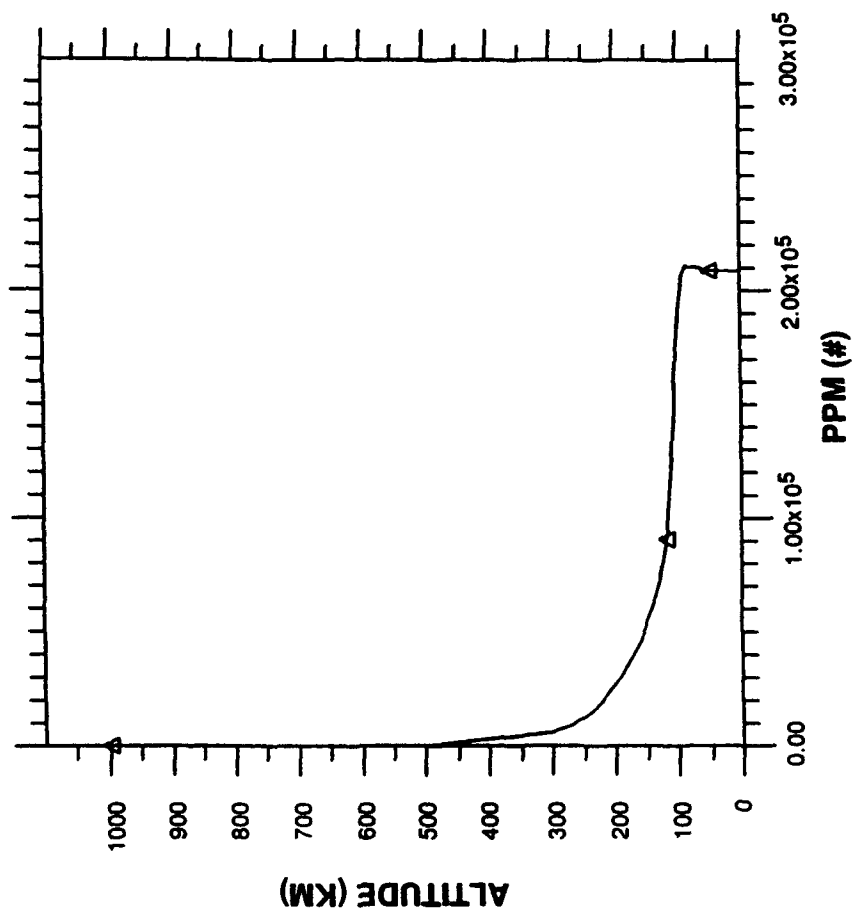
ATMOSPHERE PROFILE EXTENSION (CONT.'D)

- THE AURIC MODEL ATMOSPHERES CONTAIN 104 DATA LAYERS:
 - FROM 0km UP TO 50km 35 LAYERS, SAME AS MODTRAN
 - FROM 50km UP TO 150km 50 LAYERS SPACED EVERY 2km
 - FROM 150km THROUGH 300km 16 LAYERS SPACED EVERY 10km
 - THREE MORE LAYERS AT 500, 750, AND 1000km
- THE AURIC DAYTIME MODEL 6 ATMOSPHERE HAS ADDED SHARC CODE ATMOSPHERIC DATA FROM 50km THROUGH 300km ALTITUDES FOR THE 10 SPECIES:
 - N₂, O₂, O₃, NO, N₂O, CO, CO₂, OH, H₂O, AND CH₄ (TO 120km)
- THE AURIC DAYTIME MODEL 6 ATMOSPHERE HAS 1976 U.S. STANDARD ATMOSPHERE DATA FOR THE 500, 750, AND 1000km ALTITUDES FOR N₂ AND O₂

SYSTEMS



O2 CONCENTRATIONS



MP92:154/C B

506

SYSTEMS



CALCULATION LAYERING INCREASES

- THE ALTITUDES OR LAYER BOUNDARIES AT WHICH MODTRAN AND AURIC MAKE THEIR CALCULATIONS ARE DISTINCT FROM THE ATMOSPHERIC MODEL DATA LAYERS (EXCEPT FOR MODEL 7 USER INPUT ATMOSPHERES)
- MODTRAN ALLOWS ONLY 33 LAYERS TO BE USED
- AURIC PRESENTLY CONFIGURED TO HANDLE 97 CALCULATION ALTITUDES, CONSISTING OF 87 DEFAULT CALCULATION ALTITUDES PLUS UP TO 10 VSA ALTITUDES; THE DEFAULT CALCULATION ALTITUDES ARE:
 - FROM 0km THROUGH 25km, 26 SPACED EVERY 1km (SAME AS MODTRAN)
 - FROM 26km THROUGH 70km, 23 SPACED EVERY 2km
 - FROM 74km THROUGH 150km, 20 SPACED EVERY 4km
 - FROM 160km THROUGH 300km, 15 SPACED EVERY 10km
 - THREE MORE ALTITUDES AT 500, 750, AND 1000km





AURIC LAYERING IMPLEMENTATION

- AURIC DIMENSIONS ITS ARRAYS USING FORTRAN "PARAMETER" VALUES, INCLUDED IN SUBROUTINES FROM A PARAMETER FILE
- TO CHANGE THE CODE'S COMPILED DIMENSIONS ONLY A SINGLE FILE NEEDS TO BE CHANGED. CURRENT PARAMETER SETTINGS ARE:
 - LAYDIM = 100 FOR THE CALCULATION ALTITUDES
 - LAYDAT = 104 FOR AURIC ATMOSPHERIC DATA LAYERS
 - MODDAT = 50 FOR MODTRAN ATMOSPHERIC DATA LAYERS
 - MSPECI = 28 FOR THE CURRENT NUMBER OF ATMOSPHERIC SPECIES
 - MBANDS = 73 FOR THE AURIC NUMBER OF PATH AMOUNTS
 - MPHASE = 50 FOR THE NUMBER OF PHASE FUNCTION ANGLES
- AURIC CAN THUS BE EASILY CONFIGURED TO HANDLE ANY NUMBER OF CALCULATION ALTITUDES VIA MODEL 7 ALTITUDE INPUT, WITH PROFILE PROPERTIES DEFAULTED TO ONE OF THE STANDARD MODELS



SOLAR IRRADIANCE EXTENSION

- NEW 1987 SUSIM DATA FROM SPACELAB 2 HAVE BEEN ADDED TO AURIC TO EXTEND THE SOLAR IRRADIANCE IN THE UV
- THE DATA IS FROM $25,000\text{cm}^{-1}$ TO $83,00\text{cm}^{-1}$ (120 TO 400nm) AT 0.15nm RESOLUTION AND 0.05nm SPACING
- THE NEW SUSIM DATA REPLACES THE MODTRAN DATA FROM $25,000\text{cm}^{-1}$ TO $57,470\text{cm}^{-1}$ WHEN AURIC IS RUN; THE ORIGINAL DATA IS USED OTHERWISE
- THE NEW SUSIM DATA HAS NOT BEEN CONVERTED TO WAVENUMBER UNITS; RATHER THE WAVENUMBER IS CONVERTED TO VACUUM WAVELENGTH TO ACCESS THE DATA; THERE IS THEREFORE NO CORRUPTION OF THE ORIGINAL DATA BASE

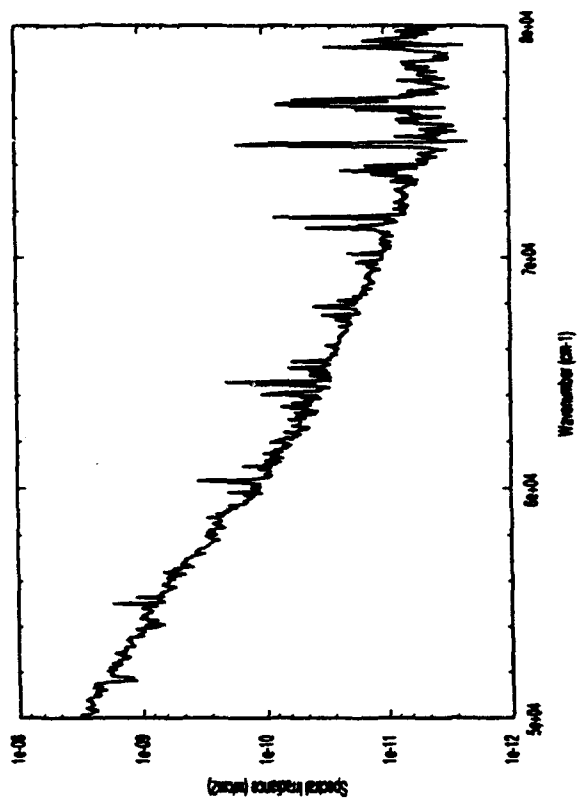


SYSTEMS



EXAMPLE AURIC SOLAR SPECTRUM

- EXTRATERRESTRIAL
SOLAR CURVE
- 125nm - 200nm



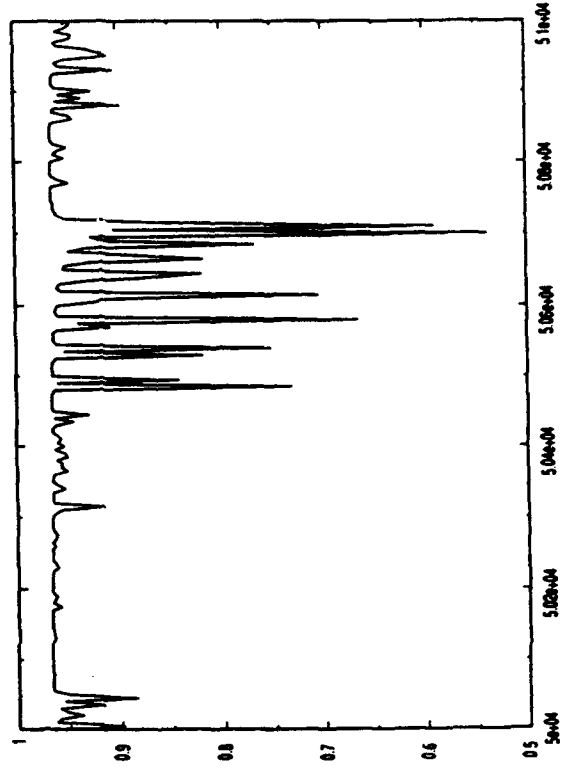
206



SYSTEMS

EXAMPLE AURIC TRANSMITTANCE SPECTRUM

SCHUMANN-RUNGE
REGION



97

SAM: SHARC AND MODTRAN MERGED

**A. Berk, D.C. Robertson, L.S. Bernstein
Spectral Sciences, Inc., 111 S. Bedford Street, Burlington, MA 01803**

**R. Sharma
Geophysics Directorate, Phillips Laboratory, Hanscom AFB, MA 01731**

An effort to merge SHARC (50-300km) and MODTRAN (0-120km) into a single, seamless, and fully correlated radiance code dubbed SAM has begun. SAM will employ a single curve-of-growth, include all MODTRAN features, and smoothly transitions into NLTE conditions as they arise above 50 km. The MODTRAN aerosol models will be incorporated into the NLTE radiance calculation, and an option to use multiple profiles for a single calculation will be made available. An equivalent width radiative transport algorithm has been developed which is applicable throughout the 0-300km altitude regime. Preliminary results will be presented.

SAM

THE SHARC AND MODTRAN CODE

PRESENTED BY

*A. BERK, D. C. ROBERTSON & L. S. BERNSTEIN
SPECTRAL SCIENCES, INCORPORATED*

R. SHARMA

PHILLIPS LABORATORY/GEOPHYSICS DIRECTORATE

PRESENTED AT

*ANNUAL REVIEW CONFERENCE ON ATMOSPHERIC MODELS
PHILLIPS LABORATORY, HANSCOM AFB*

2 JUNE 1992

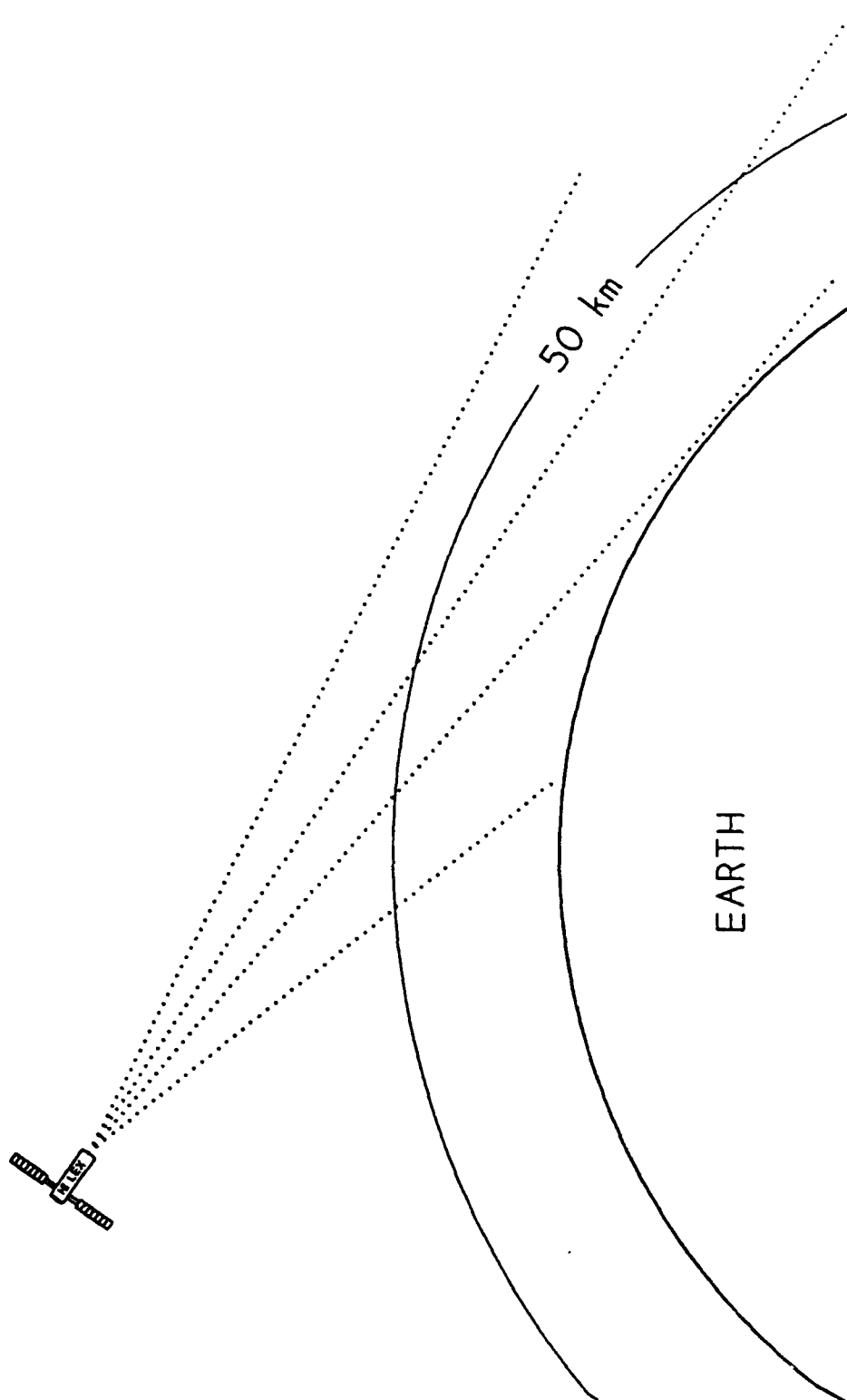


OUTLINE

- *OBJECTIVES*
- *SHARC/MODTRAN DIFFERENCES*
- *THE SAM APPROACH*
- *RESULTS*
- *CONCLUSIONS*



LIMB VIEWING



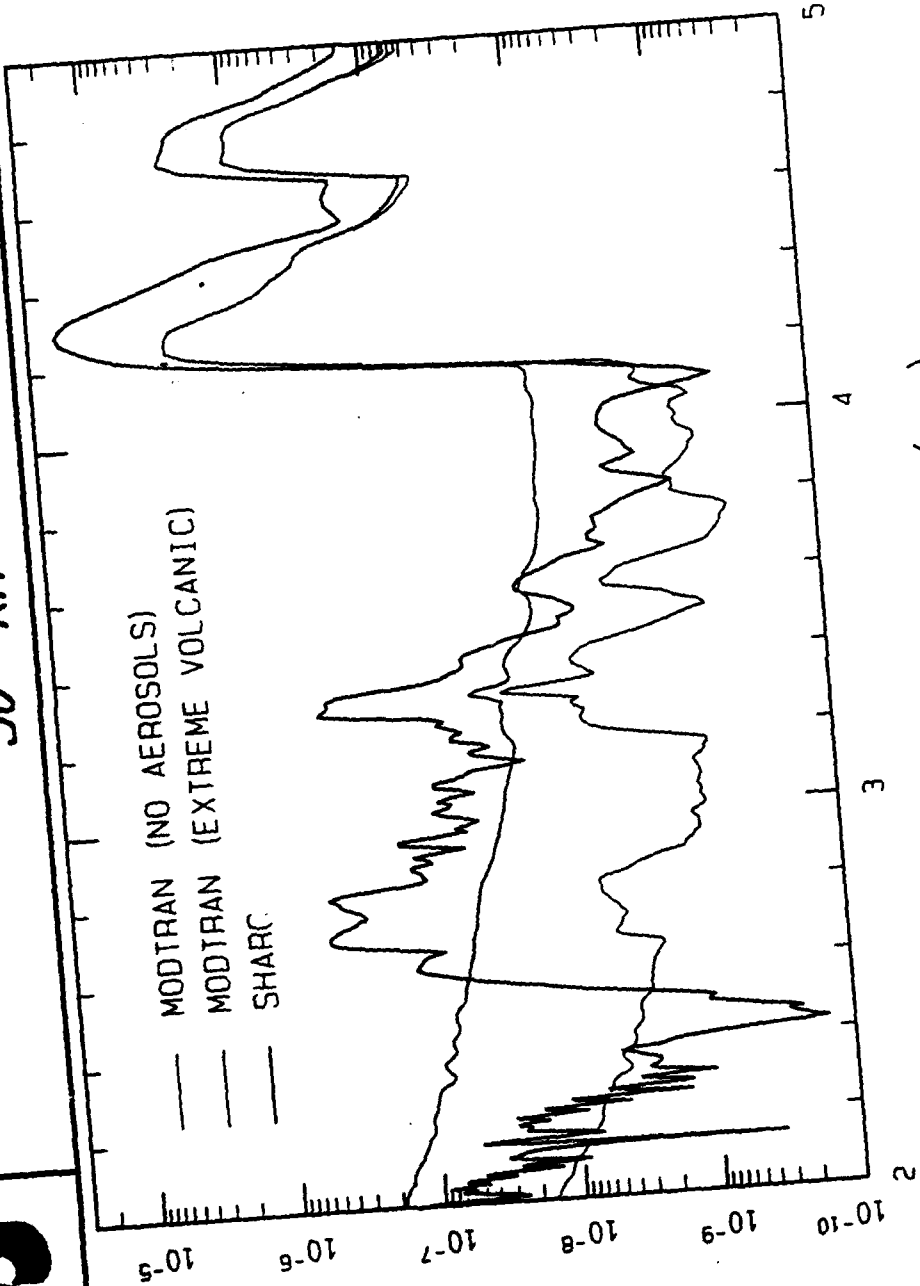


DAYTIME RADIANCE
50 KM LIMB

RADIANCE ($\text{W}/\text{CM}^{-2}/\text{SR}/\mu\text{m}$)

MODTRAN (NO AEROSOLS)
MODTRAN (EXTREME VOLCANIC)
SHARC

WAVELENGTH (μm)





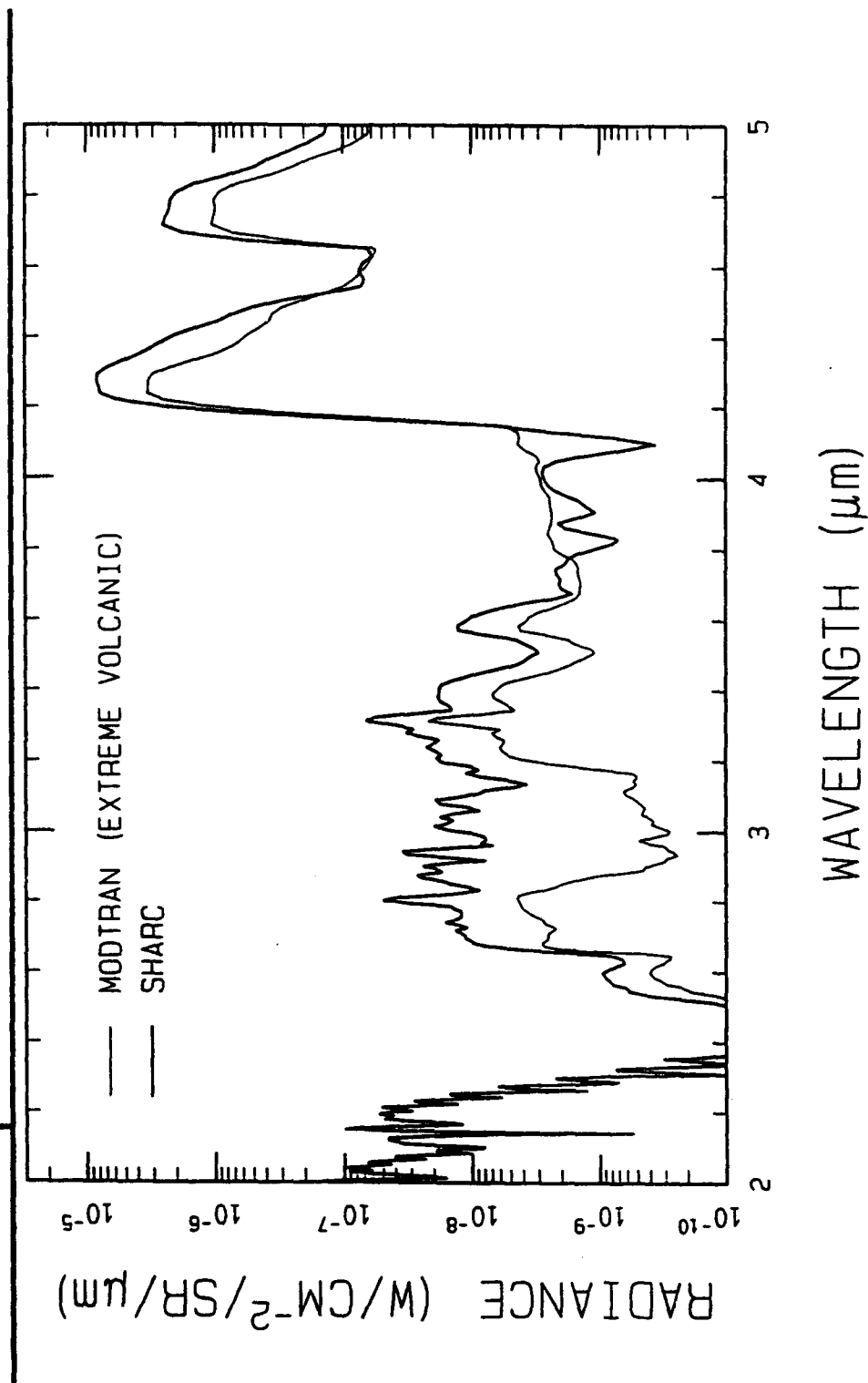
OBJECTIVES

MERGE THE HIGH ALTITUDE NLTE MODEL SHARC (50-300KM) AND THE LOW ALTITUDE LTE MODEL MODTRAN (0-120KM) INTO A SINGLE SEAMLESS RADIANCE CODE.

- EMPLOY A CORRELATED RADIANCE ALGORITHM
- INVOKE NLTE CONDITIONS ABOVE 50 KM
- INCLUDE MODTRAN FEATURES
 - AEROSOLS UP TO 100 KM
 - ARBITRARY VIEWING ANGLES
 - MULTIPLE SCATTERING
 - ETC.
- REQUIRE AGREEMENT WITH SHARC ABOVE 50 KM AND MODTRAN/FASCOD BELOW 50 KM



NIGHTTIME RADIANCE 50 KM LIMB





SHARC CAPABILITIES

STRATEGIC HIGH ALTITUDE RADIANCE CODE

- CALCULATES NLTE VIBRATIONAL EXCITATION STATE POPULATIONS
 - SOLVES CHEMICAL KINETIC MECHANISMS
 - DETERMINES REABSORBED PHOTON ENHANCEMENTS
- PREDICTS LOS SPECTRAL TRANSMITTANCES AND RADIANCES
 - EQUIVALENT WIDTH LINE-BY-LINE ALGORITHM
 - 0.1 CM⁻¹ SPECTRAL RESOLUTION
 - H₂O CO₂ O₃ CH₄ NO CO OH & NO⁺
 - 50 TO 300 KM ALTITUDE
 - 1 TO 40 MICRONS
- TREATS AMBIENT AND/OR AURORAL REGIONS



SAM APPROACH

- RADIANCE
 - EXTENDED EQUIVALENT WIDTH LINE-BY-LINE ALGORITHM FOR SHARC SPECIES
 - LINE CENTER BAND MODEL PARAMETERS FOR REMAINING SPECIES
 - LINE TAIL PARAMETERS FOR ALL SPECIES
- INTERNAL TRIANGULAR SLIT USING 1 CM^{-1} BINS
- PROFILES
 - SHARC ABOVE 50 KM
 - MODTRAN BELOW 50 KM
 - SMOOTHING BETWEEN 40 & 55 KM WHEN NECESSARY
- MODTRAN AEROSOLS
- SCATTERING
 - MODTRAN MULTIPLE SCATTERING BELOW 50 KM
 - SINGLE SCATTERING ABOVE 50 KM



SAM ARCHITECTURE

SAM DRIVER CALLS SHARC AND MODTRAN

- SHARC TASKS
 - PROBLEM DEFINITION
 - READS INPUT INTERACTIVELY W/ ERROR CHECKING
 - CREATES MODTRAN INPUT STREAM (TAPE5)
 - VIBRATIONAL EXCITATION STATE POPULATIONS
 - SOLVES CHEMICAL KINETIC MECHANISMS
 - CORRECTS POPULATIONS FOR REABSORBED PHOTONS
 - UPPER ATMOSPHERE COLUMN DENSITIES
- MODTRAN TASKS
 - LOWER ATMOSPHERE COLUMN DENSITIES
 - EMPLOYS REFRACTIVE PATH GEOMETRY
 - ALLOWS 3-D ATMOSPHERE
 - RADIANCE PREDICTIONS

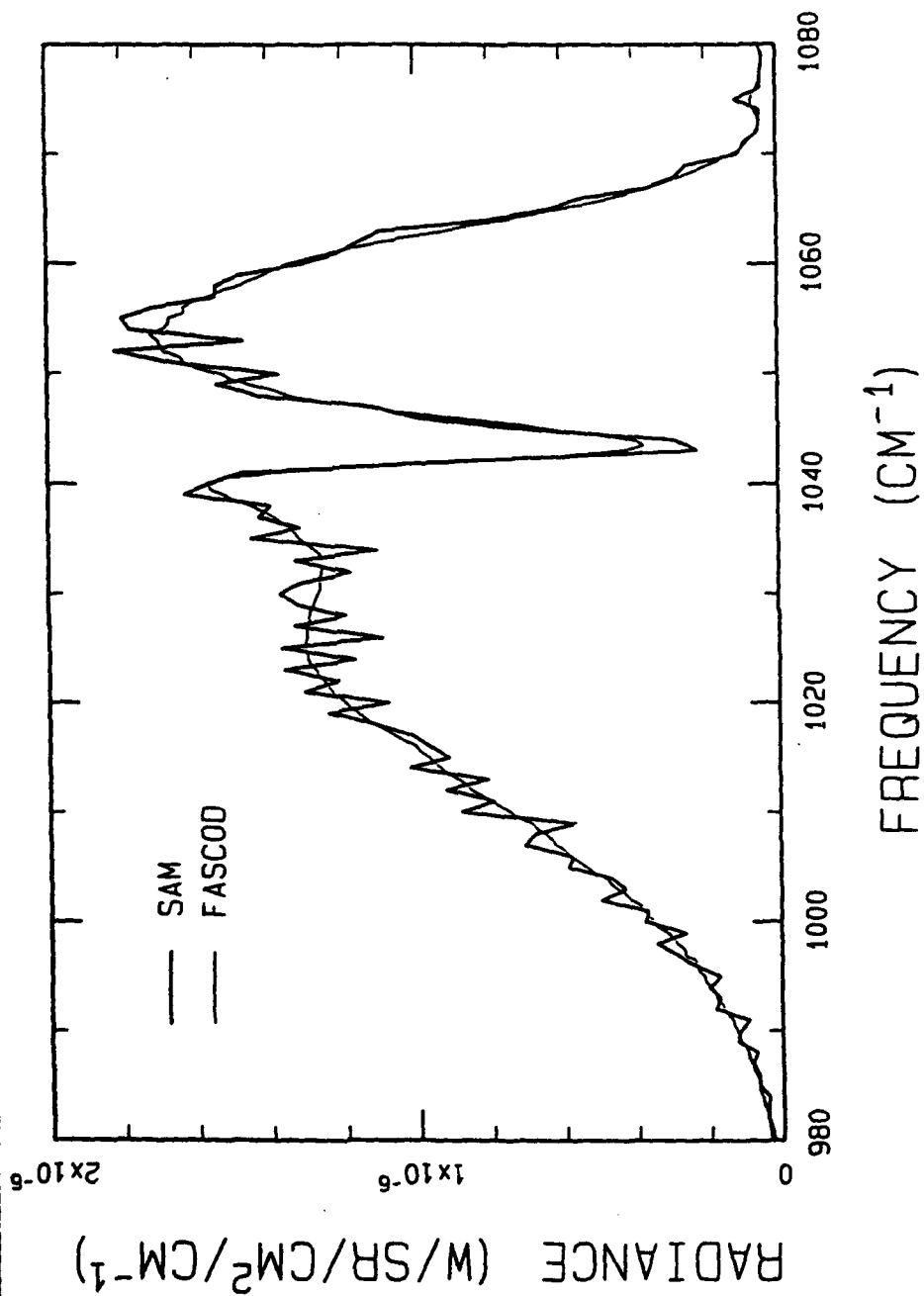


RADIATION TRANSPORT ALGORITHM

- BASED ON EQUIVALENT WIDTHS OF EACH LINE
 - RODGERS-WILLIAMS APPROXIMATION FOR VOIGT LINESHAPE
 - FAST EVALUATION OF W_D AND W_L
 - STATISTICAL APPROXIMATION FOR LINE OVERLAP (PLASS)
 - LINE TAILS MODELED USING CONTINUUM BAND MODEL PARAMETERS
- CURTIS-GODSON APPROXIMATION FOR INHOMOGENEOUS PATHS
- SOURCE TERM BASED ON POPULATION RATIOS
 - REDUCES TO PLANCK FUNCTION IN LTE LIMIT
 - OPTICAL DEPTH WEIGHTED AVERAGE IN NLTE LIMIT
- EXPLICIT USE OF LINE STRENGTHS FOR EACH INTERVAL
 - AVOIDS LINE STRENGTH DISTRIBUTION ASSUMPTION

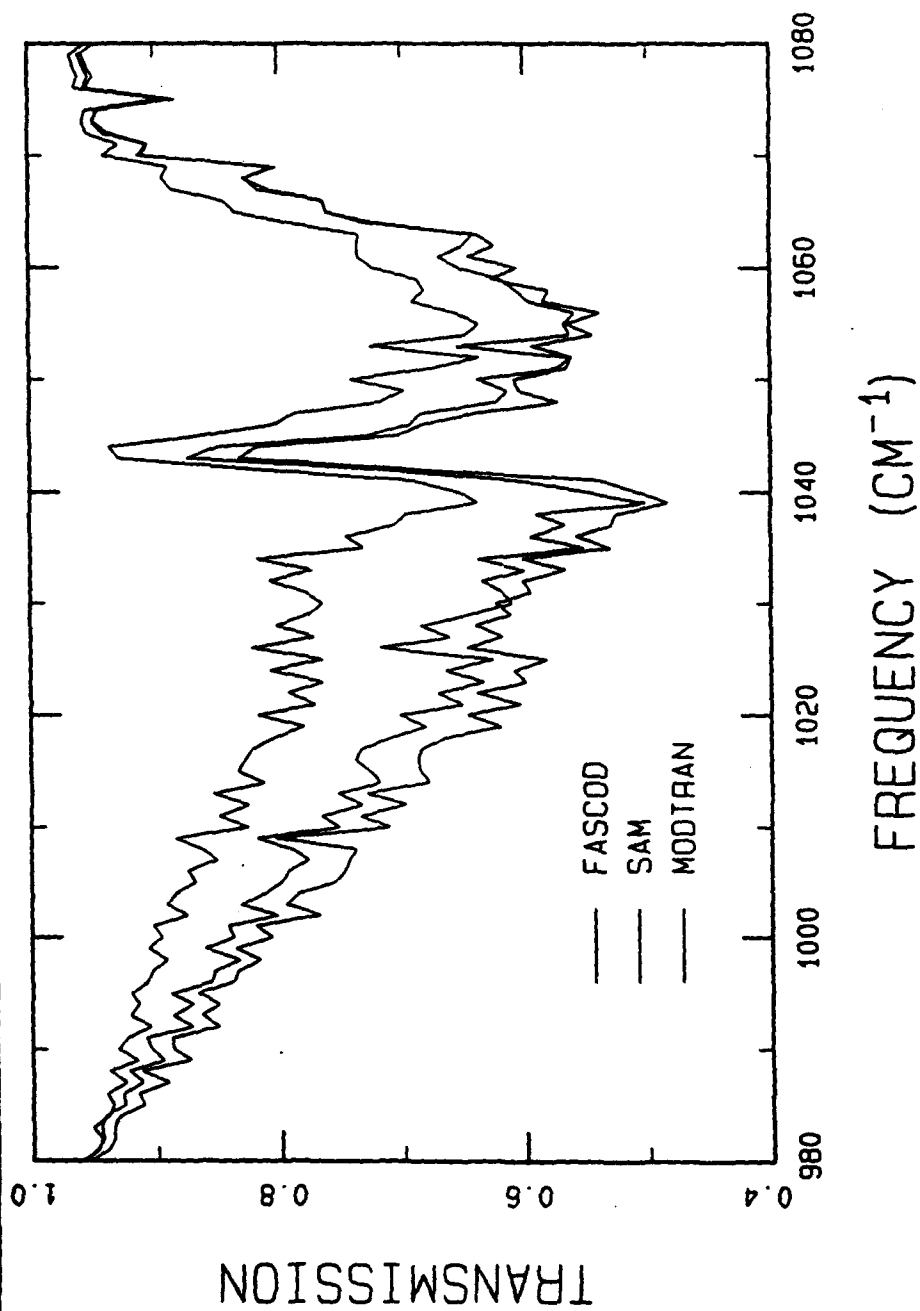


O₃ ONLY
ZENITH PATH FROM GROUND



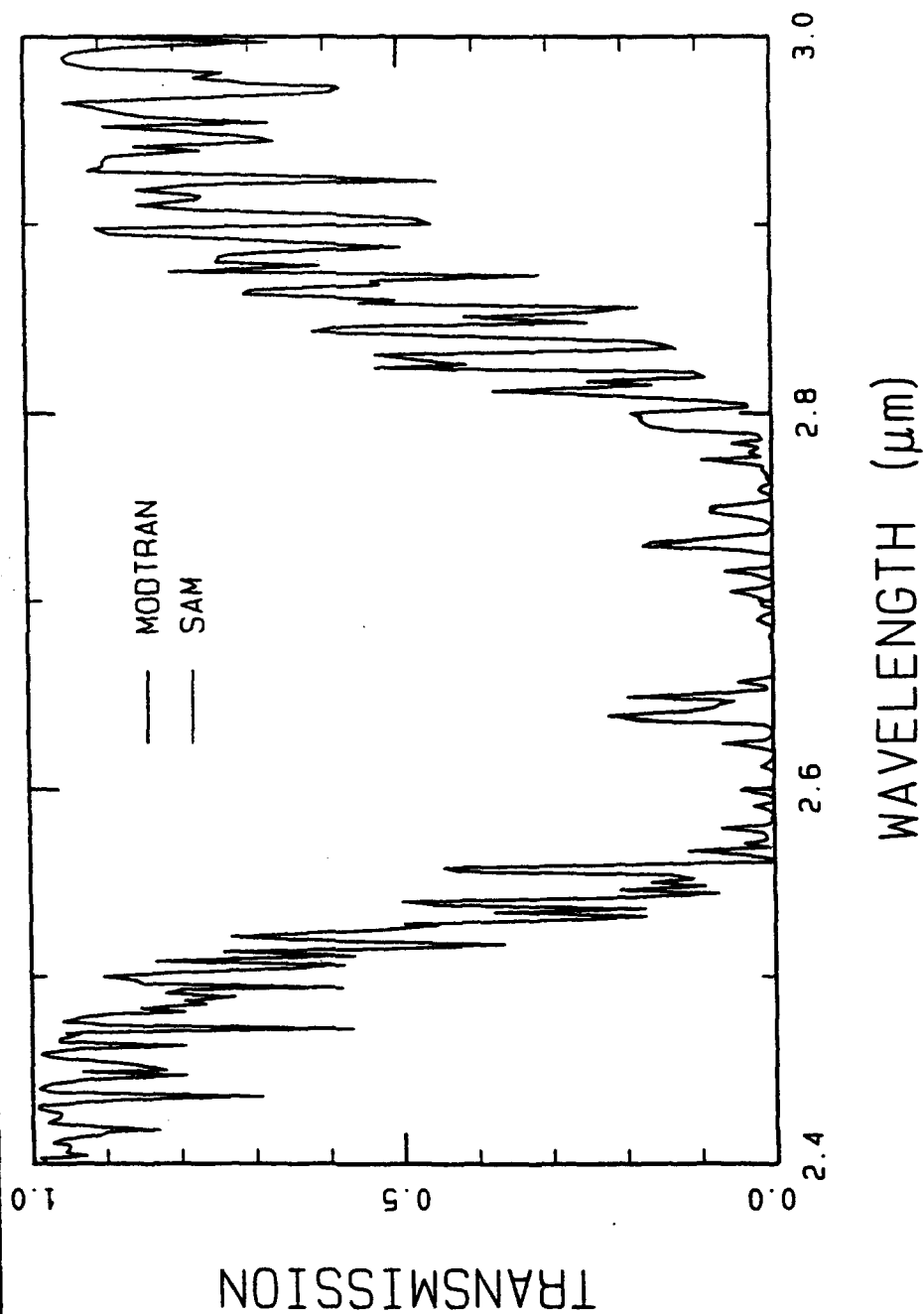


*O₃ ONLY --- 500 KM CONSTANT
PRESSURE PATH AT 40 KM ALTITUDE*



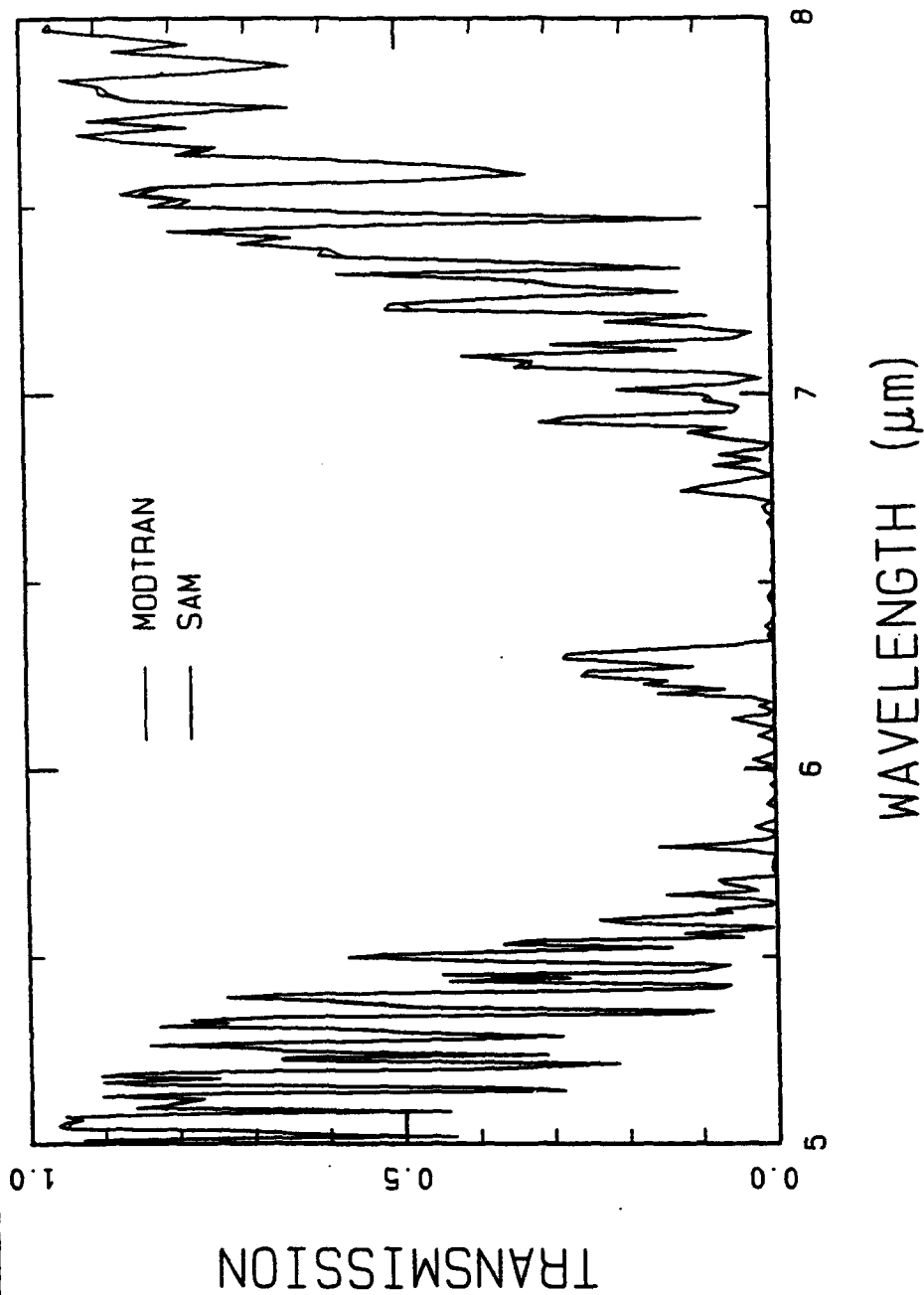


*NADIR FROM 0.1 KM
2.7 μm REGION*



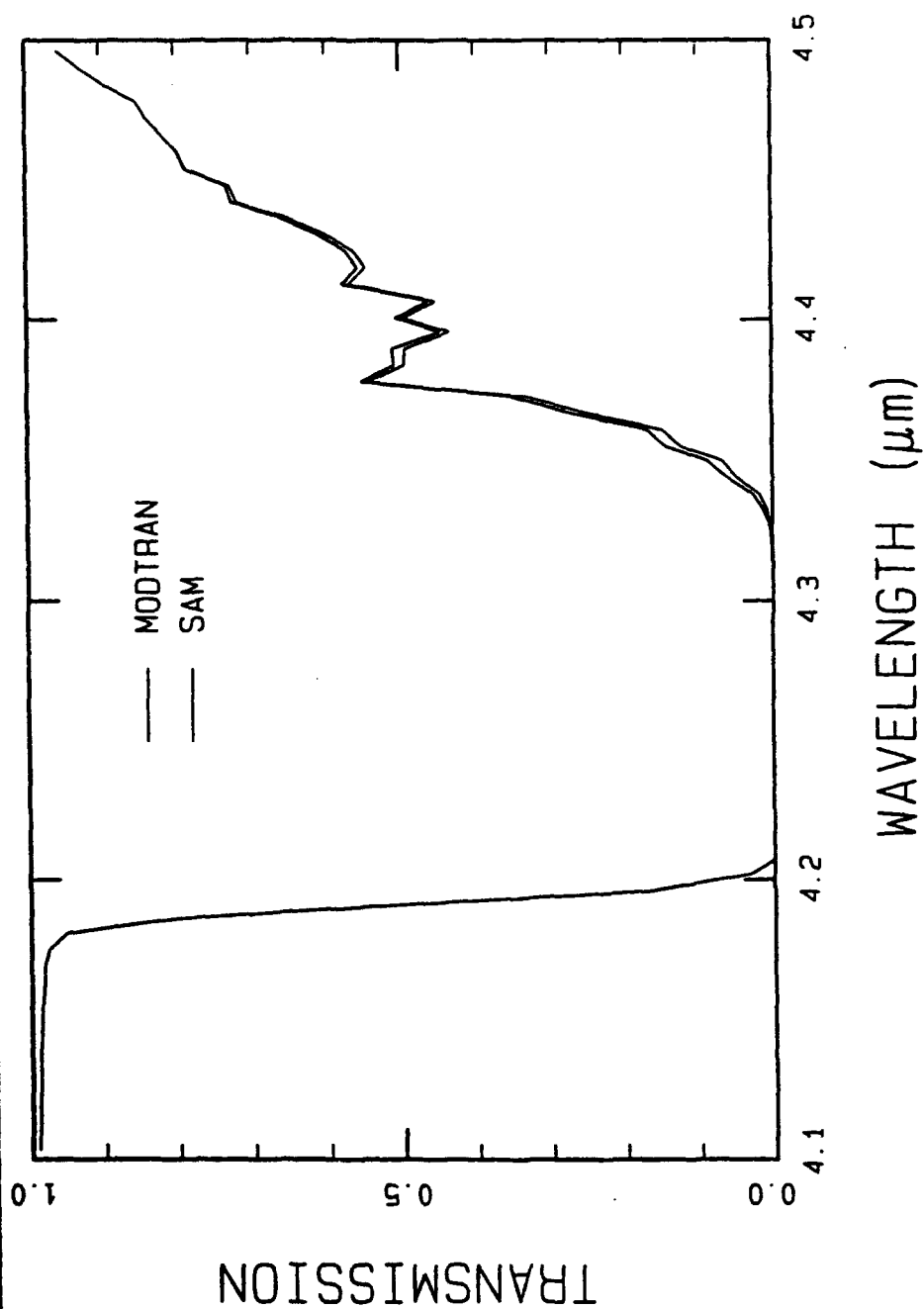


NADIR FROM 0.1 KM
6.3 μm REGION





*NADIR FROM 0.1 KM
4.3 μm REGION*





CONCLUSIONS

- SIGNIFICANT DIFFERENCES EXIST BETWEEN SHARC AND MODTRAN IN ALTITUDE REGIMES WHERE BOTH CODES ARE APPLICABLE.
- THE EQUIVALENT WIDTH LBL RADIANCE MODEL IN SHARC HAS BEEN EXTENDED TO LOW ALTITUDES
- INTEGRATION OF THIS RADIATION TRANSPORT MODEL INTO MODTRAN PRODUCES TRANSMITTANCES WHICH AGREE WITH THE ORIGINAL CODE UNDER LTE CONDITIONS.
- THE EQUIVALENT WIDTH LBL APPROACH IS APPROXIMATELY 3 TIMES SLOWER THAN MODTRAN.
- AN INITIAL VERSION OF SAM IS SCHEDULED FOR DELIVERY TO PHILLIPS LABORATORY IN EARLY 1993.

SMART MODEL FOR ATMOSPHERIC AND ASTRONOMICAL RADIANCE AND TRANSMITTANCE (SMAART)

S.B. Downer, J.P. Kennealy, P.C.F. Ip
Mission Research Corporation, One Tara Blvd, Suite 302, Nashua, NH 03062

F.O. Clark
Geophysics Directorate, Phillips Laboratory, Hanscom AFB, MA 01731

Dramatic changes are occurring in defense, requiring easily accessible background radiance descriptors for downward looking, TMD, and GPALS scenarios. A knowledge-based solution is offered which fills these needs by combining the equilibrium lower atmosphere model and non-equilibrium upper atmosphere model into a unified seamless single answer, SMAART.

SMAART includes an easily accessible guide for users in both the proper selections of the codes and their execution. It implements a single interface to models with rapid response validated data bases to permit rapid exploration of parameter space, based on DoD/SDIO Standard codes. SMAART will also contain DoD Celestial Models, and runtime capabilities for MODTRAN, SHARC and other PL Atmospheric Models. Accompanying this intelligent front end is an extensive set of data analysis tools that will allow users to readily examine and compare results for any of the SMAART modeling codes. Present and future capabilities are presented along with a demonstration of the first prototype, SMAART Version 0.5.

SMAART



Smart Model for Atmospheric and Astronomical Radiance and Transmission

*S.B. Downer, J.P. Kennealy, P.C.F. Ip
R.M. Flanders, M. A. Noah and K.J. Radermacher
Mission Research Corp., One Tara Blvd., Nashua , NH 03062*

*F.O. Clark
Geophysics Directorate, Phillips Laboratory, Hanscom AFB, MA 01731*



SMART Objectives



- Provide a Single User Interface to DOD/SDIO Standard PI Codes
- Supply Integrated Solutions Across LTE/NLTE Regimes
- Assist a Diverse User Base to Accurately Set-Up Problems
- Allow Quick Access to a Data Base of Pre-Calculated Results
- Supply Extensive Set of Data Analysis Tools to Review Results

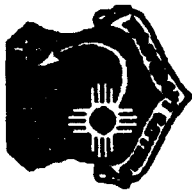




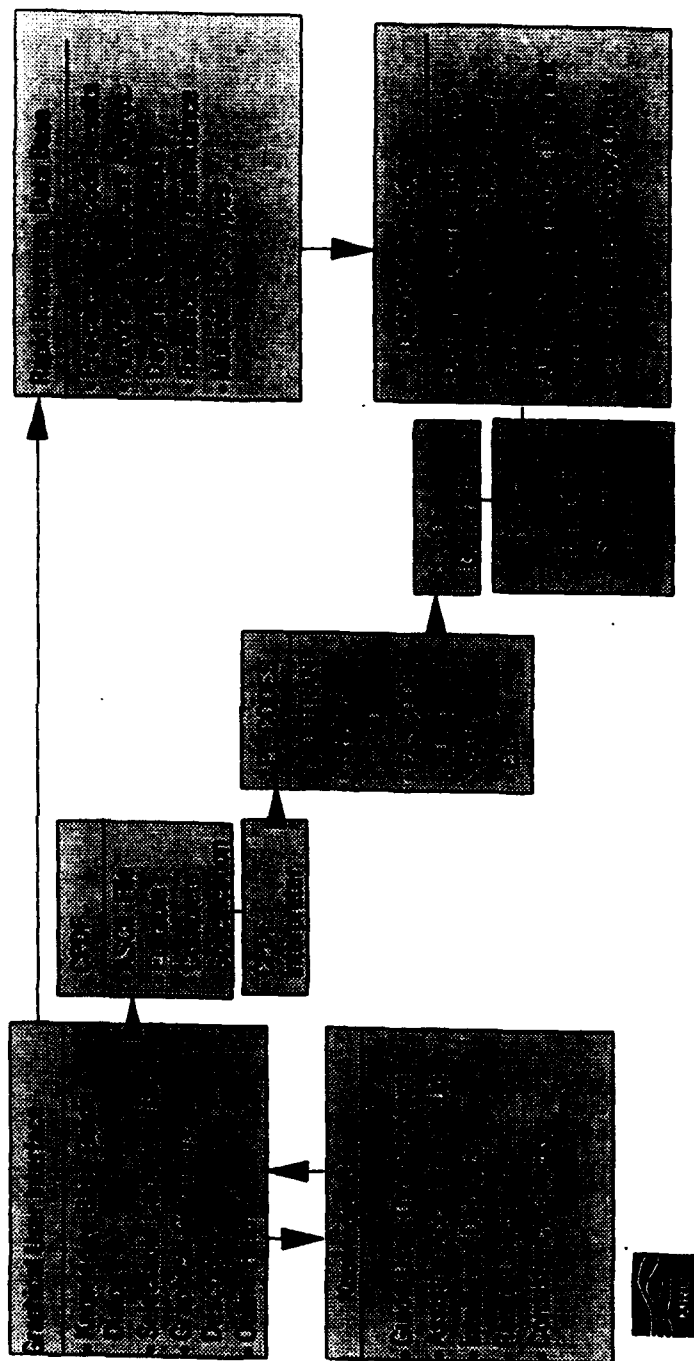
SMAART Overview

- Written in FORTRAN and C/C++
- Targeted at 386/486 Systems & Windows 3.0 or Higher
- Secondary Target UNIX Workstations & X-Windows
- Exploits Multi-Tasking Environment
- Online Hyper-Text Help
- Versatile User-Selectable Installation Package
- Extensive Graphics and Scene Imaging Capabilities





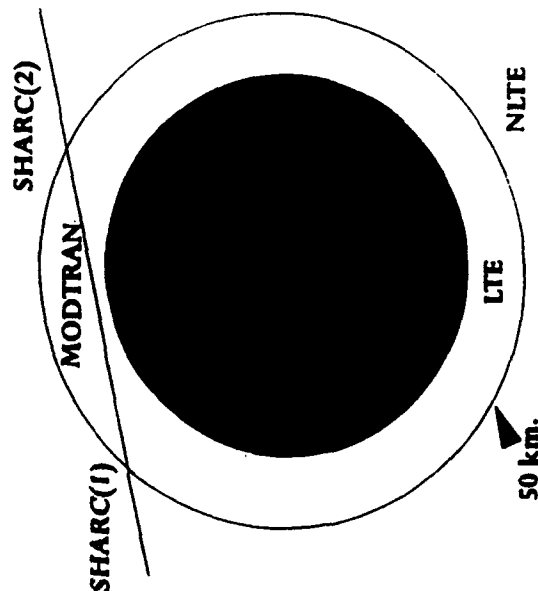
SMAART Architecture





The FAUST Method

- Developed By Harold Gardiner (PL)
- Seamless Integration LTE/NLTE Regimes
- Linear Approximation
 - Total Transmittance is Product of the Transmission for the Three Regions
 - SHARC(1) Propagate thru MODTRAN
 - SHARC & MODTRAN Propagated thru SHARC(2)
- Used in FAUST and SMAART *Rapid Response* Data Bases
- Data Base Validated by PL Scientists

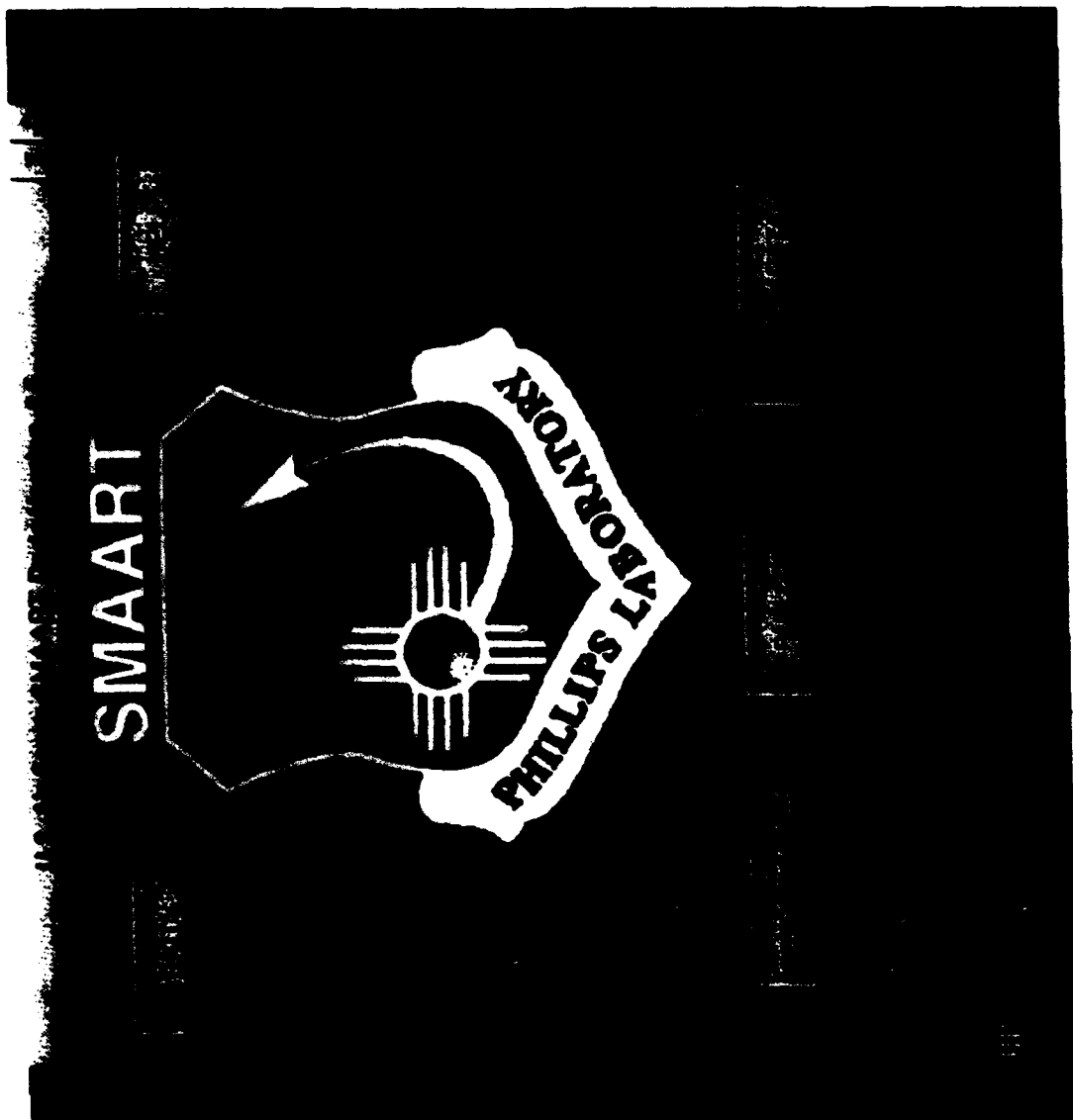


SMAART Version 0.5 Prototype



- To Be Released to Selected PL Personnel June 1992
- Runs under MS Windows 3.0 or Higher
- Supports the Following Codes
 - MODTRAN April 1992 Version
 - LOWTRAN-7 Option from MODTRAN
 - Rapid Response Data Base (FAUST)
 - CBSD Celestial Codes
- Data Analysis Tools for Examining Output
 - Displays Multiple Spectra on a Single Plot for Comparison
 - Graphically Interactive Area-of-Interest Definition
 - Provides Intensity Information at any User-Specified Point
 - Provides Integrated Intensities Over User-Defined Bands
 - Interactive Image Display





Files

File Edit Bookmark Help

Modtran Input Parameter - ITYPE

Type of Atmospheric Path

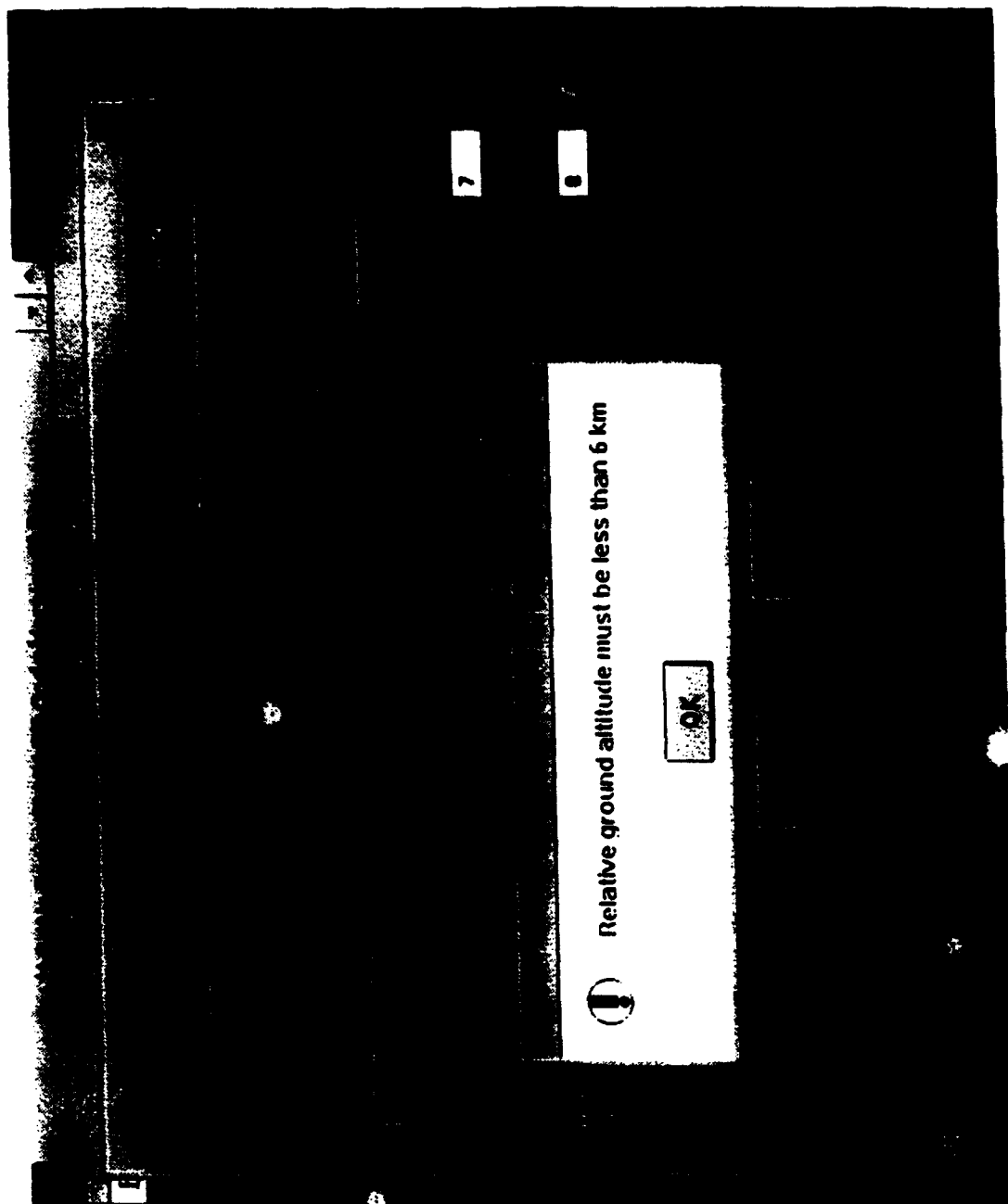
- 1=Horizontal (constant pressure) Path, read H1, RANGE
- 2=Vertical or Slant Path between two Altitudes, read H1, H2, ANGLE or H1, H2, RANGE or H1, H2, RETA, or H1, ANGLE, RANGE
- 3=Vertical or Slant Path to Space, read H1, ANGLE or H1, H2

Long and Pressure (H1)

H20 (H2)

H1 (H1)

Q10 (H4)



U.S. Air Force SMAART Cards Version 0.5

MODTRAN Input Screen 1

MODTRAN Input Screen 2

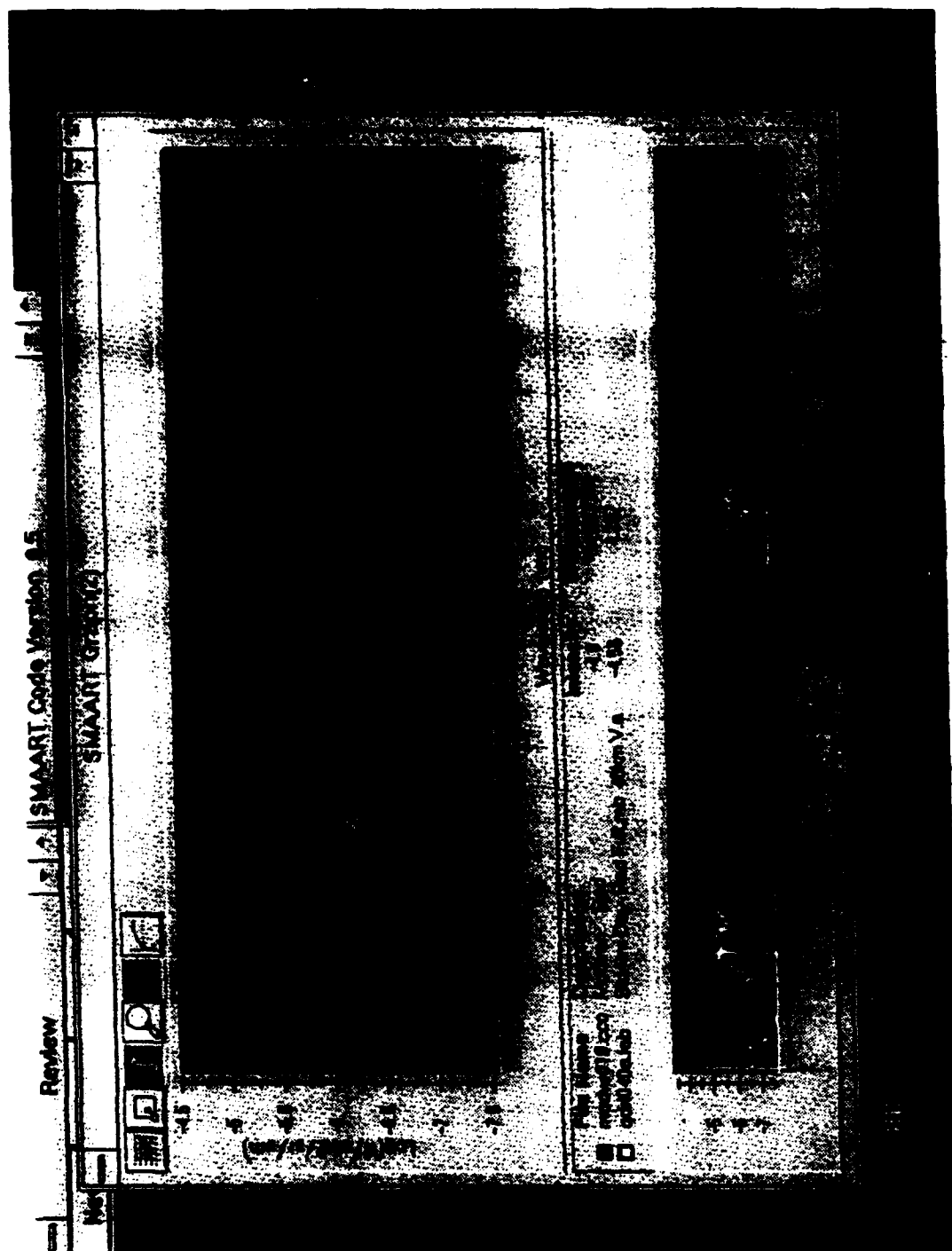
MODTRAN Input Screen 3

50

50

93.198

6371.23



SMAART FUTURE PLANS



- SMAART Version 0.9 Planned Release Fall 1992
 - Support SHARC Code and FAUST Method
 - Knowledge Base Implemented
- SMAART Version 1.0 Planned General Release Early 1993
 - Future Versions
 - X-Window Versions
 - Support FASCODE, SAM, AURIC
 - Graphical Geometry Descriptor
 - Addition of New PL codes as They Become Available
 - More Extensive Rapid Response Data Base
 - CD ROM Release
 - More Extensive Data Analysis Tools



ONCORE: THE ONTAR IMPLEMENTATION OF LOWTRAN 7

J. Schroeder

Ontar Corporation, 129 University Road, Brookline, MA 02146

Oncore [tm] is a user-friendly implementation of the Phillips Laboratory/ Geophysics Directorate's LOWTRAN 7 atmospheric transmission and radiance model. The software will operate on IBM (or compatible) personal computers in the MS-DOS environment, or the workstation UNIX environment.

The oncore package includes software for selecting inputs - with on-line help, viewing results on the computer screen, and producing hard copy outputs. Additional features include utilities for exporting compatible files for many word processing and desk top publishing packages.

This presentation will demonstrate the oncore software, and discuss sample calculations.

**ONCORE [c]: An implementation of the PL/GP's
LOWTRAN 7 Model for the Personal Computer**

**ANNUAL REVIEW CONFERENCE ON
ATMOSPHERIC TRANSMISSION MODELS**

129

PL/GP Hanscom AFB, MA

2-3 June 1992

**Ontar Corporation
129 University Road
Brookline, MA 02146-4532
Tel: 617-739-6607 FAX: 617-277-2374**



Cooperative R & D Agreement

With Geophysics Laboratory - Hanscom AFB, MA

September 1988

PC Implementation of a Software Package - LOWTRAN 7 - PCTTRAN 7 [c]



PCTRAN 7 [c] * Version 2a

PC Version of the PL/GP LOWTRAN 7 Atmospheric Radiance & Transmission Code

Complete Implementation of the LOWTRAN 7 Code

Installation Program.

Interactive User Input Software.

Help Screens for All Input Variables.

Screen and Hard Copy Graphics Output.

Tabular Output in ASCII Format.

Batch Processing Input Software.

Plotting from Different LOWTRAN Calculations.

Expert Help.

CERTIFIED for ACCURACY by the GEOPHYSICS DIRECTORATE.



Hardware and Software Requirements

Personal Computer - XT, AT, 80386, 80486 (Compatible, Clone)

1.2 Mbyte Diskette Drive, Hard Disk

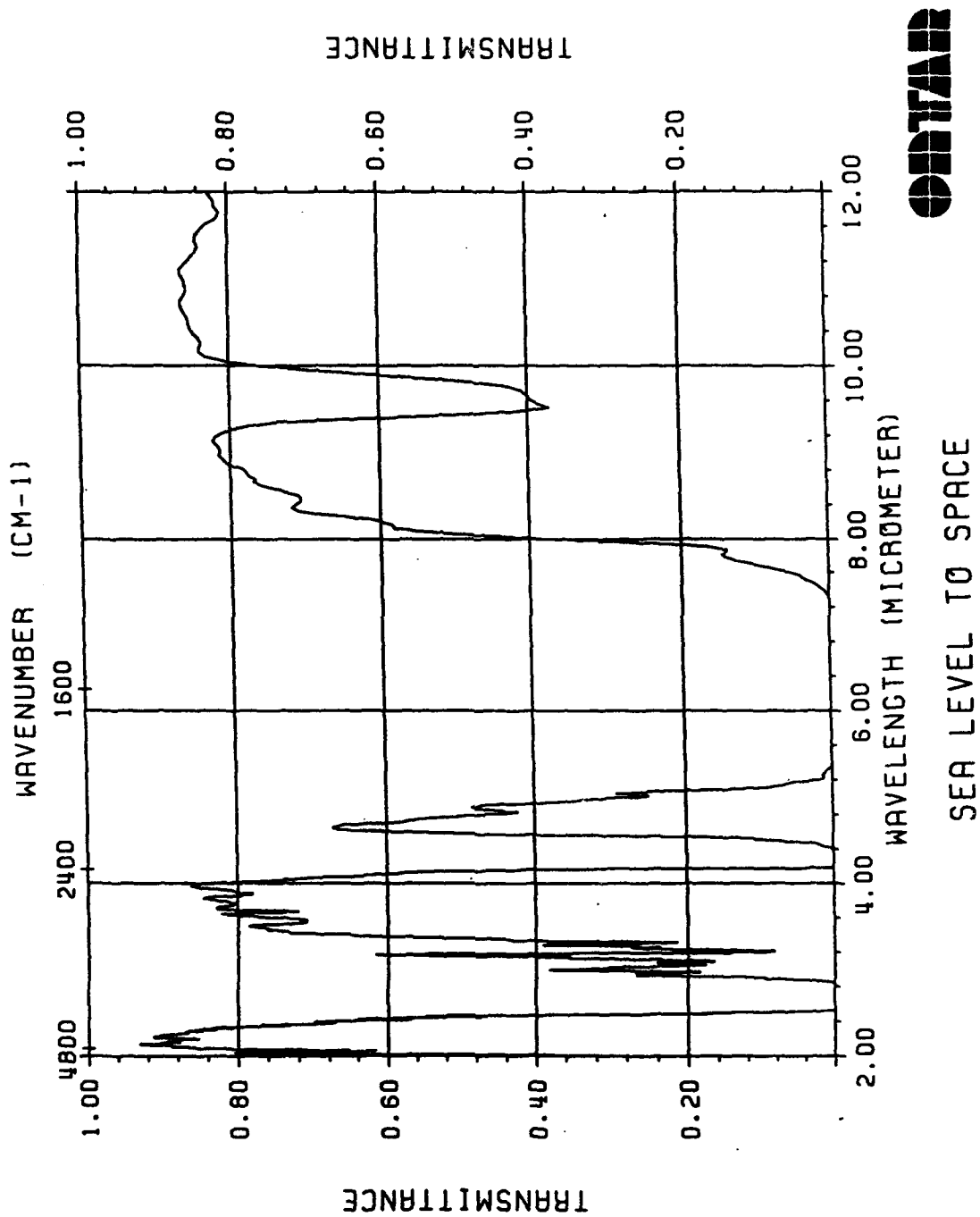
640 Kbytes of Memory

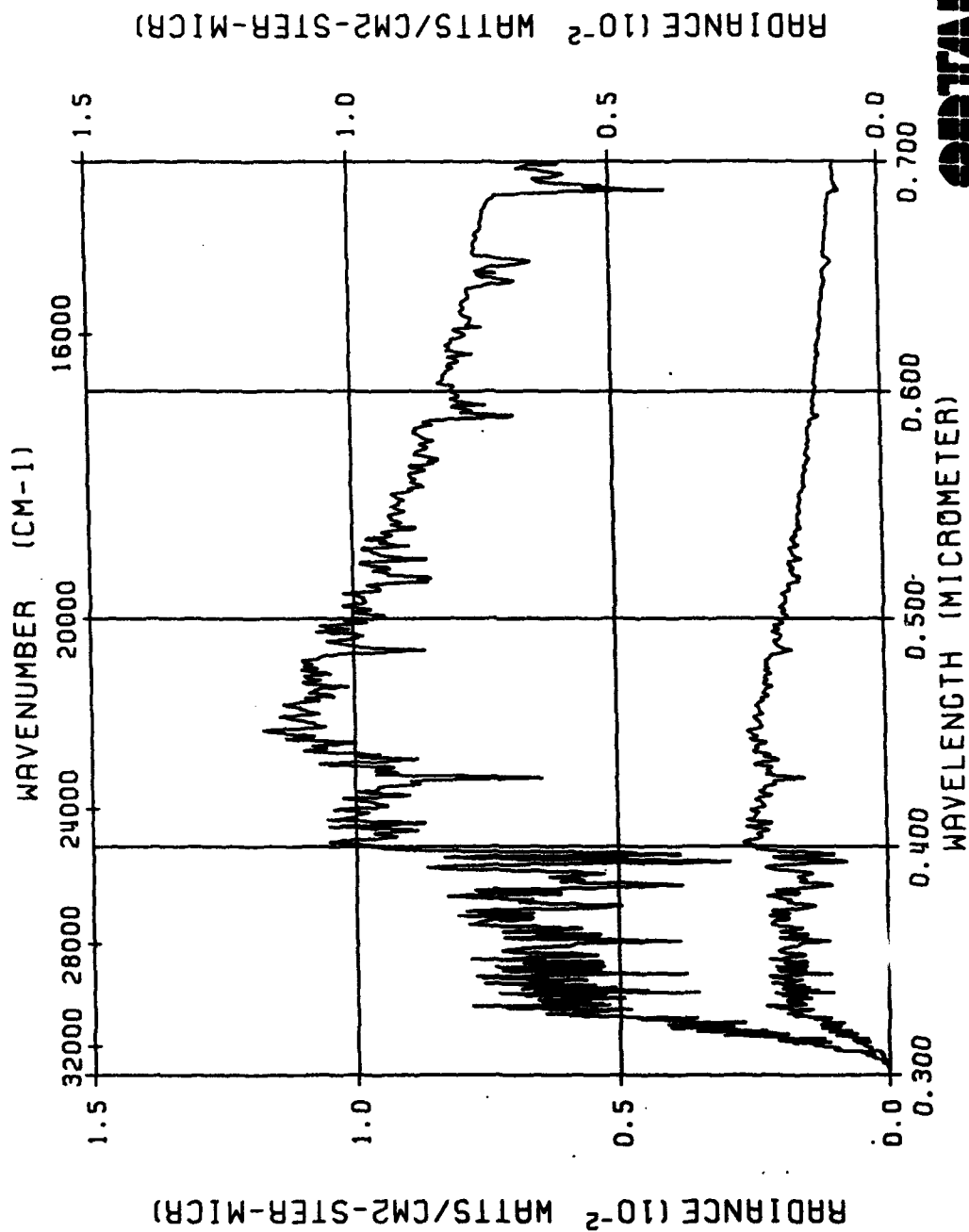
CGA, EGA, or VGA Graphics Board and Monitor - for Screen Plots

Printer - for Hard Copy

Numeric Co-processor Highly Recommended

CONTINUED





CONTINUED

MULTIPLE AND SINGLE SCATTERED SOLAR RAD

Setup Program

Semi-automatic Installation Procedure.

Copies all files to target drive.

Sets up Printer Support.

Defines Graphics Adapter Type.

Capable of Printer ONLY Installation.

Checks Available Disk Space.

ONTAR Corporation, 129 University Road, Brookline, MA 02146, 617-739-6607

ONTAR

PC-TRAN7 Batch Mode Manager.

ESC -	Quit LOWIN (write LOWIN and LOWPLT.DAT)
F2 -	Edit current run.
F3 -	Edit next run.
F4 -	Edit previous run.
F5 -	Add new run (to end) and go to that run
F6 -	Delete current run.
F7 -	Go to run.

Database name MCASE3

Number of runs in this database 4 Current run 3

LOWTRAN7

Card 5

LOWTRAN7

Multiple Run Plotting Inputs

Filename	Run	Plot Mode	Title
CASE-A	1	Transmittance	1976 U S STANDARD
CASE-A	2	Transmittance	SUBARCTIC WINTER
CASE-A	3	Radiance /w Scattering	SUBARCTIC SUMMER
CASE-A	4	Radiance	MIDLATITUDE SUMMER
CASE-B	1	Transmittance	1976 U S STANDARD
CASE-B	2	Radiance	TROPICAL MODEL
CASE-B	3	Radiance /w Scattering	MIDLATITUDE SUMMER
CASE-B	4	Transmittance	SUBARCTIC SUMMER
CASE-C	1	Transmittance	1976 U S STANDARD
CASE-C	2	Radiance	TROPICAL MODEL
CASE-C	3	Radiance /w Scattering	New Model Atmosphere
CASE-C	4	Transmittance	Met Data (Hor Path)

LOWMPIN Select Runs

LOWMPIN

PCTRAN7 Expert Help

Online Expert Help.

Guides you through common user problems.

Draws on over 5 years of PCTRAN user support.

Aides in selecting Appropriate Model:

**LOWTRAN7
MODTRAN
SENTRAN
FASCODE**

Helps in model parameter selection/setup.

PCTRAN7

LITERATURE AVAILABLE

SOFTWARE DEMONSTRATION

Ontar Corporation

129 University Road

Brookline, MA 02146 - 4532

Tel: 617-739-6607 FAX: 617-277-2374 Bulletin Board: 617-277-6299

ONTAR

**MICROWAVE REFRACTIVE PATH CALCULATIONS FOR THE PHILLIPS
LABORATORY (GL) RADTRAN ATTENUATION/TRANSMITTANCE/
CE/BRIGHTNESS TEMPERATURE COMPUTER CODE**

R.G. Isaacs, W.O. Gallery, R.D. Worsham
Atmospheric and Environmental Research, Inc., 840 Memorial Drive, Cambridge, MA 02139

V.J. Falcone
Geophysics Directorate, Phillips Laboratory, Hanscom AFB, MA 01731

The RADTRAN computer code was developed by the Air Force Geophysics Laboratory (GL) to provide atmospheric attenuation and brightness temperature calculations for typical atmospheric paths over the frequency range from 1 to 300 GHz (Falcone et al., 1982). The atmospheric attenuation submodels of the clear atmosphere, fog, cloud, and rain used in RADTRAN have been thoroughly documented (Falcone et al., 1979). The enhanced RADTRAN is described in Isaacs et al. (1989). In addition to calculation of attenuation, transmittance, and brightness temperature, this version treats surface emissivity (Isaacs et al., 1988), scattering properties of precipitation (Isaacs et al., 1987), and multiple scattering (Jin and Isaacs, 1987).

In this paper we describe an additional enhancement to include the curved earth and refraction in the determination of path properties. The atmospheric ray trace algorithm is based on the PL Optical Physics Division FSCASTM program (Gallery et al., 1983) which calculates the integrated absorber amounts for FASCODE. This algorithm has been adapted to the microwave region and is used to calculate the path absorber amounts for the attenuation and transmittance modes of RADTRAN. Applications to high incidence angle viewing will be discussed.



ANNUAL REVIEW CONFERENCE ON ATMOSPHERIC TRANSMISSION MODELS

**MICROWAVE REFRACTIVE PATH CALCULATIONS FOR
THE PHILLIPS LABORATORY RADTRAN
ATTENUATION/TRANSMITTANCE/BRIGHTNESS
TEMPERATURE COMPUTER CODE**

141

R. G. Isaacs (1), W. O. Gallery (1), R. D. Worsham (1), and V. J. Falcone (2)

*(1) Atmospheric and Environmental Research, Inc. (AER), Cambridge, MA
02139*

*(2) Phillips Laboratory / Geophysics Directorate (GPAS), Hanscom AFB, MA
01731*



The RADTRAN Computer Code

- Computes atmospheric attenuation and brightness temperature over the frequency range from 1-300 GHz
- Atmospheric attenuation submodels treat the clear atmosphere, fog, cloud and precipitation
- Gas absorption modules employ line-by-line treatment of oxygen and water vapor and a semi-empirical fit for the water vapor continuum
- fog, cloud, and precipitation attenuation properties (1-1000 GHz)
- References:
 - Falcone et al, 1979 {AFGL-TR-79-0253}
 - Falcone et al, 1982 {Proc. Soc. Photo. Opt. Instrum. Eng., 337, 62-66}
 - Isaacs et al, 1989 {GL-TR-89-0188}



Recent RADTRAN Enhancements

- Multiple scattering in the presence of precipitation for inhomogeneous, anisothermal paths {Jin and Isaacs, 1987, *JQSRT*, 37, 5, 461-469}
- Scattering properties of precipitation (extinction, single scattering albedo, phase function) {Isaacs et al., 1988, *Appl. Opt.*, 27, 14-16}
- Deterministic surface emissivity submodels {Isaacs et al., 1989, *IEEE Trans. Geosci. Remote Sensing*, 27, 4, 433-440}
- Spherical Refractive Geometry, same as in LOWTRAN and FASCODE {Gallery et al., 1983, AFGL-TR-83-0065}

der

Refraction Calculation

Snell's law for a spherical symmetric medium

$$\tilde{m} \sin \theta R(z) = \text{const}$$

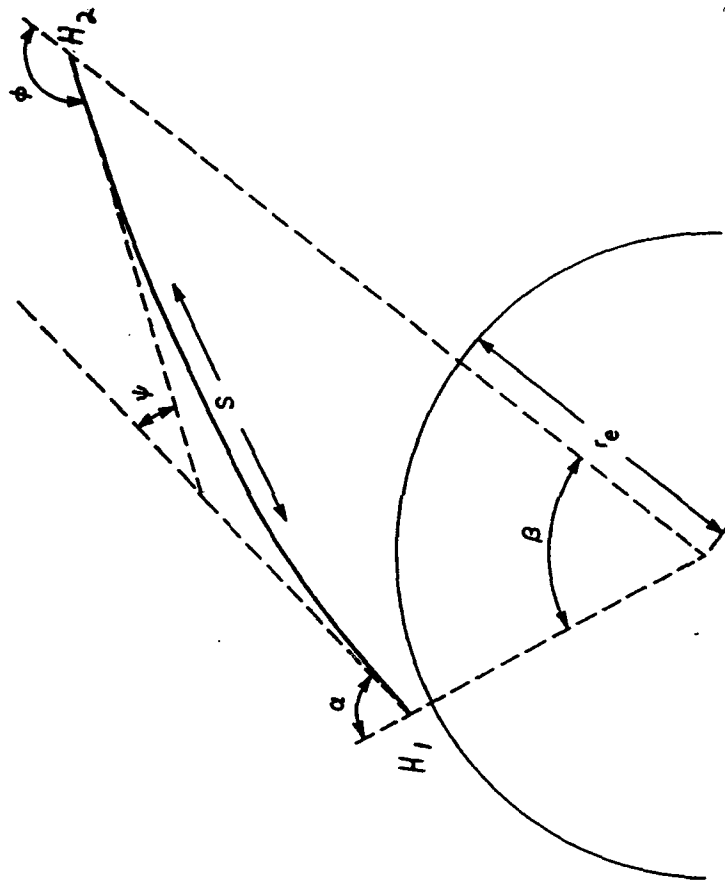
Index of Refraction $\tilde{m}(z)$

$$[\tilde{m}(z) - 1.0] \times 10^6 = 77.6 \frac{P}{T} + 3.73 \times 10^5 \frac{P_{H_2O}}{T^2}$$

Where P = pressure (mb)

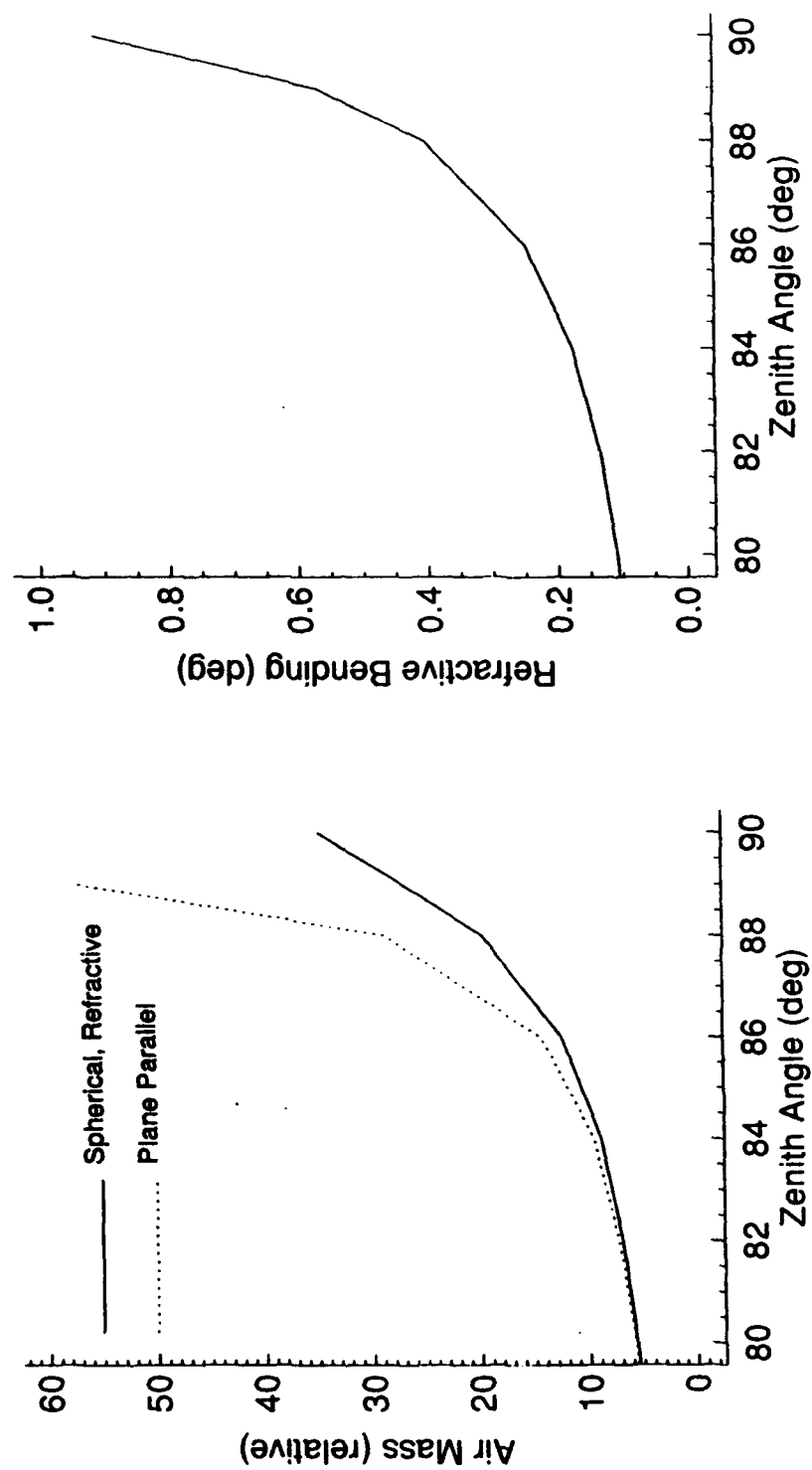
T = temperature (K)

P_{H_2O} = partial pressure of water vapor (mb)



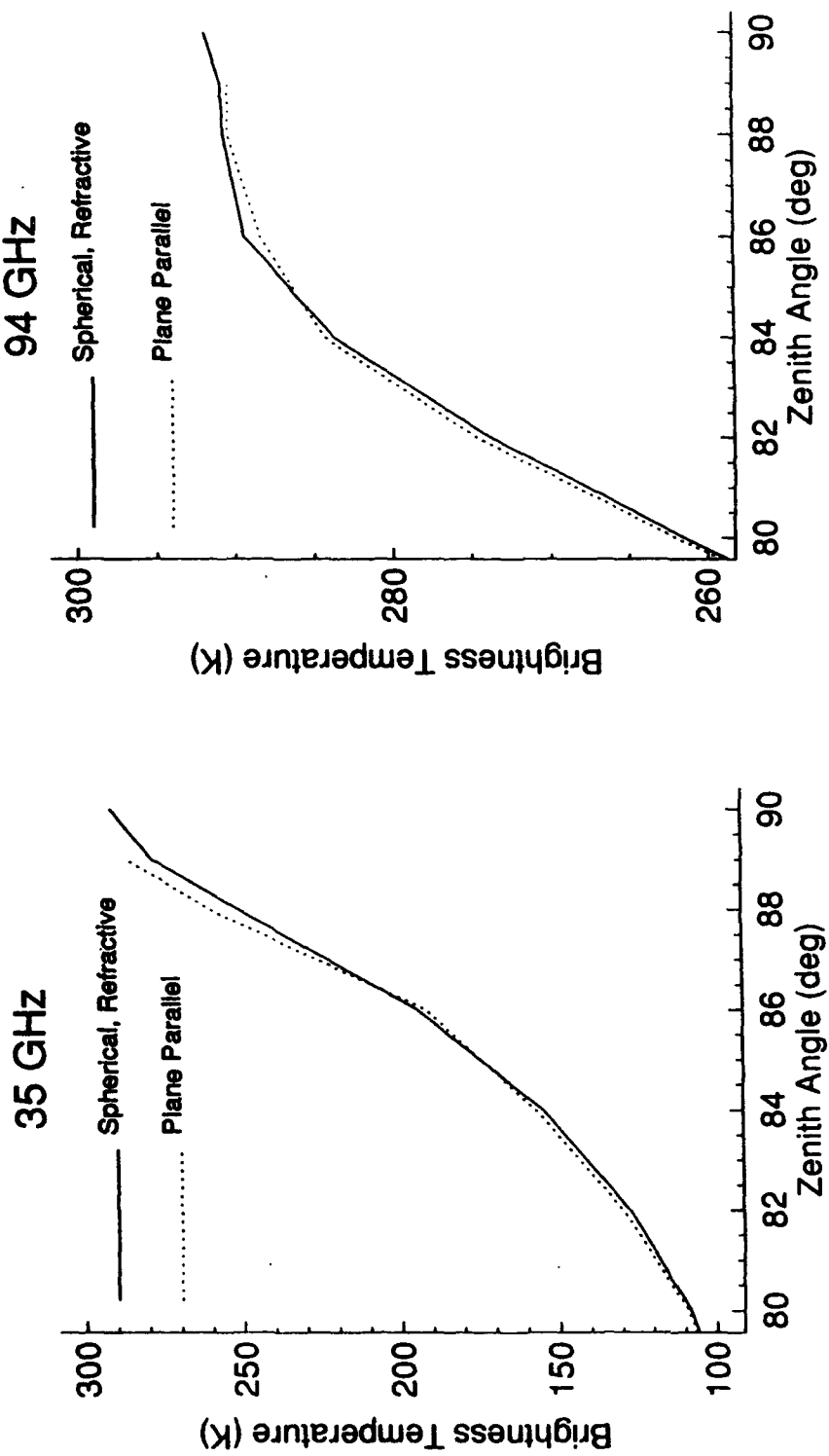
QER

Refraction Effects, Sensor at Ground



QER

Refraction Effects, Sensor at Ground (cont)



der

Conclusions

- The capability to treat refraction and spherical geometry in the computation of attenuation within RADTRAN has been accomplished;
- The approach is consistent with the microwave brightness temperature calculation allowing refracted path brightness temperatures to be evaluated;
- The algorithm does not treat extreme refractive bending such as ducting, miraging and blooming.
- The algorithm cannot include multiple scattering with spherical refractive geometry.

ATMOSPHERIC TRANSMISSION MODELS FOR PASSIVE MILLIMETER WAVE TARGET SIGNATURE SIMULATION

W.T. Kreiss

Horizons Technology, Inc., 9390 Ruffin Road, San Diego, CA 92123-1826

R.S. Dummer

R.S. Dummer and Associates, Inc., San Diego, CA 92131

Passive Millimeter Wave (MMW) sensors have been seen as an adjunct to VISEO sensors for multi-spectral surveillance, target detection, and tracking for several decades due to their superior obscurant penetrating capability. The "antenna problem" has been the main deterrent in their successful application. Current work on sensor front-end design, and on improved signal processing algorithms, are keeping the promise of combined MMW/VISEO systems alive. However, a number of problems associated with MMW atmospheric transmission and radiance modeling still remain to be resolved. For this reason several existing MMW transmission/radiance models, including LOWTRAN 7, have been examined to assess their capabilities for addressing these problems. This presentation will describe targeting scenarios, problems associated with atmospheric structure and composition, and the ability of several MMW transmission/radiance models to meet the requirements of aerial targeting applications.



**ATMOSPHERIC TRANSMISSION MODELS FOR
PASSIVE MILLIMETER WAVE TARGET SIGNATURE SIMULATION**

PRESENTED BY

**WILLIAM T. KREISS
HORIZONS TECHNOLOGY
3990 RUFFIN ROAD, SAN DIEGO, CA 92123-1826**

AND

**RICHARD S. DUMMER
R.S. DUMMER AND ASSOCIATES
9929 HIBERT STREET, SAN DIEGO, CA 92131**

AT

**THE ANNUAL REVIEW CONFERENCE ON ATMOSPHERIC TRANSMISSION MODELS
GEOPHYSICS DIRECTORATE, PHILLIPS LABORATORY
SCIENCE CENTER, BUILDING 1106
HANSCOM AFB, MA**

2 JUNE 1992



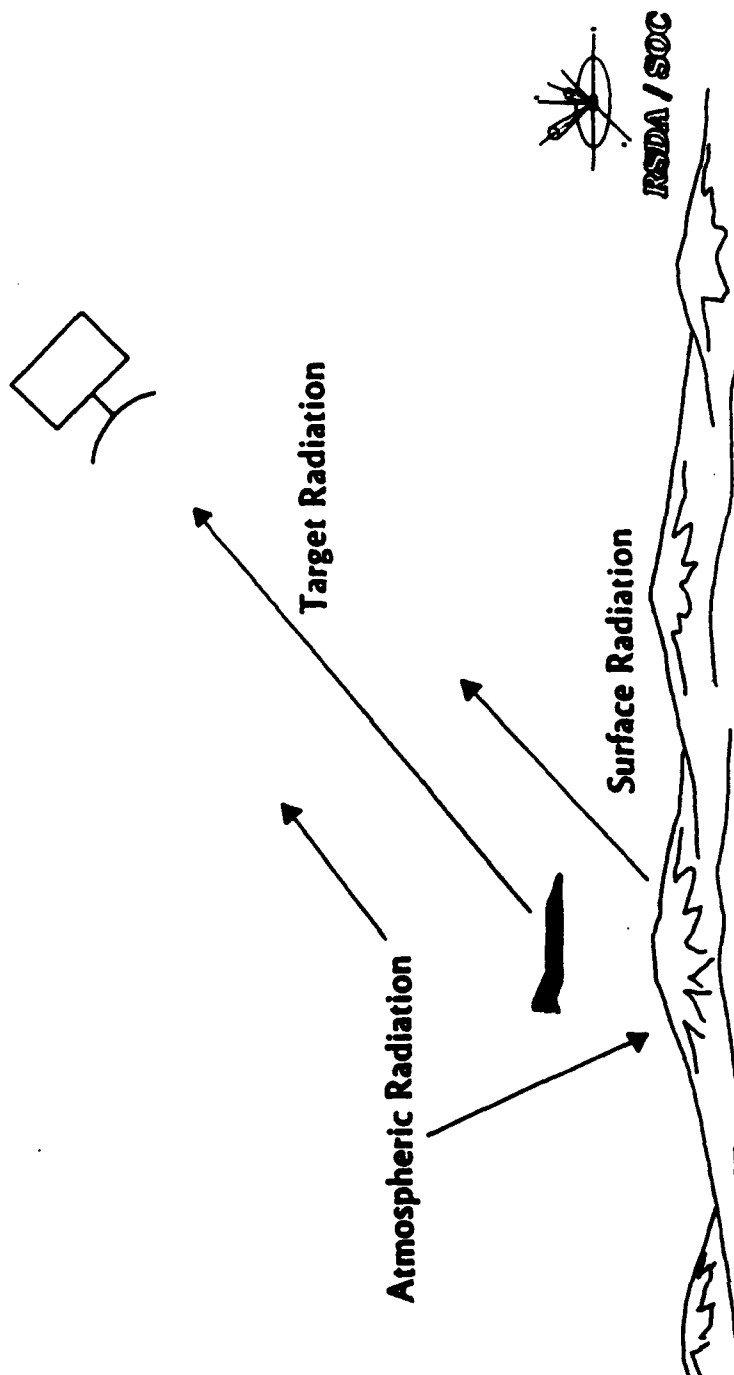
PRESENTATION CONTENT



RSDA / SOC

- 0 THE MILLIMETER WAVE SPECTRUM
- 0 WHY MILLIMETER WAVES?
- 0 MMW TARGET DETECTION CONCEPTS
- 0 THE EFFECTS OF CLOUDS ON PASSIVE MMW SURVEILLANCE
- 0 EXAMPLES OF PASSIVE MMW TARGET SIMULATION
- 0 MMW CLOUD PROPERTIES AND CLOUD-FREE LINE OF SIGHT
- 0 REQUIREMENTS FOR PASSIVE MMW TARGET DETECTION MODELS
- 0 FEATURES REQUIRED FOR MMW TRANSMISSION/RADIANCE MODELS

Target Signal Competes With Environment

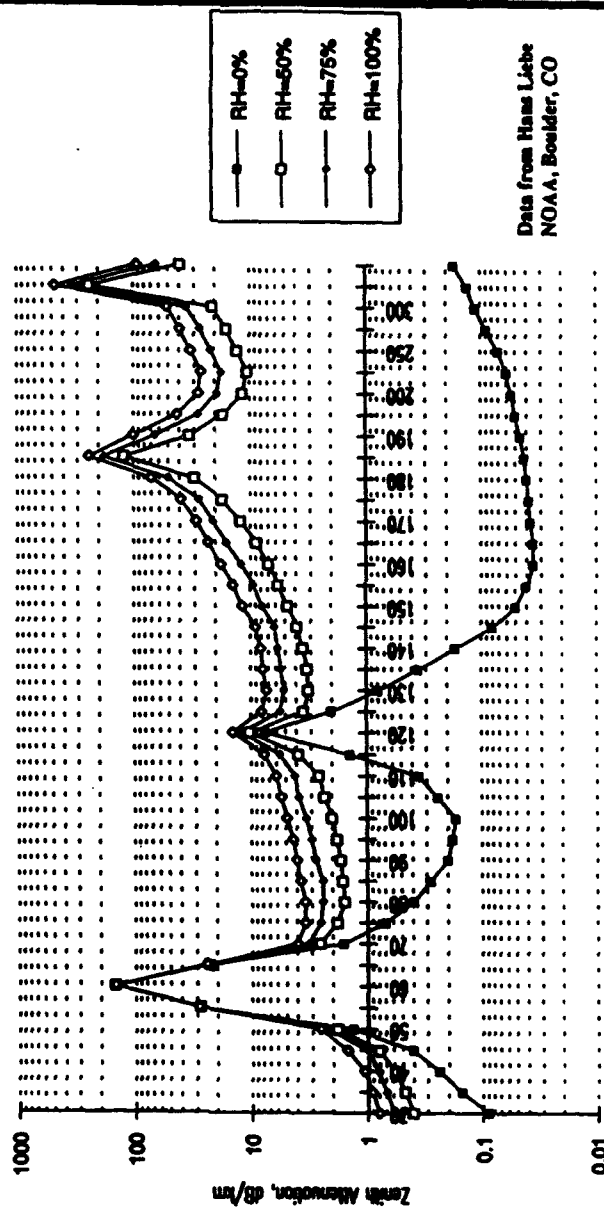




RSDA / SOC



Millimeter Wave Windows

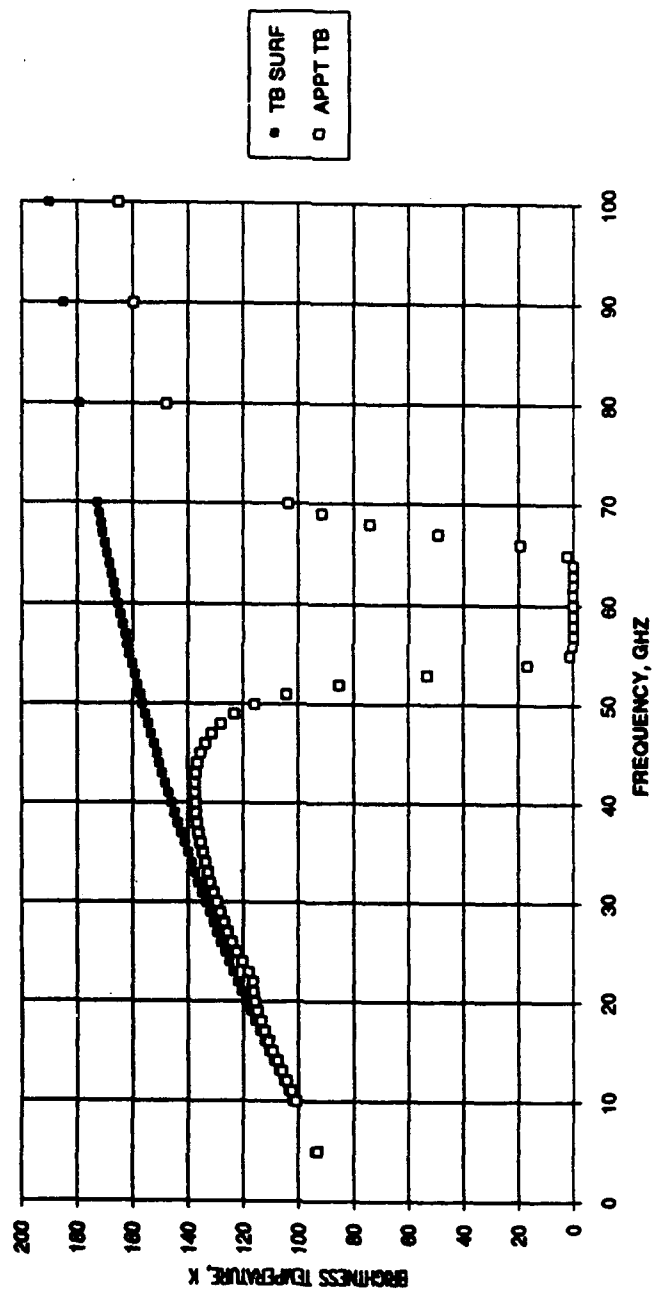


Data from Hans Liebe
NOAA, Boulder, CO

Note scale change at 200 GHz

Frequency, GHz

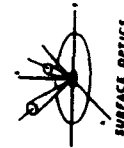
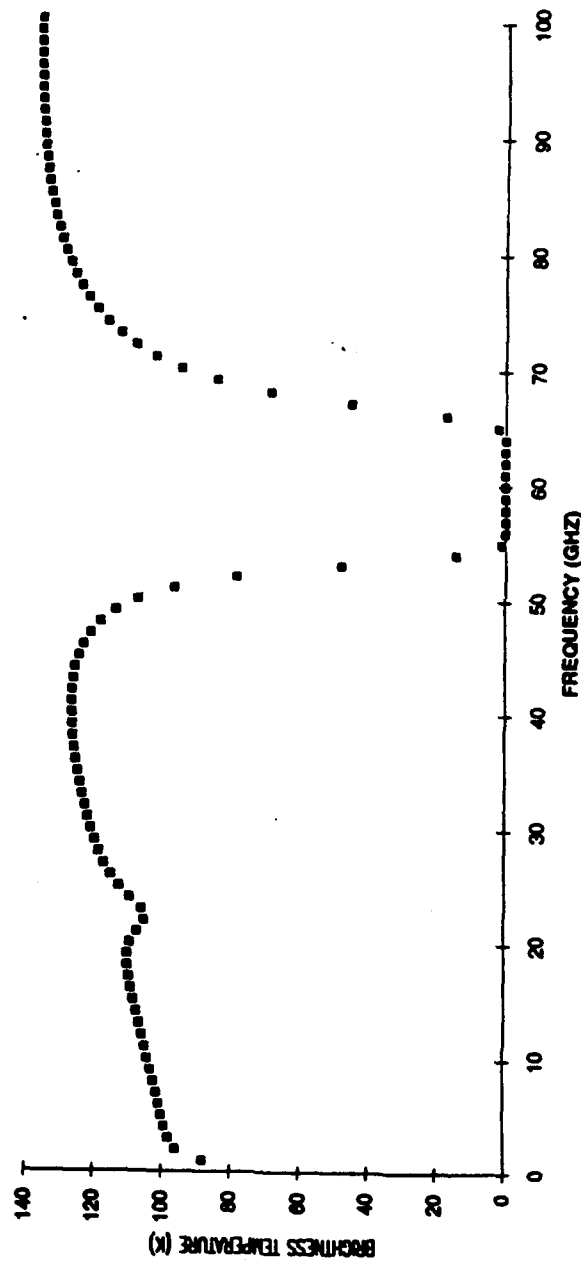
INHERENT MMW BRIGHTNESS TEMPERATURE OF AN OCEAN SURFACE AND ITS APPARENT MMW BRIGHTNESS TEMPERATURE FROM SPACE



RSDA / SOC



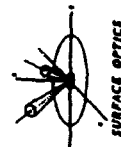
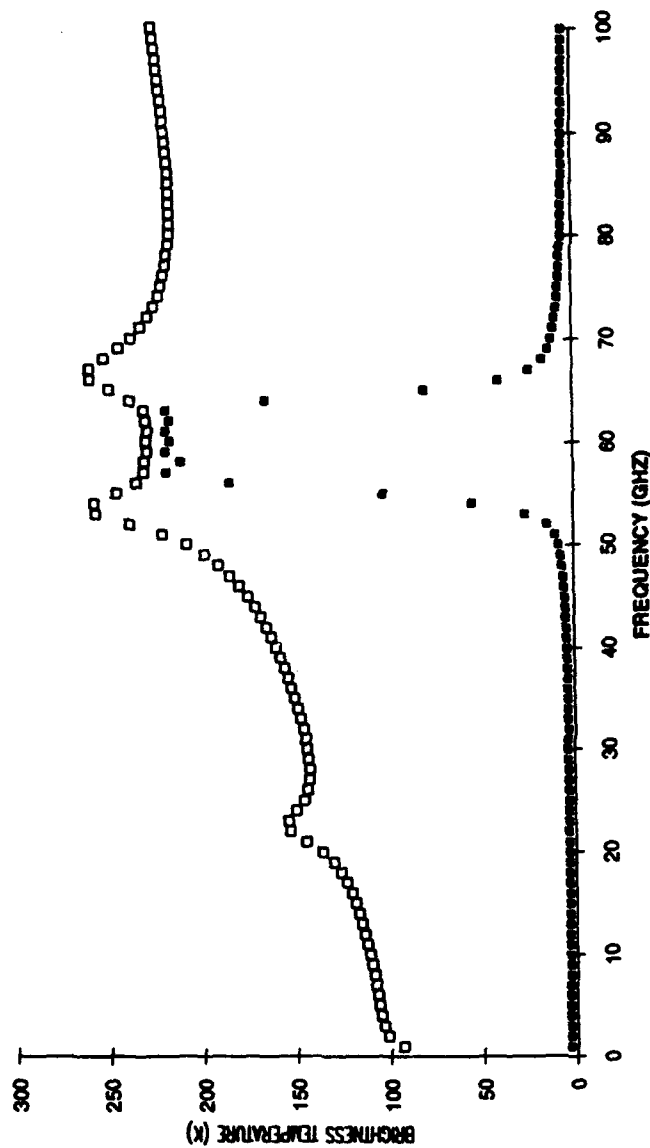
APPARENT BRIGHTNESS TEMPERATURE OF SUBTROPICAL OCEAN SURFACE FROM 10 KM



RSIDA / SOC

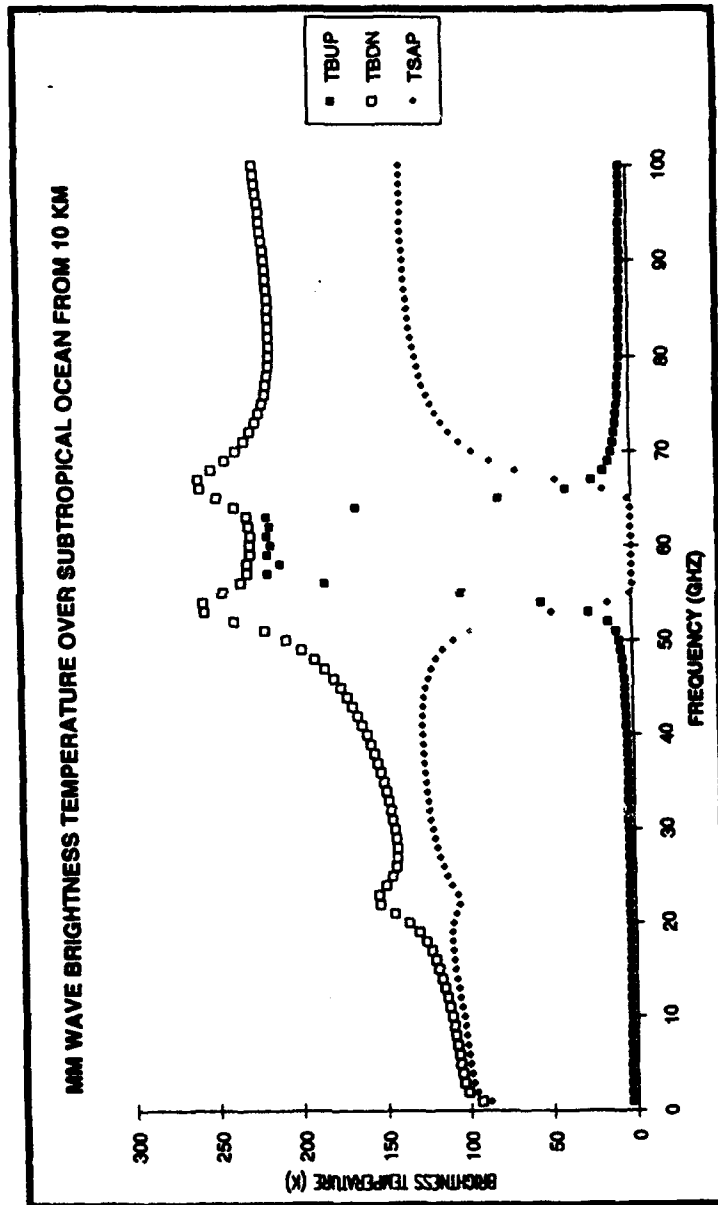
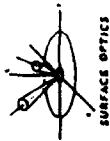


MM WAVE BRIGHTNESS TEMPERATURE OVER SUBTROPICAL OCEAN FROM 10 KM

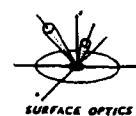
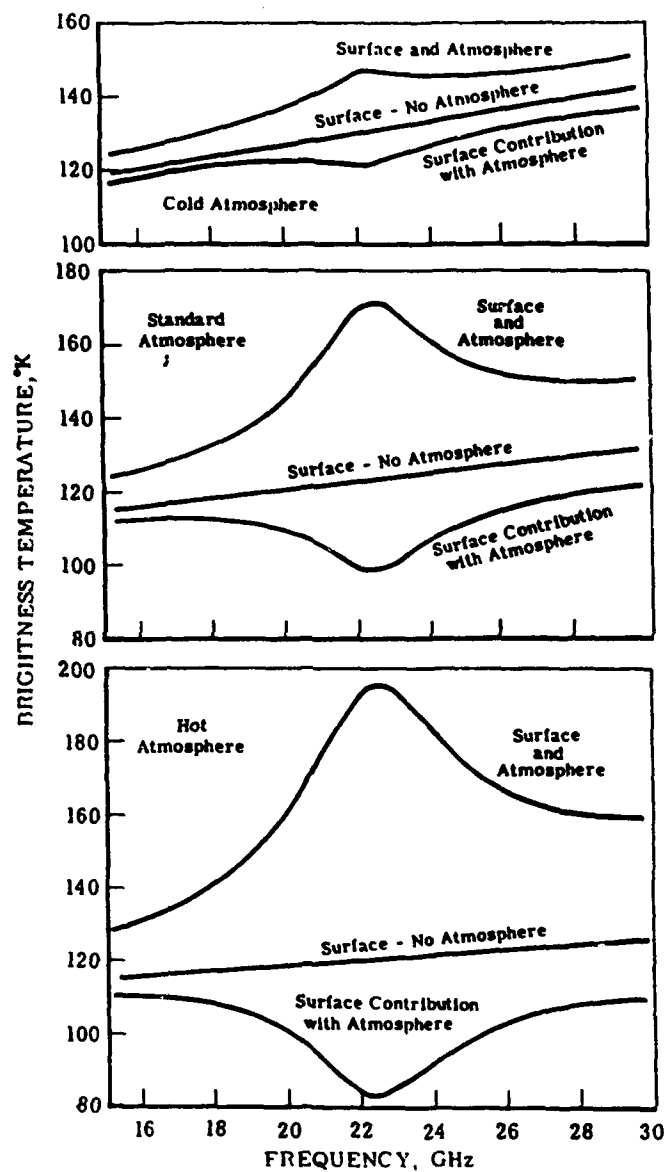


RSDA / SOC





RSDA / SOC



THE SURFACE AND ATMOSPHERE COMPONENTS OF THE DOWNWARD VIEWING
BRIGHTNESS TEMPERATURES OVER A WATER SURFACE FOR THE
THREE BASIC ATMOSPHERES WITH STANDARD HUMIDITY PROFILES

RSDA / SOC

Conventional Remote Sensor Limitations

Mission:

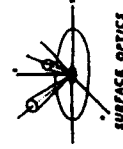
**Surveillance of Strategic Bombers and Cruise Missiles
From Space, Airborne and Surface Based Platforms**

Infrared Sensors

- Experience Difficulty In Adverse Weather

Microwave Radar

- Vulnerable To Stealth Techniques
- Not Covert, Transmitted Signal May Act As Beacon To Antiradiation Missiles



RSIDA / SOC

Passive Millimeter Wave Surveillance Features

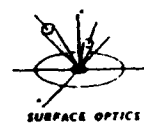
- Penetrates Fog and Clouds
- Senses Target Thermal Radiation
 - Inherent Emission
 - Reflection of Surrounding Illumination Sources
- Offers Potential Advantages
 - Adverse Weather Operation
 - Counters Target Stealth



RS&A / SOC



Figure 4. Photographs show the comparison of the visual-wavelength and millimeter-wave images of a section of freeway south of Carlsbad, California, taken on a rainy day. The sensor was flown over a layer of broken clouds, as seen on the left. The area pictured is 0.4 by 1.9 km. Helicopter altitude was 750 m. Ground speed was 90 km/hr. NASA JPL photograph.

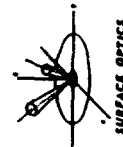


RSOA / SOC

Thermal Noise Limited Point Target Detection

$$\frac{\text{Signal}}{\text{Noise}} = \frac{A_t T_c \epsilon''}{R^2 \lambda^2} \frac{A_a \sqrt{B T_i}}{T_{\text{SYST}}}$$

$A_t T_c$	Target Radiometric Contrast Cross Section m^2k
ϵ''	Target To Sensor Path Atmospheric Transmission
R	Range (m)
λ	Wavelength (m)
A_a	Antenna Effective Area (m^2)
B	Sensor Predetection Bandwidth (Hz)
T_{SYST}	$\bar{T}_A + T_e$
	T_A --- Antenna Radiation Temperature (k)
	T_e = Receiver Internal Noise Temperature (k)

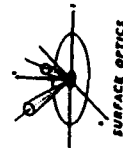


RSIDA / SOC



Antenna Gain (Area) Requirement Driven By:

- Target
 - Cross Section
 - Range
 - Detection Probability
- False Alarm Rate Allowable
- Sensor
 - Wavelength (Frequency)
 - Bandwidth
 - Integration Time - Image F.O.V.
 - Platform Velocity
- Adverse Weather Performance Needs



RSDA / SOC

Critical Areas In Phenomenology

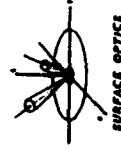
- Quantitative Knowledge of
- Spatial Variations
 - Temporal Variations
- } Land and Ocean Surfaces
Atmosphere

Dependence On

- Specific Geographical Locations and Features
- Climatic Zone
- Time of Year, Day
- Sensor Frequency and Polarization

Need:

- Definition of Measurement: Goal and Approach
- Models For Data Analysis To Extract Operationally Significant Information



RSDA / SOC

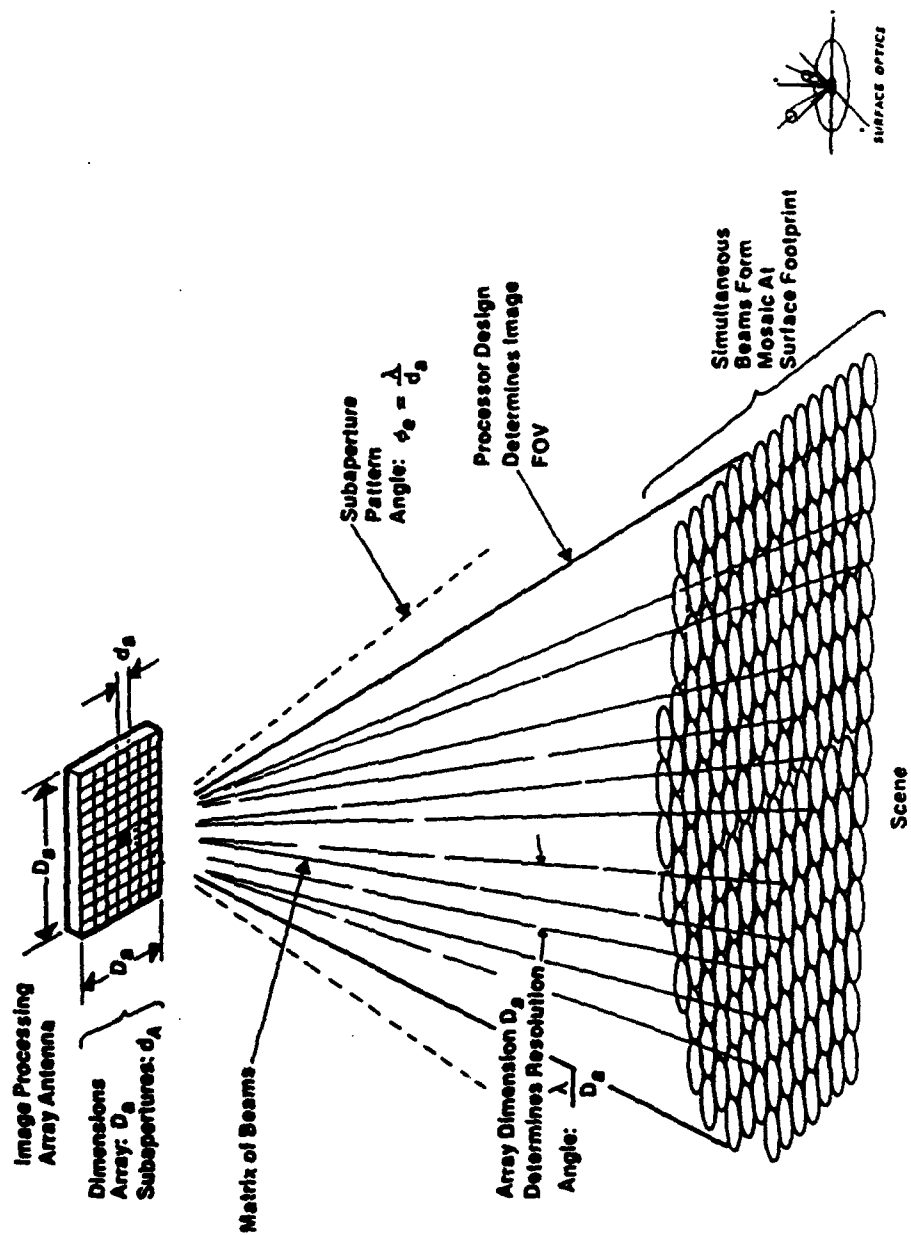
Multibeam (Imaging) Antenna Key To Moving Target Detection

- Simultaneous Observation of All Pixels In Extended Scene – Permits Cancellation of Stationary Background With Frame To Frame Differencing
- Extended Integration Times With Streak Detection Improve Thermal Noise Limited Sensitivity



RSDA / SOC

PASSIVE MILLIMETER MULTIBEAM ARRAY ANTENNA

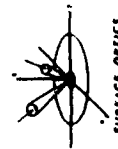


RSIDA / SOC



Fixed Target Detection

- Problem:
 - Background Scene Features Introduce Clutter Noise Exceeding Target Signal
- Approach:
 - An Imaging Sensor With Sufficient Spatial Resolution and Contrast Sensitivity To Permit Target Detection On Basis Of
 - (a) Its Associated Pixel Intensity Exceeding Those of the Scene
 - (b) Shape Recognition (Require High Spatial Resolution)
 - (c) Or In the Case of Temporally Varying Backgrounds (e.g., Oceans) Sufficient Averaging To Reduce the Residual Spatial Variations To Below the Target Signal



RSDA / SOC

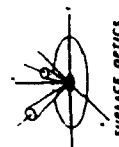
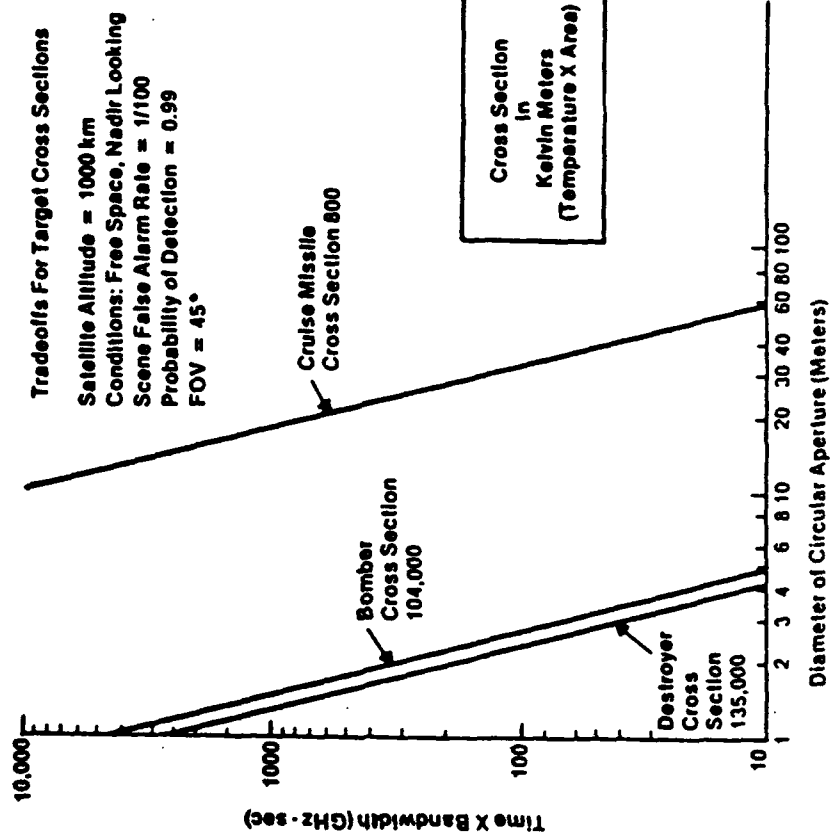
Moving Target Detection

- Problem:
 - Scene Features Introduce Clutter Noise Obscuring Target Signal
- Basic Approach:
 - Coherent Process To Image Scene
 - Post Detection Process To Difference Successive Images of Same Scene
 - Cancellation of Stationary Scene Features Reduces Clutter To Level of Thermal Noise
 - Motion Results In Full Strength Target Signal
- Design For Clutter Cancellation Requires:
 - Accurate Quantitative Measurement and Analysis of Surfaces and of Atmospheric Radiation Sources
 - Spatial and Temporal Variations of Land and Ocean Surfaces and of Atmospheric Radiation Sources



SORDA / SOC

35 GHz Antenna Diameter - (Time-Bandwidth) Tradeoffs For Target Cross Sections

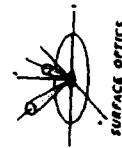
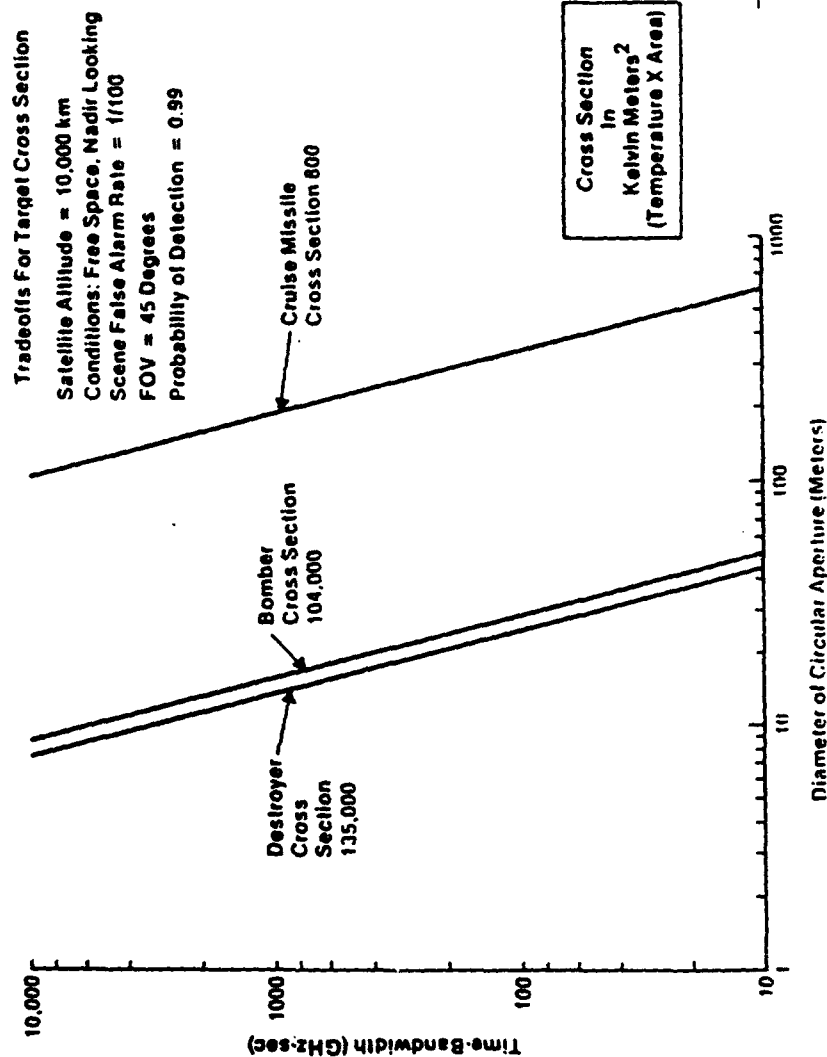


SURFACE OPTICS

RSIDA / SOC



35 GHz Antenna Diameter - (Time-Bandwidth) Tradeoffs For Target Cross Sections

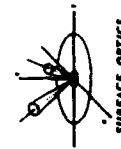
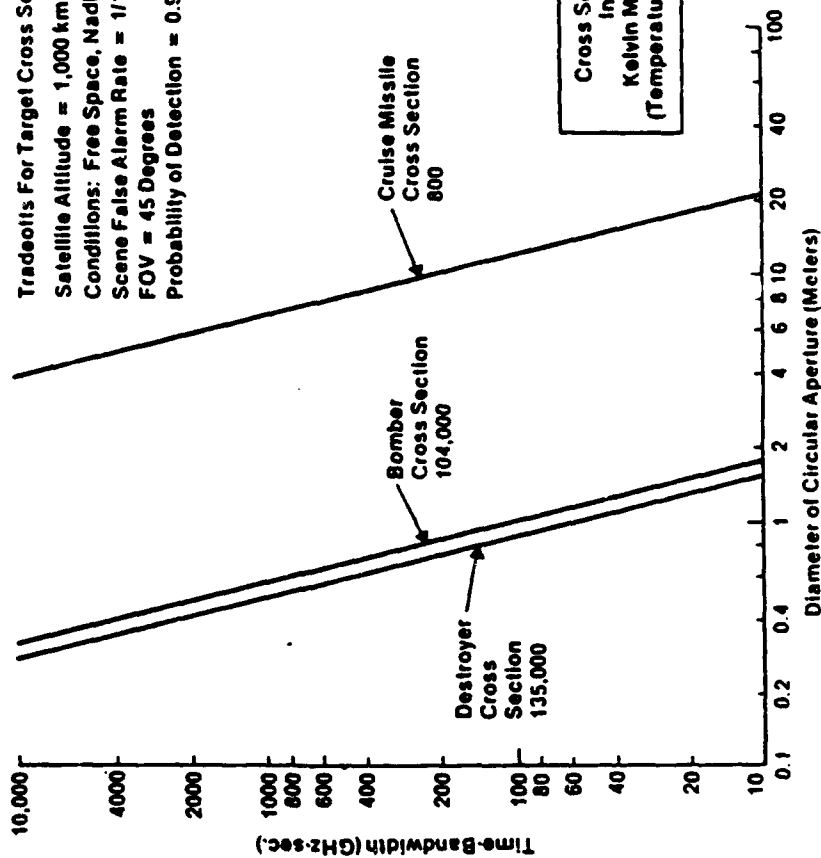


RSDA / SOC



95 GHz Antenna Diameter - (Time-Bandwidth) Tradeoffs For Target Cross Sections

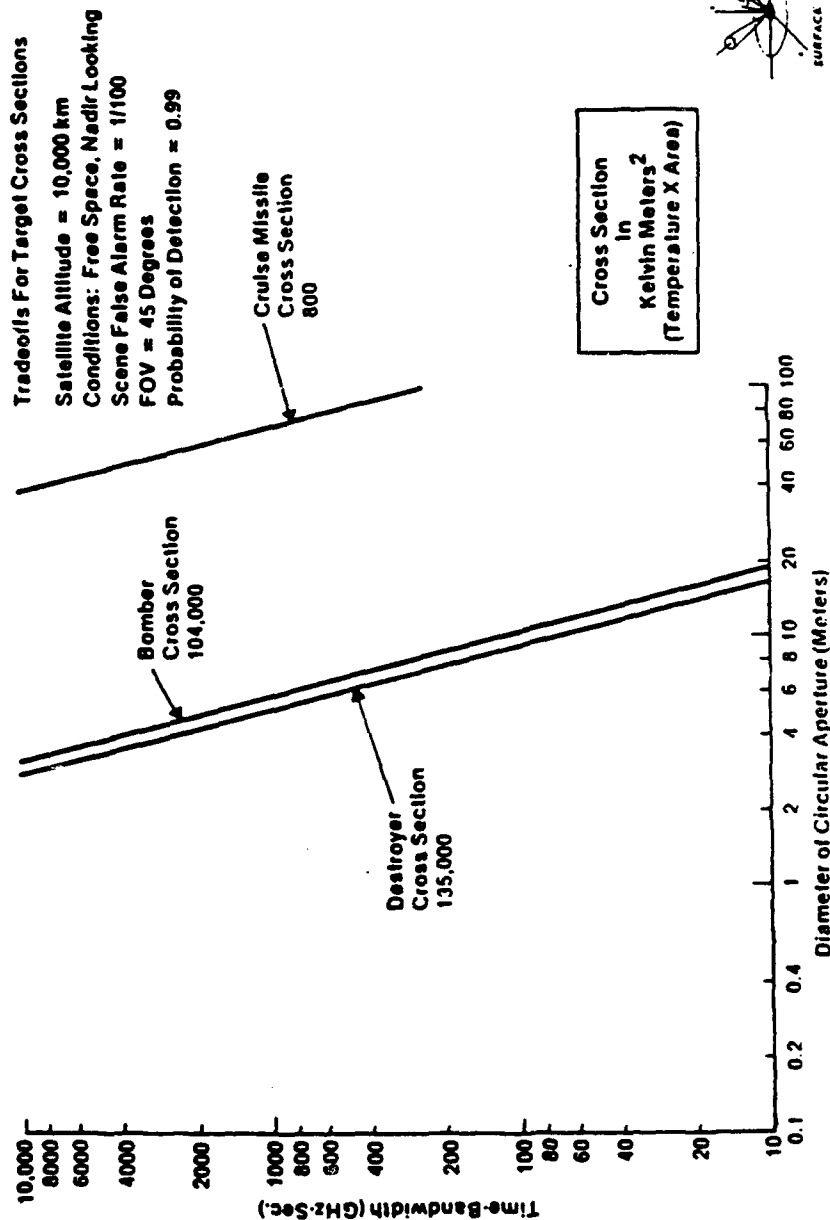
Tradeoffs For Target Cross Sections
 Satellite Altitude = 1,000 km
 Conditions: Free Space, Nadir Looking
 Scene False Alarm Rate = 1/100
 FOV = 45 Degrees
 Probability of Detection = 0.99



RSDA / SOC



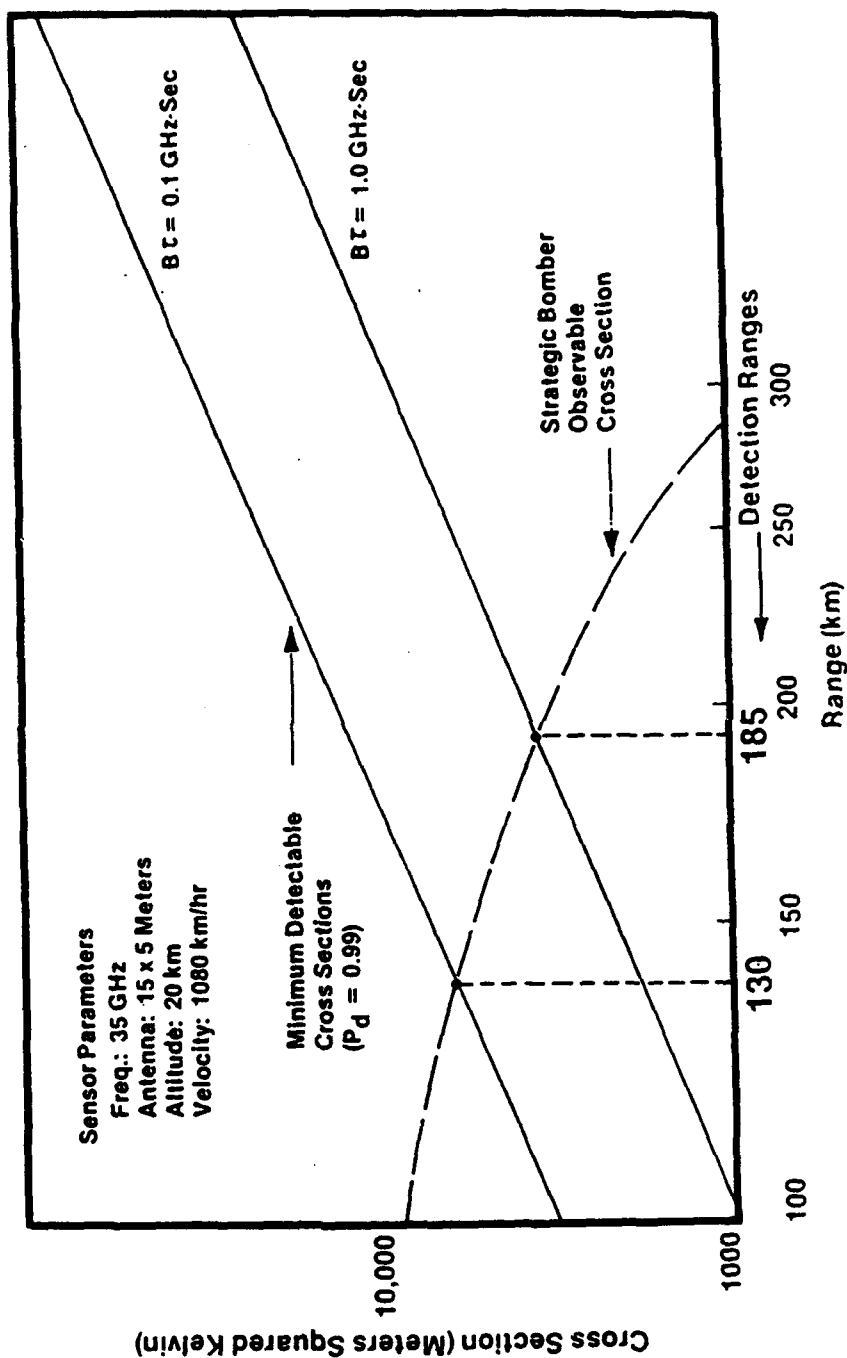
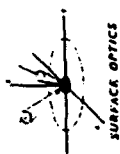
95 GHz Antenna Diameter - (Time-Bandwidth) Tradeoffs For Target Cross Sections



RSIDA / SOC

hite

Airborne Passive Microwave Sensor Detection Ranges For Strategic Bomber



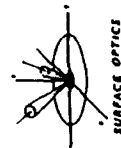
RSIDA / SOC



Target Contrast Cross Sections

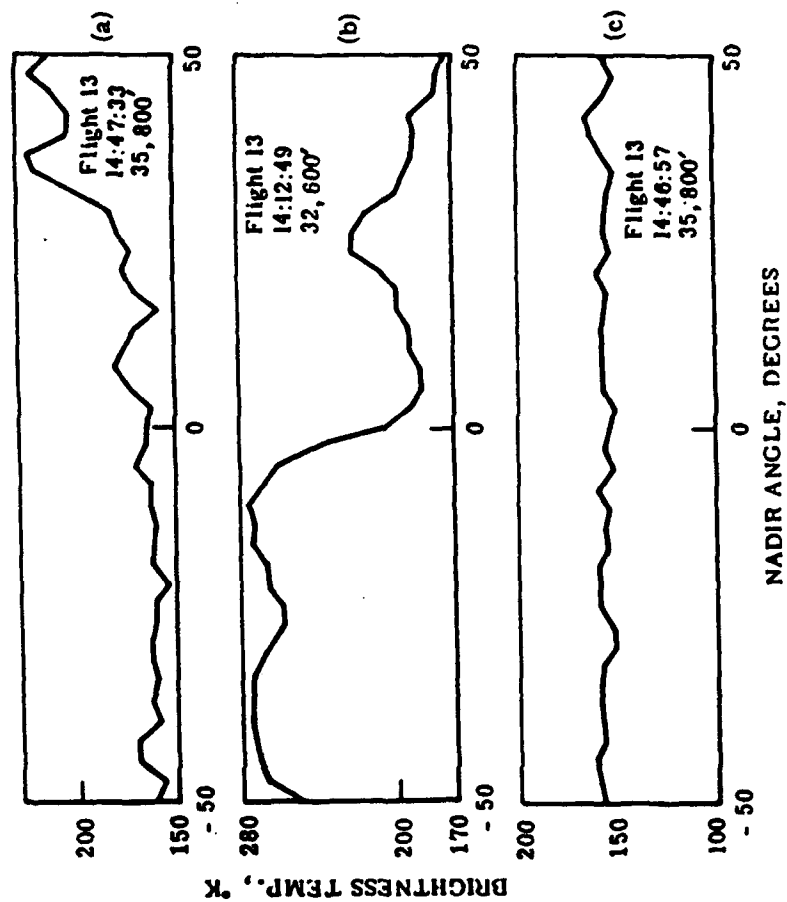
Type	Area A_s m^2	Back- ground	Emissivity Contrast $\Delta \epsilon$	Cross Section $A_s \Delta \epsilon T_h$ ($m^2 \circ K$)
PT Boat	185	Ocean	0.4	21000
Destroyer	1300	Ocean	0.4	135000
Str. A/C	400	Land	0.9	104000
Tank	15	Land	0.9	4000
LSF	2.6	Land	0.9	700

Target Areas - Metal $\epsilon = 0$, $T_r = 290^\circ K$
 $\Delta \epsilon$ Same At 35 GHz and 95 GHz



RSDA / SOC





RSDA / SOC

THE EFFECT OF CLOUDS ON MILLIMETER WAVE BRIGHTNESS TEMPERATURES



RSDA / SOC

17600

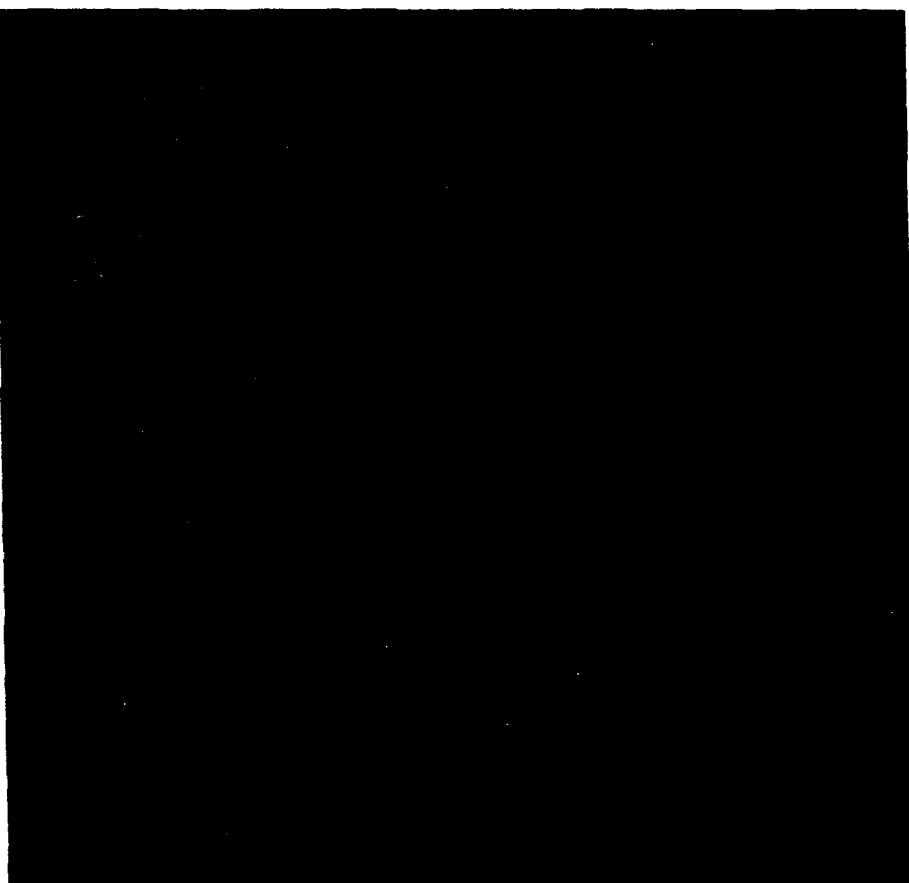


Scan (b) from previous figure

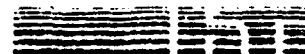
AIRCRAFT
↑
HEADING

MODEL = BACKFIRE
ALT = 10 KM
HEADING = 0.0
YAW = PITCH = ROLL = 0.0 DEG
EARTH CENTRAL ANG = 0.0 DEG
TGT TEMP = 250 K
SENSOR ALT = 0.0 KM
CENTRAL OBS FREQ = 35 GHZ
BANDWIDTH = 1 GHZ
ATMO = US STD
SOLAR IRRAD = 0.0 W M**2

SURFACE = LAND
SFC TEMP = 290 K
SFC TYPE = VEGETATION
SFC FRACTIONAL COVER = 0.75
SFC DIELECTRIC CONST = 10
SFC BACKSCATT COEF = 0.2
CLOUD = NONE
CLOUD BOTTOM =
CLOUD THICK =
CLOUD LWC =

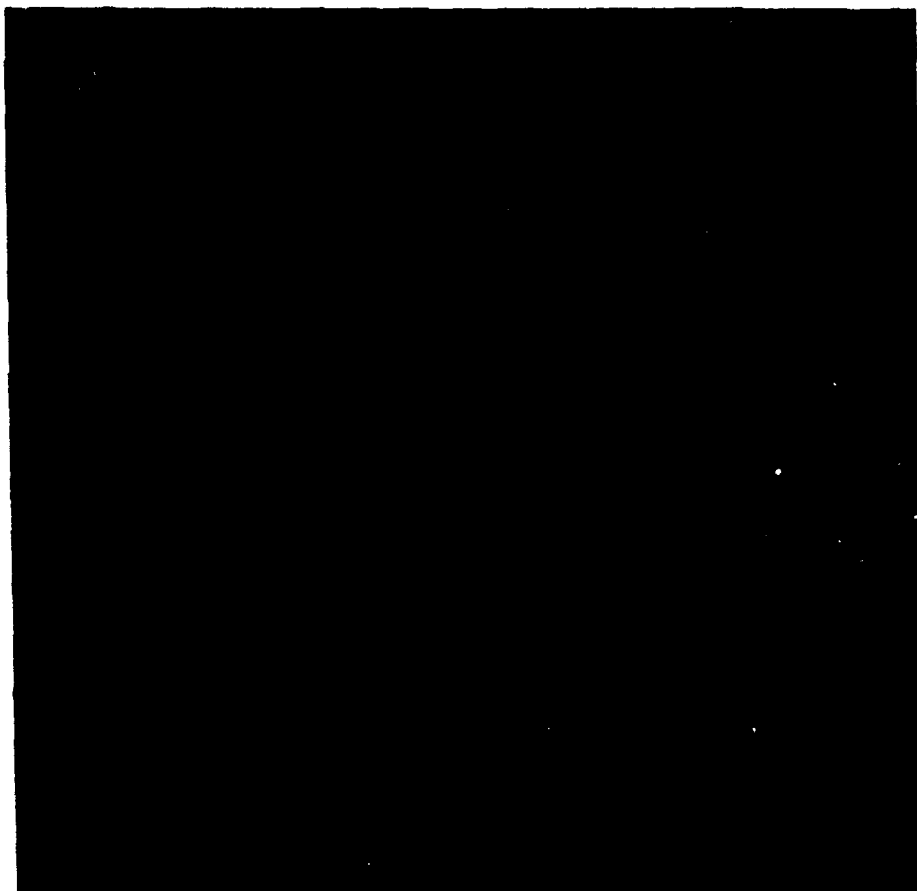


OBSERVER DISTANCE = 10 KM
MEAN ATMO XMISSION = 0.9350
TGT PROJ AREA = 290.9 SQ M
BACKGND TEMP = 21.1 K
MEAN TGT TEMP = 249.7 K
MEAN APPARENT TEMP = 213.7 K
MEAN INHERENT TEMP = 228.6 K
TGT APPARENT CONTRAST = 10.13
TGT INHERENT CONTRAST = 10.83
APPARENT / INHERENT RATIO = 0.9350

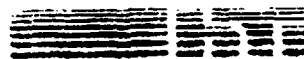


MODEL = BACKFIRE
ALT = 10 KM
HEADING = 0.0
YAW = PITCH = ROLL = 0.0 DEG
EARTH CENTRAL ANG = 0.0 DEG
TGT TEMP = 250 K
SENSOR ALT = 0 K
CENTRAL OBS FREQ = 35 GHZ
BANDWIDTH = 1 GHZ
ATMO = US STD
SOLAR IRRAD = 0.0 W / M**2

SURFACE = LAND
SFC TEMP = 290 K
SFC TYPE = VEGETATION
SFC FRACTIONAL COVER = 0.75
SFC DIELECTRIC CONST = 10
SFC BACKSCATT COEF = 0.2
CLOUD = WATER
CLOUD BOTTOM = 1 KM
CLOUD THICK = 1 KM
CLOUD LWC = 0.25 GM / M**3



OBSERVER DISTANCE = 10 KM
MEAN ATMO XMISSION = 0.88
TGT PROJ AREA = 290.9 SQ M
BACKGND TEMP = 36.3 K
MEAN TGT TEMP = 252.7 K
MEAN APPARENT TEMP = 190.5 K
MEAN INHERENT TEMP = 216.4
TGT APPARENT CONTRAST = 5.244
TGT INHERENT CONTRAST = 5.959
APPARENT / INHERENT RATIO = 0.88

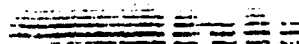


MODEL = BACKFIRE
ALT = 10 KM
HEADING = 0.0
YAW = PITCH = ROLL = 0.0 DEG
EARTH CENTRAL ANG = 0.0 DEG
TGT TEMP = 250 K
SENSOR ALT = 20 KM
CENTRAL OBS FREQ = 35 GHZ
BANDWIDTH = 1 GHZ
ATMO = US STD
SOLAR IRRAD = 0.0 W M**2

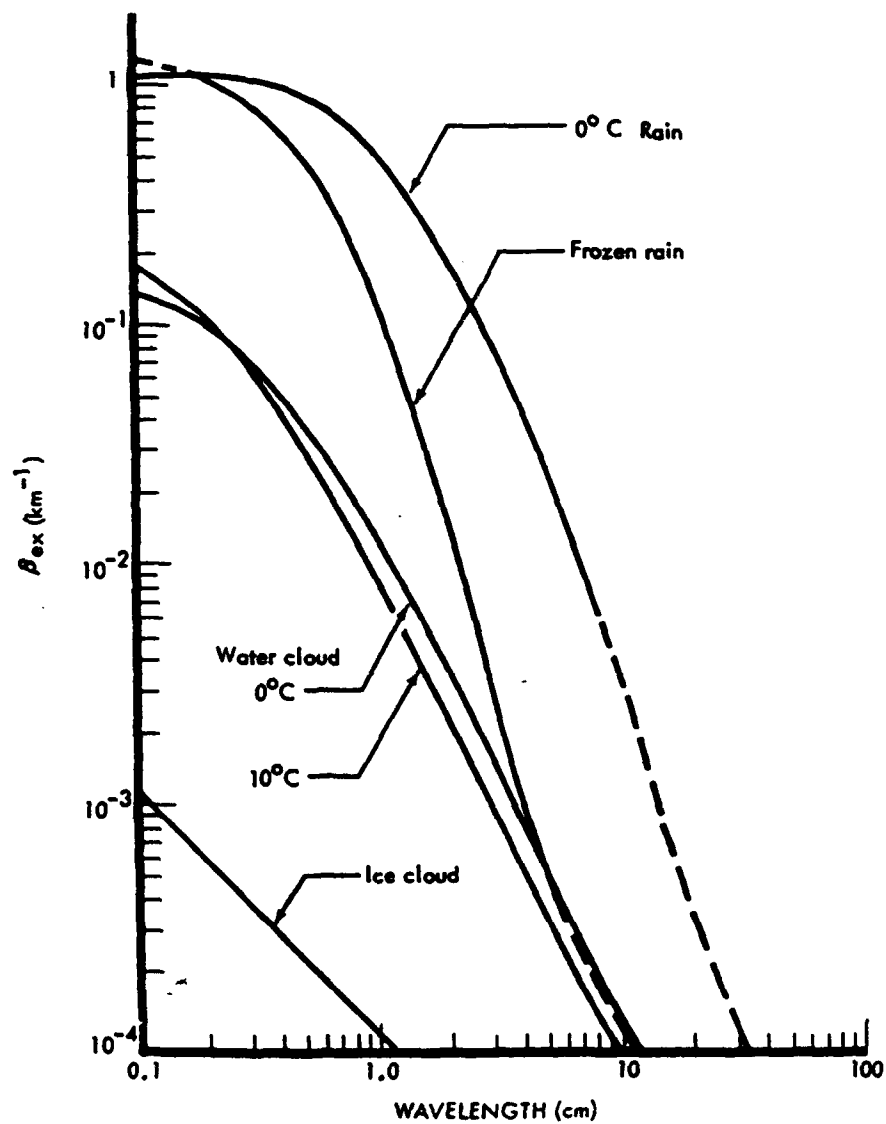
SURFACE = LAND
SFC TEMP = 290 K
SFC TYPE = VEGETATION
SFC FRACT IONAL COVER = 0.75
SFC DIELECTRIC CONST = 10
SFC BACKSCATT COEF = 0.2
CLOUD = NONE
CLOUD BOTTOM =
CLOUD THICK =
CLOUD LWC =



OBSERVER DISTANCE = 10 KM
MEAN ATMO XMISSION = 0.9963
TGT PROJ AREA = 288.3 SQ M
BACKGND TEMP = 260.9 K
MEAN TGT TEMP = 30.96 K
MEAN APPARENT TEMP = 229.1 K
MEAN INHERENT TEMP = 229.9 K
TGT APPARENT CONTRAST = -0.8781
TGT INHERENT CONTRAST = -0.8813
APPARENT / INHERENT RATIO = 0.9963



PSDA / SOC

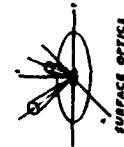
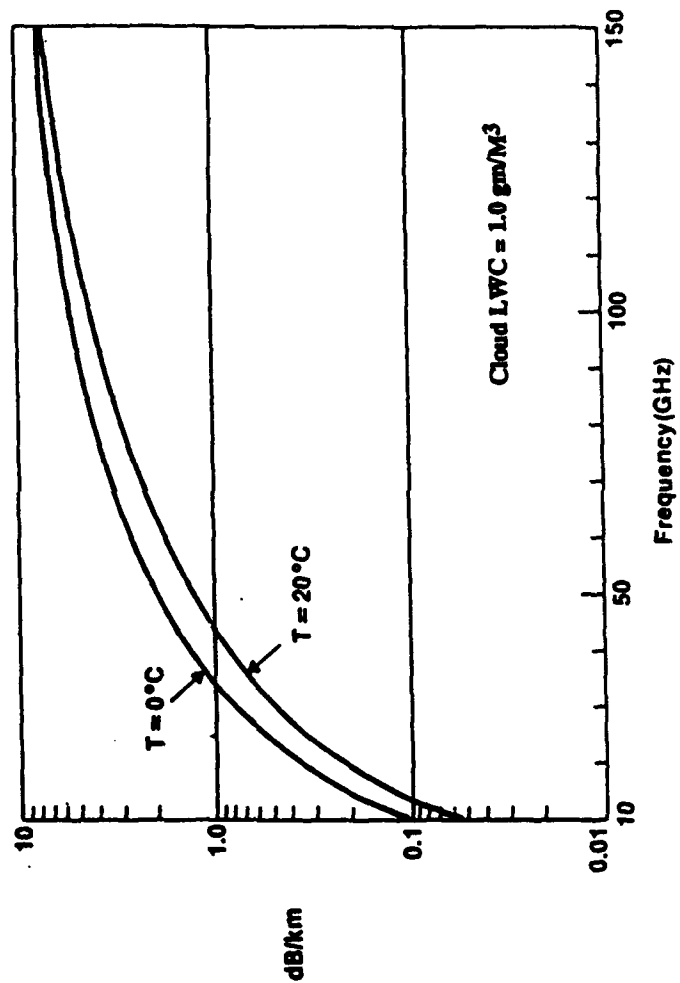


COMPUTED EXTINCTION CURVES FOR CLOUDS AND PRECIPITATION

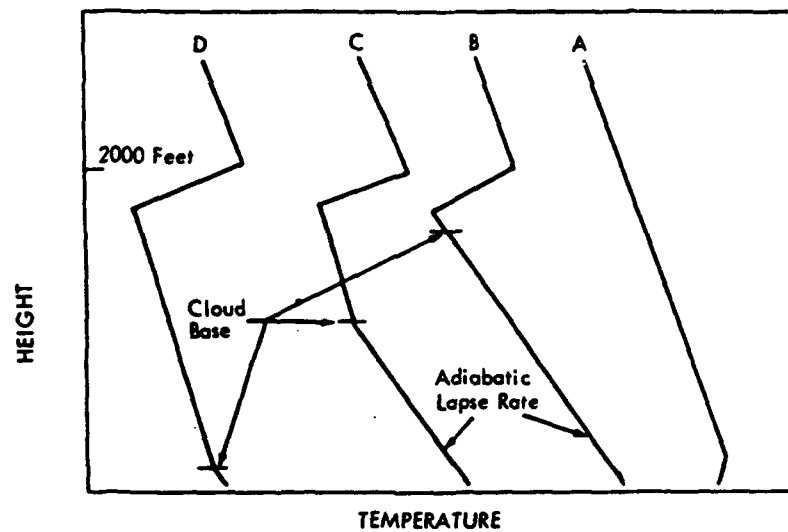
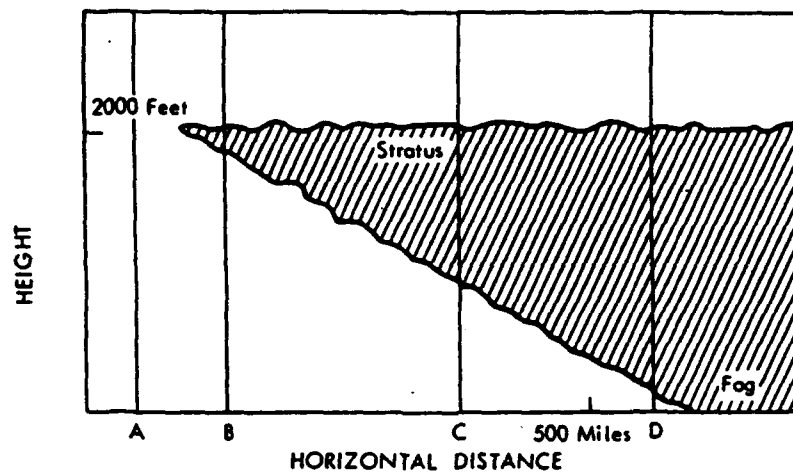


RSDA / SOC

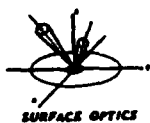
Atmospheric Liquid Water Absorption



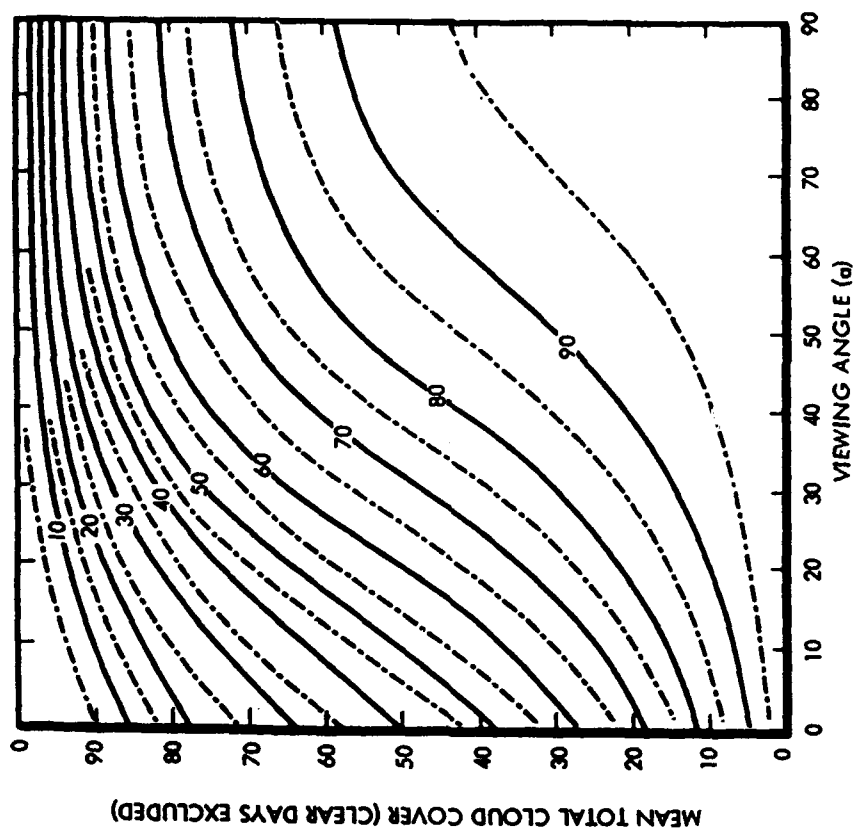
RSIDA / SOC



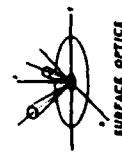
EFFECT OF CLOUDS ON TEMPERATURE-LAPSE RATE



RSDA / SOC

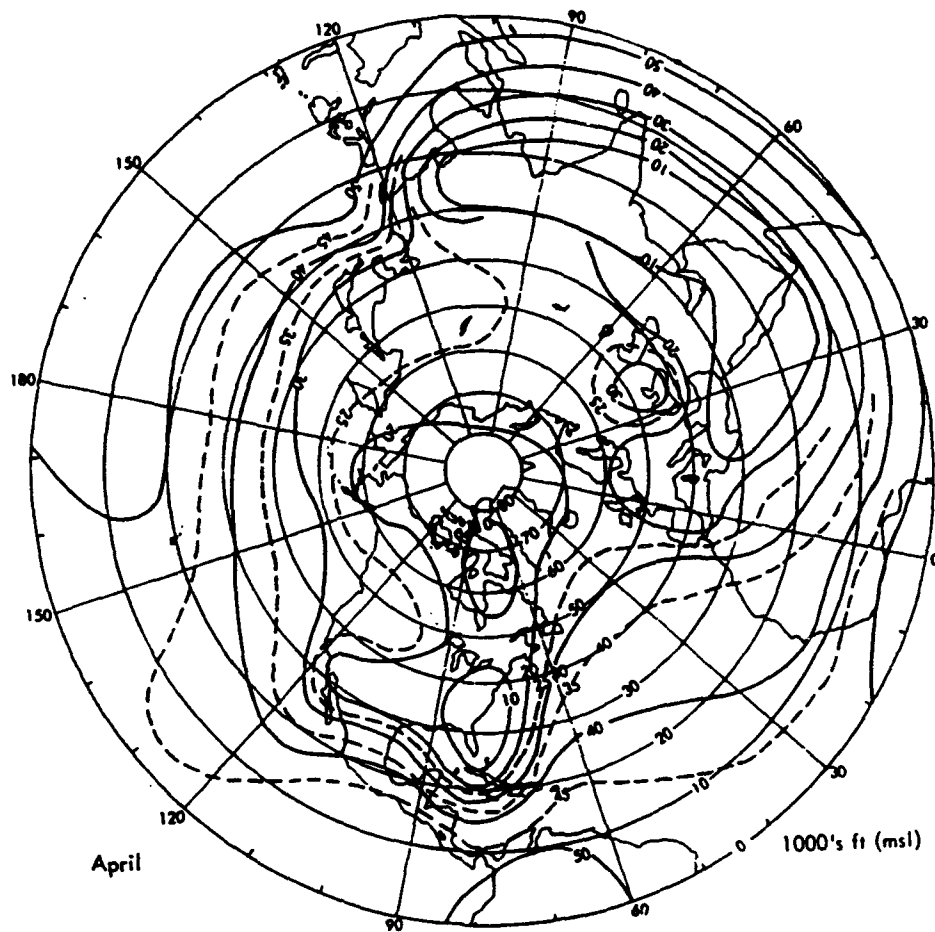


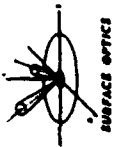
PROBABILITY OF A CLEAR LINE OF SIGHT



RSDA / SOC



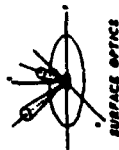




RSIDA / SOC

REQUIREMENTS FOR TRANSMISSION / RADIANCE (T/R) MODELS FOR PASSIVE MILLIMETER WAVE TARGET DETECTION

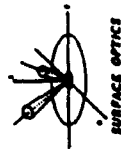
- o TO MINIMIZE ATMOSPHERIC INTERFERENCE AND MAXIMIZE RANGE PERFORMANCE, MMW SENSORS OPERATE IN ATMOSPHERIC WINDOWS i.e., CENTERED ABOUT 10, 35, 95, 140, 220 GHZ (30, 8.6, 3.2, 2.1, OR 1.4 MM)
- o UNOBSERVED WINDOWS BECOME LESS CLEAR AS WAVELENGTH DECREASES
- o ATMOSPHERIC OPTICS AND CLUTTER TAKE ON NEW IMPORTANCE
- o SINCE MMW PROPAGATE THROUGH, OR AT LEAST PENETRATE OBSCURANT "CLOUDS", THE T/R MODEL MUST TREAT THE RADIATION PHYSICS AT THE "CLOUD" BOUNDARIES AND WITHIN THE CLOUD
- o SINCE THE SIGNATURES OF MOST TARGETS OF INTEREST ARE "SEEN" THROUGH REFLECTION OF THE TARGET SURROUNDS, THE T/R MODEL MUST ACCOMMODATE A MULTITUDE OF PATHS AND BACKGROUNDS
- o THE SUN BECOMES A MORE IMPORTANT GLINT SOURCE



FEATURES REQUIRED FOR PASSIVE MMW T/R MODELS

RSDA / SOC

- 0 COMPLETE AND ACCURATE DESCRIPTION OF O₂ AND H₂O MOLECULAR ABSORPTION OVER TOTAL MMW SPECTRUM
- 0 SPHERICAL STRATIFICATION FOR MODEL LAYERS
- 0 ADEQUATE NUMBER OF LAYERS TO ACCOMMODATE ALL ATMOSPHERIC STRUCTURE PHENOMENA
- 0 RAY TRACING TO ACCOUNT FOR RAY BENDING AND DUCTING
- 0 MEANS TO FACILITATE COMPUTATION OF SPATIAL AND TEMPORAL DEPENDENCE
- 0 MODELS FOR WARM CLOUD TYPES, ICE CLOUDS, AND PRECIPITATION
- 0 MULTIPLE CLOUD LAYERS



FEATURES REQUIRED FOR PASSIVE MMW T/R MODELS (CON'T)

RSDA / SOC

- 0 CLOUD CLIMATOLOGIES AND CFLOS MODEL
- 0 MODEL ATMOSPHERES FOR CLOUDED CONDITIONS
- 0 EXTINCTION MODELS FOR LARGE HYDROSOLS
- 0 POLARIZATION
- 0 DEPENDENCE ON GEOGRAPHICAL LOCATION AND FEATURES, AND MODELS TO ACCOUNT FOR LOCAL FEATURES
- 0 CLIMATIC ZONE
- 0 EPHEMERIS

MEASUREMENTS
and
MODELS

ABSORPTION CROSS SECTION MEASUREMENTS OF SCHUMANN-RUNGE CONTINUUM OF O₂ AT 78 K AND 295 K

**K. Yoshino, J.R. Esmond, W.H. Parkinson
Harvard-Smithsonian Center for Astrophysics, Cambridge, MA 02138**

We measured the photoabsorption cross sections of the S-R continuum at 78 K and 295 K in the wavelength region 130-175 nm. The 1-m Seya-Namioka vacuum spectrometer on the BL-12A beam line at the Photon Factory, KEK, Japan was used, in the first order, with synchrotron radiation as a background continuum. The measurements have been performed on a relative scale in scanning mode and also on the absolute scale at every 5 nm interval. These absolute cross sections measurements of O₂ have been used to put the relative cross sections on a firm absolute basis throughout the region 130-175 nm. Temperature effects on the cross sections of the S-R continuum are clearly seen and cross sections at 78 K are about 80% of those at 295 K. The observed cross sections at 78 K are limited to absorption originating from only the $v''=0$ level.

This work is supported by NASA grant NAG5-484 to Smithsonian Astrophysical Observatory.

Absorption Cross Section Measurements of Schumann-Runge

Continuum of O₂ at 78 K and 295 K

K. Yoshino, J.R. Esmond and W.H. Parkinson

Harvard-Smithsonian Center for Astrophysics, Cambridge, MA 02138, U.S.A.

We measured the photoabsorption cross sections of the S-R continuum at 78 K and 295 K in the wavelength region 130-175 nm. The 1-m Seya-Namioka vacuum spectrometer on the BL-12A beam line at the Photon Factory, KEK, Japan was used, in the first order, with synchrotron radiation as a background continuum. The measurements have been performed on a relative scale in scanning mode and also on the absolute scale at every 5 nm interval. These absolute cross sections measurements of O₂ have been used to put the relative cross sections on a firm absolute basis throughout the region 130-175 nm. Temperature effects on the cross sections of the S-R continuum are clearly seen and cross sections at 78 K are about 80% of those at 295 K. The observed cross sections at 78 K are limited to absorption originating from only the $v''=0$ level.

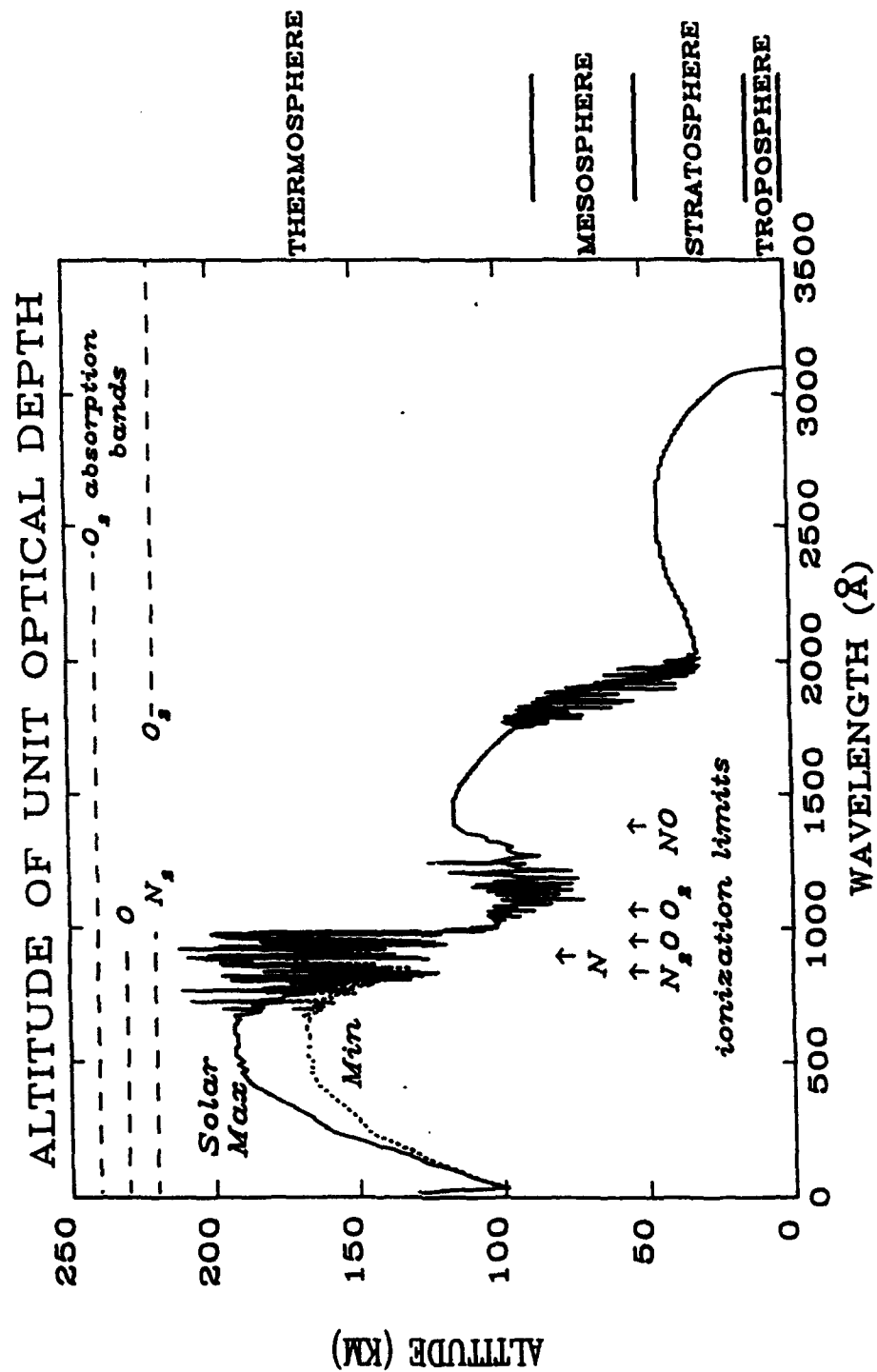
This work is supported by NASA grant NAG5-484 to Smithsonian Astrophysical Observatory.

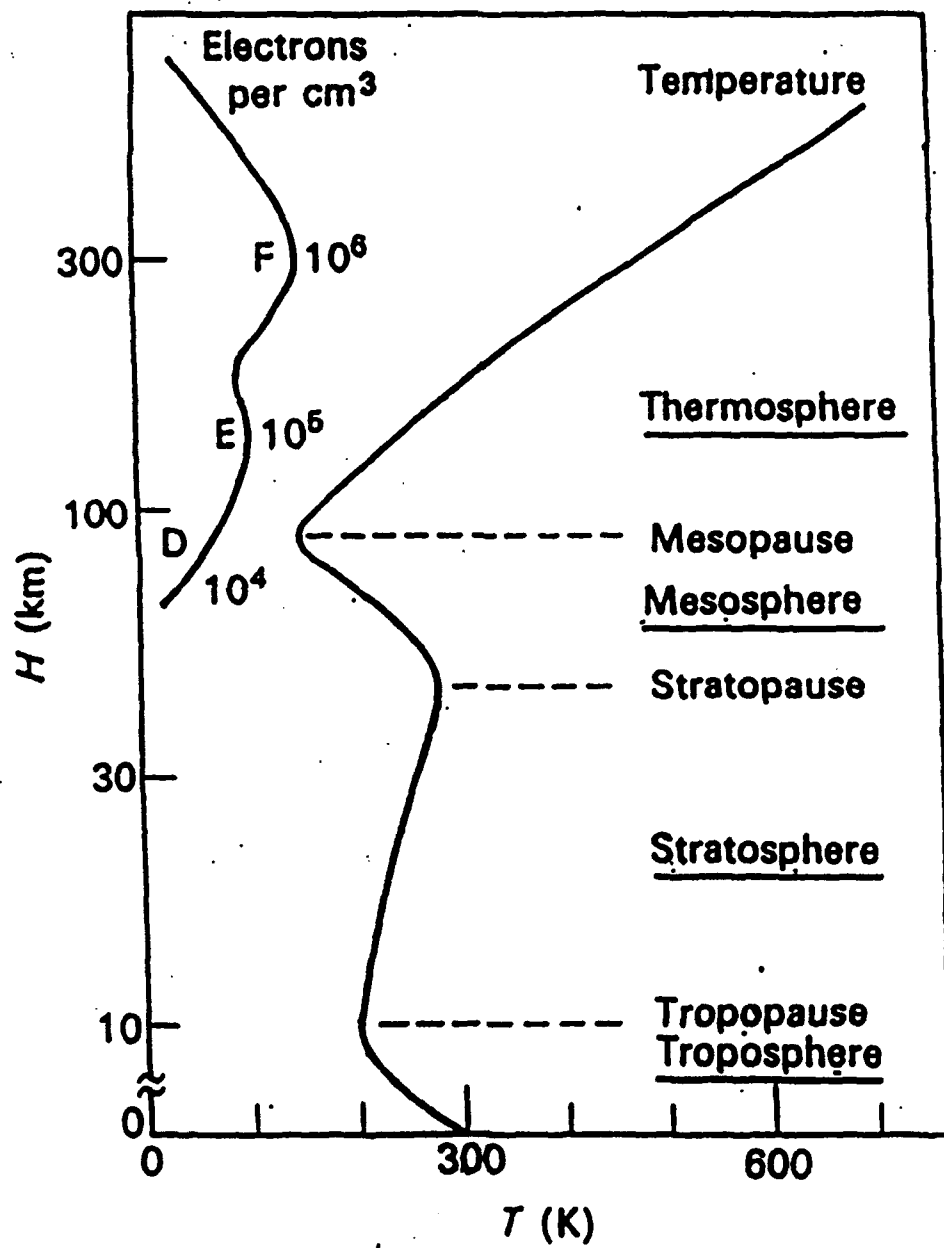
**Absorption Cross Sections Measurements of the Schumann-Runge
Continuum of O_2 at 78 K and 295 K**

K. Yoshino, J.R. Esmond, and W.H. Parkinson,

Harvard-Smithsonian Center for Astrophysics
60 Garden Street, Cambridge, MA 02138, U.S.A.

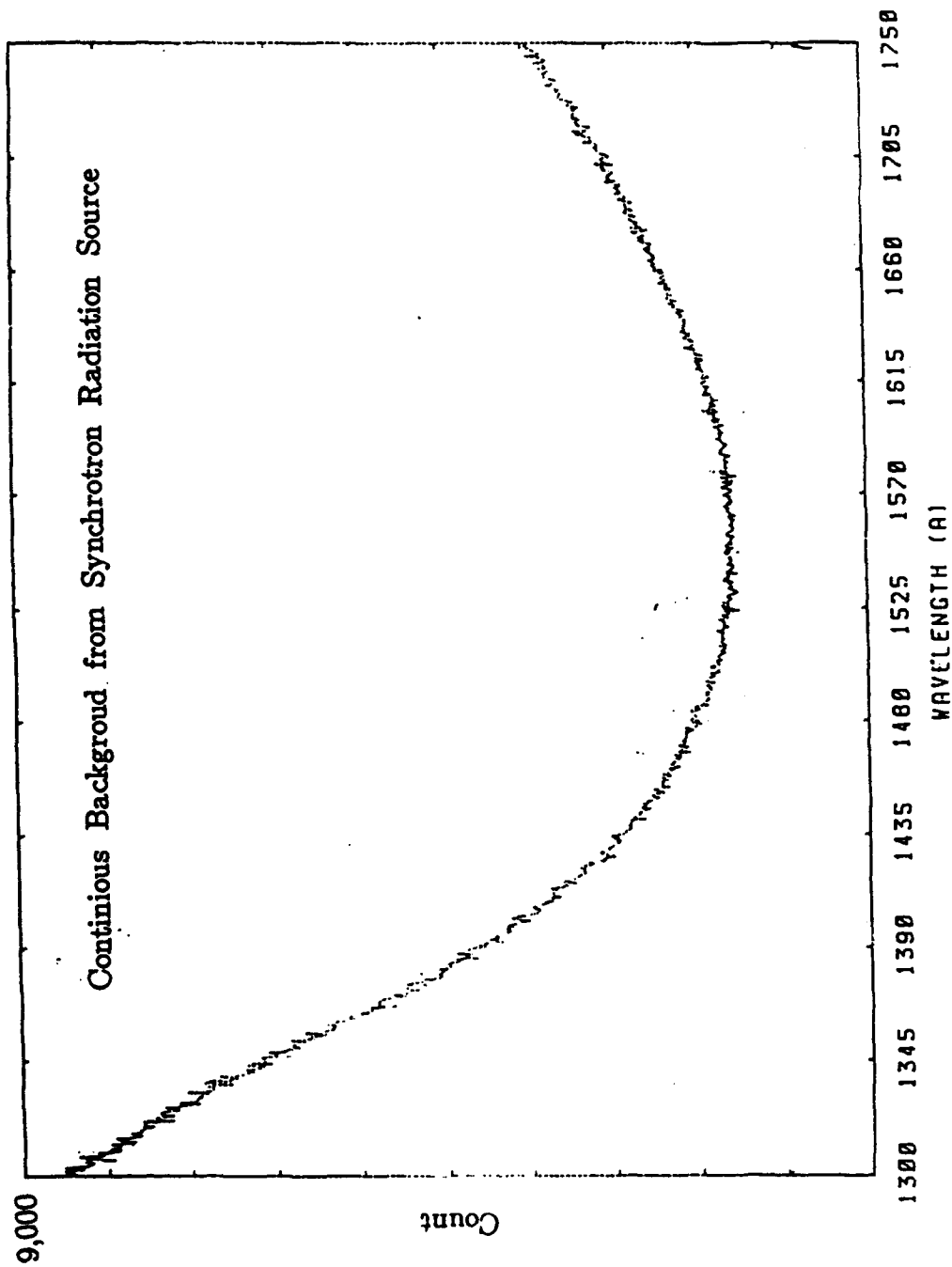
Supported by the NASA Upper Atmospheric Research Program

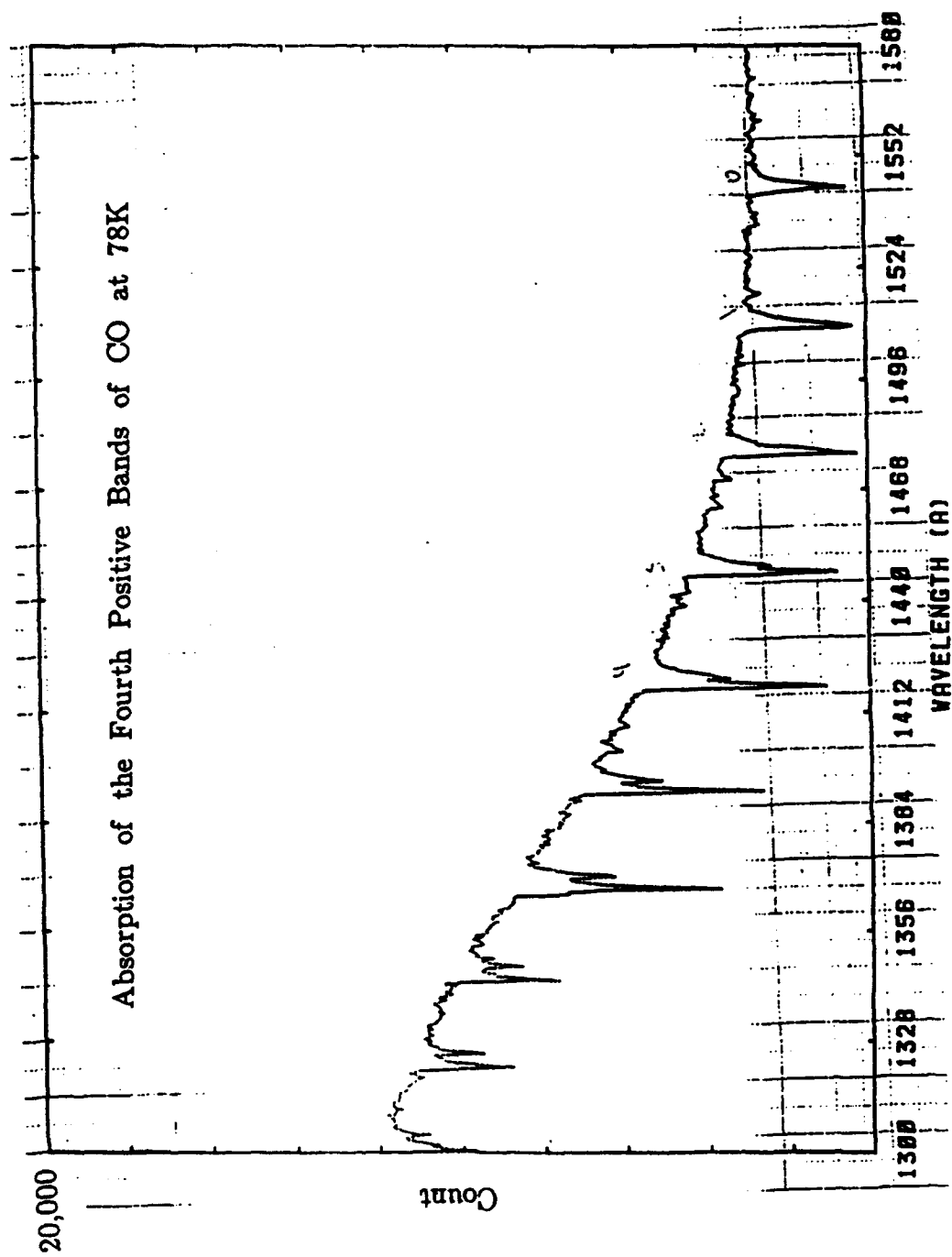




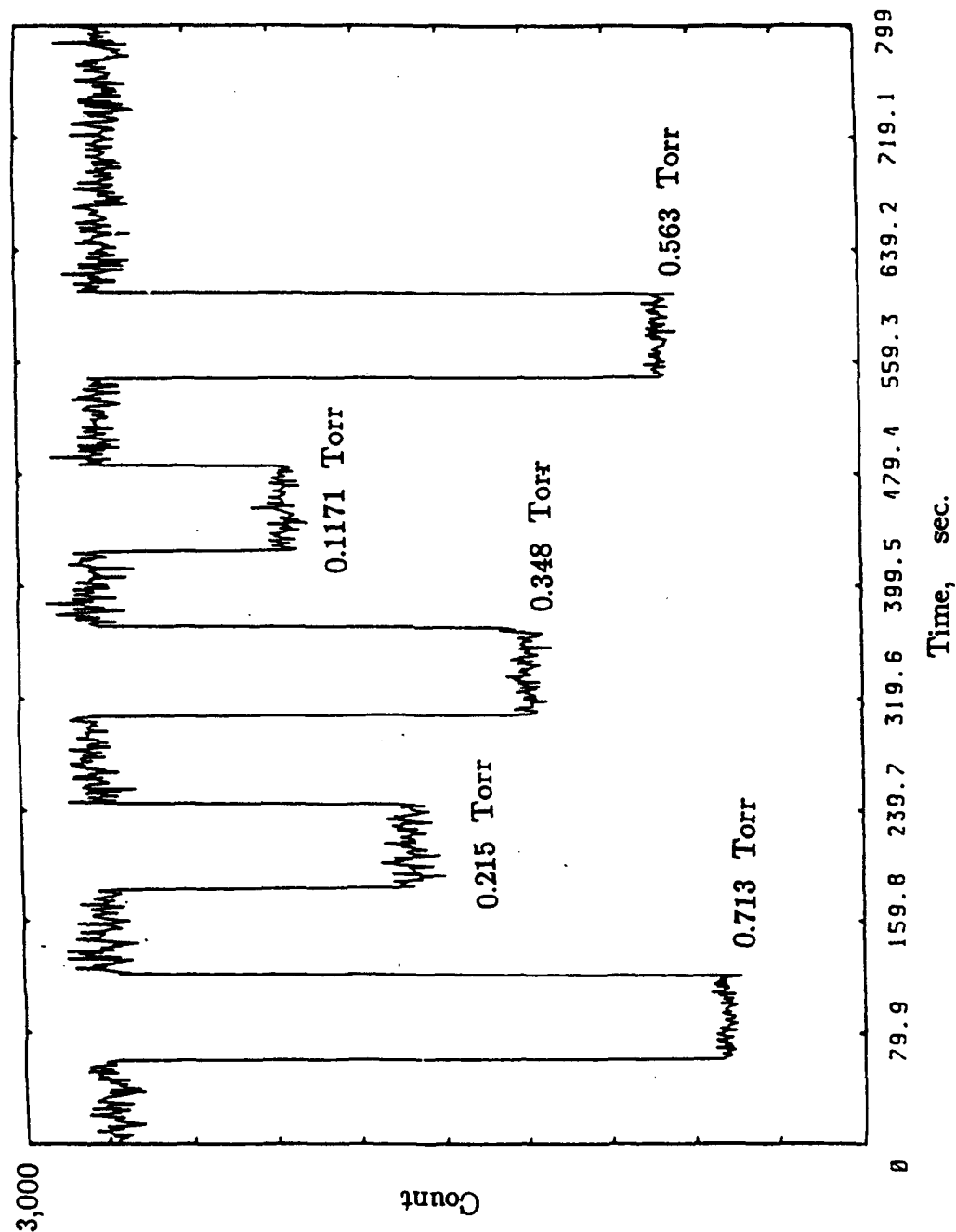
EXPERIMENTAL CONDITIONS

Spectrometer	1-m Seya-Namioka
Grating	1200 1/mm in the first order
Source	Synchrotron, Photon Factory, Japan
Spectrometer bandwidth (FWHM)	0.066 nm or 0.6 Å
Interval between data points	0.05 nm or 0.5 Å
Wavelength Region	130 - 175 nm or 1300 - 1750 Å
Period of accumulating account	1 sec
Temperature	78 K and 295 K
Optical path length	12.08 cm
Pressure range	0.05 - 10.0 Torr





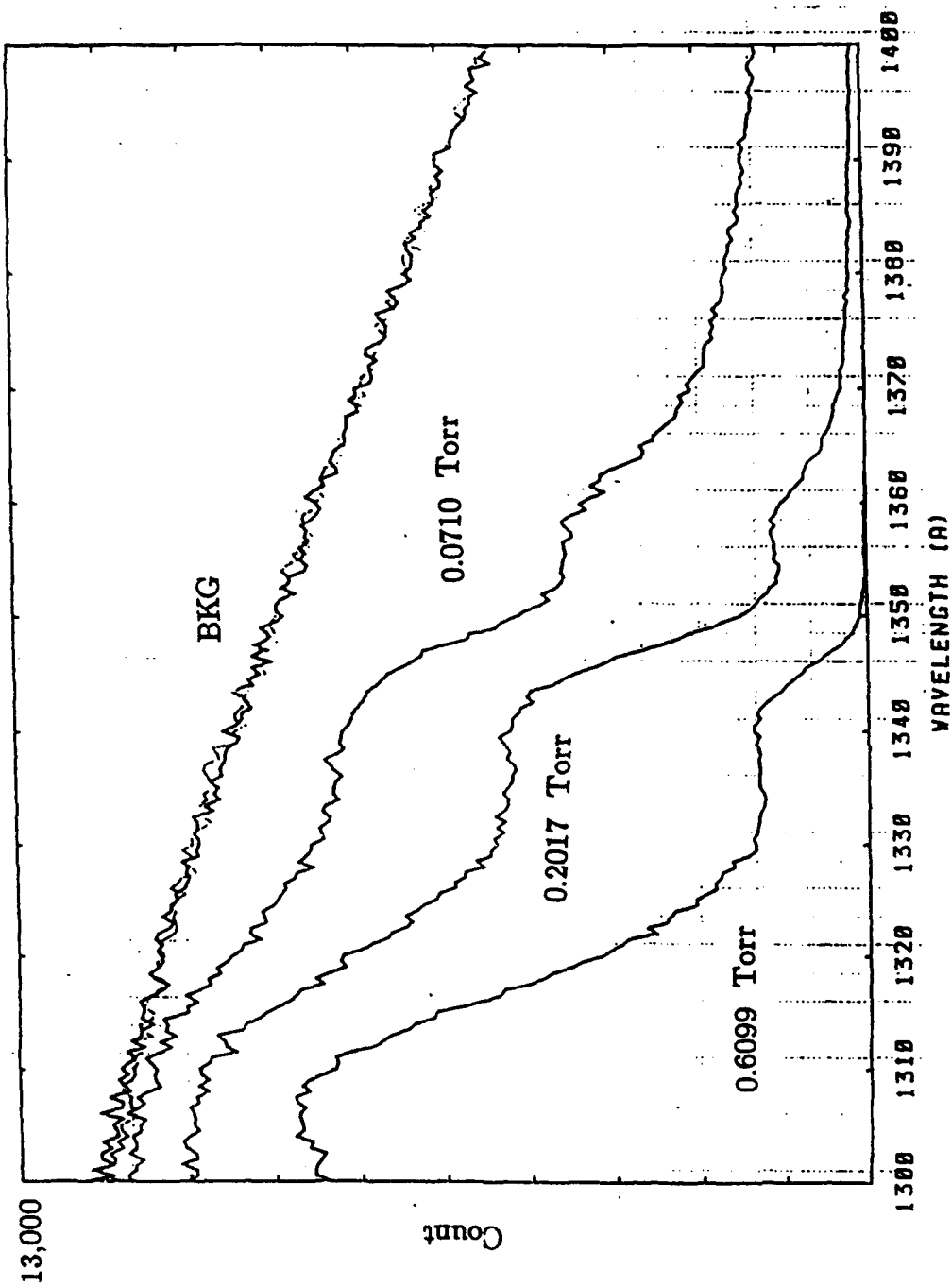
Absolute Absorption Cross Sections Measurements

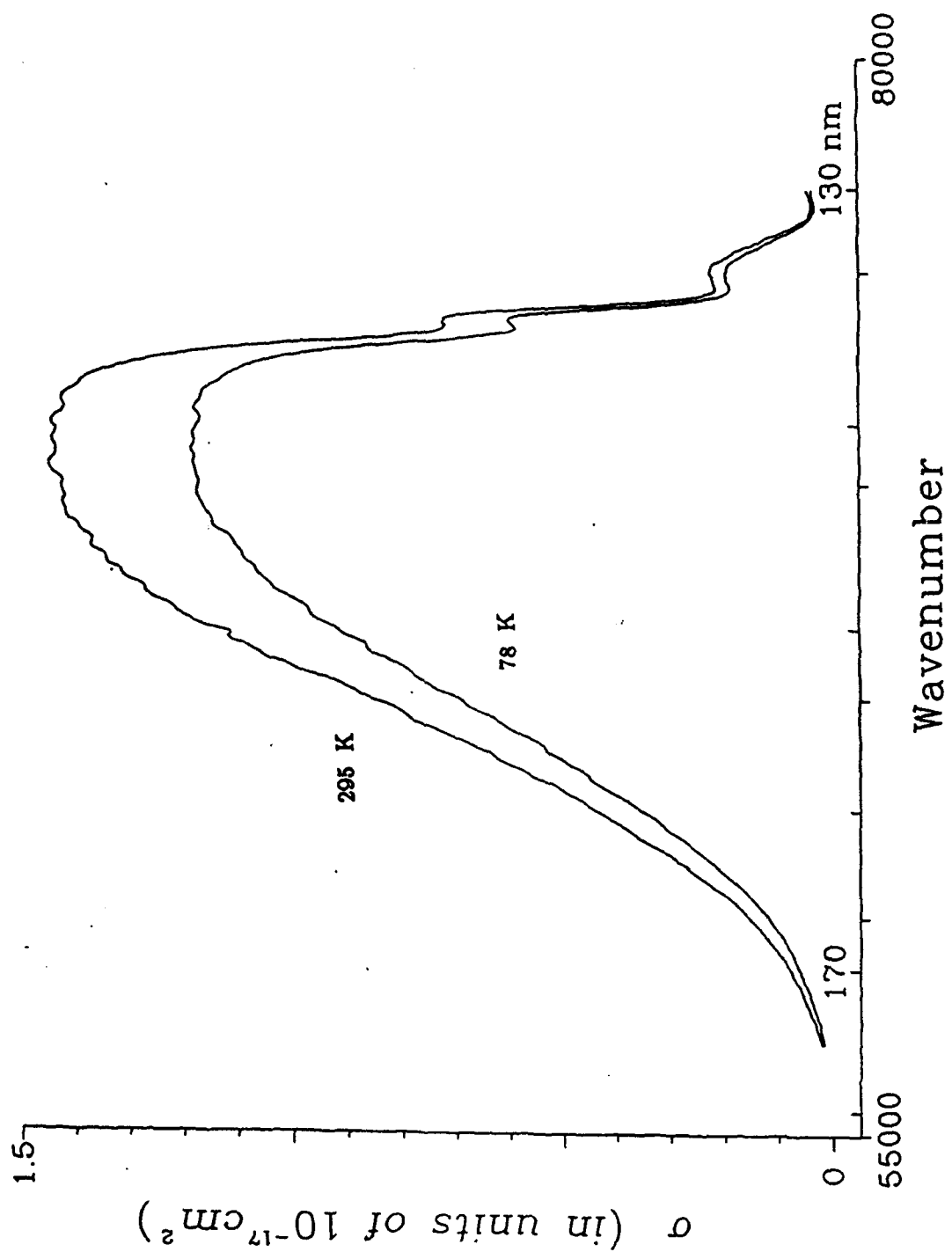


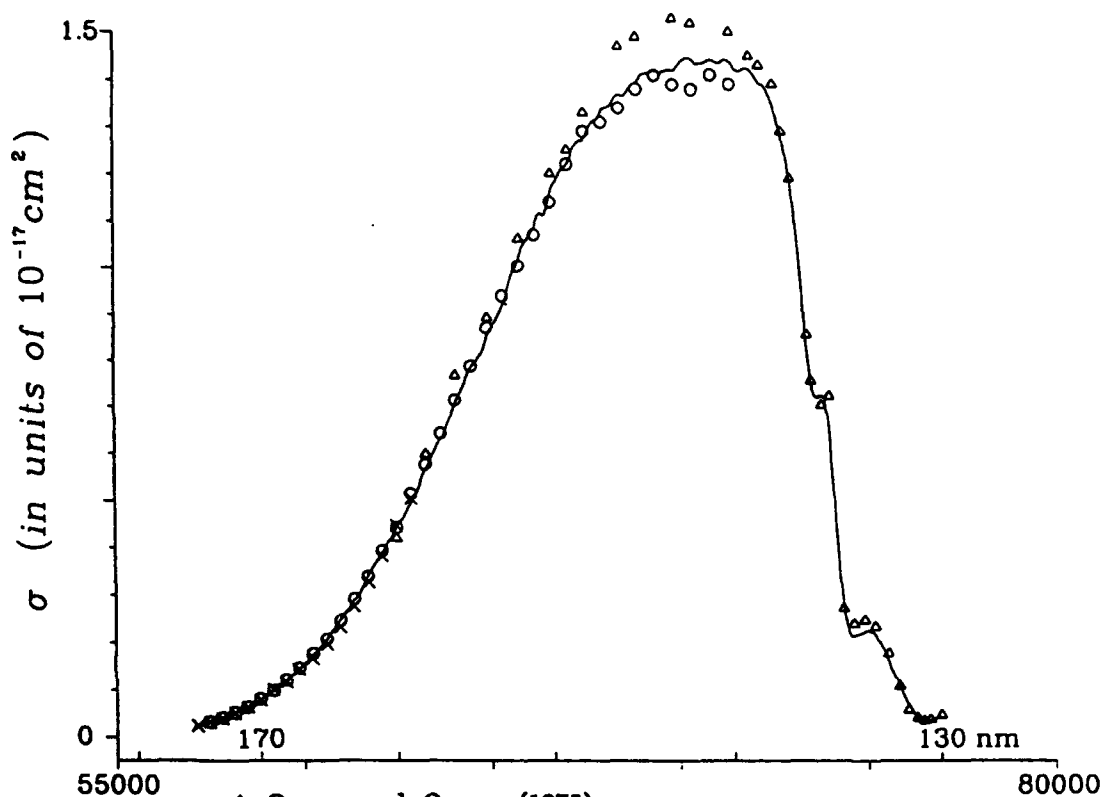
The absolute cross section measurements of Schumann-Runge
continuum at fixed wavelengths.

WL nm	Temp K	P _{high} Torr	P _{low} Torr	n	σ 10 ⁻¹⁸ cm ²
174.0	78 295	3.96 7.301	0.808 2.305	5 4	0.246 ± 0.003 0.311 ± 0.002
170.0	78 295	1.569 6.240	0.503 0.941	5 5	0.613 ± 0.006 0.792 ± 0.009
165.0	78 295	0.713 2.44	0.1171 0.3603	5 4	1.598 ± 0.014 2.05 ± 0.01
160.0	78 295	0.307 1.142	0.1044 0.1709	5 5	3.54 ± 0.03 4.40 ± 0.03
155.0	78 295	0.1794 0.647	0.0717 0.1026	4 5	6.25 ± 0.09 7.78 ± 0.07
150.0	78 295	0.1325 0.354	0.0718 0.0810	3 5	9.26 ± 0.09 11.47 ± 0.05
145.0	78 295	0.1166 0.351	0.0612 0.0834	3 5	11.39 ± 0.15 13.97 ± 0.08
140.0	78 295	0.1275 0.361	0.0729 0.0687	4 5	11.71 ± 0.08 14.36 ± 0.09
135.0	78 295	0.1994 0.800	0.0518 0.1058	5 5	4.87 ± 0.04 5.98 ± 0.07
130.1	78 295	2.942 10.40	0.802 1.636	4 5	0.351 ± 0.003 0.418 ± 0.005

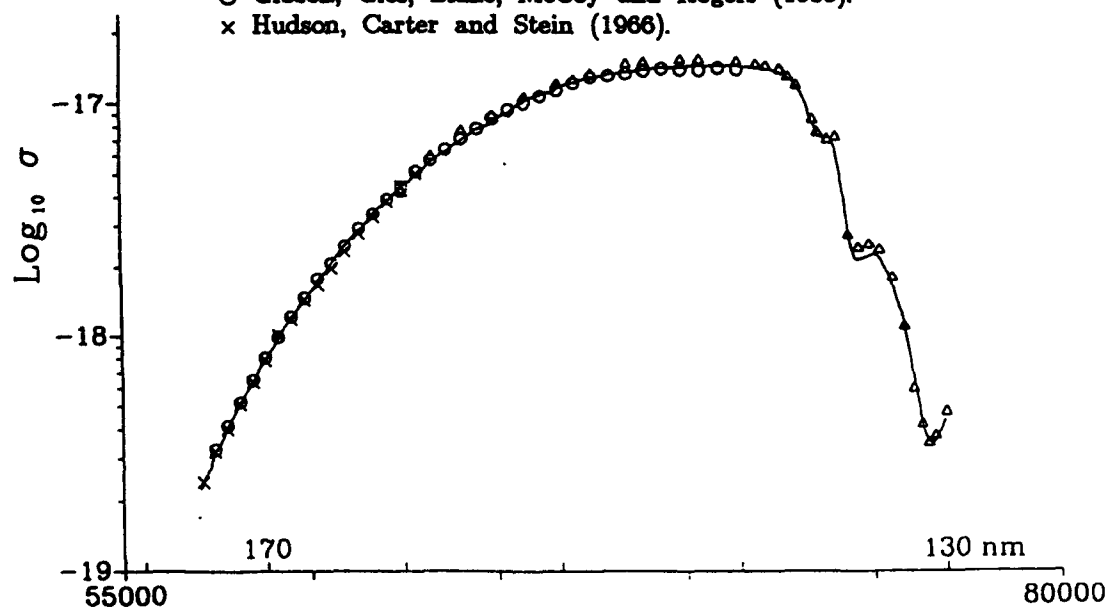
Scan Mode of Cross Section Measurements

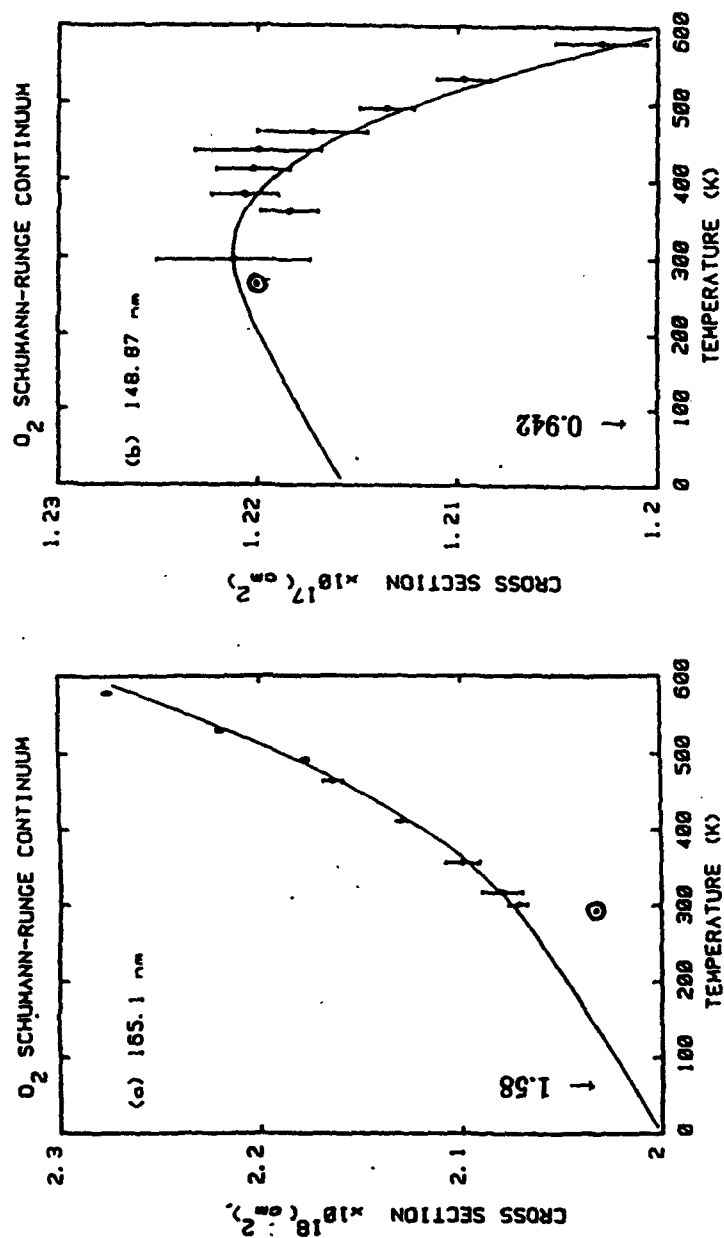






Δ Ogawa and Ogawa (1975).
 \circ Gibson, Gies, Blake, McCoy and Rogers (1983).
 \times Hudson, Carter and Stein (1966).





Gibson *et al.* (1983)

**THE SPECTRAL RADIATION EXPERIMENT (SPECTRE): AN OVERVIEW -
CLEAR-SKY OBSERVATIONS AND THEIR USE IN ICRCCM**

R.G. Ellingson

Department of Meteorology, University of Maryland, College Park, MD 20742

W.J. Wiscombe, V. Kunde, H. Melfi

NASA Goddard Space Flight Center, Code 613, Greenbelt, MD 20771

J. DeLuisi

Air Resources Laboratory, NOAA/Environmental Research Laboratory, Boulder, CO 80303

D. Murcray

Department of Physics, University of Denver, 2400 S. Vine, Denver, CO 80208

W. Smith

**Space Science & Engineering Center, University of Wisconsin,
1225 W. Dayton Street, Madison, WI 53706**

Surface-based, high resolution observations of the spectral radiance in the 3 to 20 μm region were obtained simultaneously by three FTIR spectrometers concurrently with insitu and remote observations of atmospheric temperature and water vapor profiles and trace gases CO_2 , CH_4 , N_2O , O_3 , F11 and F12 as part of the FIRE Cirrus II field experiment. The spectrometers were self- and inter-calibrated in the field to achieve close to 1% accuracy. The presentation will summarize the data obtained for selected clear-sky cases, and comparisons of model calculations with observations will be used to illustrate how the data may be used to clarify uncertainties associated with calculations of the effects of trace gases as found by the international Intercomparison of Radiation Codes in Climate Models (ICRCCM).

ON THE USE OF GROUND-BASED REMOTE SENSORS TO PROVIDE TEMPERATURE AND MOISTURE SOUNDINGS FOR ATMOSPHERIC TRANSMISSION MODELS

J.C. Liljegren

Battelle, Pacific Northwest Laboratory, Richland, WA 99352

R.O. Knuteson

University of Wisconsin, 1225 W. Dayton Street, Madison, WI, 53706

A general goal of the Atmospheric Radiation Measurement (ARM) Program of the DOE is to advance the state-of-the-art for models of atmospheric transmission through comparison of model-calculated radiance spectra with measured spectra. ARM will rely primarily on ground-based remote sensors to acquire the input temperature and moisture profiles simultaneously with the radiance measurements. To support this strategy, we present comparisons of measured infrared radiance spectra with spectra calculated using FASCODE for two balloon-borne systems, NCAR-CLASS and NWS, and two remote sensing systems, the NOAA/WPL 6-channel microwave profiler (MWP) and the High-resolution Infrared Sounder (HIS), which were co-located and simultaneously operated during the Ground-based Atmospheric Profiling EXperiment (GAPEX) described by Smith et al. (1990). Our results show that, at least for the relatively dry conditions which prevailed during GAPEX, the calculations based on the remote sensor-based profiles were at least as accurate as those using the balloon-borne systems.



**On the Use of Ground-Based Remote Sensing
to
Provide Temperature and Moisture Profiles
for
Atmospheric Transmission Models**

**James C. Liljegren
Pacific Northwest Laboratory**

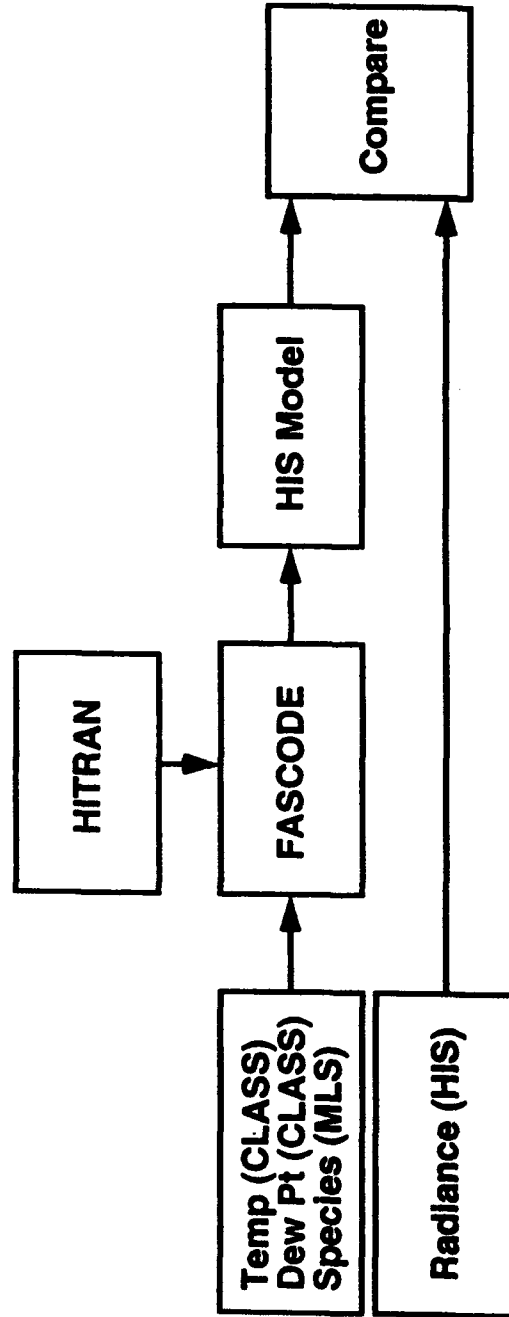
**Robert O. Knuteson
University of Wisconsin**

**Review Conference on Atmospheric Transmission Models
Hanscom AFB, MA
June 3, 1992**

Experiment Design

Science Team Experiment (GAPEX)

- Compare remote sensors against radiosondes
- Compare FASCODE / HITRAN against HIS





The GAPEX Data Set

"Ground-based Atmospheric Profiling Experiment"
Denver Stapleton Airport, 29 Oct. - 4 Nov. 1988

CLASS Radiosondes - NCAR

Pressure, Temperature and Humidity using Vaisala RS-80L

NWS Radiosonde - NWS

Pressure, Temperature and Humidity (using VIZ carbon hygristor)

Microwave Profiler (MWP) - NOAA/WPL

2-channel water vapor radiometer - total vapor and cloud liquid plus
crudely resolved vertical profiles of water vapor

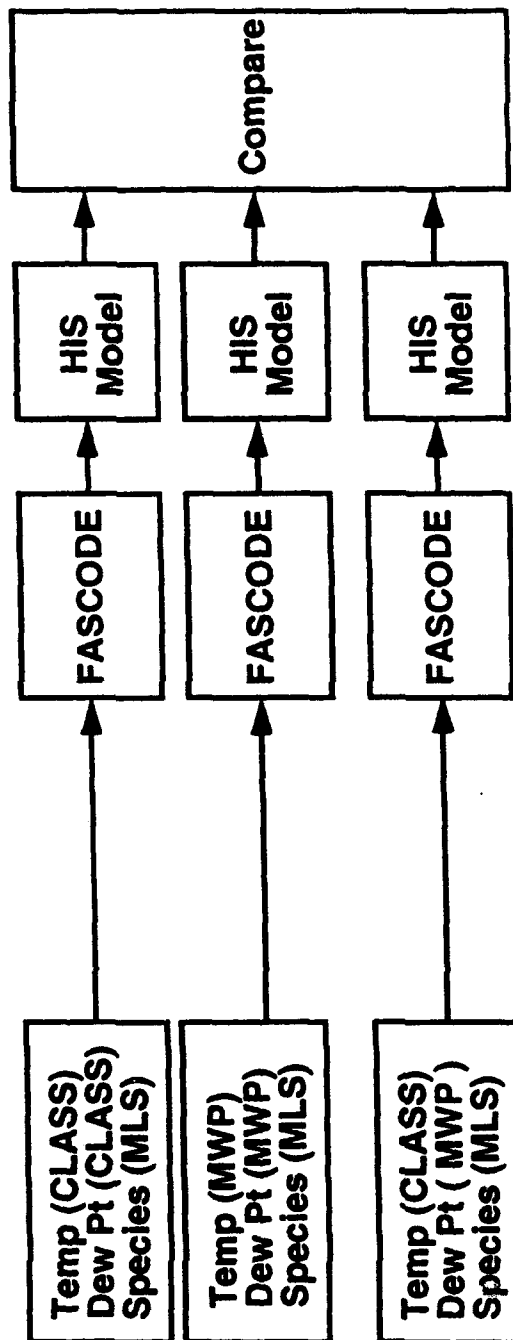
4-channel microwave temperature profiler - vertical profiles of
temperature

High-resolution Interferometer Sounder (HIS) - U of Wisc

IR radiances

Retrieved vertical profiles of temperature and humidity

Testing Method

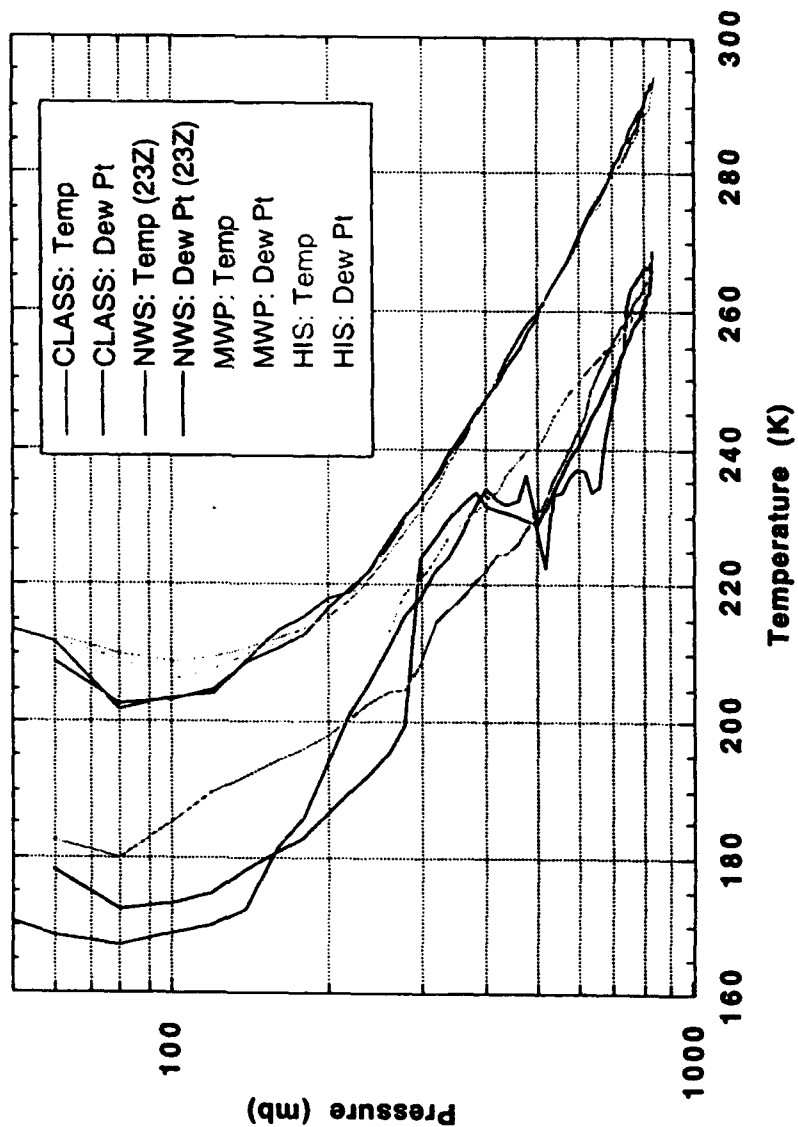


ARM



Vertical Profiles

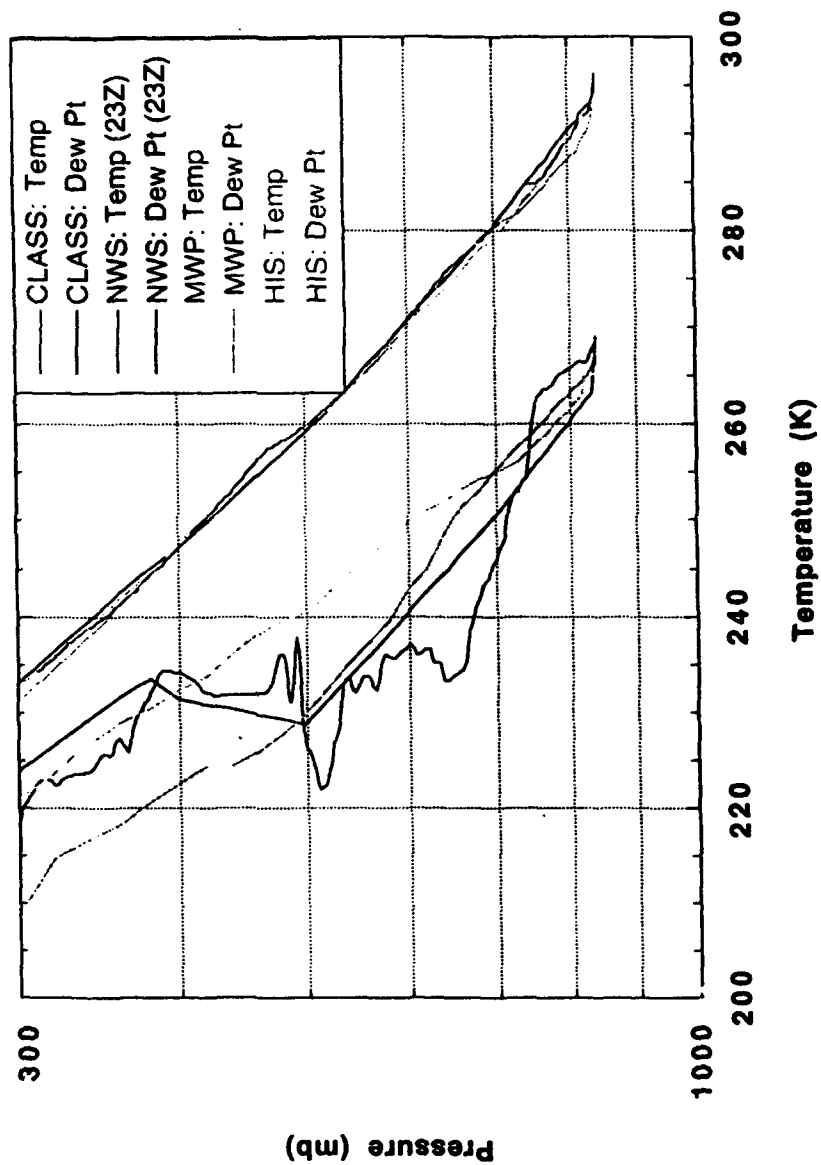
GAPEX - 31 Oct 88, 20Z





Profiles Revisited

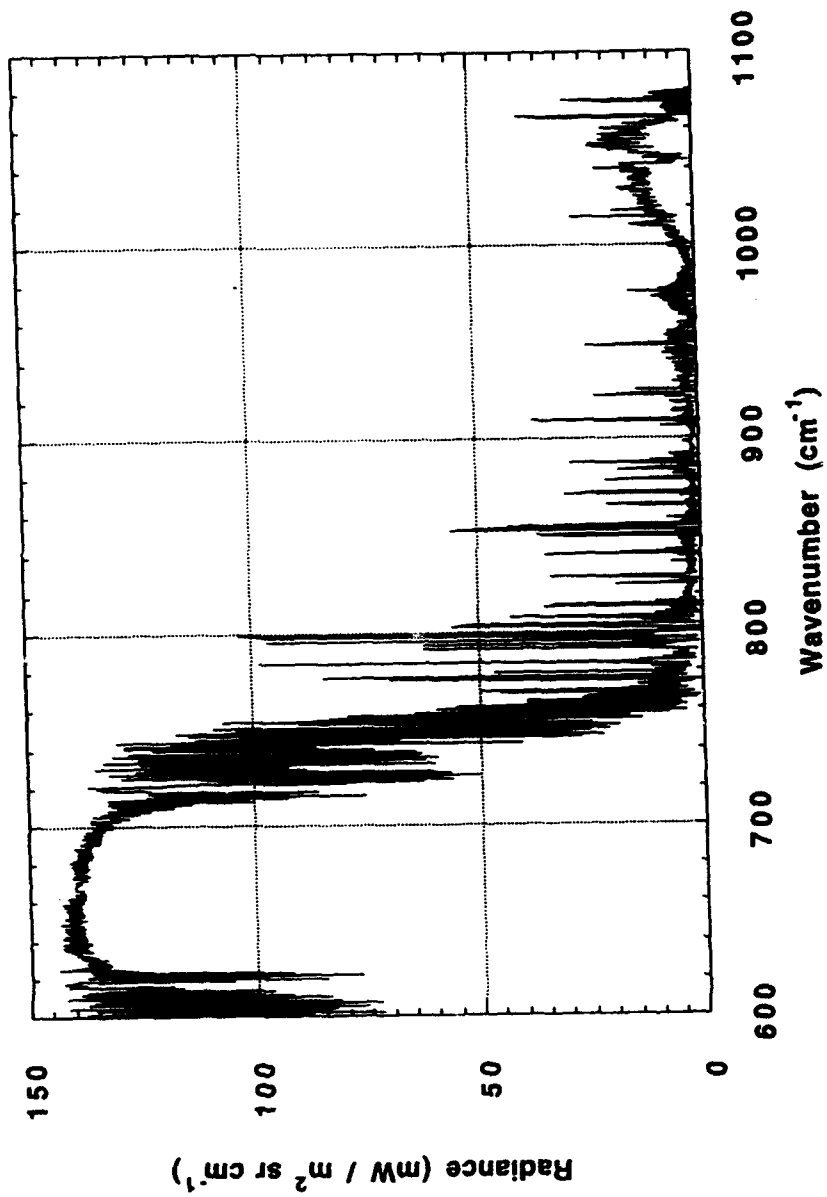
GAPEX - 31 Oct 88, 20Z





HIS Radiances

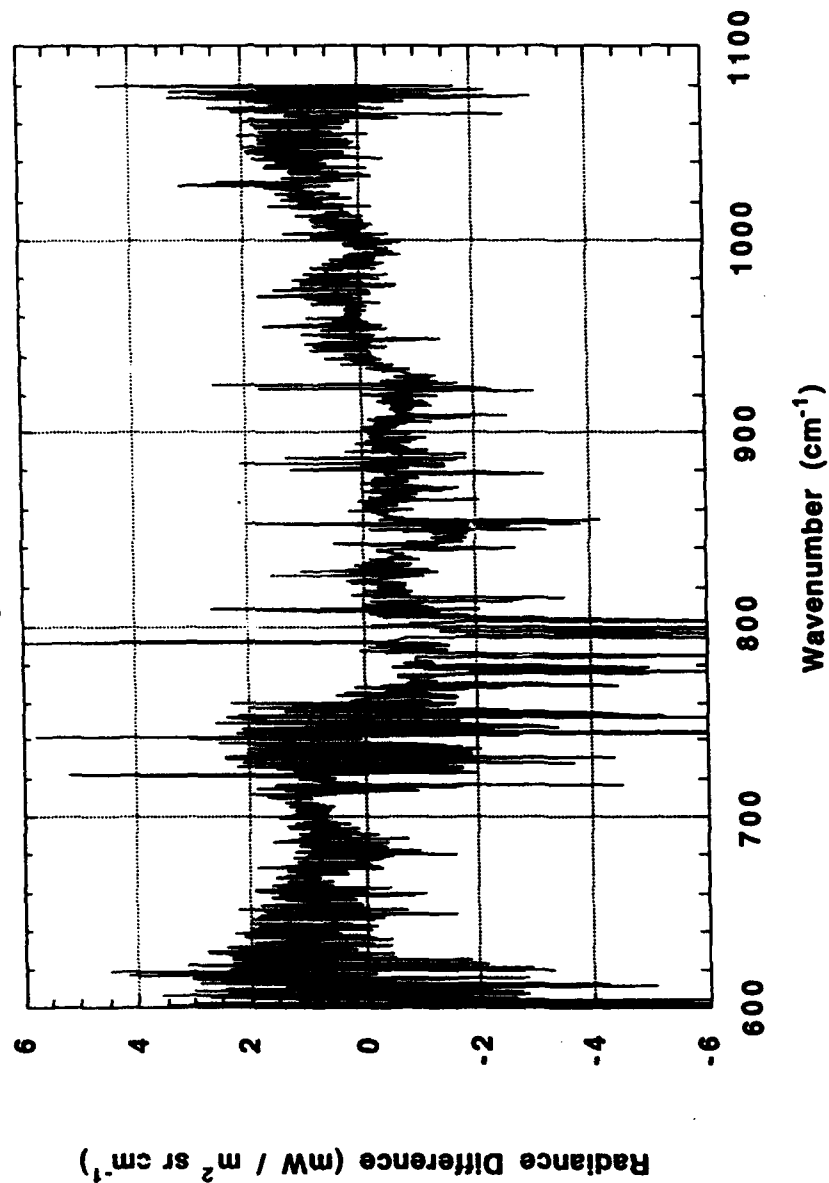
GAPEX 31 Oct 88 - HIS Observations



ARM

Comparison

GAPEX 31 Oct 88
FASCODE calcs using CLASS minus HIS radiances



ARM

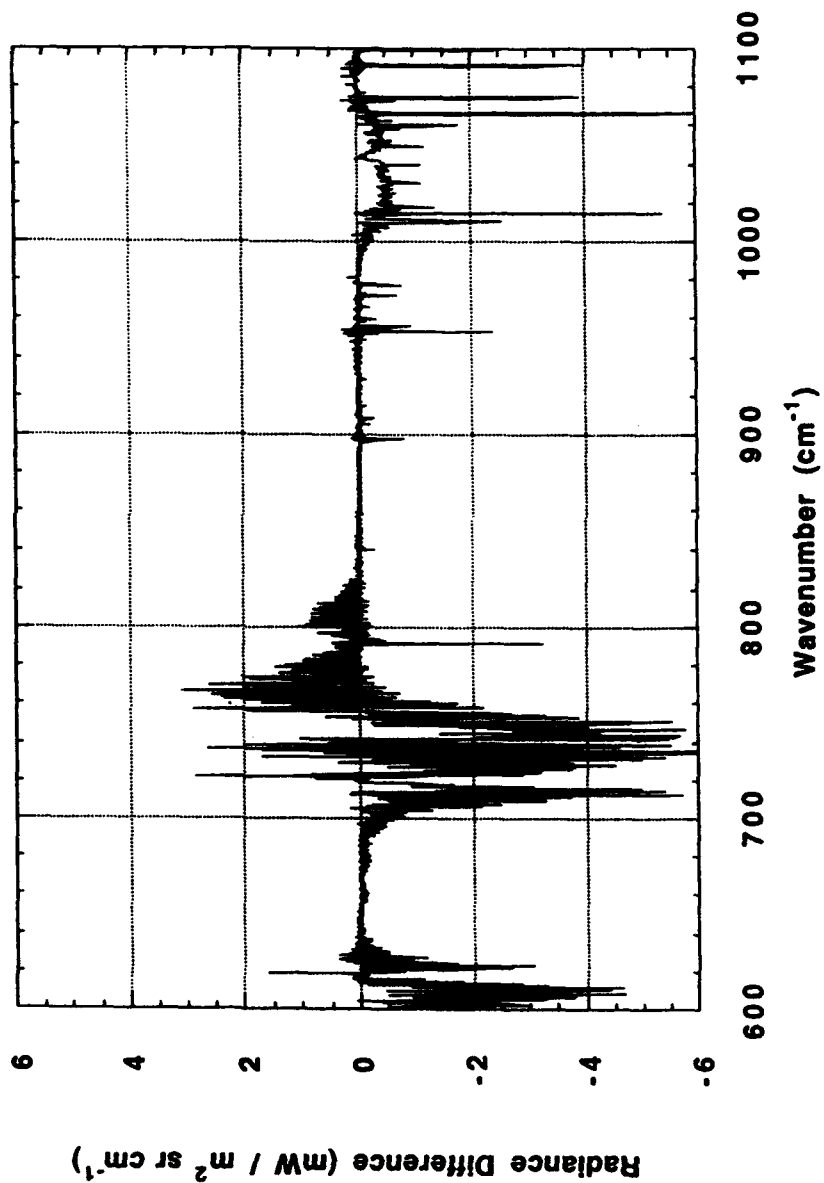


HITRAN 86 VS 91

GAPEX 31 Oct 88

FASCODE calcs using CLASS

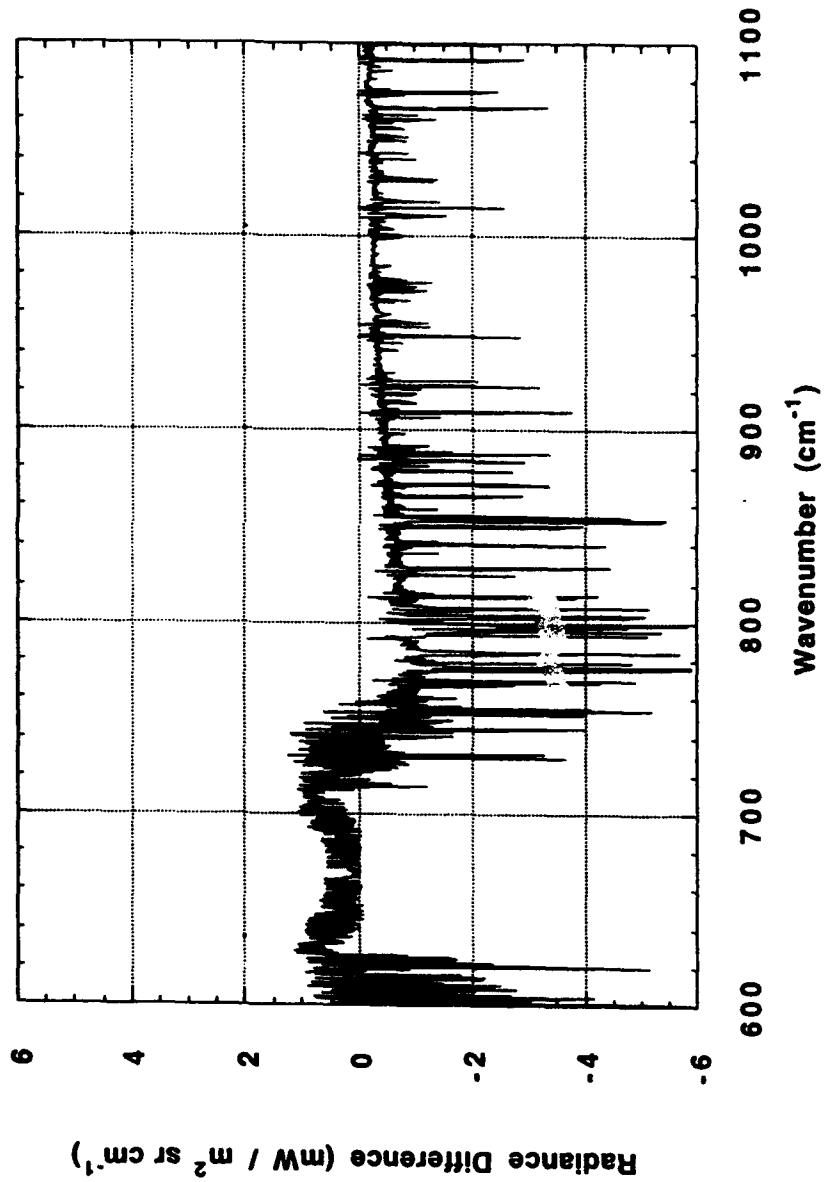
HITRAN91 - HITRAN86





NWS

GAPEX 31Oct 88
F(NWS,NWS)-F(CLASS,CLASS)

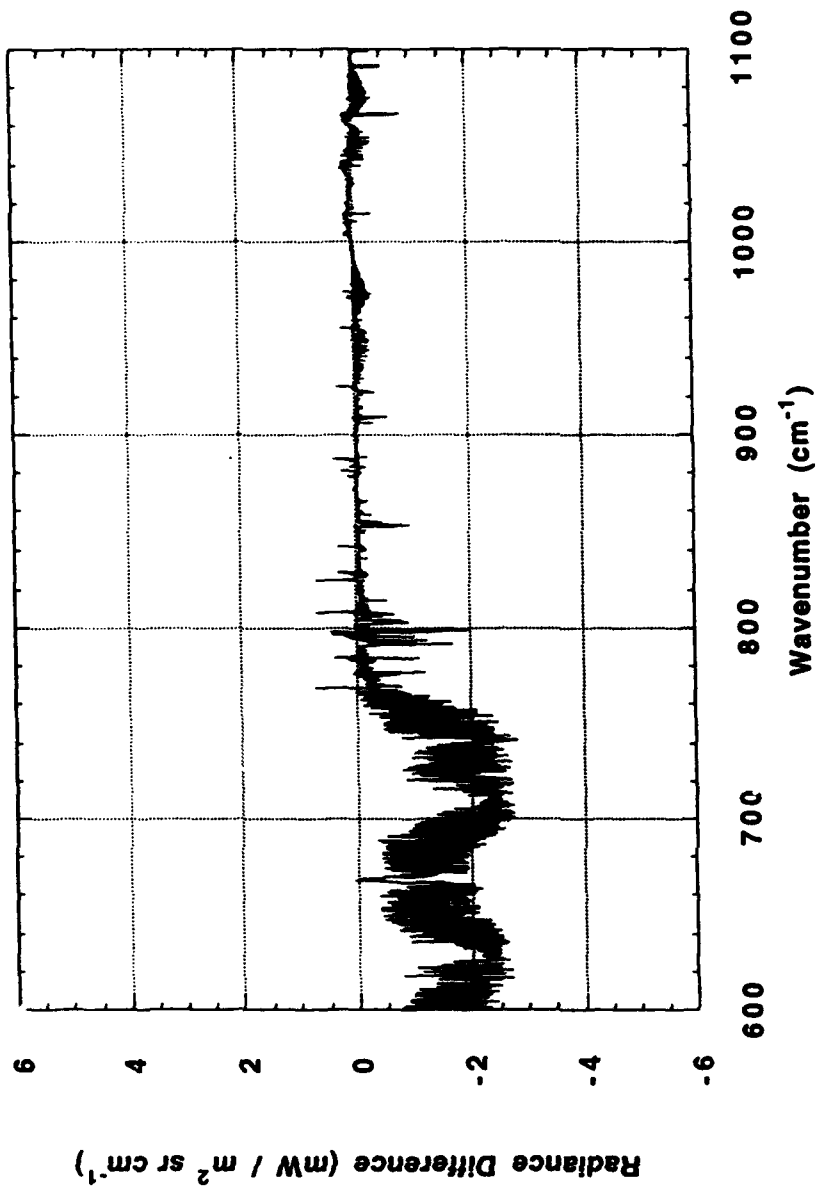


ARM



MWP

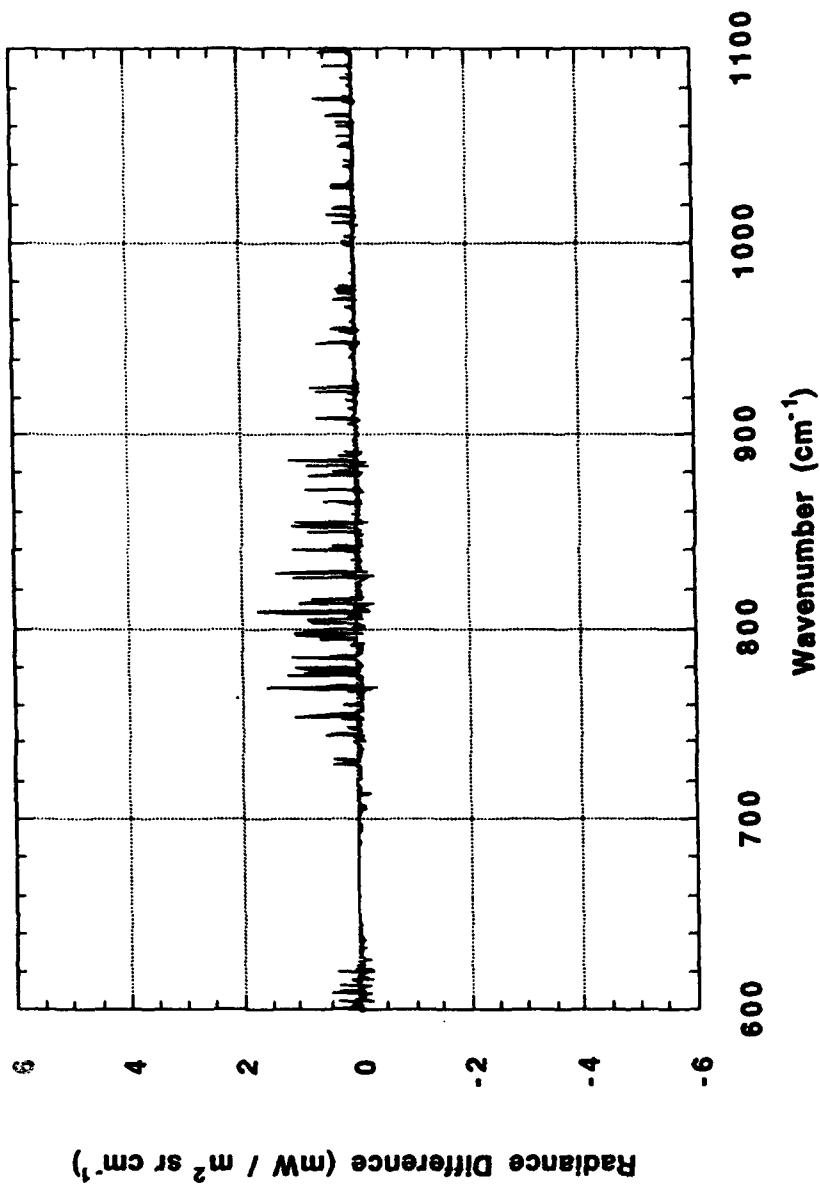
GAPEX 31 Oct 88
F(MWP,MWP)-F(CLASS,CLASS)



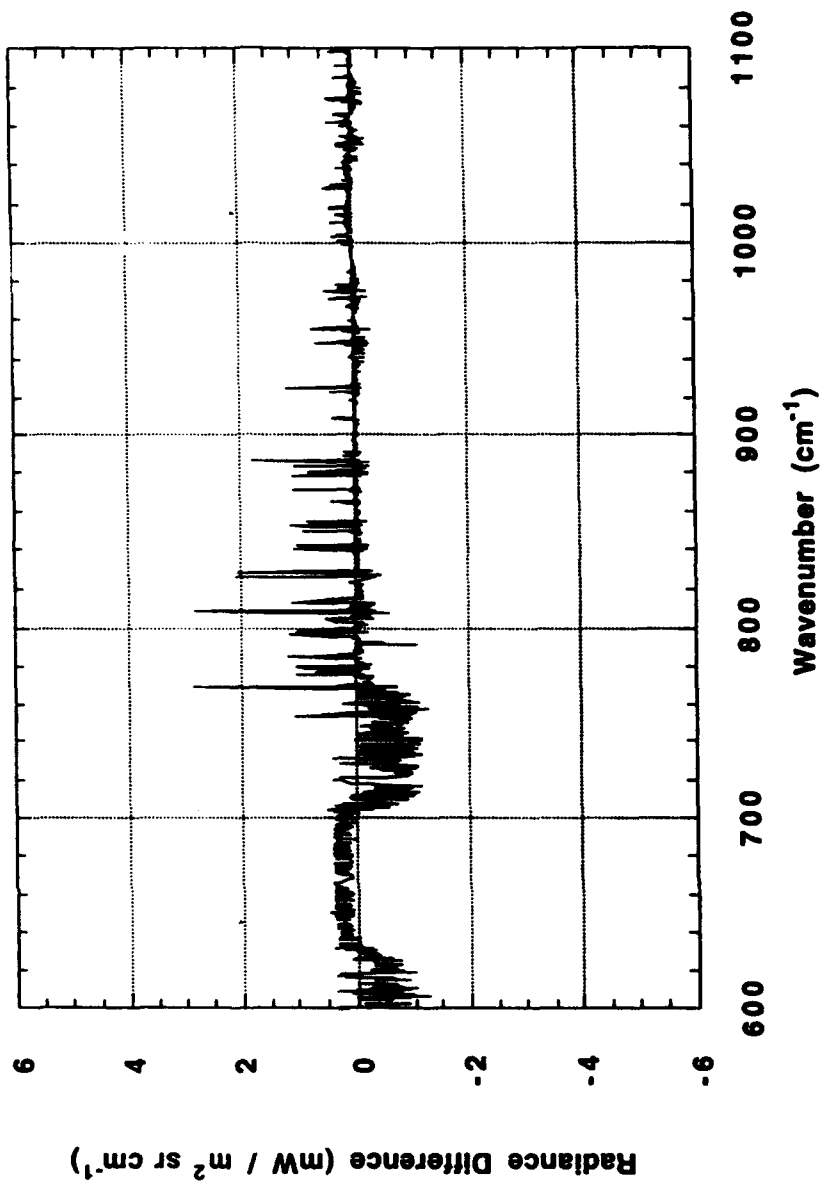
ARM

MWP: Dew Pt Only

GAPEX 31 Oct 88
F(CLASS,MWP)-F(CLASS,CLASS)



GAPEX 31 Oct 88
F(HIS,HIS)-F(CLASS,CLASS)





Integrated Radiance Differences

GAPEX Oct 31, 1988
Residual Integration/Normalization

ΔI	$\int_{600}^{1080} \Delta I(\nu) d\nu$	$\frac{\int \Delta I d\nu}{\int \Delta I_{F(C,C)-HIS} d\nu}$	$\frac{\int \Delta I d\nu}{\int I_{HIS} d\nu}$
Residual Calculation	$mW / m^2 sr$		
F(C,C) - HIS	504.4329	1.0	0.02356
F(C,C) ₉₁ - F(C,C) ₈₆	235.1824	0.46623	0.01099
F(M,M) - F(C,C)	310.053	0.61466	0.01448
F(C,M) - F(C,C)	41.606	0.08248	0.00194
F(N,N) - F(C,C)	351.616	0.69705	0.01643
F(H,H) - F(C,C)	107.312	0.21274	0.00501
HIS	21406.140		

Discussion

Residual errors using remote sensors are small

Results reproducible for other GAPEX data (1 Nov 88, 11Z)

Humidity was low during GAPEX study

Examination of higher humidity cases necessary

Remote sensors representative of model physics

Instantaneous, concurrent, co-located, spatial averages

Correct column-integrated vapor amount



Additional Studies Useful

Higher humidity cases

WISP / ARM91 (Platteville, CO)

FIRE II / SPECTRE (Coffeyville, KS)

Other radiative quantities

Heating/cooling rates through the atmosphere

Multiple sensors

915 and 50 MHz RASS, satellites, etc

Test merging / retrieval algorithms

MODEL CLIMATOLOGIES OF TRACE SPECIES IN THE ATMOSPHERE

M.E. Summers

Naval Research Laboratory, Upper Atmospheric Physics Branch, Washington, DC 20375

W.J. Sawchuck

Computational Physics, Inc., P.O. Box 788, Annandale, VA 22003

G.P. Anderson

Geophysics Directorate, Phillips Laboratory, Hanscom AFB, MA 01731

A set of model climatologies of important chemically and optically active trace species in the atmosphere has been developed for use with atmospheric radiance/transmittance codes. The new climatologies include monthly mean pressure/temperature/density fields along with N₂, O₂, O₃, O, H₂O, CH₄, CO₂, CO, NO₂, N₂O, and HNO₃ which represent zonally averaged abundances for the altitude range 0 - 120 km, at 10 degree latitude intervals. For O₃ and O, day/night ratios are tabulated. The climatologies incorporate observations of trace species abundances where available and validated model extrapolations in other regions. Variances about the monthly mean values have been deduced from selected observational data sets and provide estimates of variability in the constituent fields. The generation of the climatologies will be discussed and selected portions will be shown. Community access to the climatologies will also be discussed.

MODEL CLIMATOLOGIES OF TRACE SPECIES IN THE ATMOSPHERE

M.E. Summers, Naval Research Laboratory

W.J. Sawchuck, Computational Physics, Inc.

G.P. Anderson, Geophysics Directorate, Phillips Laboratory

Presentation at:

**ANNUAL REVIEW CONFERENCE ON ATMOSPHERIC TRANSMISSION MODELS
2-3 June 1992
Geophysics Directorate, Phillips Laboratory
Hanscom AFB, MA 01742**

MODEL CLIMATOLOGIES OF TRACE SPECIES IN THE ATMOSPHERE

M.E. Summers

Naval Research Laboratory, Upper Atmospheric Physics Branch, Washington, DC 20375

W.J. Sawchuck

Computational Physics, Inc., P.O. Box 788, Annandale, VA 22003

G.P. Anderson

Geophysics Directorate, Phillips Laboratory, Hanscom AFB, MA 01731

A set of model climatologies of important chemically and optically active trace species in the atmosphere has been developed for use with atmospheric radiance/transmittance codes. The new climatologies include monthly mean pressure/temperature/density fields along with N₂, O₂, O₃, O, H₂O, CH₄, CO₂, CO, NO₂, N₂O, and HNO₃ which represent zonally averaged abundances for the altitude range 0 - 120 km, at 10 degree latitude intervals. For O₃ and O, day/night ratios are tabulated. The climatologies incorporate observations of trace species abundances where available and validated model extrapolations in other regions. Variances about the monthly mean values have been deduced from selected observational data sets and provide estimates of variability in the constituent fields. The generation of the climatologies will be discussed and selected portions will be shown. Community access to the climatologies will also be discussed.

TRACE CONSTITUENT CLIMATOLOGY DATABASE

GRAPHICAL INTERFACE

and

TAPE FORMATS

William J. Sawchuck

Computational Physics, Inc.

Annandale, VA

and

Michael E. Summers

E. O. Hulburt Center for Space Research

Naval Research Laboratory, Washington, DC

18 May 1992

I. INTRODUCTION

The Trace Constituent Climatology Database represents a self-consistent combination of observational data sets and photochemical-dynamical model simulations of atmospheric trace constituents for the altitude region between the surface and 120 km. It provides a zonally averaged global description of the monthly mean distributions of O_3 , H_2O , CO , CO_2 , CH_4 , NO_2 , N_2O , HNO_3 , O , O_2 , and N_2 for each month of the year. In addition, climatologies of the average night/day variation of ozone mixing ratio, reference atmospheres (pressure, temperature, density) and trace species statistical variability fields have been incorporated into the database.

This document provides a brief overview of the contents, file structures, and record formats which are needed to access the Trace Constituent Climatology Database tape. In addition, descriptions and source listings are given for all FORTRAN and IDL programs which have been provided with the database. A representative set of cross sectional plots is provided which illustrates the output of the Trace Constituent Climatology Graphical Interface (TCCGI). A detailed description of the data sources and models which were used to generate this climatological database is provided in a separate report.

II. DATABASE CONTENT

The Trace Constituent Climatology Database currently consists of 27 individual parameter fields. These fields are classified as follows:

Reference Atmosphere Climatology

- (1) Pressure
- (2) Temperature
- (3) Density

Ozone Diurnal Variability

- (4) Average Night/Day Variation of O_3 mixing ratios

Trace Species Climatology (Mixing Ratios)

- (5) O_3
- (6) H_2O
- (7) CO
- (8) CO_2
- (9) CH_4
- (10) NO_2
- (11) N_2O
- (12) HNO_3
- (13) O
- (14) O_2
- (15) N_2

Trace Species Variability (Std. Dev.)

- (16-17) O_3
- (18-19) H_2O
- (20-21) NO_2
- (22-23) HNO_3
- (24-25) N_2O
- (26-27) CH_4

The trace species variability fields (fields 16-27) in the above list, represent the standard deviations of daily zonal mean trace species profile measurements about the monthly zonal mean. They have been incorporated into the climatology database in terms of mixing ratios and as deviations (in percent) from the monthly mean for each constituent. Therefore, there are two parameter fields associated with each trace constituent for which these variability values were calculated.

The database contains monthly mean climatologies (January-December) for each of the 27 parameter fields as listed above. Each of these parameter fields have been mapped onto a standard Latitude-Altitude grid with a spatial coverage and resolution as follows:

LATITUDE GRID

90°S - 90°N (10° resolution)

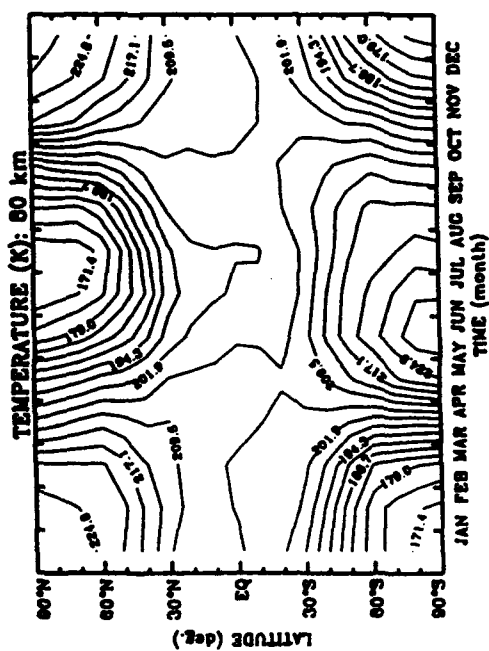
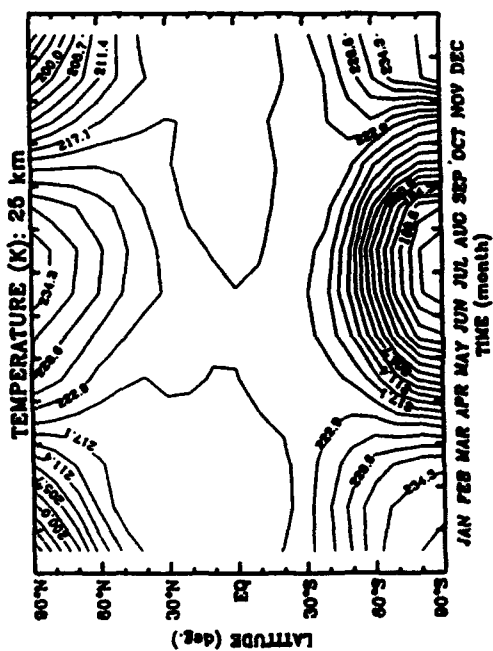
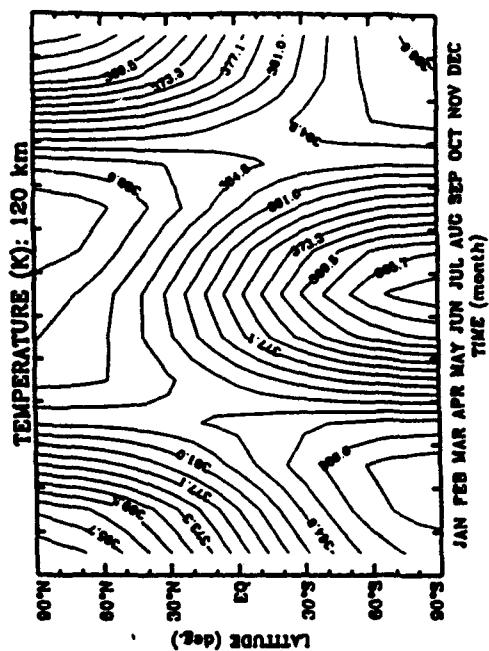
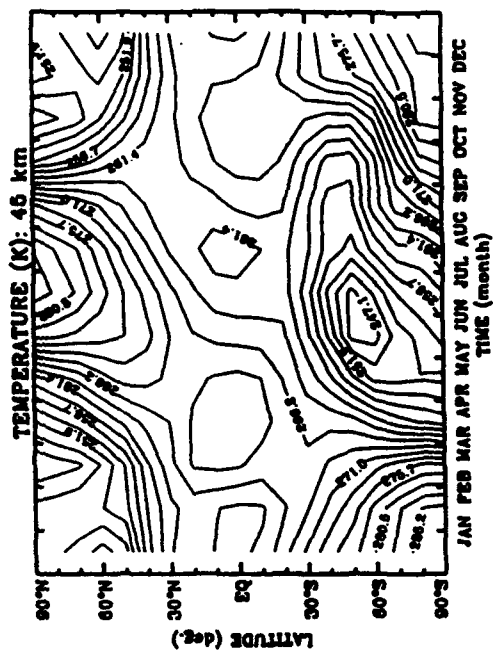
ALTITUDE GRID

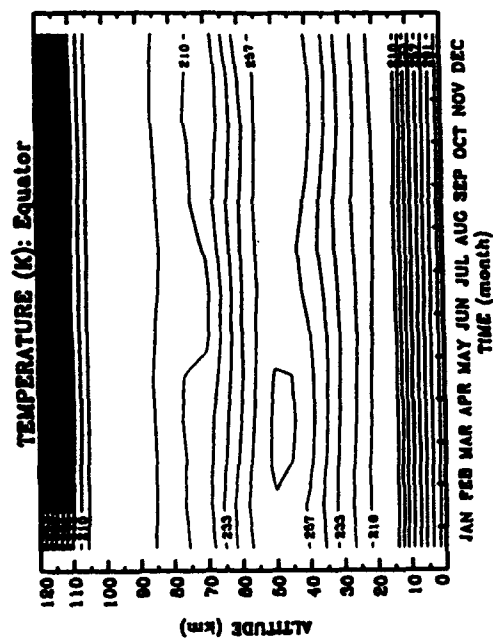
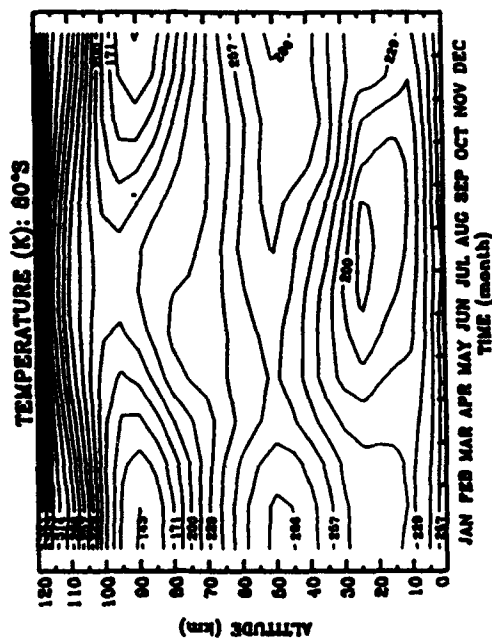
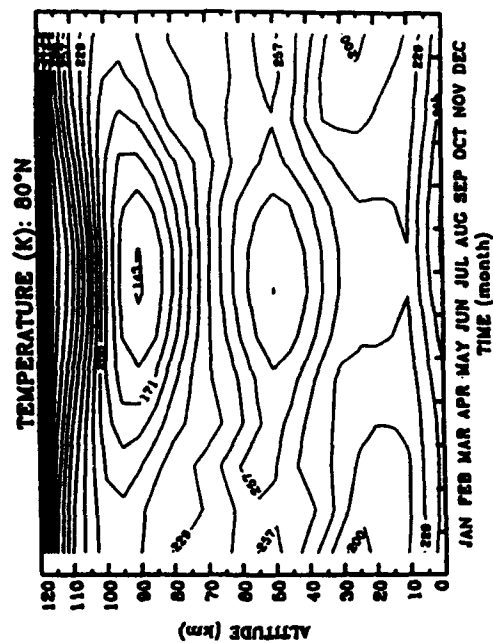
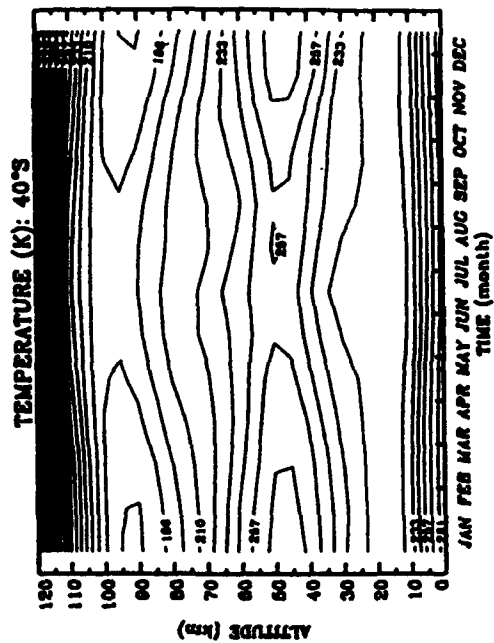
0 km - 25 km (1 km resolution)

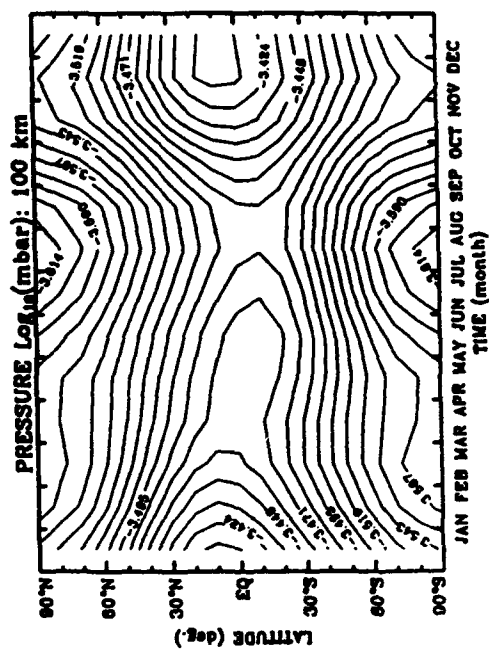
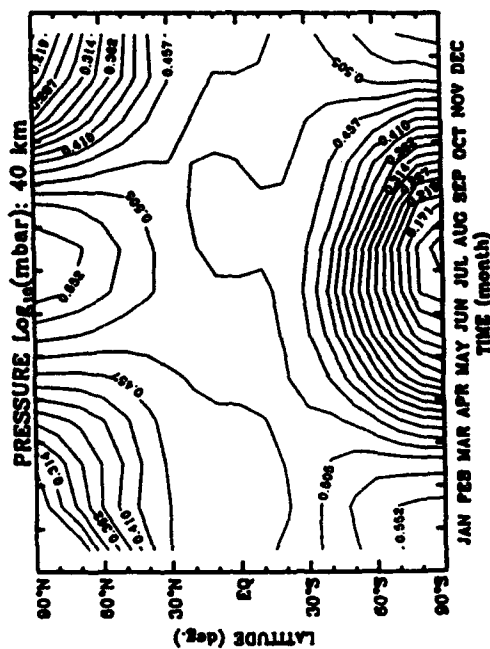
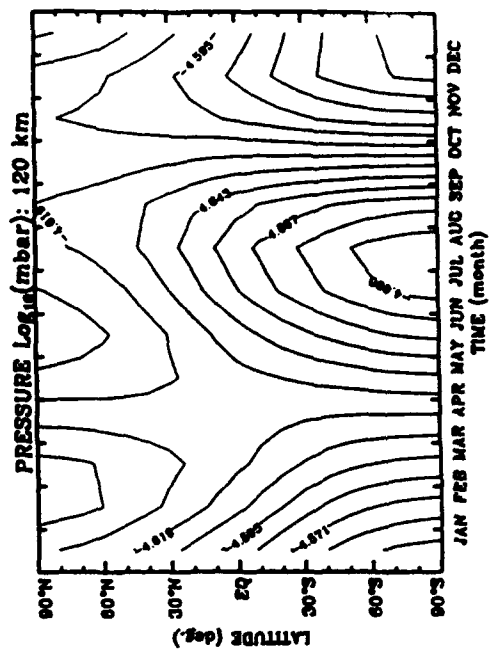
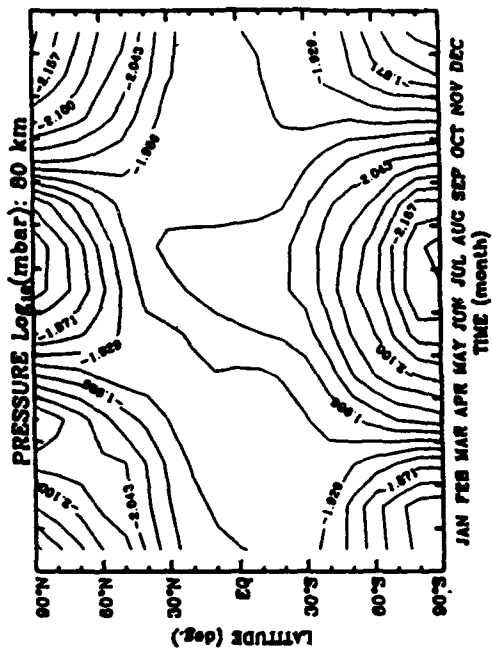
25 km - 120 km (5 km resolution)

APPENDIX H

Figures: Reference Atmosphere Climatology

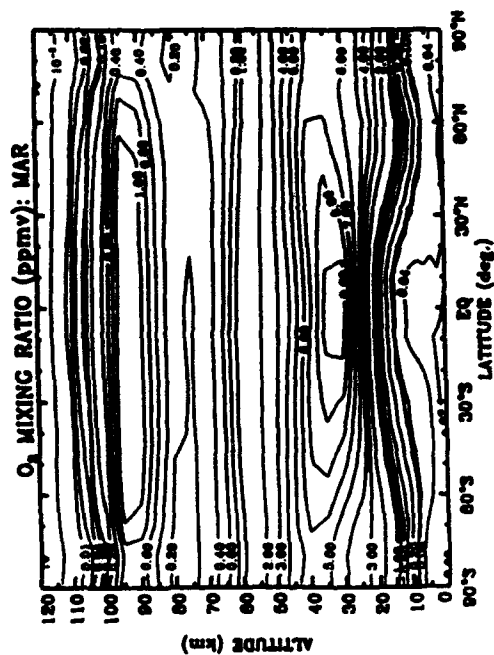
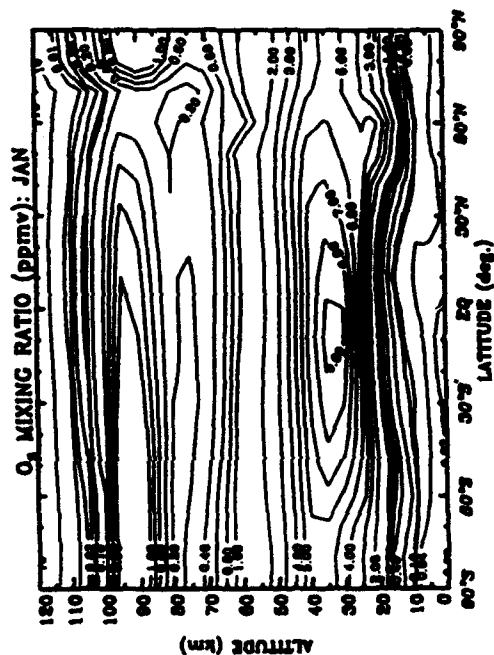
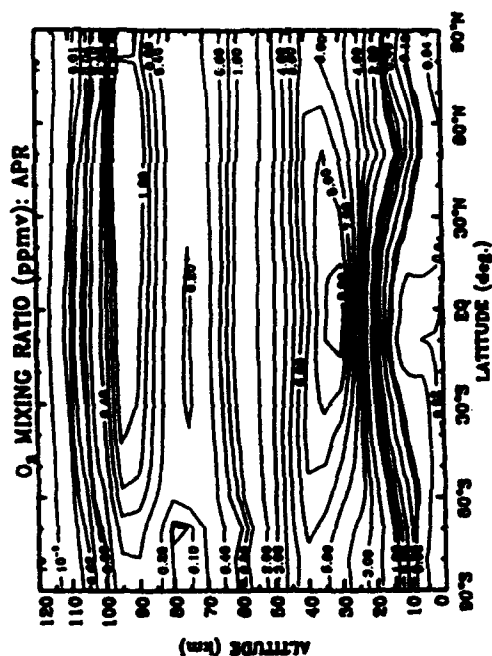
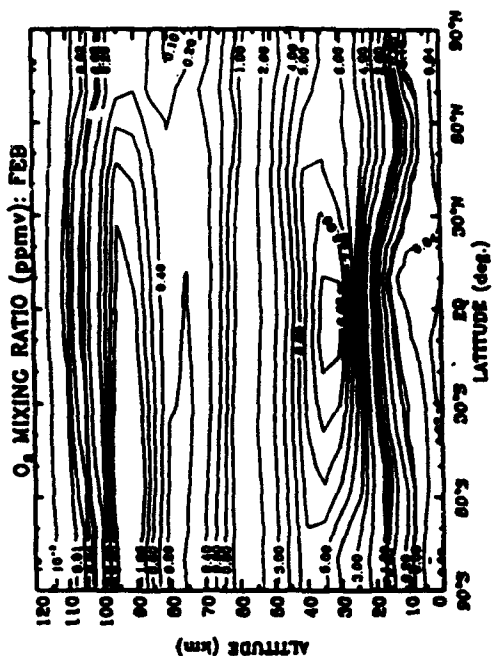


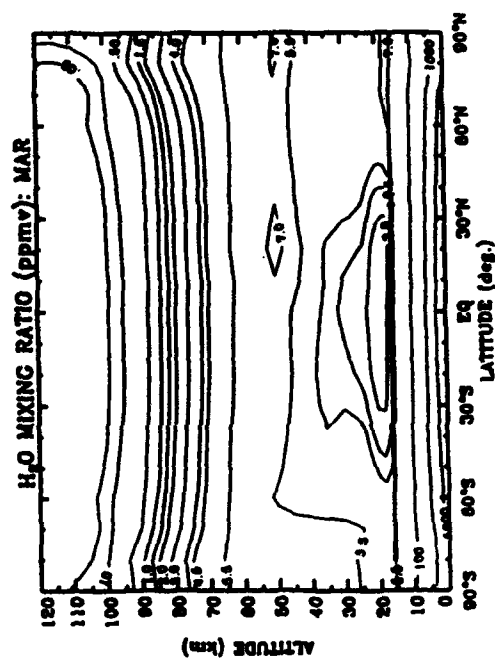
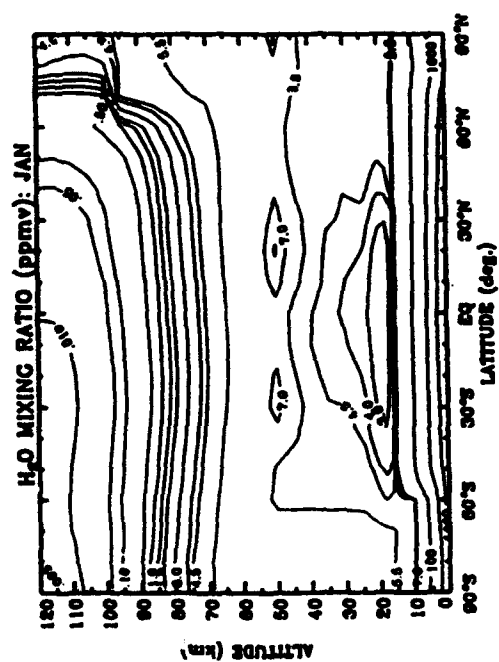
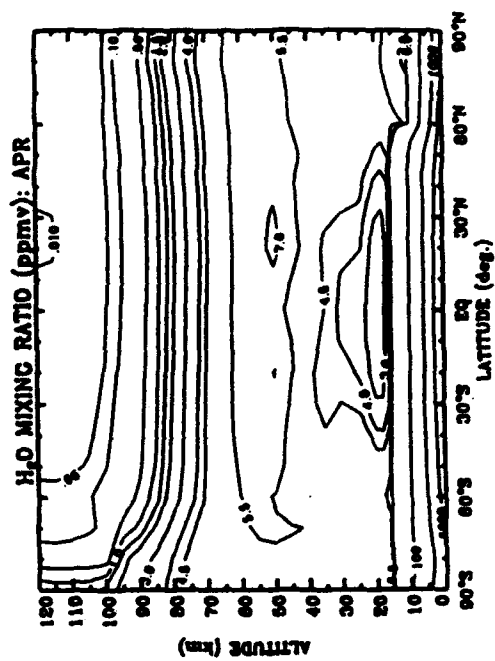
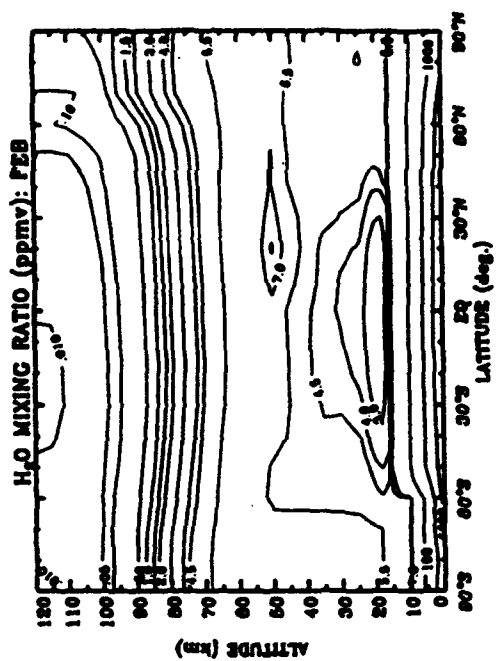


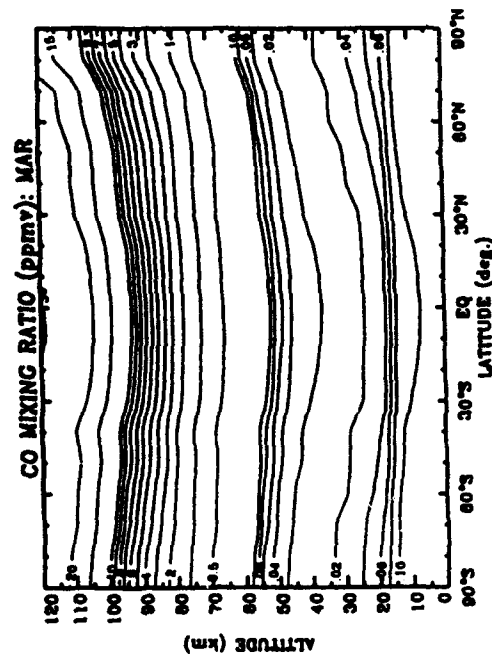
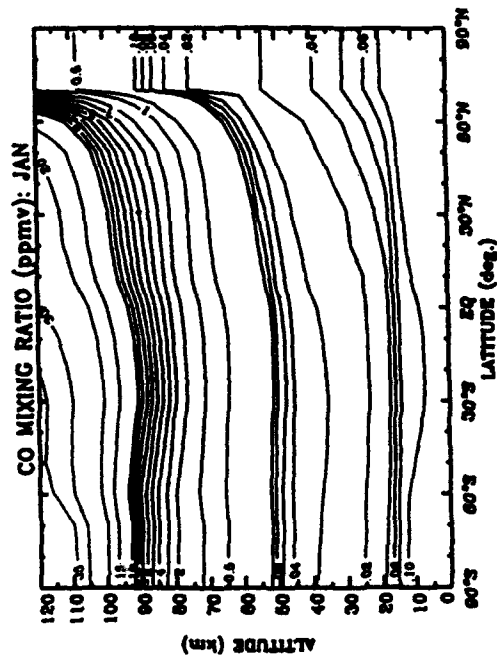
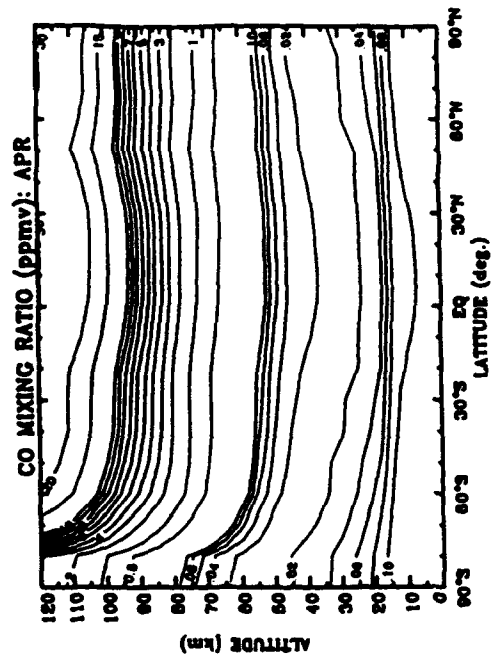
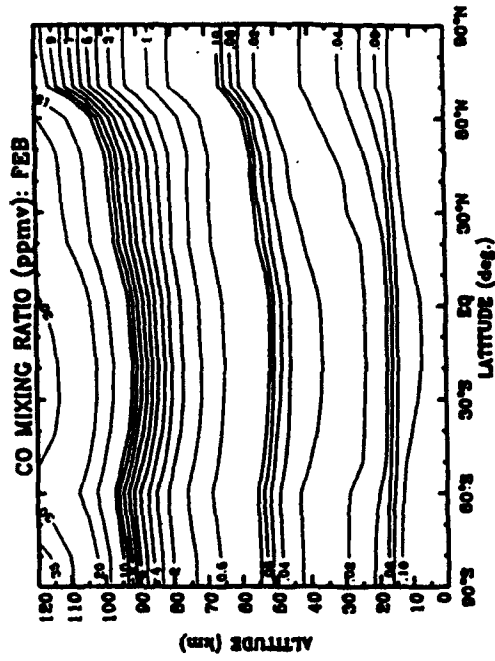


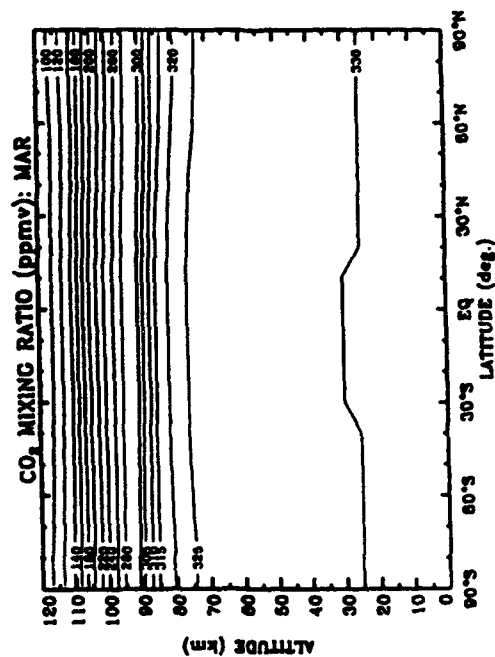
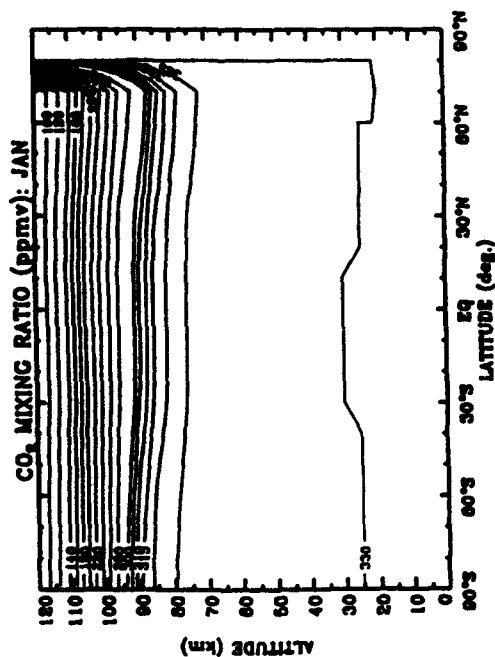
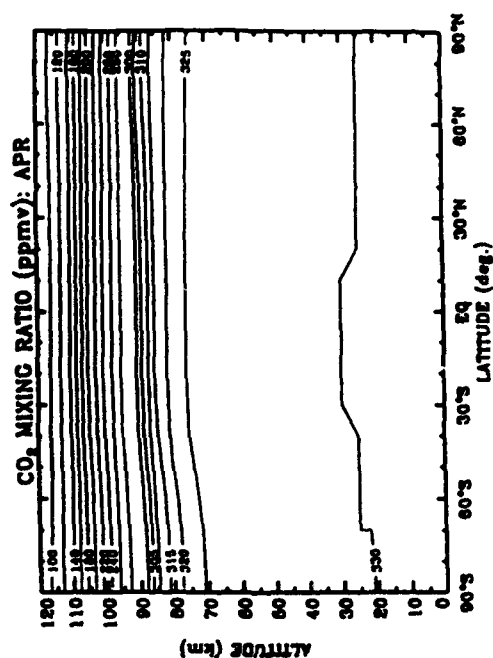
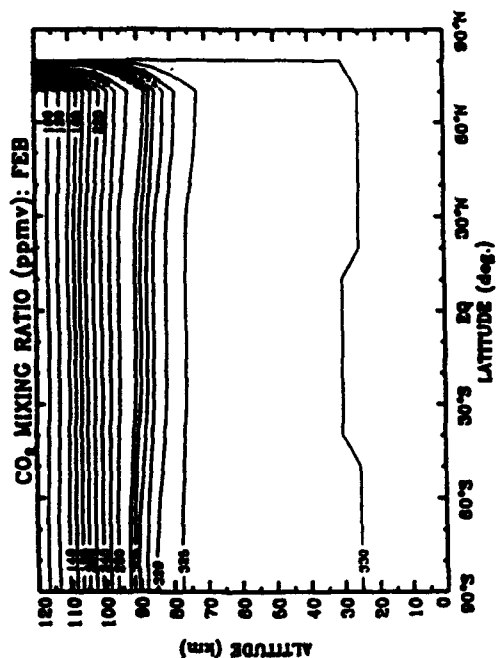
APPENDIX J

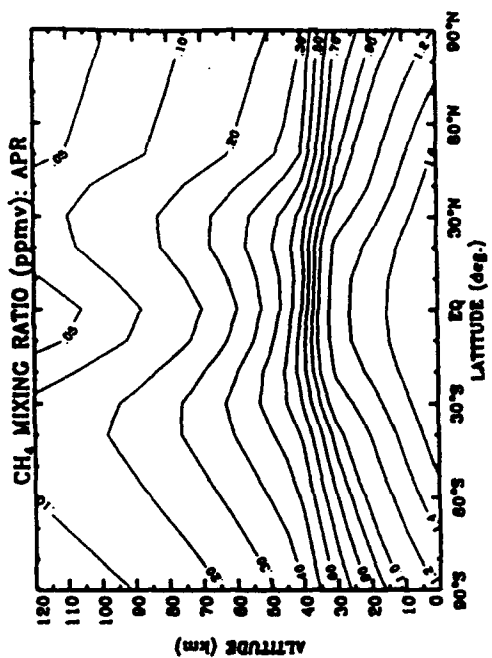
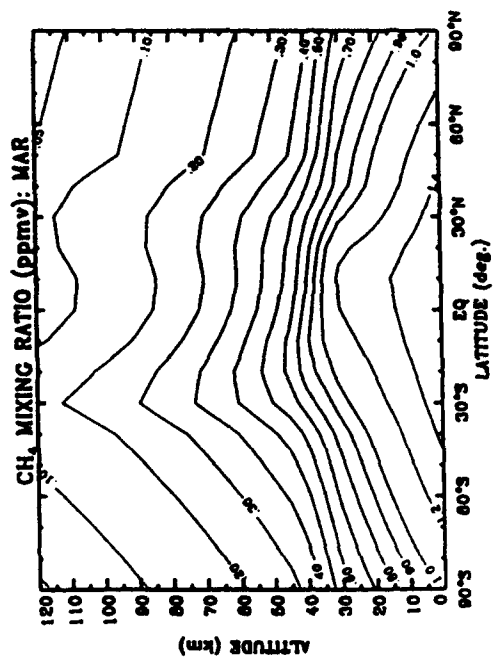
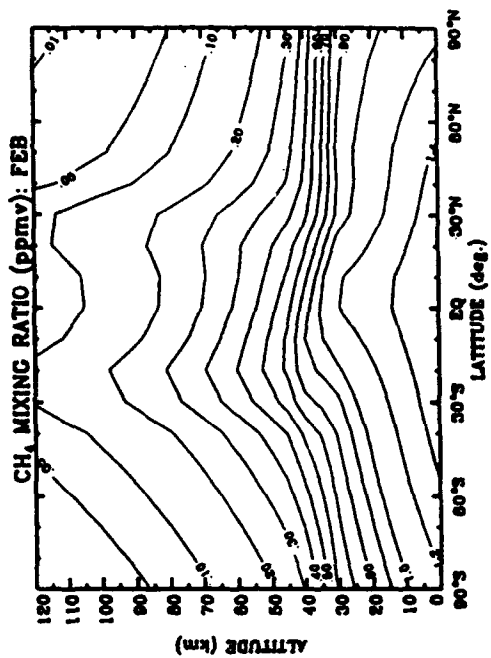
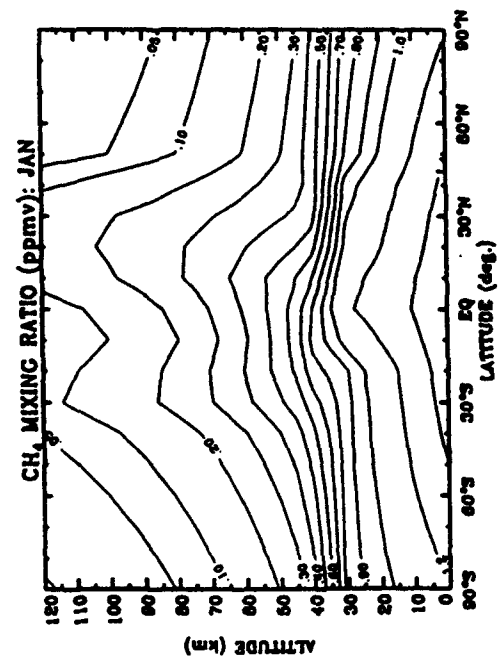
Figures: Trace Species Climatology

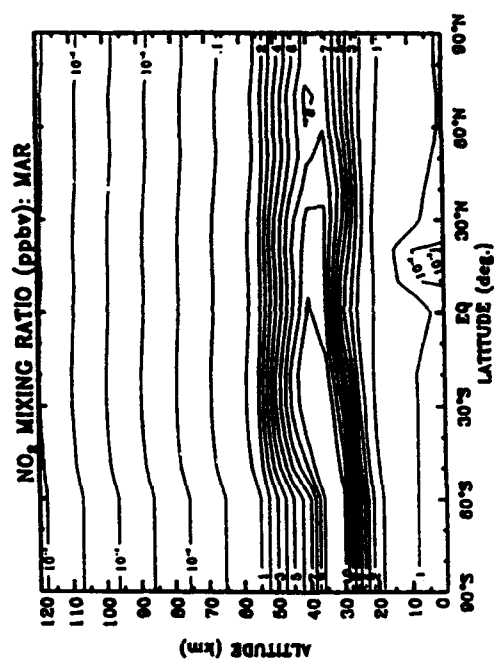
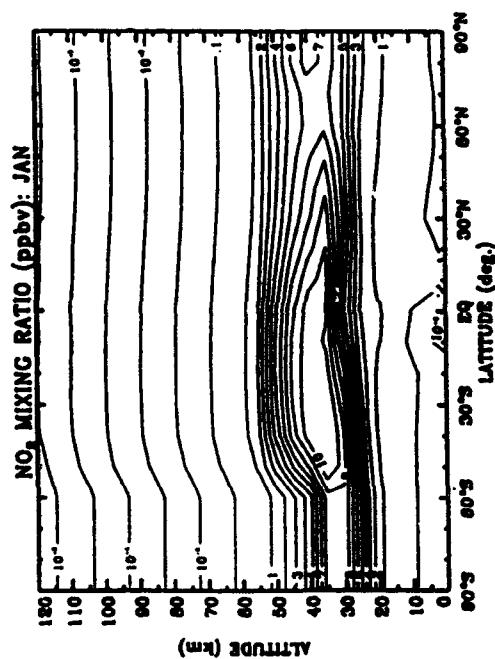
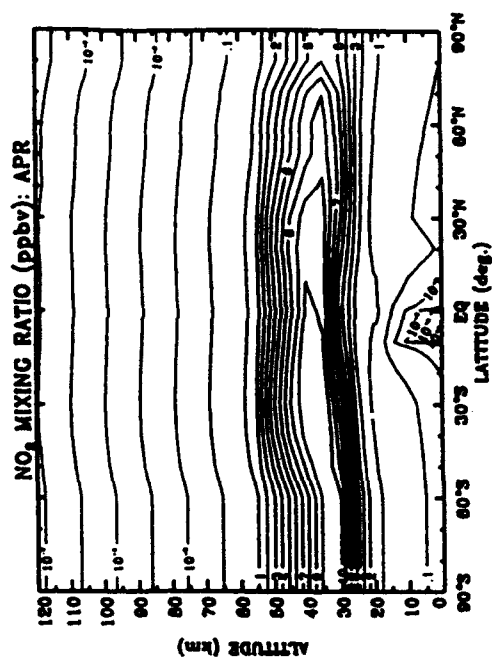
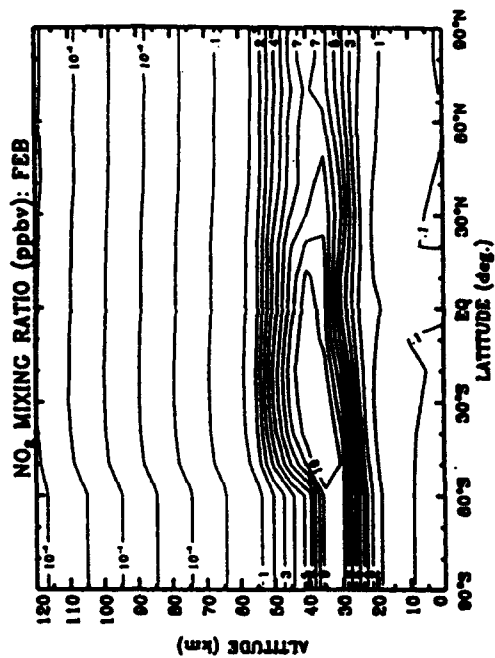


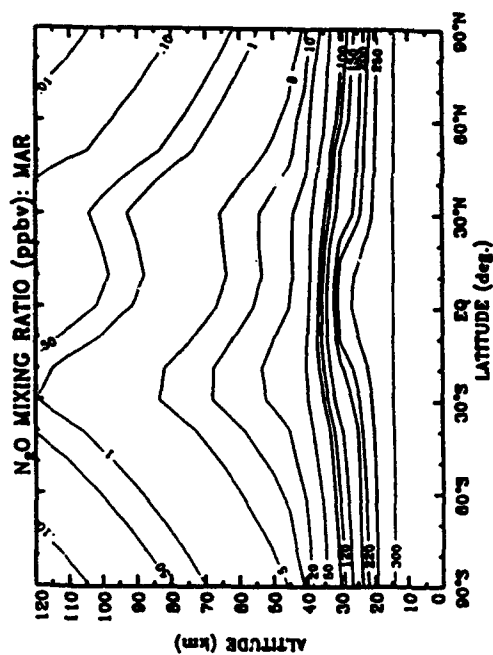
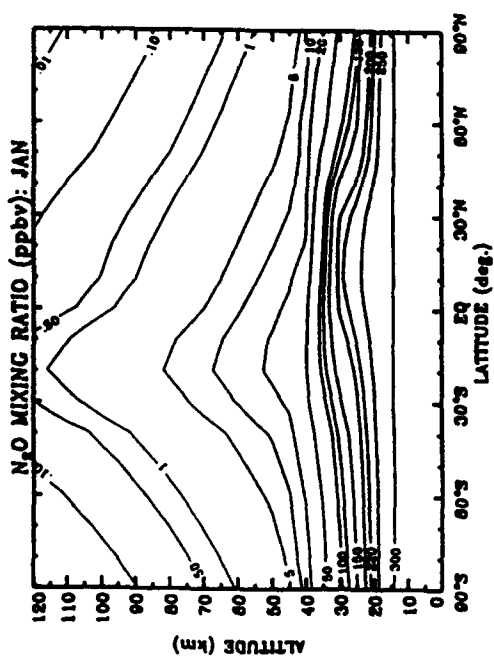
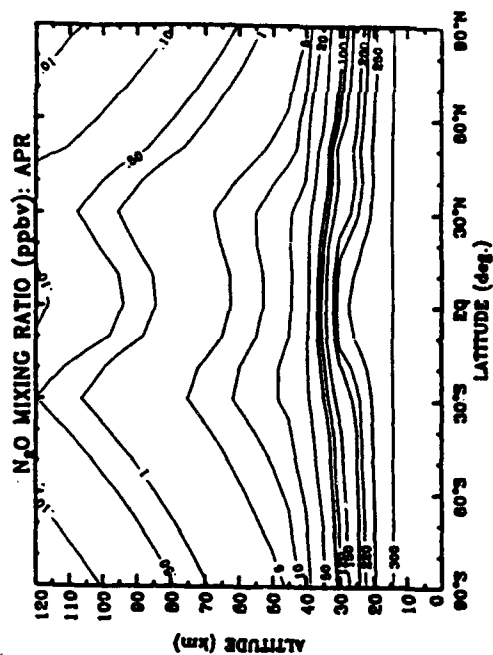
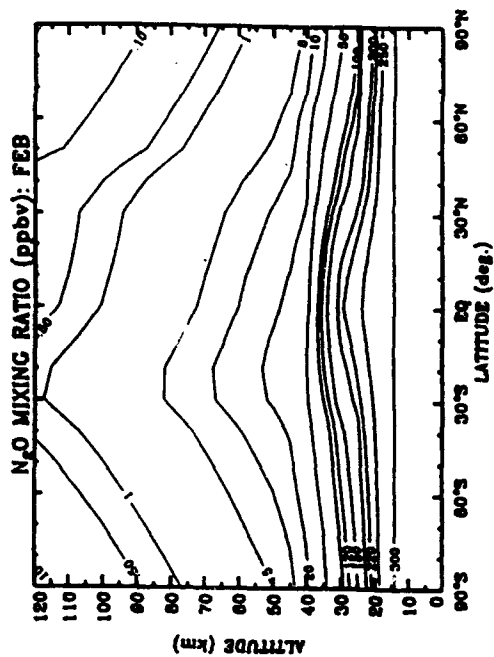


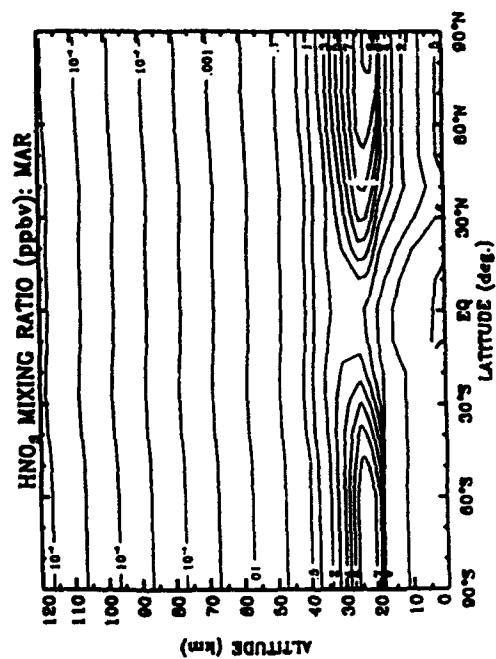
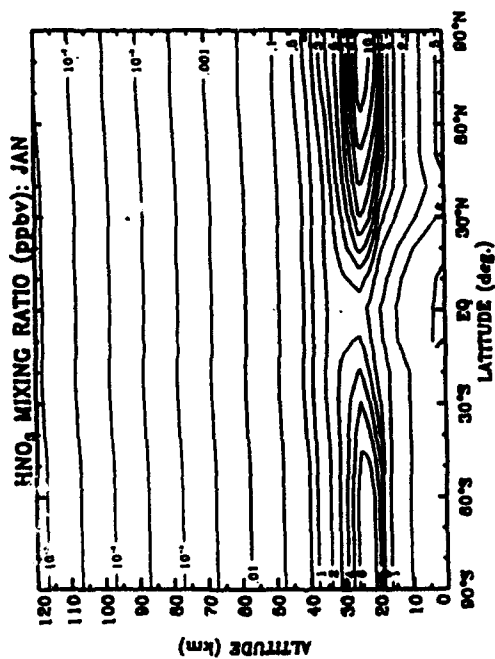
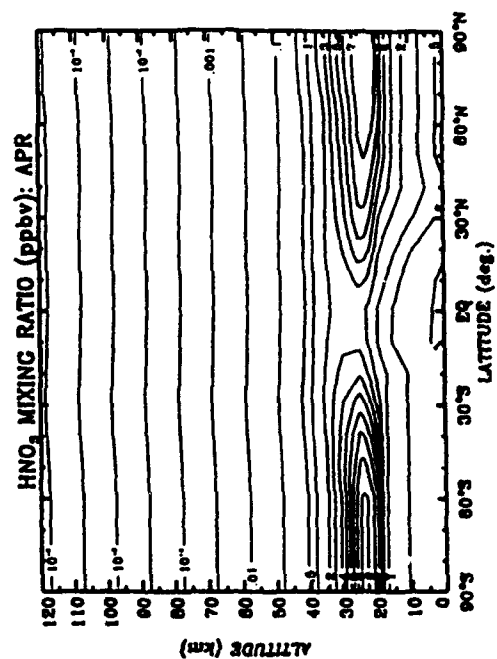
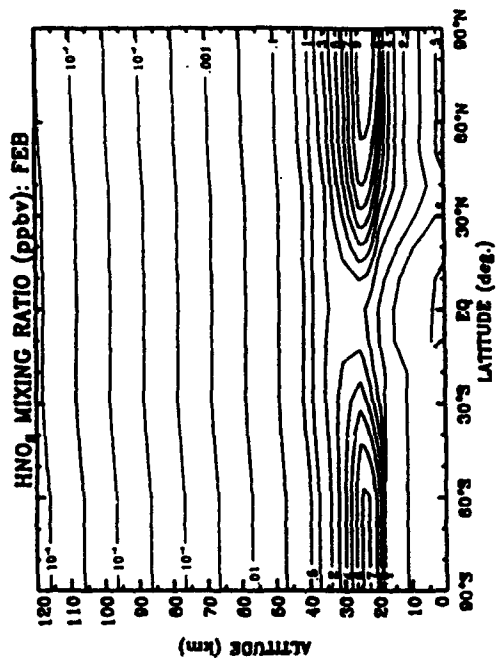






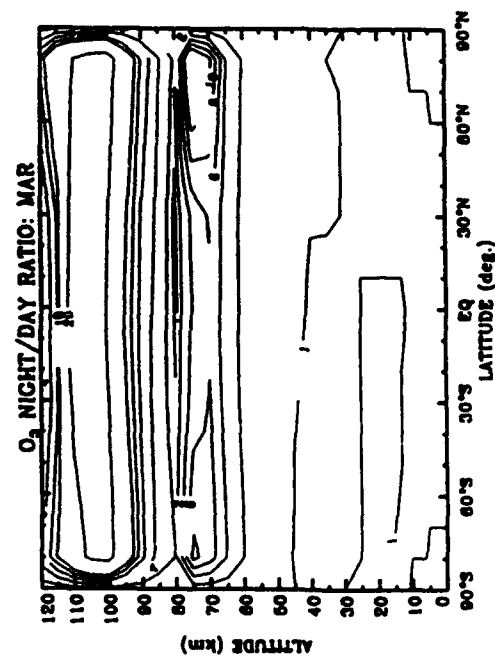
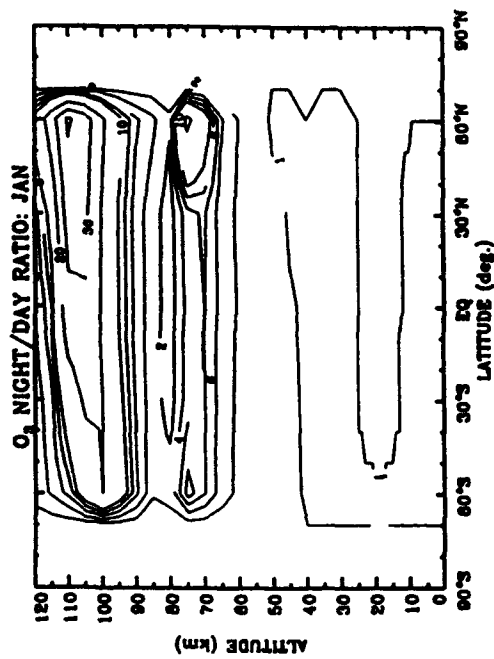
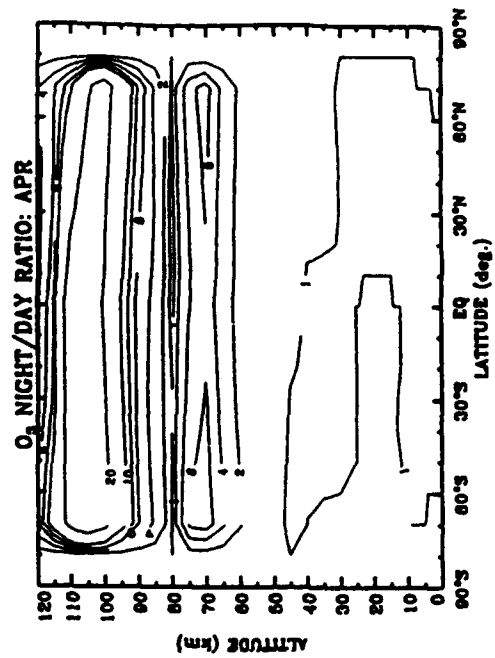
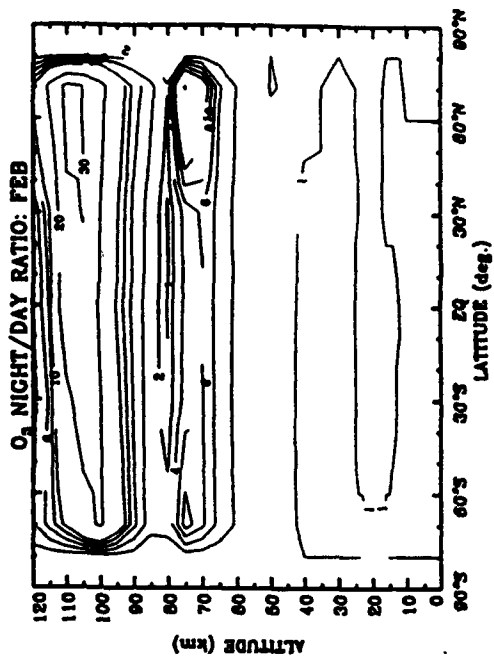






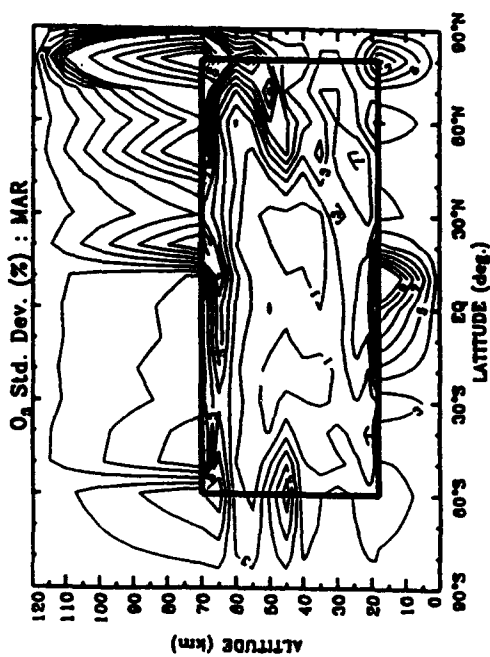
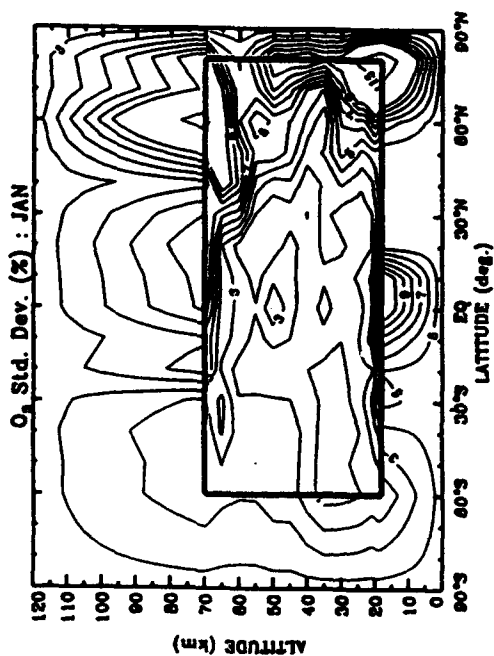
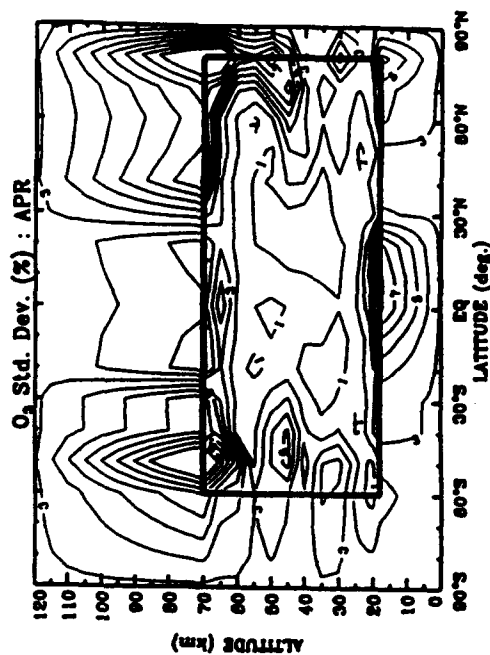
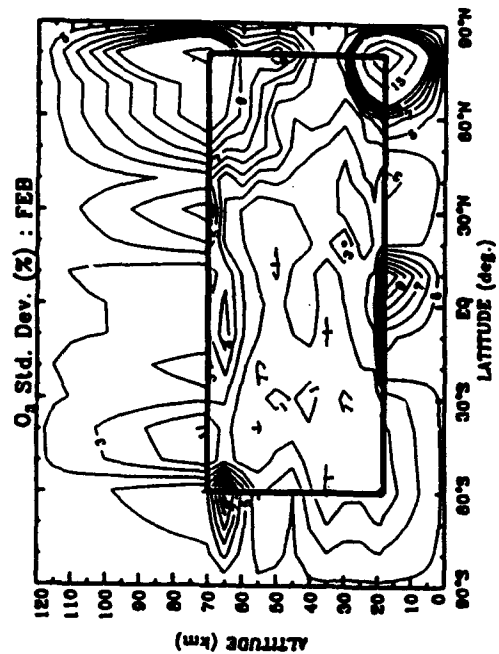
APPENDIX I

Figures: Ozone Diurnal Variability



APPENDIX K

Figures: Trace Species Variability



FAR-WING LINE SHAPE CONTRIBUTION TO THE WATER CONTINUUM: RECENT RESULTS AND FUTURE DIRECTIONS

R.H. Tipping

Department of Physics and Astronomy, University of Alabama, Tuscaloosa, AL 35487

Q. Ma

Institute for Space Studies, Goddard Space Flight Center, New York, NY 10025

A far-wing line shape theory has been developed and applied to the calculation of both self- and N₂-broadened water lines. This theory is based on the quasistatic and binary collision approximation and utilizes only known parameters obtainable from other measurements (line strengths, positions, interaction potential parameters, and multipole moments). The resulting continuous absorption coefficient is in good agreement, in both its magnitude and its temperature dependence, with existing experimental laboratory measurements. Some refinements in the model and future directions will be discussed briefly.

**FAR-WING LINE SHAPE CONTRIBUTION TO THE WATER CONTINUUM:
RECENT RESULTS AND FUTURE DIRECTIONS**

R. H. Tipping

University of Alabama, Tuscaloosa, AL 35487

and

Q. Ma

Institute for Space Studies, Goddard Space Flight Center

New York, NY 10025

1. INTRODUCTION

2. FAR-WING LINE SHAPE THEORY

APPROXIMATIONS

INPUT DATA

3. COMPARISON WITH EXPERIMENTAL DATA

4. FUTURE DIRECTIONS

INTRODUCTION

1.1) IMPORTANCE OF MILLIMETER AND INFRARED RADIATION IN ATMOSPHERES

- (1) Controls the energy balance and affects the climate of the Earth.
- (2) Widely used in remote sensing, atmospheric communications, etc.
- (3) To determine characteristics of planetary atmospheres from experiment data.

1.2) ATMOSPHERIC WINDOWS AND CONTINUUM ABSORPTION

OPAQUE REGIONS AND WINDOWS:

The opaque regions are mainly determined by H_2O lines, along with O_2 and CO_2 lines. Between them there are "WINDOWS".

THE WEAK ABSORPTION IN WINDOWS:

- (1) Some weak local lines of H_2O , O_2 and CO_2 .
- (2) A gradually varying background, i.e. continuum absorption.

1.3) BASIC CHARACTERISTICS OF CONTINUA

There are two kinds of water continua:

- (1) $\text{H}_2\text{O} - \text{H}_2\text{O}$ (self) continuum
- (2) $\text{H}_2\text{O} - \text{N}_2, \text{O}_2$ (foreign) continuum

Usually, the self-continuum is dominant.

CHARACTERISTICS OF THE SELF-CONTINUUM:

- (1) Varies smoothly with frequency.
- (2) Proportional to n^2 .
- (3) Very strong negative temperature dependence.

1.4) MAIN THEORIES OF WATER CONTINUUM

THREE MECHANISMS FOR SELF-CONTINUUM:

- (1) Collision broadened far-wings of
allowed water vapor lines.
- (2) Collision-induced absorption.
- (3) Water dimers.

All three mechanisms vary as n^2 ,
but there are large differences in the
temperature dependencies and in the
magnitudes of the absorption.

2. FAR-WING LINE SHAPE THEORY

$$\alpha(\omega) = (4\pi^2/3\hbar c) n_s \omega \tanh(\hbar\omega/2kT) [F(\omega) + F(-\omega)] \quad (1)$$

$$F(\omega) = \text{Im} (2\pi^2 i)^{-1} \int_{-\infty}^{\infty} d\omega' \text{Tr}[\mu_a \cdot (\omega - \omega' - L_1)^{-1} \\ \times <(\omega' - L_1)^{-1} \rho^{(in)}>_b \rho^{(a)} \mu_a] \quad (2)$$

P. W. Rosenkranz, J. Chem. Phys. **83**, 6139 (1985).

P. W. Rosenkranz, J. Chem. Phys. **85**, 163 (1987).

Q. Ma and R. H. Tipping, J. Chem. Phys. **93**, 7066 (1990).

Q. Ma and R. H. Tipping, J. Chem. Phys. **93**, 6127 (1990).

Q. Ma and R. H. Tipping, J. Chem. Phys. **95**, 6290 (1991).

Q. Ma and R. H. Tipping, J. Chem. Phys. **96**, May 15 (1992).

Q. Ma and R. H. Tipping, J. Chem. Phys. **97**, July 15 (1992).

APPROXIMATIONS

1. BINARY COLLISION APPROXIMATION

$$\rho^{(int)} = n_b e^{-V(r)/kT}$$

$$V(r) = V_{aniso}(r) + V_{iso}(r)$$

$$V_{iso}(r) = C\sigma^{-6}[(\sigma/r)^{12} + (\sigma/r)^6]$$

2. QUASISTATIC APPROXIMATION

$$\langle (\omega' - L_1)^{-1} \rho^{(int)} \rangle_b$$

$$\langle \dots \rangle \rightarrow 4\pi \int \dots r^2 dr$$

3. BAND-INDEPENDENT APPROXIMATION

$$\alpha(\omega) = \sum_{v \neq j} \alpha_{vij}(\omega)$$

$$\alpha_{vij}(\omega) = n_s \sum_{\omega_{vij} > 0} S_{vij} [\omega \sinh(\hbar\omega/2kT)] / [\omega_{vij} \sinh(\hbar\omega_{vij}/2kT)]$$

$$\times \pi^{-1} \{ \chi_+ (\omega - \omega_{vij}) / (\omega - \omega_{vij})^2 + \chi_- (\omega + \omega_{vij}) / (\omega + \omega_{vij})^2 \}$$

INPUT DATA

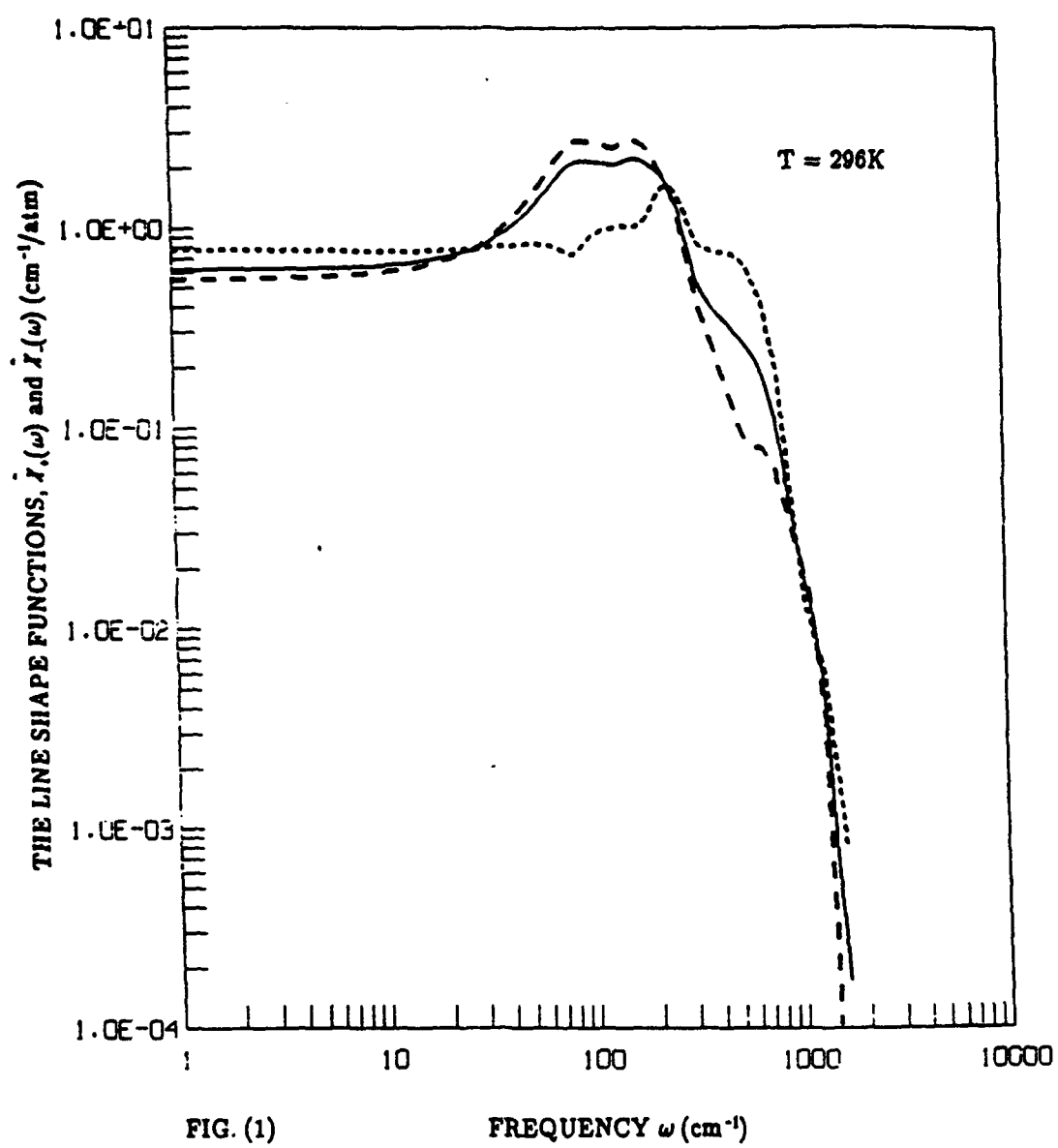
POTENTIAL PARAMETERS

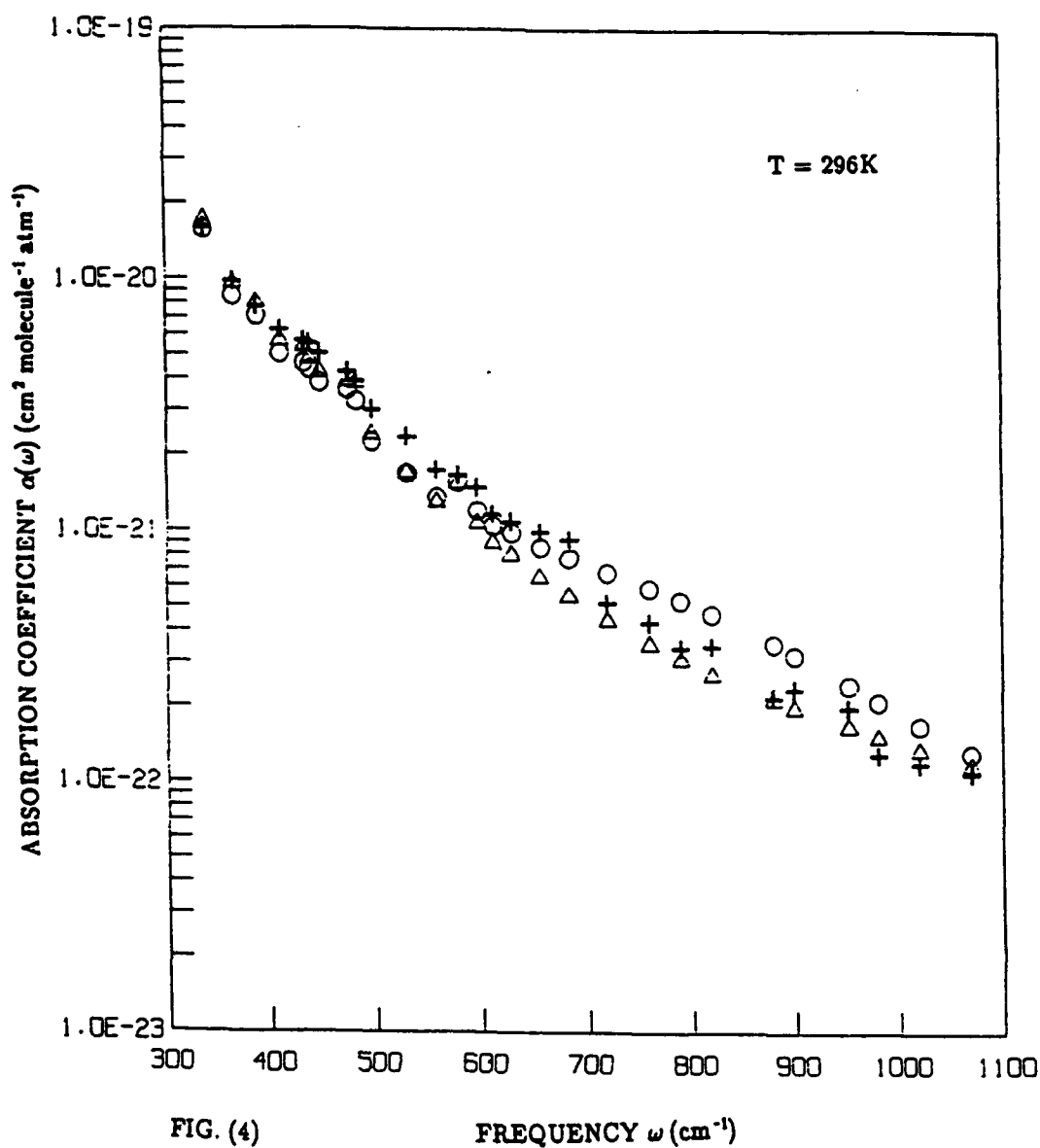
C, σ, t, μ, Q

SPECTROSCOPIC PARAMETERS

(HITRAN DATABASE)

S_{ij}, E_i, ω_{ij}





+ Burch et al.

Δ now

O "Rosenkranz"

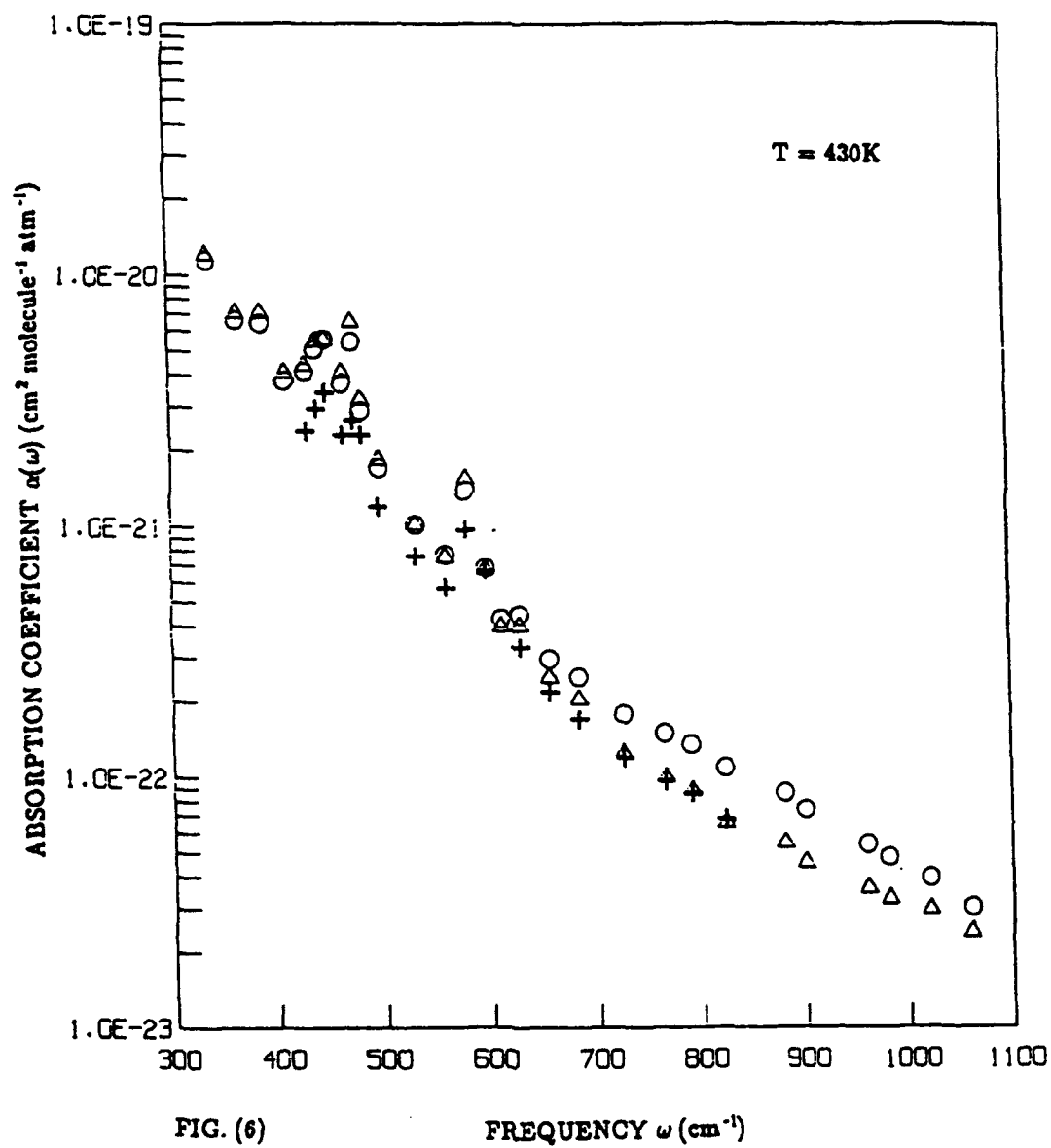


FIG. (6)

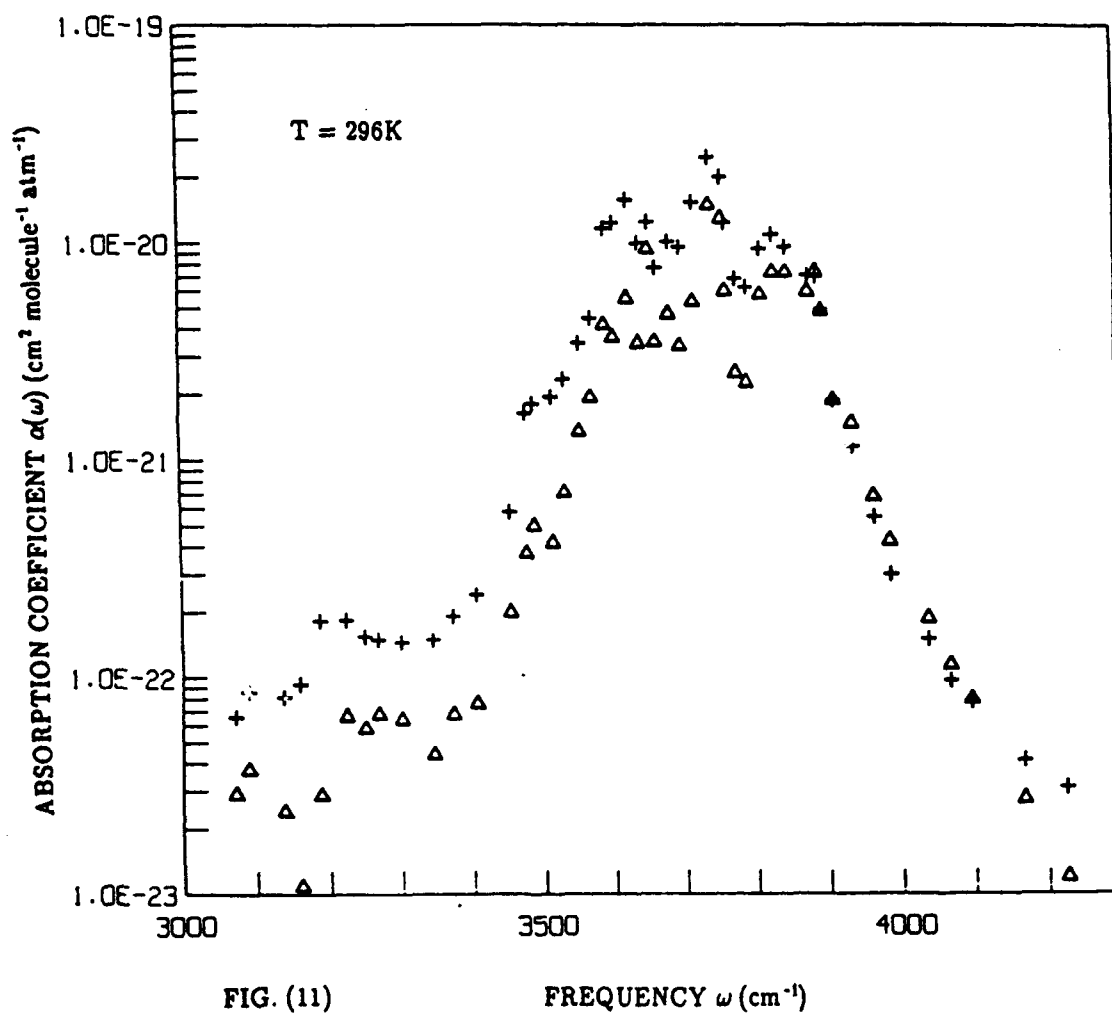
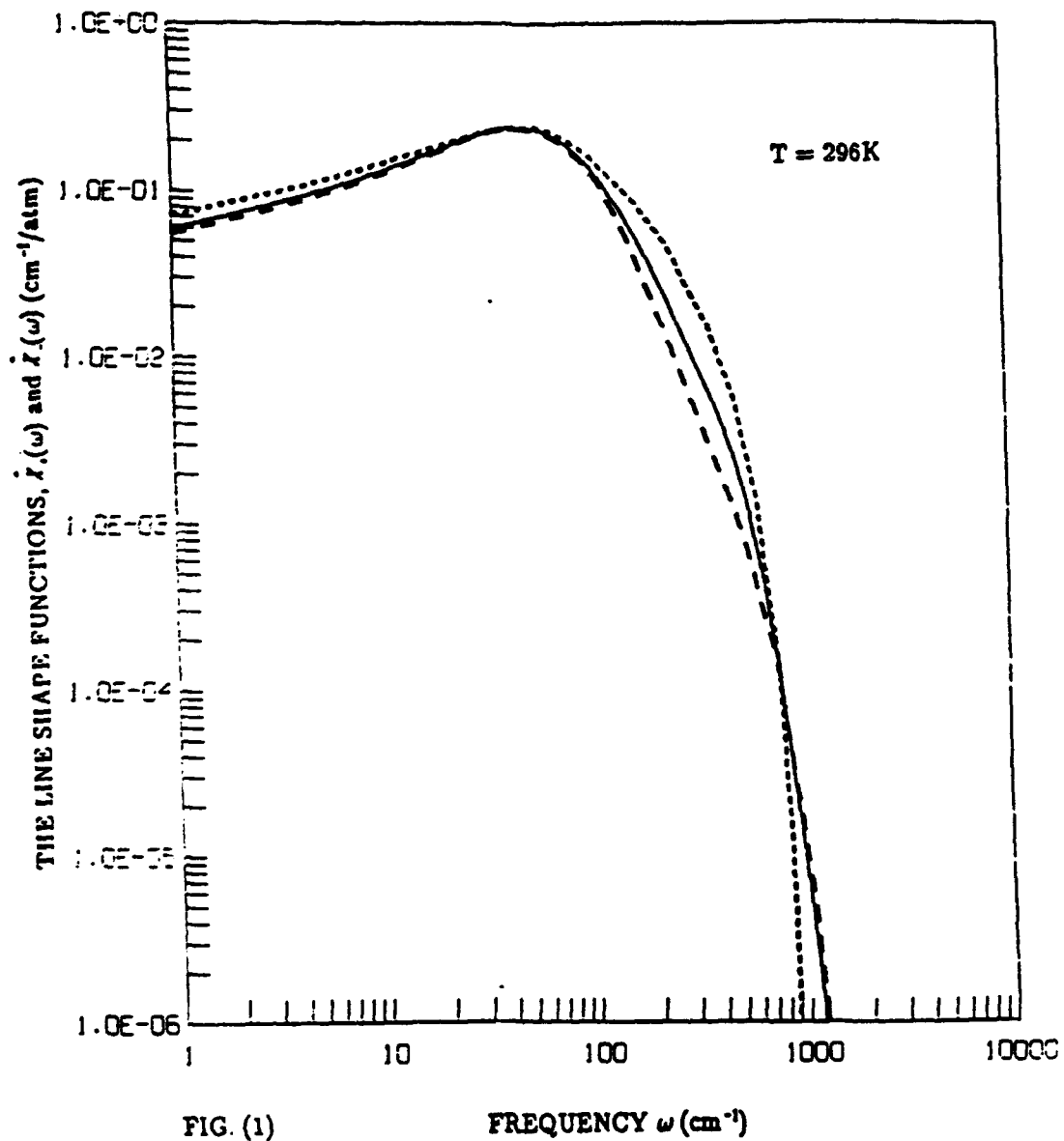
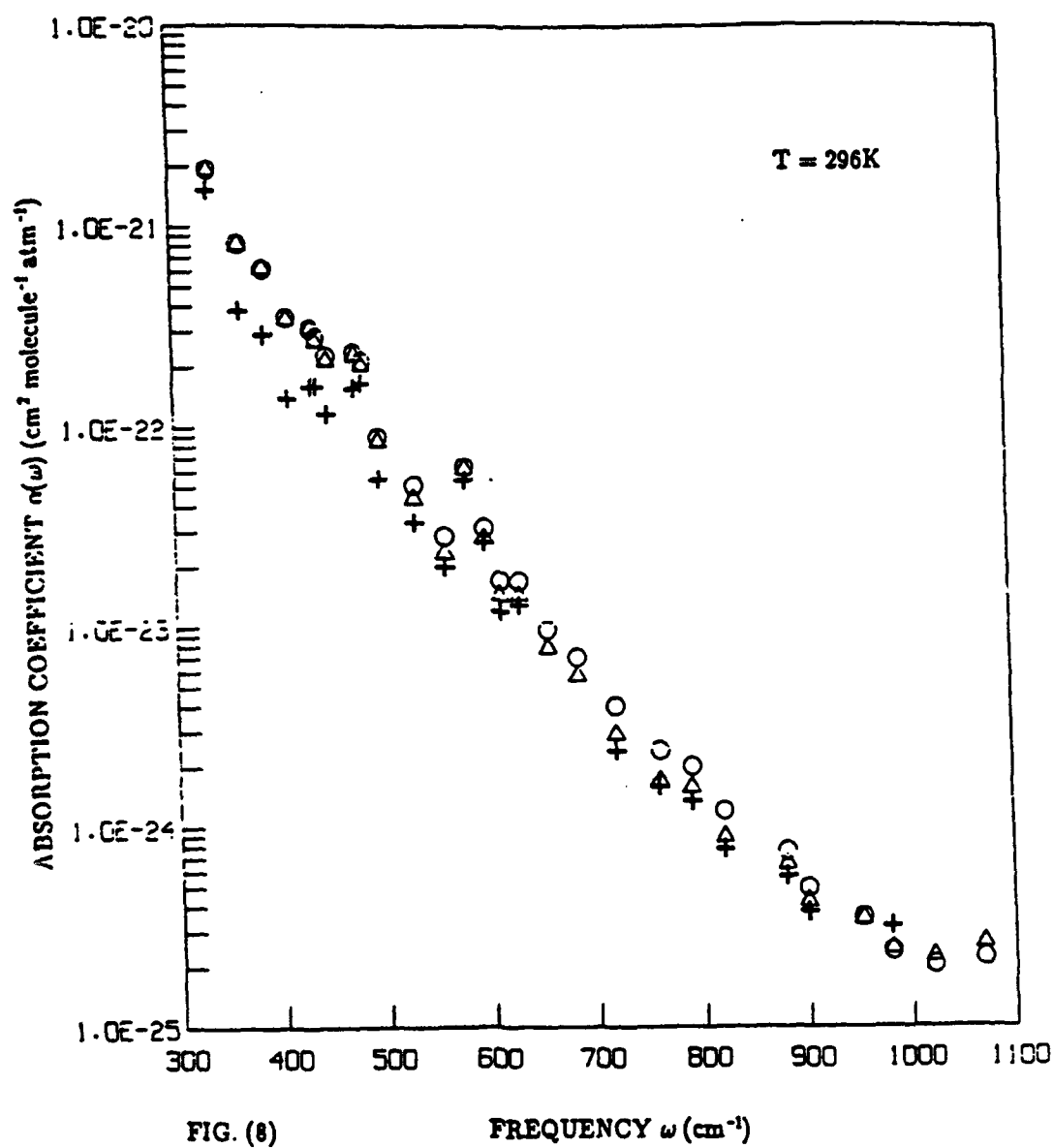


FIG. (11)





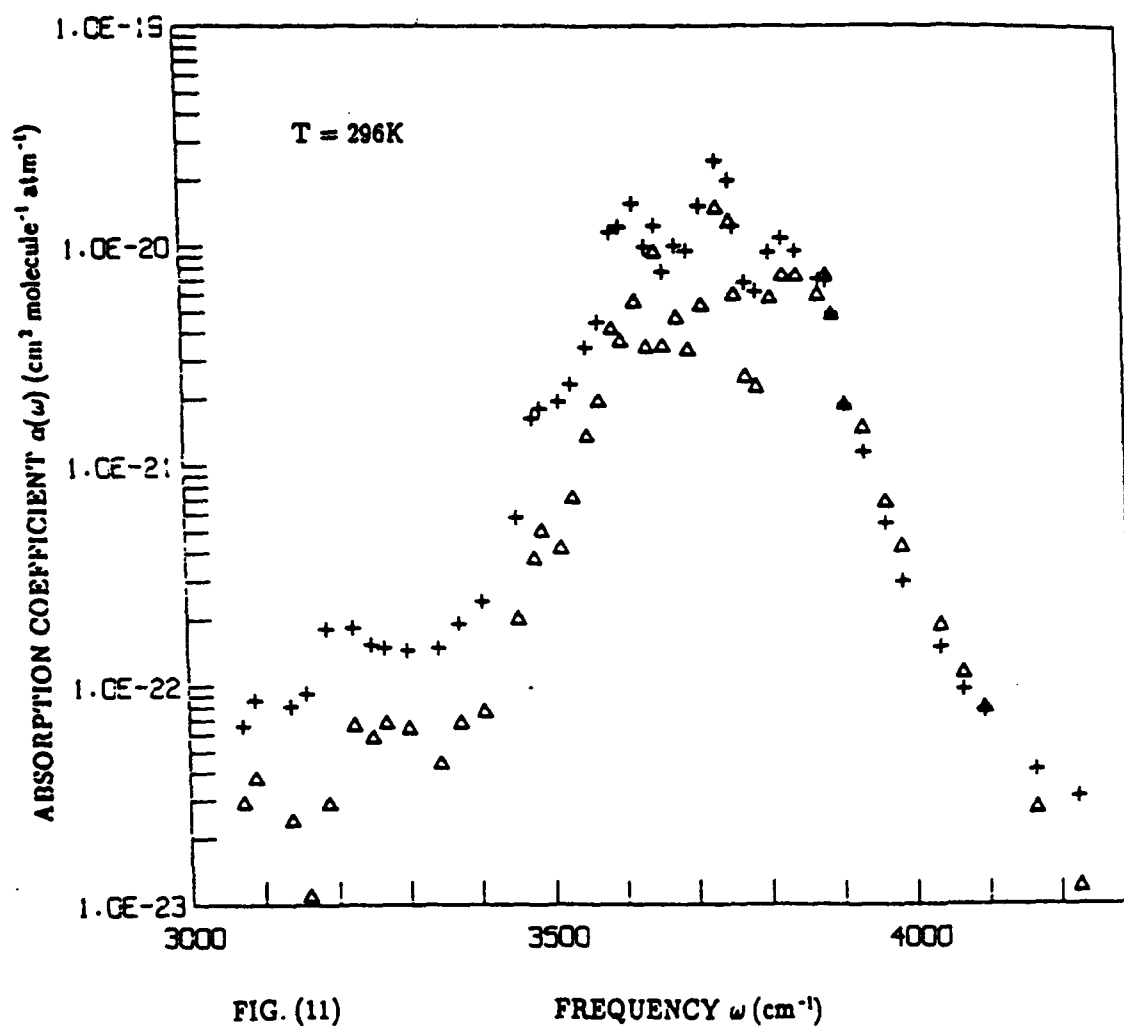
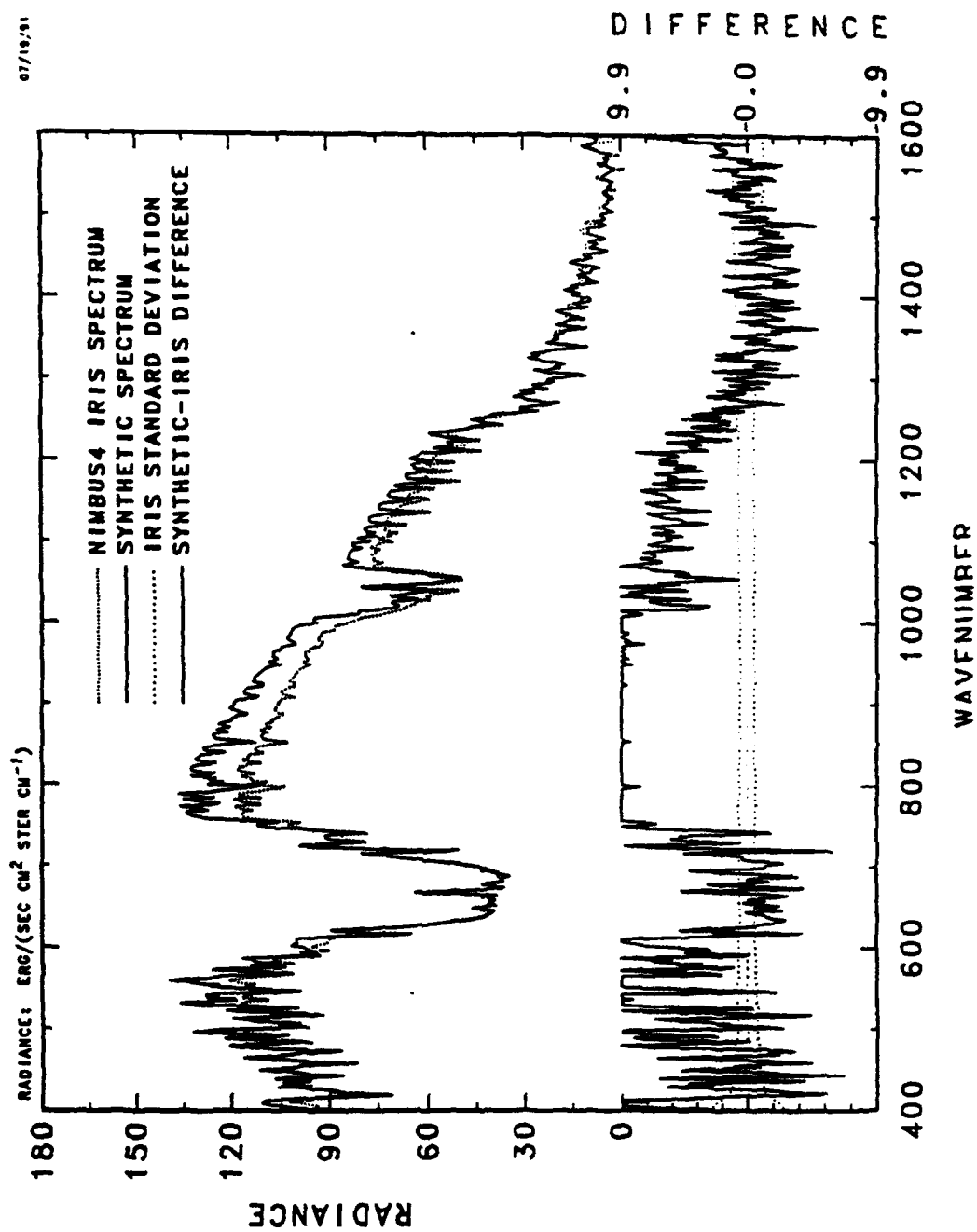


FIG. (11)

without H_2O continuum

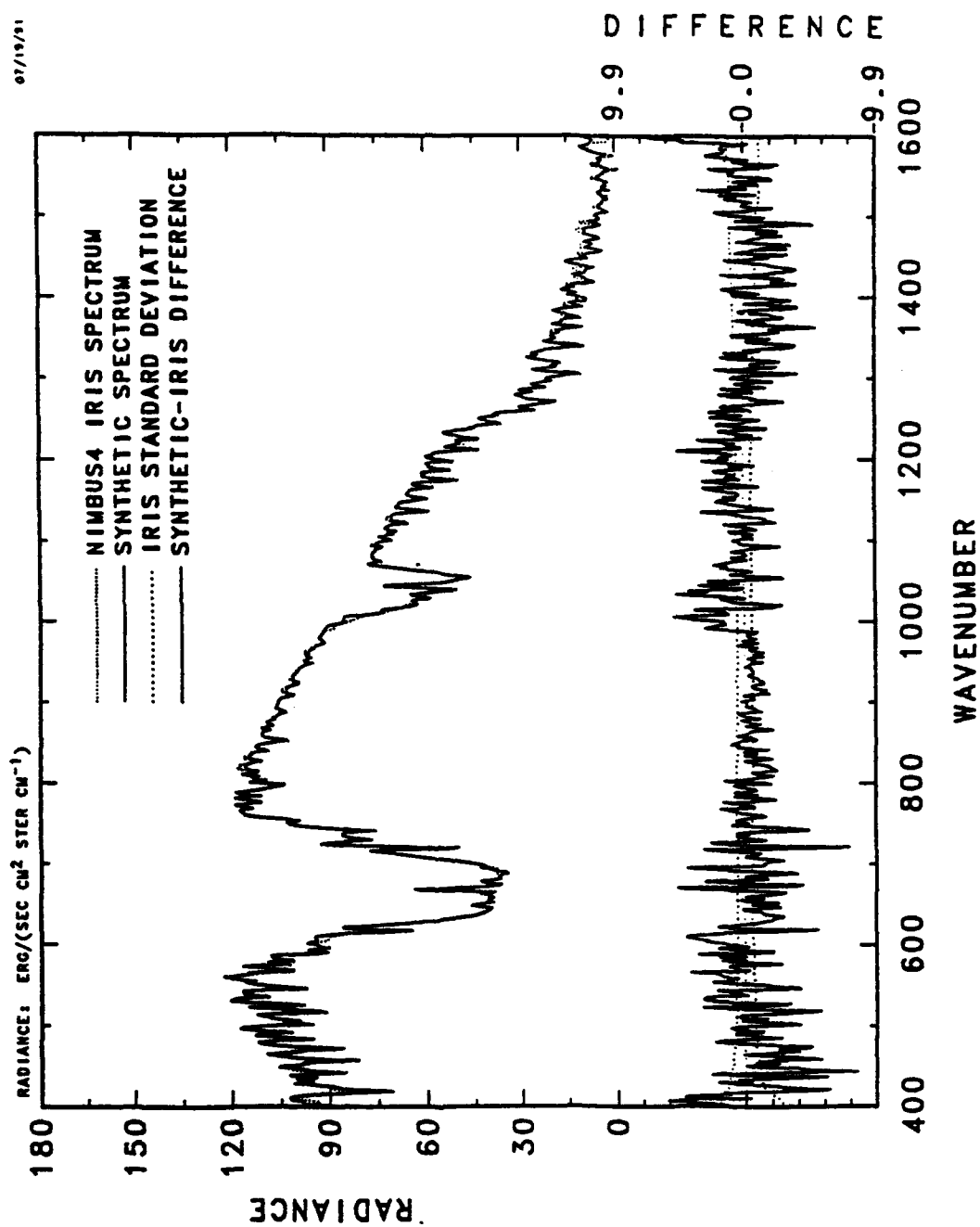
1102001
07/19/91



with H_2O continuum

115001

07/19/91



4. FUTURE DIRECTIONS

- A. MORE REALISTIC POTENTIAL MODEL**
- B. CORRECTIONS TO QUASISTATIC APPROXIMATION**
- C. INTERFERENCE BETWEEN ALLOWED AND
INDUCED DIPOLE MOMENTS**
- D. VALIDATION WITH NEW DATA WHEN AVAILABLE**

TOWARD AN IMPROVED WATER VAPOR CONTINUUM MODEL

S.A. Clough

Atmospheric and Environmental Research, Inc., 840 Memorial Drive, Cambridge, MA 02139

A model for the water vapor continuum based on the measurements of Burch [1], has been reported by Clough et al. [2,3]. Since the definition of the continuum is inextricably related to the line contribution associated with the radiative transfer program with which it is used, a consistent analysis of the data is essential to the proper treatment of the problem. To obtain an improved water vapor continuum model, the local line contribution consistent with the line-by-line program FASCODE has been carefully and systematically removed from the extinction measurements made in the microwindows of the water vapor spectrum by Burch [1]. Other measurements based on the transmittance over a homogeneous atmospheric path and radiances for an inhomogeneous atmospheric path are being considered in the analysis. An improved line shape including the effects of detail balance is being developed on the basis of these measurements. The results from the present model are compared with recent theoretical results of Ma and Tipping [4].

1. Burch, D. E., Continuum absorption by H₂O, Rep. AFGL-TR-81-0300, 32 pp, Air Force Geophys. Lab., Hanscom AFB, MA, 1981. ADA112264
2. Clough, S. A., F. X. Kneizys, R. W. Davies, R. Gamache, and R. H. Tipping, Theoretical line shape for H₂O vapor: application to the continuum, in Atmospheric Water Vapor, edited by A. Deepak, T. D. Wilkerson, and L. H. Rhunke, pp. 25-46, Academic Press, London, 1980.
3. Clough, S. A., F. X. Kneizys, and R. W. Davies, Line shape and the water vapor continuum, Atmospheric Research, **23**, 229-241, 1989b.
4. Ma, Q., and R. H. Tipping, A far wing line shape theory and its application to the water continuum absorption in the infrared region (II), J. Chem. Phys., in press, 1992.

A CORRELATED K-DISTRIBUTION MODEL OF THE HEATING RATES FOR CH₄ AND N₂O IN THE ATMOSPHERE BETWEEN 0 AND 60KM*

K. Grant, A.S. Gross

Lawrence Livermore National Laboratory, P.O. Box 808, L-262, Livermore, CA 94551-9900

An infrared radiative transfer model using the correlated-k technique is being developed for use in atmospheric chemistry and climate models at LLNL, as well as for stand-alone radiative diagnostics. This implementation of the correlated-k algorithm will provide a computationally efficient means to calculate atmospheric radiative fluxes and heating rates. It will also allow for both time-varying gas concentrations and for the rapid inclusion of new gases into the model.

We present the results of our prototype model of absorption by CH₄ and N₂O in the 7-9 micron wavelength band. The correlated-k algorithm maps the highly structured absorption coefficient versus wavelength relationship into a substantially smoother monotonic relationship between the absorption coefficient and its cumulative probability distribution. This provides a substantial reduction in computational complexity relative to line-by-line calculations, while maintaining a high degree of accuracy.

*Work performed under the auspices of the U.S. Dept. of Energy by the Lawrence Livermore National Laboratory under contract No. W-7405-Eng-48.

A Correlated k -Distribution Model of the Heating Rates for CH_4 and N_2O in the Atmosphere Between 0 and 60 Km

Keith Grant
Allen S. Grossman
Lawrence Livermore National Laboratory
Livermore, California 94550

and

James B. Pollack
Richard Freedman
Space Sciences Division
NASA-Ames Research Center
Moffett Field, California 94035

March 27, 1992

Abstract

An infrared radiative transfer model using the correlated- k technique is being developed for use in atmospheric chemistry and climate models at LLNL, as well as for stand-alone radiative diagnostics. This implementation of the correlated- k algorithm will provide a computationally efficient means to calculate atmospheric radiative fluxes and heating rates. It will also allow for both time-varying gas concentrations and for the rapid inclusion of new gases into the model.

We present both a general background of the c - k method and the results of applying our prototype model to absorption by CH_4 and N_2O in the 7-9 micron wavelength band. The correlated- k algorithm maps the highly structured absorption coefficient versus wavelength relationship into a substantially smoother monotonic relationship between the absorption coefficient and its cumulative probability distribution. This provides a substantial reduction in computational complexity, relative to line-by-line calculations, while maintaining a high degree of accuracy.

1. Introduction

Infrared radiative transfer models are used at LLNL both as stand-alone diagnostic tools and as important components of more general atmospheric models. As diagnostic models, we use radiative transfer models to calculate the radiative forcing to the surface-troposphere system due to potential changes in trace gases concentrations, aerosols, or clouds. For example, such radiative forcing calculations are an essential step in deriving global warming potentials (GWPs) for trace gases. These GWPs provide an approximate index of the time-cumulative radiative effects of a unit emission of a specified trace gas relative to the comparable effect for CO_2 . Another diagnostic application of our efforts in atmospheric radiative transfer modeling has been the calculation of stratospheric temperature changes forced by observed decadal changes of ozone mixing ratio profiles.

As integral parts of global and regional chemistry models and of climate models, we use infrared radiative transfer models in calculating vertical profiles of net heating rates. Such heating rate profiles are a vital part both of calculating the atmospheric circulation within global models and of estimating the chemical and temperature feedback effects from potential

anthropogenic trace gas emissions. As a requirement of our global modeling efforts, we are emphasizing the development of radiative transfer models that maintain accuracy into the upper stratosphere and that are implemented with the flexibility to handle time varying profiles of temperature and radiatively active overlapping trace gases.

A current focus of our efforts is the development of an infrared radiative transfer model which can provide a substantial reduction in computational complexity, relative to line by line calculations, while maintaining a high degree of accuracy. In a recent publication (Lacis and Oinas, 1991, "LO"), a method was described for treating transmission calculations in infrared radiative transfer problems for a vertically inhomogeneous atmosphere in which there is non-gray gaseous absorption. The method known as the correlated k -distribution utilizes a mapping of the opacity-frequency relation into an opacity-probability relation within a particular frequency interval. The probability variable $g(k)$, the cumulative distribution function, is defined as

$$g(k) = \int_0^k f(k') dk' , \quad (1)$$

where $f(k')dk'$ is the fraction of the frequency interval occupied by absorption coefficients between k' and $k'+dk'$ (Goody and Jung, 1989, "G1"; Goody *et al.*, 1989, "G2"; and West *et al.*, 1990, "W1"). The limits of $g(k)$ range between 0 and 1 within the frequency interval. The inverse of Equation 1, $k(g)$, the k -distribution, has been shown by LO, G2, and W1 to be a monotonic function across the frequency interval for a particular atmospheric layer. The correlated- k method can mathematically provide an exact procedure for calculating the transmission and heating rates in a homogeneous atmosphere. For the case of inhomogeneous atmospheric paths the method is, in practice, inherently inexact since somewhat different sets of frequencies will associate with a given ordering of the k terms as the pressure and temperature vary over the path. If the fractional error caused by the use of the correlated- k method to calculate the transmission for inhomogeneous paths is tolerable, then the method offers an attractive means for computing radiation fields in real atmospheres.

The calculation of the transmission can be expressed in the three physically equivalent forms:

$$\begin{aligned} T(u) &= 1 / \Delta v \int_{\Delta v} \exp(-k_v u) dv , \\ &= \int_0^1 f(k') \exp(k' u) dk' , \\ &= \int_0^1 \exp(-k(g)u) dg , \end{aligned} \quad (2)$$

where u is the absorber column density. Using the k -distribution form, the calculation can be performed using far fewer k - g points than the same calculation using $k-v$ (frequency) points. Thus the k -distribution method has the potential of being a much more computationally efficient method of doing radiative transfer calculations within the earth's atmosphere when compared to line by line or narrow band models while retaining many of the numerical advantages of an explicitly exponential, monochromatic calculation. For example, scattering may be readily handled with the correlated k -distribution model, but not with band models.

The opacity model used by LO for the molecules CH₄ and N₂O was a Malkmus band model (Malkmus, 1967; Rodgers, 1968) for the transmission function,

$$T(u) = \exp\left\{-\pi B/2\left[\left(1 + 4Su/\pi B\right)^{1/2} - 1\right]\right\} , \quad (3)$$

where the parameters S and B are obtained by fits to the mean absorption line strength, mean absorption line half width, and mean line spacing in the frequency interval. The probability function $f(k)$ in Equation 1 has been shown to be the inverse Laplace transform of Equation 3 by Domoto (1974) and is given by the expression (LO);

$$f(k) = 0.5k^{-3/2} (BS)^{1/2} \exp\left\{\pi B/4\left[2 - S/k - k/S\right]\right\} . \quad (4)$$

The k -distributions used by LO for CH₄ and N₂O were obtained using the $f(k)$ relations derived from the Malkmus band model. Excellent fits to the CH₄ and N₂O heating rates were obtained by LO using the Malkmus model with parameters empirically fit to give the best agreement with line by line calculations.

An more direct and inherently more accurate method of obtaining k -distributions has been used by G2 and by Freedman and Pollack (1990, "FP"). This method involves a direct line by line calculation of the opacity-frequency relation and a direct numerical sorting of this data to obtain $f(k)$ and the k -distribution, $k(g)$. The advantage of doing this is that the Malkmus formulation is bypassed and the assumptions, such as Lorentz line shape introduced into the problem by the Malkmus model are avoided.

The main purpose of this paper is to review the theory necessary to implement the correlated- k model for a vertically inhomogeneous atmosphere, and to apply the direct FP method to calculate k -distributions for the transmission of the molecules CH₄ and N₂O. For the wavelength interval of 7 to 9 microns and altitude range of 0 to 62 km, a calculation of the atmospheric cooling rates, upward fluxes, and downward fluxes will be made for each molecule and compared to the LO values.

II. The K-Distribution Method

For a non-homogeneous atmospheric path, containing j discrete layers, the transmission expression given by Equation 2 becomes;

$$T(u) = 1/\Delta u \int_{\Delta u} \exp\left(-\sum_j k_{uj} \Delta u_j\right) du , \quad (5a)$$

$$= \int_0^1 \exp\left(-\sum_j k_{gj} \Delta u_j\right) dg . \quad (5b)$$

The exact equivalence of Equations 5a and 5b for an inhomogeneous atmosphere is limited to a few special cases. G1 has shown that these expressions are equivalent for the case of $k_{uj} = k_{uo} f_j$, where the subscript "o", indicates a particular layer and f_j is a function of the pressure and temperature of the j th layer. G2 has shown that the two expressions are also equivalent for the case of the strong line limit for pressure broadened lines. When the exponential

terms in Equations 5a and 5b are expanded and the integrals are compared term by term, G1 has shown that in the weak line limit,

$$\left(\sum_j k_j \Delta u_j \right)^n \ll \left(\sum_j k_j \Delta u_j \right) \quad n \geq 2,$$

the two expressions are equivalent. G1 also states that since terms of the kind,

$$\left(\sum_j k_j \Delta u_j \right)^n,$$

contain the expressions $(k_j \Delta u_j)^n$ which are equivalent in the two transmission models, the k distribution method will be a more accurate method than the weak line approximation. In general, the term integrals which involve the cross product terms will not be equivalent unless there is a unique $k(g)$ relation which is correlated for all the layers. Both LO and W1 have discussed the validity of the k -distribution method from this point of view. For the method to work precisely, the $k(g)$ relations must be such that a particular g value selects the same set of frequencies in all the layers; i.e. the frequency ordering of the opacity groups is preserved layer to layer. In LO and W1 examples are presented which show the consequences that can occur when specific g values do not select the same frequency sets in different layers. Via the separate $k(g)$ relationships for two layers, the $k(v)$ distribution for a layer can be scaled on to the range of k values appropriate for the second layer by selecting a set of frequencies appropriate to a particular g value for the first layer and using this set of frequencies with the k value, for the same g , in the second layer as the scaling relation. The scaled $k(v)$ relation, thus obtained for the second layer, will differ from the original $k(v)$ relation for the second layer, with the difference increasing as the correlation between the $k(v)$ relations of the two layers decreases. The k -distribution derived from the scaled $k(v)$ relation will become significantly non monotonic as the correlation between the layers decreases; i.e. the k value for a given g will no longer show a small dispersion about a well defined mean value. As pointed out in G2, the k -distribution method cannot be valid for all conditions and its use under all circumstances must be accompanied by numerical validity tests or comparison with asymptotic forms. The monotonic nature of the k -distributions allow transmission calculations to be performed, over a frequency interval, using a few tens of $k(g)$ points as opposed to large numbers of $k(v)$ points ($\Delta v \sim \Delta v_H/4$; Δv_H =line half width) required for a line by line calculation. The resulting computational economy using the k -distribution method is sufficient to warrant the numerical validity tests necessary for its use.

The calculation of the k -distributions for CH_4 and N_2O by the FP method contains the following steps. First, the HITRAN-91 database (Rothman *et al.*, 1991) is utilized to determine the line transitions and physical properties of the selected lines. Second, a version of the FASCODE2 code (Clough *et al.*, 1986), modified by FP, is used to calculate a finely gridded ($\Delta v \sim \Delta v_H/4$) set of monochromatic absorption coefficients, with full allowance for the overlap of neighboring lines, for each layer in the atmosphere. Third, a sorting code developed by FP, ABSORT, is used to calculate the $f(k)$, $g(k)$, and $k(g)$ functions for each homogeneous layer. A block diagram of the process is shown in Figure 1. Initial input to the SELECT code which accesses the HITRAN-91 database consists of the wave number range, and the choice of molecular species and isotopes. The SELECT code output contains the central wave number, intensity, half width, and lower state energy for each line as well as an intensity weighted average half width for all the lines. The weighted average half width calculation in the SELECT

code was a modification added by FP. The modified FASCODE program takes the line data generated by the SELECT code, fits an absorption line profile (Voigt Profile) to each line and calculates the absorption coefficient $k(\text{cm}^2/\text{air mol})$ as a function of wave number. The wave number grid spacing is controlled by the value of the weighted average half width. A typical value of the opacity grid spacing for the CH_4 calculations is 0.0005 cm^{-1} at pressures of the order of 1 mb. The normal cutoff point in the line profile is set at 25 cm^{-1} from line center. This is done both for reasons of economy (beyond 25 cm^{-1} a given line contributes little opacity) and because deviations from Lorentz behavior can become appreciable. In addition to the input from the SELECT code. The values of temperature, pressure, and nominal mixing ratios (X 's) of the absorbing species are required for the FASCODE program. These values are obtained from a model atmosphere specification which will be discussed later. The ABSORT code takes the absorption coefficient files generated by the FASCODE program and sorts the opacity into bins of equal logarithmic width, $\Delta \log k(v)$, to produce a distribution, $f(k)$, based on the relative probability of occurrence within the wave number interval (proportional to the number of entries in each bin). The cumulative distribution function, $g(k)$ (Equation 1), is obtained by numerical integration of the $f(k)$ function. The k -distribution is obtained by a reverse interpolation of the $g(k)$ relation using a spline function. For the calculations in this paper a 201 bin model was used. FP suggests a number greater than 100 bins for normal atmospheric problems. The inputs to the ABSORT code are the maximum and minimum values of the opacity in each atmospheric layer (determines the range of k 's covered by the bins), the number of sorting bins (determines the width of each bin), the choice of linear or spline interpolation, and the line by line opacity results from FASCODE for each layer. The output from the ABSORT code is the 201 point $k(g)$ relation for each layer.

In order to make a direct comparison with the LO calculations, the wavelength range chosen for the CH_4 and N_2O calculations in this paper is 1100 to 1340 cm^{-1} or 7.5 to 9.1 microns. This wave number interval was divided into subintervals having a 20 cm^{-1} width. For this subinterval width the variation of the value of the Planck function is less than 10 percent across the band at the maximum and minimum atmospheric temperatures, i.e., the use of the average value of the Planck function over the wave number interval is accurate to the order of about 5 percent of the actual value. The use of wider bands will require averaging opacities weighted by the Planck function

The model atmosphere chosen for the calculations is the McClatchey mid-latitude, summer, pressure-temperature distribution (McClatchey *et al.*, 1972). The altitude resolution was chosen as 1 km between 0 and 20 km and 2 km between 20 and 62 km. Mixing ratios of CH_4 and N_2O were chosen to be 1.75 and 0.3 ppm respectively. Both the LO calculations and those of this paper assume that the mixing ratios are constant with altitude, although G1 indicates that the mixing ratios decrease significantly above ~ 25 km altitude. This point will be discussed later in terms of the stratospheric cooling rates.

Figures 2 and 3 show the $f(k)$, $g(k)$, and $k(g)$ functions for CH_4 in the wave number band 1300 – 1320 cm^{-1} at the temperatures and pressures representative of the surface layer, $T = 291.7 \text{ K}$ and 945.7 mb (Figure 2), and a layer at $\sim 50 \text{ km}$, $T = 272.2 \text{ K}$ and $P = 1.48 \text{ mb}$ (Figure 3). It is interesting to note that the k -distributions exhibit very different behavior at g values between ~ 0.9 and 1.0 . For the high pressure surface layer the k variation is less than an order of magnitude, while for the low pressure high altitude layer the k variation is approximately four orders of magnitude. Figure 4 shows the k -distributions for five representative atmospheric layers, $P = 1.48, 18.05, 102.44, 542.36$, and 945.28 mb . These curves are constructed from the 201 $k(g)$ points produced by the ABSORT code. For pressures greater than $\sim 100 \text{ mb}$ (altitudes below $\sim 18 \text{ km}$) the curves are reasonably well behaved. At pressures below $\sim 100 \text{ mb}$ the curves have large opacity excursions at g value greater than 0.9 . These excursions can be up to four orders of magnitude at the lowest pressures. This kind of behavior at low pressures is thought to be due to the absence of pressure broadening effects on the absorption lines in the wave number

band; i.e. the lines are dominated by doppler broadening near line center. Inspection of Figures 2 and 3 shows that the existence of narrow, high opacity line cores in the wave number band causes the distribution function $f(k)$ to have small but finite values at high opacities, which results in a sharply peaked $k(g)$ function at high g values. These variations in the k -distributions require a careful numerical integration strategy in the transmission expression, Equation 5b, in order to accurately reproduce the $k(g)$ functions. The integral over g in Equation 5b can be approximated by a summation,

$$T(u) = \sum_{i=1}^N a_i \exp \left[- \sum_j k_{gi} \Delta \mu_j \right] g_i \quad (6)$$

where the a_i 's represent the integration weights. The k -distributions for the lower pressures require a larger number of $k(g)$ points in Equation 6 to accurately reproduce the transmission integral. The integration strategy which was adopted after test calculations was a 43 point, variable spaced trapezoidal model. For g values between 0.0 and 0.6, a Δg spacing of 0.1 was chosen. For g values between 0.6 and 0.9, a Δg spacing of 0.02 was chosen. For g values between 0.9 and 1.0, a Δg spacing of 0.005 was chosen (this is the spacing for the 201 point ABSORT code output data).

III. Radiative Transfer Model

In order to determine the atmospheric heating rates and upward and downward fluxes, the radiative transfer equations must be solved for the specific monochromatic intensities, $I_\nu(\tau_\nu, \mu)$, in the atmosphere. The classical radiative transfer equations for a plane parallel atmosphere are (Liou, 1980);

$$\mu \frac{dI_\nu(\tau_\nu, \mu)}{d\tau_\nu} = I_\nu(\tau_\nu, \mu) - B_\nu \quad (7a)$$

$$d\tau_\nu = -k_\nu \rho dz \quad (7b)$$

$$\mu \equiv \cos \theta \quad (7c)$$

τ_ν is the monochromatic optical depth at frequency ν ($\tau_\nu=0$ at the top of the atmosphere), B_ν is the Planck function, ρ is the mass density, z is the altitude, and θ is the zenith angle. The formal solution of Equation 7a is

$$I_\nu(\tau_\nu, \mu) = I_\nu(\tau_{\nu_0}, \mu) e^{-(\tau_\nu - \tau_{\nu_0})/\mu} - \int_{\tau_{\nu_0}}^{\tau_\nu} \frac{B_\nu(\tau_{\nu'})}{\mu} e^{-(\tau_\nu - \tau_{\nu'})/\mu} d\tau_{\nu'} \quad (8)$$

For downward radiances, $\tau_{\nu_0}=0$, $-1 \leq \mu < 0$, $I_\nu(0, -\mu) = 0$, and Equation 8 becomes

$$I_\nu^-(\tau_\nu, \mu) = \int_0^{\tau_\nu} B_\nu(\tau_{\nu'}) e^{-(\tau_\nu - \tau_{\nu'})/\mu} \frac{d\tau_{\nu'}}{\mu} \quad (\mu < 0) \quad (9)$$

For upward radiances, $\tau_{\nu_0} = \tau_{\nu s}$ (surface), $I_\nu(\tau_{\nu s}, \mu) = B_\nu$ (ground), $1 \leq \mu < 0$, and Equation 8 becomes

$$I_v^+(\tau_v, \mu) = B_v(\text{ground})e^{-(\tau_w - \tau_v)/\mu} - \int_{\tau_w}^{\tau_v} B_v(\tau_v') e^{-(\tau_v' - \tau_v)/\mu} \frac{d\tau_v'}{\mu} \quad (10)$$

Integration of Equations 9 and 10 by parts gives

$$I_v^-(\tau_v, \mu) = B_v(\tau_v) - B_v(0)e^{-\tau_v/\mu} - \int_0^{\tau_v} e^{-(\tau_v - \tau_v')/\mu} \frac{dB_v(\tau_v')}{d\tau_v'} d\tau_v' \quad (11)$$

for the downward radiance and

$$I_v^+(\tau_v, \mu) = B_v(\tau_v) + [B_v(\text{ground}) - B_v(\tau_w)]e^{-(\tau_w - \tau_v)/\mu} - \int_{\tau_w}^{\tau_v} e^{-(\tau_v' - \tau_v)/\mu} \frac{dB_v(\tau_v')}{d\tau_v'} d\tau_v' \quad (12)$$

for the upward radiance. Note that a distinction has been made between the ground temperature and the air temperature of the zero altitude point. The flux, $F_{\Delta v}$, in a particular frequency band Δv is given by the equation

$$F_{\Delta v}^{\pm} = \int_{\Delta v} 2\pi \int_0^1 I_v^{\pm}(\tau_v, \mu) \mu d\mu \quad (13)$$

This can be approximated by the expression

$$F_{\Delta v}^{\pm} \approx \int_{\Delta v} \sum_{i=1}^N a_i I^{\pm}(\tau_v, \mu_i) \mu_i dv \quad (14)$$

where the a_i 's are the weights for the numerical integration scheme. Under the usual assumption of the constancy of the Planck function across the frequency band Δv , the flux equation becomes

$$F_{\Delta v}^{\pm} \approx \sum_{i=1}^N b_i f^{\pm}(T_{\Delta v}, \mu_i) \mu_i \quad (15)$$

where $T_{\Delta v}$ is the transmission function for the frequency interval Δv , calculated between the appropriate levels in the atmosphere, and the b_i 's are the integration weights.

The f^{\pm} expressions are:

$$f^- = B_{\Delta v}(z) - B_{\Delta v}(z_{\max}) T_{\Delta v}(z, z_{\max}, \mu_i) + \int_z^{z_{\max}} T_{\Delta v}(z, z', \mu_i) dB_{\Delta v}(z') \quad (16)$$

$$f^+ = B_{\Delta v}(z) - [B_{\Delta v}(\text{ground}) - B_{\Delta v}(0)]T_{\Delta v}(z, 0, \mu_i) - \int_0^z T_{\Delta v}(z, z', \mu_i) dB_{\Delta v}(z'), \quad (17)$$

and

$$B_{\Delta v}(z) = \int_{\Delta v} B_v(z) dv. \quad (18)$$

This set of equations plus the transmission equations between appropriate levels (cf. Equation (6)), are solved for ten evenly spaced μ values between 0 and 1.0 for every level in the atmosphere. Once the upward and downward fluxes are obtained at each level, the heating rates for each atmospheric layer can be determined. For a particular layer the heating rate is

$$\frac{dT}{dt} = \frac{\Delta F}{c_p \Delta m} \quad (19)$$

where ΔF is the net flux into the layer,

$$\Delta F = F_{UP_i} + F_{DN_{i+1}} - F_{UP_{i+1}} - F_{DN_i}, \quad (20)$$

c_p is the specific heat, and Δm is the mass per unit area in the layer. The subscripts $i+1$ and i denote, respectively, the upper and lower boundaries of the layer. The hydrostatic equilibrium condition $\Delta m = \rho \Delta z = -\Delta P/g$, can be substituted into Equation (19) to obtain the expression

$$\frac{dT}{dt} (^{\circ}\text{C/day}) = \frac{-8.4672}{\Delta P} \frac{\Delta F}{(mb)} \frac{(w/m^2)}{(mb)}, \quad (21)$$

where ΔP is the pressure difference ($P_{i+1} - P_i$) across the layer.

IV. Results and Discussion

Upward and downward fluxes and heating rates have been calculated for CH_4 and N_2O using the correlated- k transmission model for the following problem specifications:

1. McClatchey mid latitude, summer, model atmosphere temperature-pressure distribution.
2. Altitude resolution;
 - a. 1 km, 0-20 km altitude,
 - b. 2 km, 20-60 km altitude.
3. A ground temperature of 294 K.
4. A CH_4 mixing ratio of 1.75 ppm, constant with altitude.
5. An N_2O mixing ratio of 0.31 ppm, constant with altitude.
6. A wavenumber range of 1100 to 1340 cm^{-1} (~7.5-9 microns), in 20 cm^{-1} bands.

Figures 5 (CH_4) and 6 (N_2O) show the downward flux (a), the heating rate (b), the upward flux (c), and the net upward flux (d), as a function of altitude for the wavenumber range 1100-1340 cm^{-1} . The net upward flux is defined as the upward flux at each atmospheric level minus the upward flux due to the ground at the bottom of the atmosphere. The net upward flux is illustrated for the purpose of direct comparison to the LO results. The line by line calculations of

LO for the downward flux, net upward flux, and heating rates are shown as dotted lines in Figures 5a, b, d and 6a, b, d. The wave number spacing for the line by line calculations was 0.005 cm^{-1} for altitudes below 15 km and 0.0005 cm^{-1} for altitudes above 15 km, yielding between 4000 and 40000 points within the 20 cm^{-1} wave number band. These numbers are to be compared with the 43 k(g) points for the same 20 cm^{-1} wave number band for the k -distribution transmission model. The results for CH_4 (Figure 5) show that fluxes agree to ~ 8 percent with the line by line calculations. The heating rate calculations show good agreement up to an altitude of ~ 45 km with the line by line results. The quality of the agreement below 45 km is of the same order as that given by the LO results. Above 45 km the heating rate shows a large negative excursion which is correlated with a temperature maximum at 47 km. In the region between 45 and 60 km the k -distribution model produces heating rates which are greater than the line by line results by ~ 4 percent. Test calculations seem to indicate that the agreement of the heating rates in these altitude regimes depends on how accurately the high opacity end of the low pressure k -distributions can be resolved.

The results for N_2O (Figure 6) exhibit similar behavior to the CH_4 results. The fluxes agree with the line by line values to better than ~ 15 percent. The heating rates below ~ 45 km show good agreement with the line by line values and is of the same quality as the CH_4 results. Above 45 km there is a disagreement in the heating rates which amounts to ~ 5 percent.

As a test of the sensitivity of the method to the size of the wavenumber subintervals, a set of heating rate calculations were made using a subinterval size of 40 cm^{-1} . The heating rate variation as a function of altitude at the 40 cm^{-1} interval size for CH_4 and N_2O is shown in Figures 7a and 7b respectively. The accuracy of the 40 cm^{-1} interval calculation in the 45 to 60 km altitude range decreases compared to 20 cm^{-1} interval size calculation. For CH_4 the error in the heating rate goes from ~ 4 percent to ~ 12 percent as the interval size goes from 20 cm^{-1} to 40 cm^{-1} . For N_2O the error in the heating rate goes from ~ 5 percent to ~ 42 percent as the interval size increases from 20 cm^{-1} to 40 cm^{-1} . The decrease in the heating rate error is due to two factors, a smaller variation of the Planck function across the interval and increase in resolution of the k -distribution. The allocation of the error difference between these two factors depends on the spectral characteristics of the gases being considered.

The CH_4 and N_2O heating rate calculations of LO, using k -distributions based on the Malkmus Band Model to calculate the transmissions, agree with the line by line results to within approximately 5 percent on the 45 to 60 km altitude region (since this is the altitude region when doppler line cores become important). The agreement at the lower altitudes is much better. In the 0-60 km altitude region, the FP k -distribution model used in this paper and the Malkmus k -distribution model, used by LO, produce approximately the same results. The calculations in this paper have been done using a wave number band spacing of 20 cm^{-1} and 43 k intervals for the k -distribution in order to resolve the sharply peaked k distributions in the stratosphere. These numbers are to be compared with the LO band spacing of 10 cm^{-1} and 36 k intervals for the k -distribution.

The results of the CH_4 and N_2O calculations indicate that the correlated- k method of calculating transmissions appears to be a computationally efficient method which yields good accuracies when compared with line by line calculations. Future work will address the overlap capabilities of the k -distributions for different species as well as the inclusion of more molecules in order to produce a complete longwave radiation transport model. Additional efforts will include numerical improvements to optimize quadratures, allow wider frequency bands, the implementation of a new code to calculate the finely gridded set of monochromatic absorption coefficients used by the ABSORT code, and the addition of clouds and aerosols.

V. Acknowledgment

Work was performed under the auspices of the U.S. Department of Energy by the Lawrence Livermore National Laboratory under contract No. W-7405-Eng-48 and was supported in part by the Department of Energy Office of Environmental Analysis, Office of Health and Environmental Research's Environmental Sciences Division, the U.S. Environmental Protection Agency, and the National Aeronautics and Space Administration. The authors would like to acknowledge the assistance of Raymond Gentry with the numerical calculations.

References

- Clough, S.A., F.X. Kneizys, E.P. Shettle, and G.P. Anderson, 1986: Atmospheric radiance and transmittance: FASCODE2. *Proceedings of the Sixth Conference on Atmospheric Radiation*, 141-144, Williamsburg, VA.
- Domoto, G.A., 1974: Frequency integration for radiative problems involving homogeneous non-gray cases: The inverse transmission function. *J. Quant. Spectrosc. Radiat. Transfer*, 14, 935-942.
- Freedman, R., and J.B. Pollack, 1991: unpublished NASA Report, (FP).
- Goody, R.M., and Y.L. Yung, 1989: *Atmospheric Radiation, Theoretical Basis*, 2nd. Ed., 519 pp., Oxford, New York, NY, (G1).
- Goody, R.M., R. West, L. Chen, and D. Crisp, 1989: The correlated- k method for radiation calculations in nonhomogeneous atmospheres. *J. Quant. Spectrosc. Radiat. Transfer*, 42, 539-550, (G2).
- Lacis A., and V. Oinas, 1991: A description of the correlated k distribution for modeling nongray gaseous absorption, emission, and multiple scattering in vertically inhomogeneous atmospheres. *J. Geophys. Res.*, 96, D5, 9027-9063, (LO).
- Malkmus, W., 1967: Random lorentz band model with exponential tailed s^{-1} line intensity distribution function. *J. Opt. Soc. Am.*, 57, 323-329.
- Rodgers, C.D., 1968: Some extensions and applications of the new random model for molecular band transmission. *Q.J. Royal Met. Soc.*, 94, 399, 99-102.
- Rothman, L.S., R.R. Gamache, R.H. Tipping, C.P. Rinsland, M.A.H. Smith, D.C. Benner, V. Malathy Devi, J.-M. Flaud, C. Camy-Peyret, A. Perrin, A. Goldman, S.T. Massie, L.R. Brown, and R.A. Toth, 1992: The HITRAN molecular database: Editions of 1991 and 1992. *J. Quant. Spectrosc. Radiat. Transfer*, in press.
- West, R., D. Crisp, and L. Chen, 1990: Mapping transformations for broad band atmospheric radiation calculations. *J. Quant. Spectrosc. Radiat. Transfer*, 43, 191-199, (W1).

Figure Captions

- Figure 1. A block diagram of the calculation of the upward and downward fluxes and the heating rates. The SELECT Code accesses the HITRAN-91 data base and outputs the appropriate line transition data for the selected molecular species. The FASCODE Code takes the output of the SELECT Code plus the temperature-pressure relation and mixing ratio values from the model atmosphere and produces a line by line opacity vs. wave number data base for the selected wave number band. The ABSORT Code uses the line by line data base output from the FASCODE Code to calculate the $f(k)$, $g(k)$, and $k(g)$ relations for each atmospheric point. The CORKI Code uses the $k(g)$ relations calculated in the ABSORT Code and the model atmosphere to calculate fluxes and heating rates at each atmospheric level.
- Figure 2. The CH_4 opacity distribution function, $f(k)$ (Figure 2a), cumulative probability, $g(k)$ (Figure 2b), and k -distribution, $k(g)$ (Figure 2c), for the wave number band 1300–1320 cm^{-1} , at $T = 272.23 \text{ K}$ and $P = 1.48 \text{ mb}$.
- Figure 3. The CH_4 opacity distribution function, $f(k)$ (Figure 3a), cumulative probability, $g(k)$ (Figure 3b), and k -distribution, $k(g)$ (Figure 3c), for the wave number band 1300–1320 cm^{-1} , at $T = 291.66 \text{ K}$ and $P = 945.2 \text{ mb}$.
- Figure 4. The CH_4 k -distributions for the wave number band 1300–1320 cm^{-1} , at five atmospheric pressure levels, $P = 1.48, 18.05, 102.44, 542.36$, and 945.28 mb .
- Figure 5. The altitude variation of the radiative fluxes and heating rate for CH_4 in the wave number band 1100–1340 cm^{-1} using a 29 cm^{-1} subinterval size. Figure 5a shows the altitude variation of the downward flux (W/m^2). Figure 5b shows the altitude variation of the heating rate (deg C/day). Figure 5c shows the altitude variation of the upward flux (W/m^2). Figure 5d shows the altitude variation of the net upward flux (W/m^2). The net upward flux is defined as the upward flux at a particular atmospheric level minus the upward flux due to the ground at the bottom of the atmosphere. The dotted lines shown in Figures 5a, 5b, and 5c are the line by line values of LO.
- Figure 6. The altitude variation of the radiative fluxes and heating rate for N_2O in the wave number band 1100–1340 cm^{-1} using a 29 cm^{-1} subinterval size. Figure 6a shows the altitude variation of the downward flux (W/m^2). Figure 6b shows the altitude variation of the heating rate (deg C/day). Figure 6c shows the altitude variation of the upward flux (W/m^2). Figure 6d shows the altitude variation of the net upward flux (W/m^2). The net upward flux is defined as the upward flux at a particular atmospheric level minus the upward flux due to the ground at the bottom of the atmosphere. The dotted lines shown in Figures 6a, 6b, and 6c are the line by line values of LO.
- Figure 7. The altitude variation of the heating rate (deg C/day) in the wave number band 1100–1340 cm^{-1} , using a 40 cm^{-1} subinterval size. Figure 7a shows the CH_4 heating rate variation and Figure 7b shows the N_2O heating rate variation.

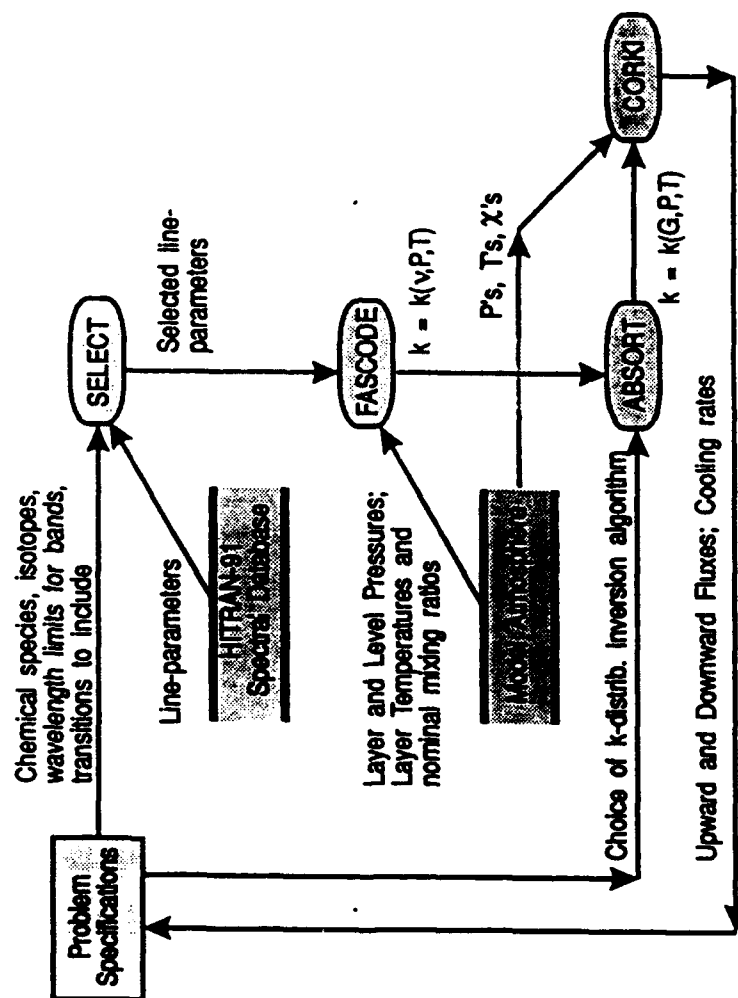
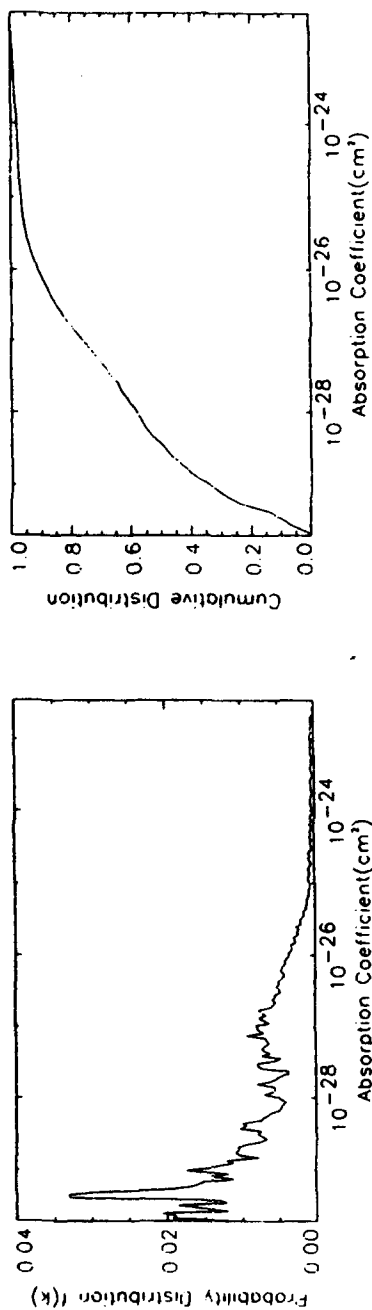
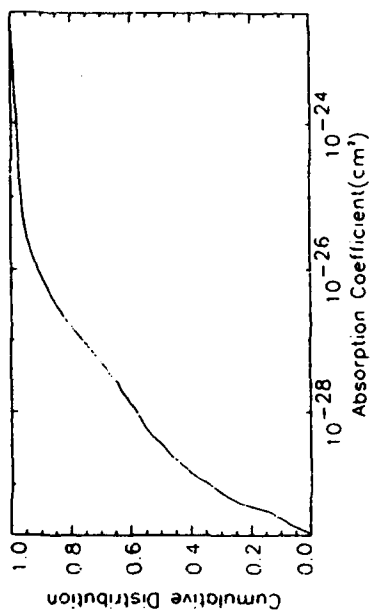


Figure 1

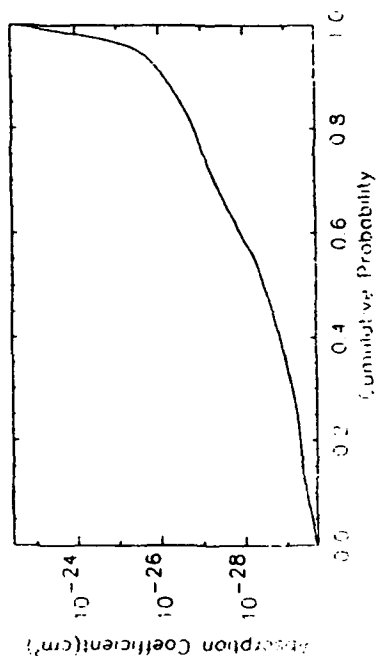
CH₄



(a)



(b)



(c)

Pressure	1.480
Temperature	272.23
Bond Low	1300.0
Bond High	1320.0

Figure 2

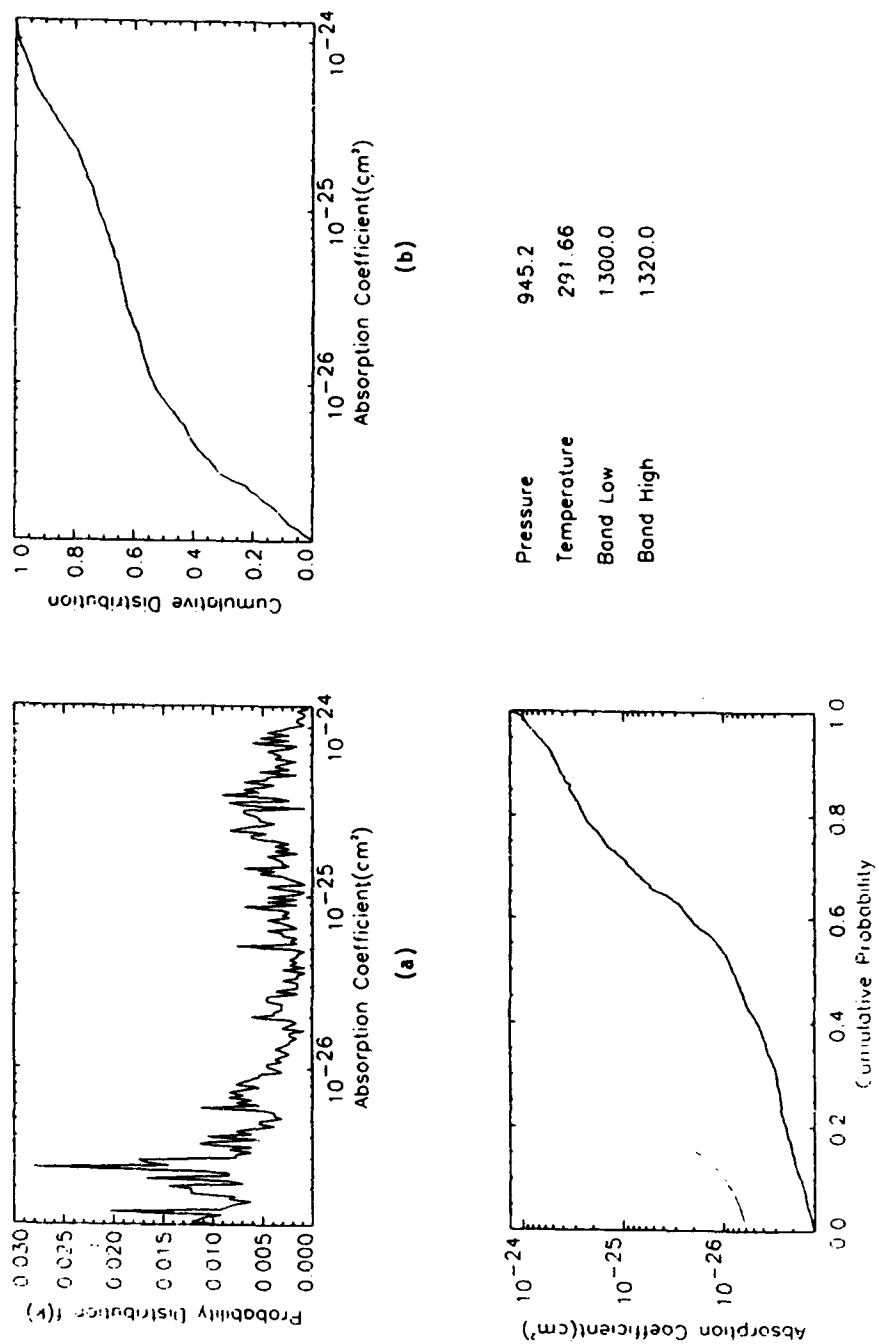
CH₄

Figure 3

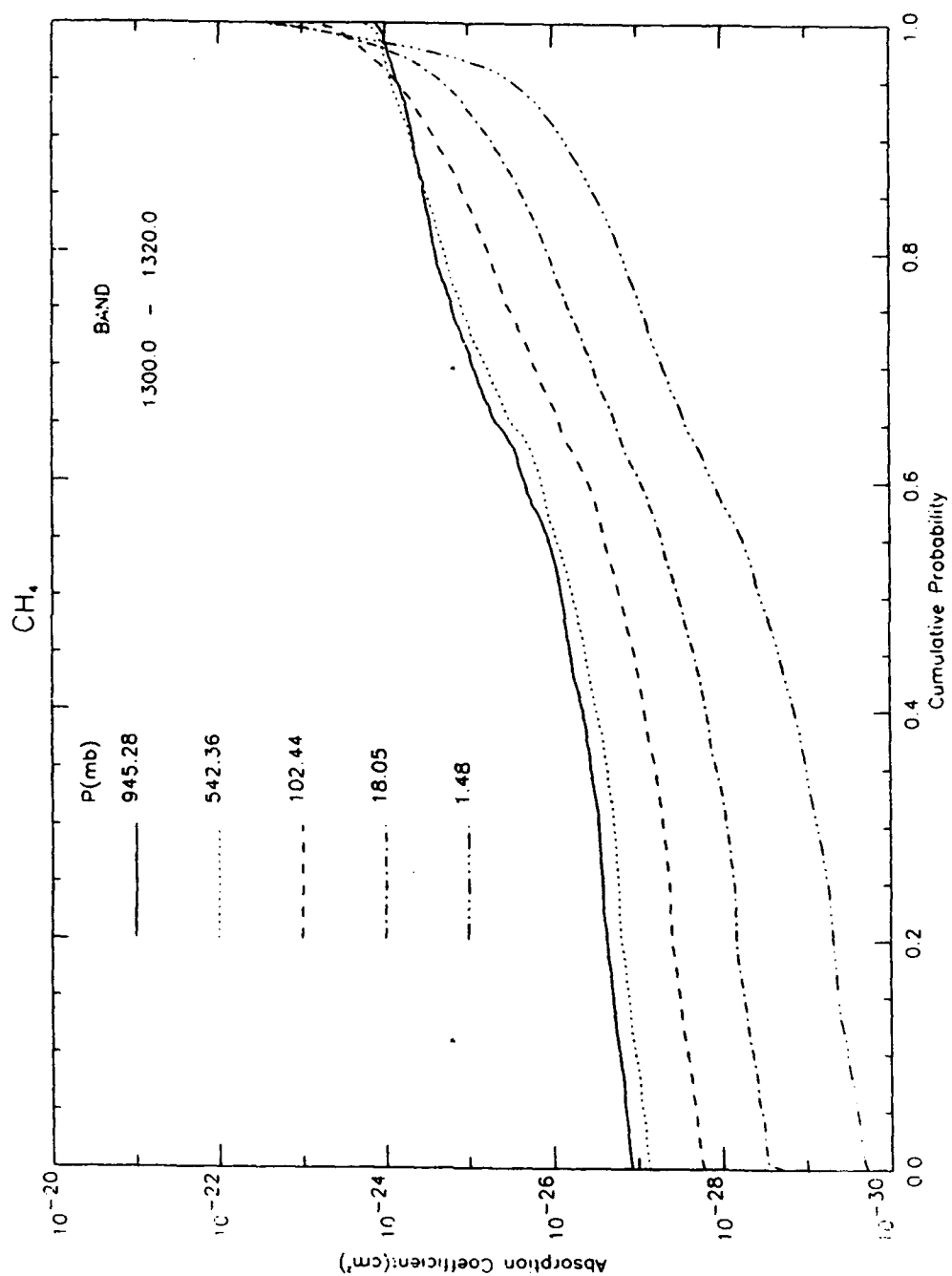


Figure 4

CH, 40 points

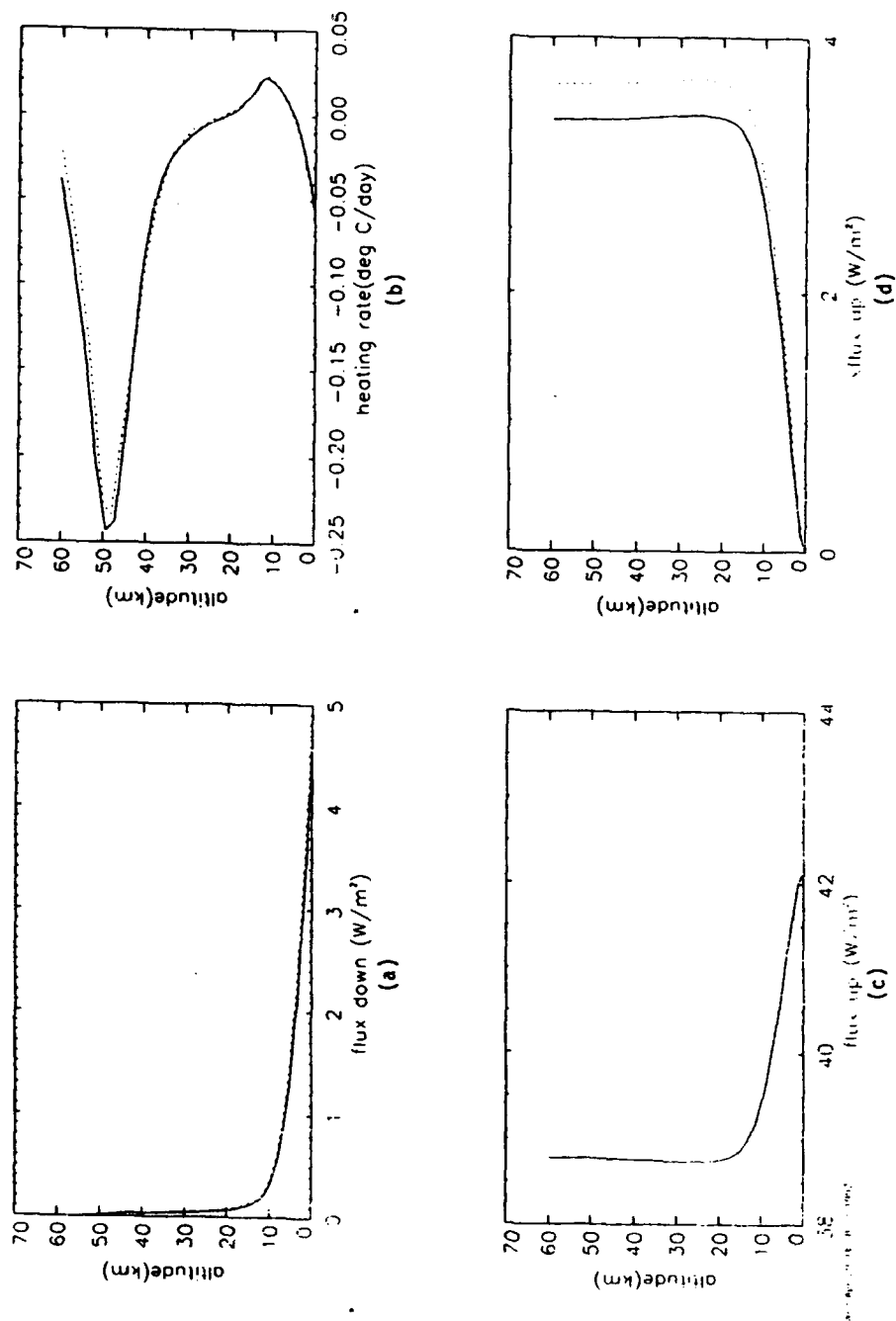


Figure 5

N₂O 40 points

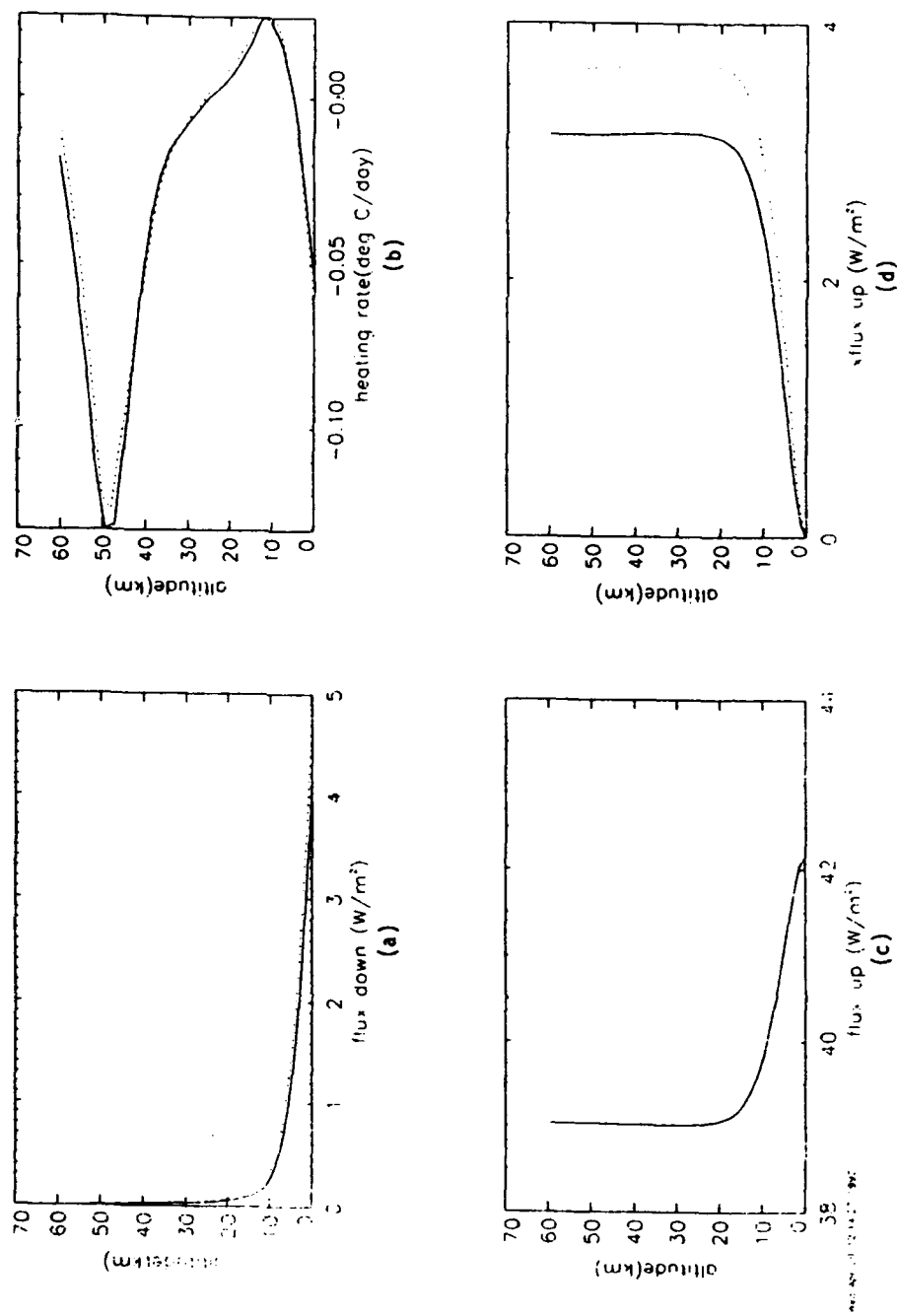
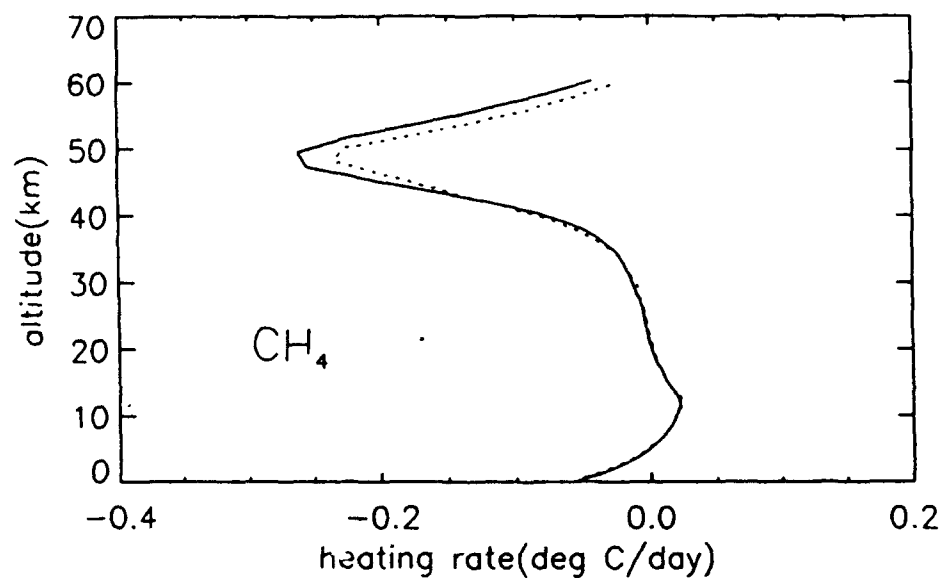
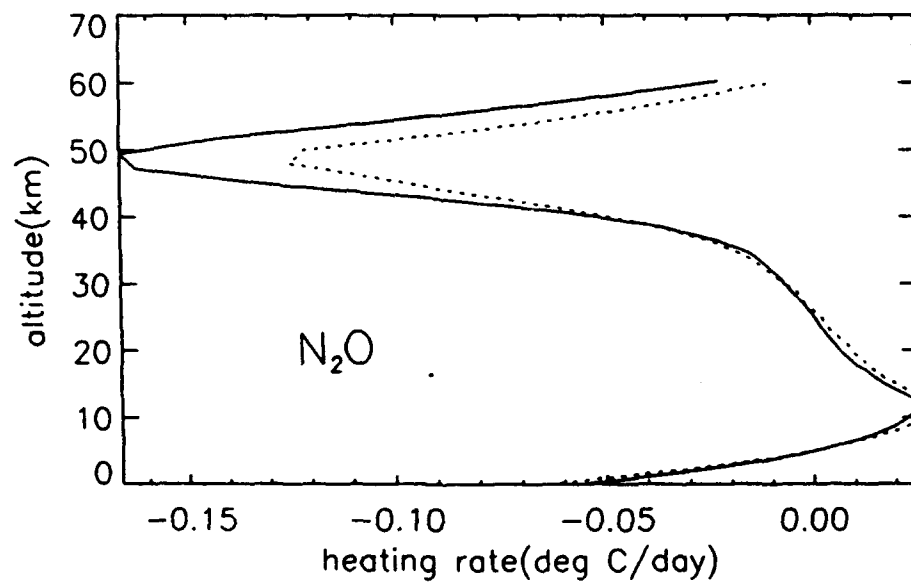


Figure 6



(a)



(b)

Figure 7

LINE BY LINE CALCULATION OF ATMOSPHERIC FLUXES AND COOLING RATES: APPLICATION TO WATER VAPOR, OZONE, CARBON DIOXIDE AND THE FLUOROCARBONS

**S.A. Clough, M.J. Iacono, J.-L. Moncet
Atmospheric and Environmental Research, Inc.,
840 Memorial Drive, Cambridge, MA 02139**

Line by line calculations of atmospheric fluxes and heating rates for the long wave spectral region have been performed to assess methods of treating the overlap of carbon dioxide and water vapor and to study approximate methods for including the effects of heavy molecules including the fluorocarbons. In developing these results we have explicitly considered the role of the water vapor continuum [1] and the effect of doubling carbon dioxide. The role of the water vapor continuum is explicitly considered. Comparisons with results from ICRCCM will be presented. A vectorized version of FASCODE with the capability of obtaining fluxes has been utilized for these calculations. The strong correlation of the spectral cooling rates and the outgoing spectral radiance is emphasized as well as the importance of the spectral region from 0 - 600 cm^{-1} .

1. Clough, S.A., F.X. Kneizys and R.W. Davies, 1989: Line Shape and the Water Vapor Continuum, *Atmospheric Research*, **23**, 229-241.

AEROSOLS

and

CLOUDS

BACKSCAT LIDAR SIMULATION: VERSION 3.0

**J.R. Hummel, D.R. Longtin, N.L. DePiero, R.J. Grasso
SPARTA, Inc., 24 Hartwell Avenue, Lexington, MA 02173**

The Geophysics Directorate of Phillips Laboratory is developing a number of lidar systems for use in probing the atmosphere. These systems include backscatter lidars to study atmospheric aerosols, Doppler lidar systems to measure wind fields, and Raman lidars to study the distributions of different molecular species. To aid in the design and use of such lidar systems, SPARTA has developed a lidar simulation program, BACKSCAT. Originally developed to include only the backscattered return from aerosols, the simulation package has evolved to also include Raman scattering processes. This paper describes a new version of the simulation system, BACKSCAT Version 3.0.

BACKSCAT Version 3.0 includes two significant improvements. The first is the inclusion of user-defined aerosol layers and the second is the consideration of Raman scattering processes. (The description of the Raman scattering options within BACKSCAT Version 3.0 will be described in a companion paper.)

In BACKSCAT Version 3.0, a user-defined aerosol layer is defined by a number density profile, a size distribution shape, and an index of refraction. Aerosol attenuation properties are computed using an efficient Mie scattering program that is coupled to the BACKSCAT simulation system. Users can select from a library of aerosol indices of refraction for common aerosols, or they can input specific values.

Research Supported by Phillips Laboratory, Geophysics Directorate, Contract F19628-91-C-0093.

BACKSCAT LIDAR SIMULATION VERSION 3.0

By:
J.R. Hummel, D.R. Longtin, N.L. DePiero,
and R.J. Grasso
SPARTA, Inc.
24 Hartwell Avenue
Lexington, MA 02173

3 June 1992
Annual Review Conference on
Atmospheric Transmission Models
Hanscom AFB, MA

Funded By Contract F19628-91-C-0093

model 1.0.0.3



BRIEFING OUTLINE

SPARTA, INC.

- Background and Objectives of Work
- Overview of BACKSCAT Version 3.0
- Changes and New Features
- Summary and Recommendations for Future Work

back2.m3



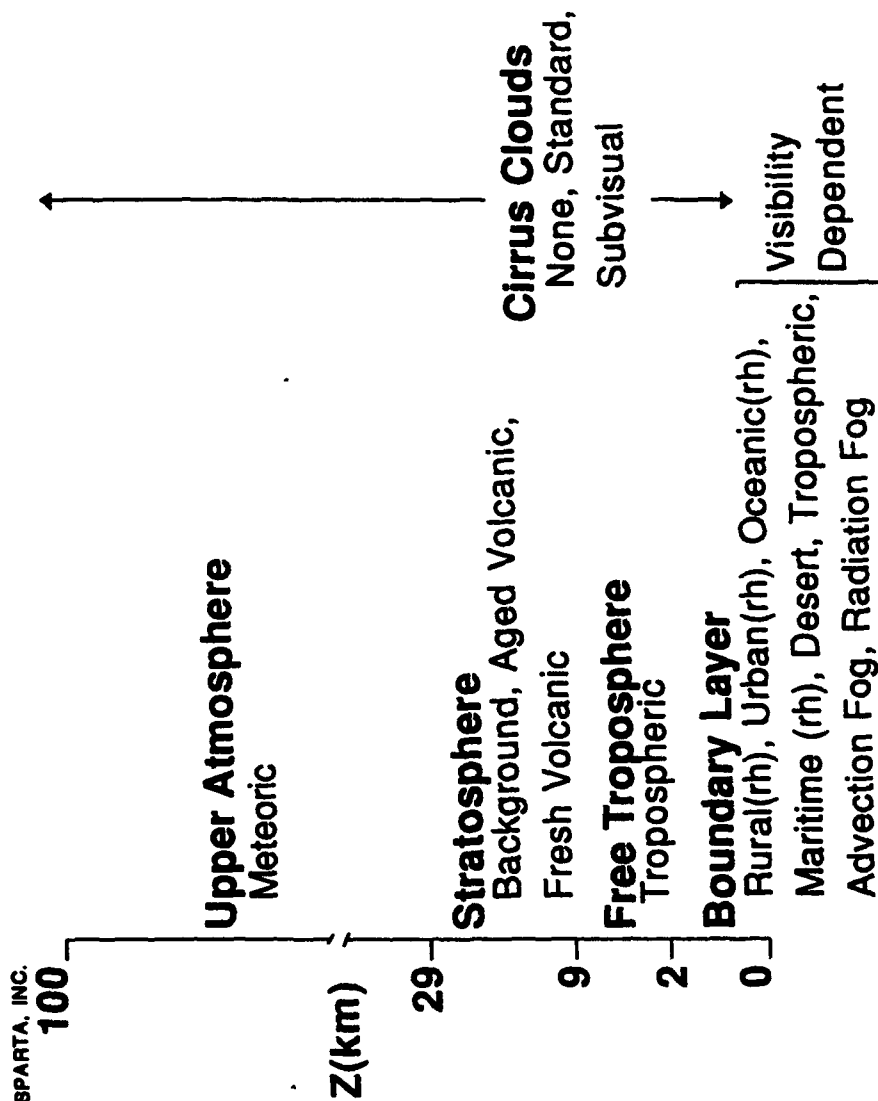
OVERVIEW OF BACKSCAT VERSION 3.0

SPARTA, INC.

- BACKSCAT Was Designed as a Tool For Use in Studying the Performance of Lidar Systems Under Realistic Environmental Conditions
- BACKSCAT Offers the User the Option of:
 - Describing the Atmosphere With a Library of Built-in Aerosol and Atmospheric Models
 - Inputting Actual Propagation Profiles, Such as From a Field Program



OVERVIEW OF BACKSCAT VERSION 3.0 (Cont.)



bcat3b



EVOLUTION OF THE BACKSCAT LIDAR SIMULATION SYSTEM

SPARTA, INC.

1990 Version 1.0

FORTTRAN Based System With
AFGL Aerosol Models as
Built-in Defaults

1991 Version 2.0

- New C-Based Menu System
- Cirrus Clouds and Desert
Aerosols Added

1992 Version 3.0

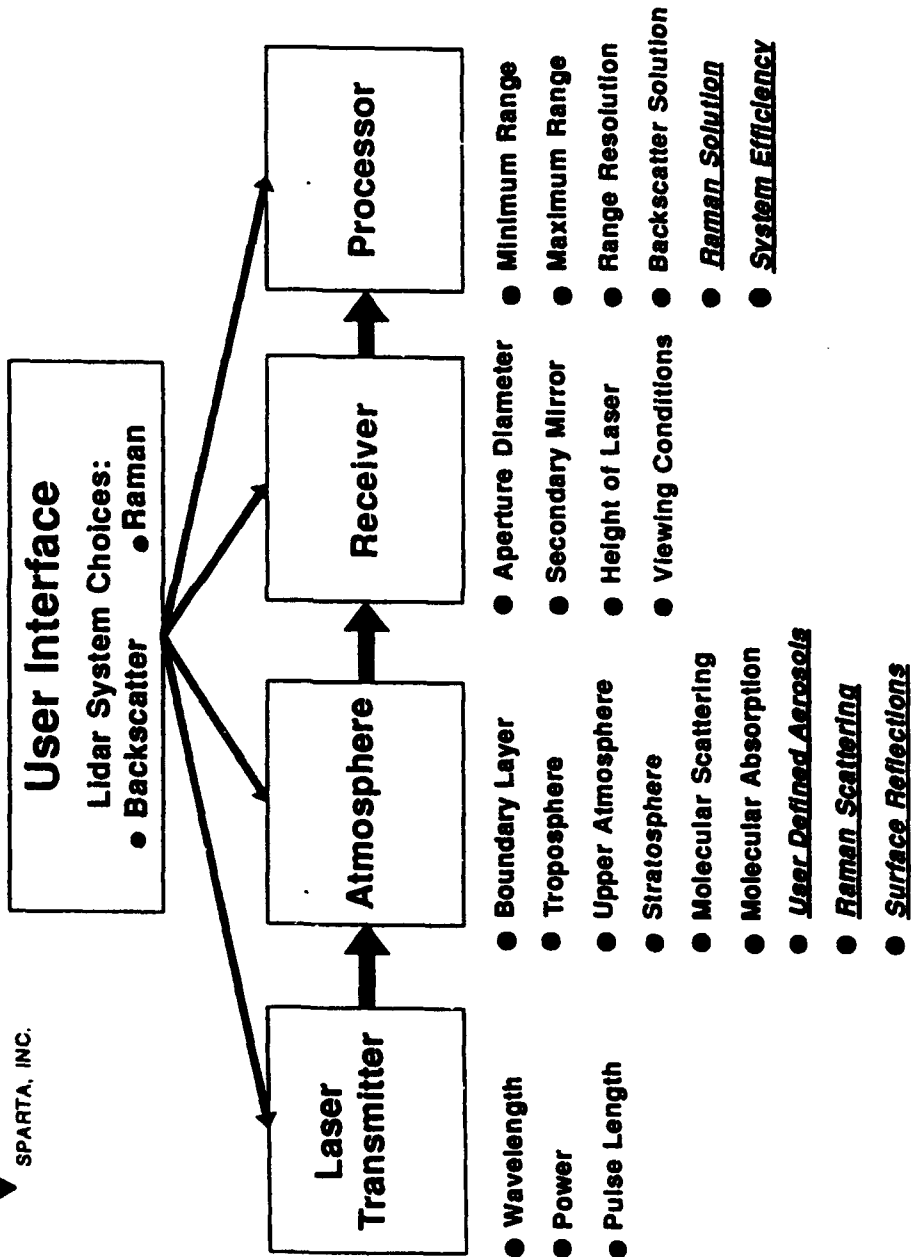
- Surface Reflections Added
- User-Defined Aerosols
- System Efficiency Considered
- Raman Lidars Simulated



OVERVIEW OF BACKSCAT VERSION 3.0

LIDAR SIMULATION SYSTEM

SPARTA, INC.



BACKSCAT



OVERVIEW OF CHANGES AND NEW FEATURES

SPARTA, INC.

CHANGES

- Improvements to the Menu System
- Corrections of Errata

NEW FEATURES

- Surface Reflections
- User-Defined Aerosols
- Raman Lidar Can Be Simulated
- System Efficiency Added

hw015.010



SPARTA, INC.

CHANGES IN BACKSCAT VERSION 3.0

- Improvements to the Menu System
 - Listing of Available Files
 - Improved File Handling
- Corrections of Errata
 - Improper Accounting of Cirrus Backscattering
 - Error in Adjusting Molecular Contributions When Cirrus Clouds are Present



NEW FEATURES IN BACKSCAT VERSION 3.0

SPARTA, INC.

- Addition of Surface Reflections
- Inclusion of System Efficiency
- Ability to Add User-Defined Aerosol Layers
- Ability to Model Raman Lidar Systems



NEW FEATURES IN BACKSCAT VERSION 3.0 (Cont.)

SPARTA, INC.

- Addition of Surface Reflections
 - Wavelength-Dependent Surface Albedo
a New User Input
- Inclusion of System Efficiency
 - All System Loss Terms Lumped Into a
Single System Efficiency Term
 - Serves as a Basis for Developing a
Full Single-to-Noise Treatment



NEW FEATURES USER-DEFINED AEROSOLS

SPARTA, INC.

- BACKSCAT's Aerosol Choices are Based on the AFGL Aerosol Models
- Numerous Users Wished to Study Aerosols Different From Those Built Into BACKSCAT
 - Different Altitudes
 - Different Aerosol Types



NEW FEATURES USER-DEFINED AEROSOLS (Cont.)

SPARTA, INC.

- The Mie Scattering Code (FMIE3B) of Shettle and Longtin Has Been Coupled to BACKSCAT Version 3.0
- User Inputs:
 - Normalized Size Distribution Shape
 - Total Number Density Profile at a Maximum of Five Altitudes
 - Particle Complex Index of Refraction



NEW FEATURES

USER-DEFINED AEROSOLS (Cont.)

SPARTA, INC.

- Normalized Size Distribution Shape
 - Log Normal
 - Modified Gamma
 - User Defined
- Particle Complex Index of Refraction
 - User Defined
 - Choose From Built-in Library of Values:

Water

Ice

Dust

Smoke

Maritime Aerosols

Stratospheric Aerosols

0000110.003

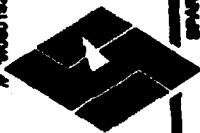


NEW FEATURES USER-DEFINED AEROSOLS (Cont.)

SPARTA, INC.

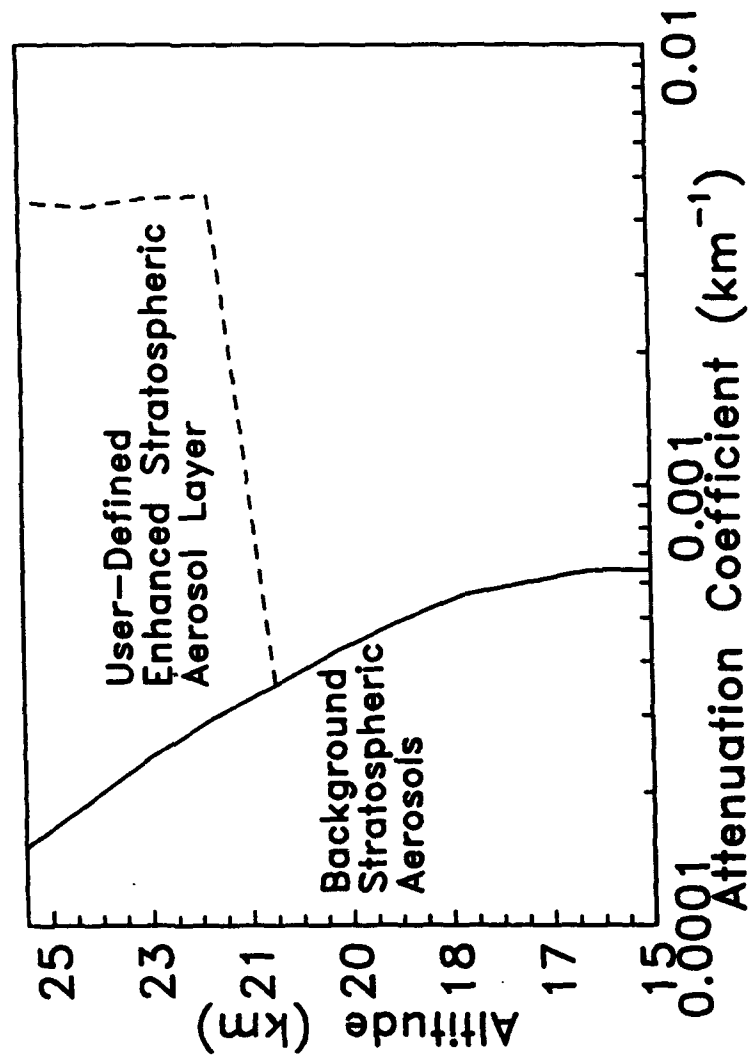
- FMIE3B Utilizes Different Approximations for the Mie Calculations in Order to Provide Rapid Execution Times
- FMIE3B Provides Accuracy Within +/- 20% for Large Particles Relative to a Full Mie Calculation

SPARTA INC.



NEW FEATURES USER-DEFINED AEROSOLS (Cont.)

SPARTA INC.





NEW FEATURES MODELING RAMAN LIDAR (Cont.)

SPARTA, INC.

- Option for Simulating Raman Scattering Processes
- User Selects the Molecule (N_2 , CO_2 , H_2O , O_3 , or O_2)
- Raman Cross Sections Calculated Internally or User-Supplied



SUMMARY AND RECOMMENDATIONS

SPARTA, INC.

SUMMARY

- Version 3.0 of BACKSCAT, a Lidar Simulation System Will be Available Summer 1992

- Changes and New Features Include:
 - Improvements to the Menu System
 - Corrections of Errata
 - Addition of Surface Reflections
 - Addition of System Efficiency
 - Addition of User-Defined Aerosols
 - Additions of a Raman Lidar Option



SUMMARY AND RECOMMENDATIONS (Cont.)

SPARTA, INC.

RECOMMENDATIONS FOR FUTURE WORK

- Continue the Evolutionary Growth of BACKSCAT to Include the Simulation of Additional Lidar Systems (*i.e.* Doppler, DIAL)
- Include a Full Treatment of Signal-to-Noise for Performance Studies
- Include the Capability to Invert Solutions From Actual Lidar Profiles

SPART11.023

DEVELOPMENT OF A RAMAN LIDAR SIMULATION OPTION WITHIN BACKSCAT VERSION 3.0

**R.J. Grasso, J.R. Hummel
SPARTA, Inc., 24 Hartwell Avenue, Lexington, MA 02173**

Raman lidar is a useful and powerful tool for remote probing of the atmosphere. With Raman lidars, one can accurately determine the identification and concentration of a particular molecular specie present in the atmosphere. Results are presented from an effort to develop a simulation capability of Raman lidar systems for the remote detection of atmospheric gases and/or air polluting hydrocarbons. Our model, which integrates remote Raman spectroscopy with SPARTA's BACKSCAT Version 3.0 atmospheric lidar simulation package, permits accurate determination of the performance of a Raman lidar system.

The accuracy of the model results from the accurate calculation, at any given excitation wavelength, of the differential scattering cross section for the molecular specie under investigation. We show excellent correlation of our calculated cross section data with experimental data from the published literature. In addition, the use of BACKSCAT Version 3.0 package, which provides a user friendly environment to define the operating conditions, provides an accurate calculation of the atmospheric extinction at both the excitation and Raman shifted wavelengths. The Raman option within BACKSCAT Version 3.0 can be used to accurately predict the performance of a Raman lidar system, the concentration and identification of a specie in the atmosphere, or the feasibility of making Raman measurements.

Research Supported by Phillips Laboratory, Geophysics Directorate, Contract F19628-91-C-0093

DEVELOPMENT OF A RAMAN LIDAR SIMULATON OPTION WITHIN BACKSCAT VERSION 3.0

By:

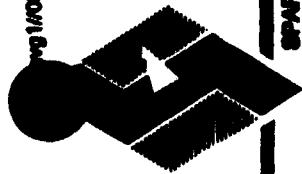
**Robert J. Grasso and John R. Hummel
SPARTA, Inc.
24 Hartwell Avenue
Lexington, MA 02173**

3 June 1992

Presented To:

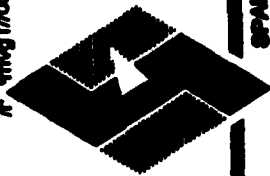
**Annual Review Conference on Atmospheric Transmission Models
Hanscom AFB, MA 01731-5000**

Funded By Air Force Contract F19628-91-C-0093



OUTLINE OF BRIEFING

- Background and Purpose of the Study
- Overview of the Raman Effect
- Results of a Literature Review for Sources of Raman Scattering Cross Sections
- Development of a Model for Raman Cross Sections
- Implementing a Raman Simulation in the BACKSCAT Version 3.0 System



SPARTA INC.

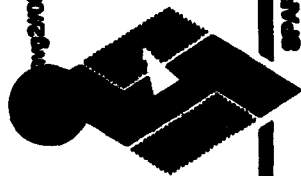
BACKGROUND AND PURPOSE OF THE STUDY

BACKGROUND

- Raman Lidars Provide a Powerful Tool for Probing the Atmosphere to Obtain Information on the Distribution of Various Molecular Constituents
- SPARTA has Developed for Phillips Laboratory/Geophysics Directorate a Lidar Simulation System, BACKSCAT, That Provides a Framework for the Addition of a Raman Lidar Simulation Capability

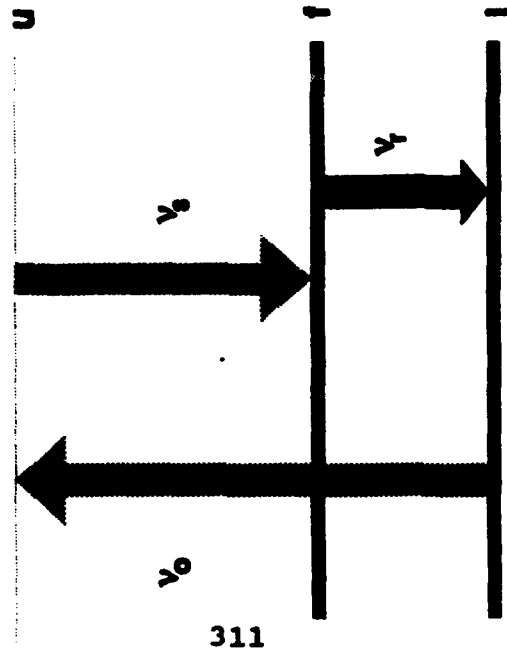
PURPOSE OF STUDY

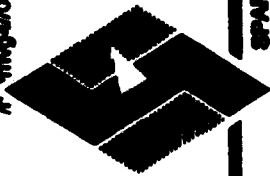
- Describe the Physics Necessary to Perform a Raman Lidar Simulation
- Review the Literature to Identify Sources of Raman Scattering Cross Sections
- Implement a Raman Lidar Simulation Capability Within the BACKSCAT Version 3.0 Framework



OVERVIEW OF THE RAMAN EFFECT

- A Photon of Exciting Energy is Absorbed by a Molecule of a Given Initial State, ν_0
- The Molecule is Elevated to a Virtual State Through an Inelastic Collision
- The Molecule Relaxes to a Final State, ν_s , and Becomes the Stokes Line
- A Photon is Emitted With a Raman Shifted Frequency Corresponding to the Energy Difference Between the Two States, $\nu_r = \nu_0 - \nu_s$





IMPLEMENTING A RAMAN SIMULATION IN THE BACKSCAT FRAMEWORK

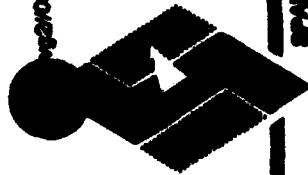
SPARTA INC.

- The Lidar Equation for a Raman Lidar With a Filtered Receiver is:

$$P_r(\lambda_r, R) = \frac{P_o(\lambda_o)\tau c\eta_{sys}A}{2R^2} \left[\beta_m(\lambda_r, R) + \beta_a(\lambda_r, R) + \frac{d\sigma(\lambda_o)}{d\Omega} N_i(R) \right] T(\lambda_o, R) T(\lambda_r, R)$$

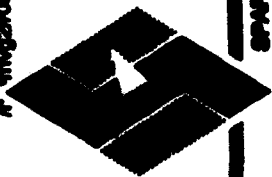
Where:

- $P_r(\lambda_r, R)$ and $P_o(\lambda_o)$ are the Received and Transmitted Laser Power at the Raman Shifted (λ_r) and Transmitted (λ_o) Wavelengths, Respectively
- τ is the Pulse Length, c is the Speed of Light, η_{sys} is the Total System Efficiency, A is the Collecting Area of the Receiver and R is the Range
- $\beta_m(\lambda_r, R)$ and $\beta_a(\lambda_r, R)$ are the Molecular and Aerosol Backscattering
- $\frac{d\sigma}{d\Omega}$ is the Differential Raman Scattering Cross Section as a Function of Solid Angle and $N_i(R)$ is the Concentration of the Species Being Probed
- $T(\lambda_o, R)$ and $T(\lambda_r, R)$ are the One-Way Total Atmospheric Transmissions



RAMAN LIDAR LITERATURE SEARCH

- Reviewed References to Raman Cross Sections of Simple Molecules Based Upon Empirical Measurements at Specific Excitation Wavelengths
- Reviewed Literature to Formulate a Theoretical Model for the Raman Cross Section for Simple and Complex Molecules at Any Excitation Wavelength
- Empirical Data Reviewed Consisted of Pre-Laser (H_g Lamp) and Laser (CW and Pulsed) Excitation of Samples
- Most Cross Section Data Measurements Were Made Using Argon-Ion Lasers at 488 nm and 514.5 nm



SPARTAN INC.

- Complete Data Exist for Most Atmospheric Gases (N_2 , CO_2 , H_2O , and O_2) and Most "Air Polluting" Hydrocarbons (C_2H_2 , NO_2 , CH_4 , CO , H_2S , and SO_2)
- Lack of Data Exist for O_3 , Two References Found, Only One Appears Valid
- Review Article by Schrotter and Klockner (1979) Presents the Most Complete Compilation of Experimental Cross Section Data
- Definite Lack of Published Data on Cross Section Measurements at Wavelengths Shorter Than 337 nm

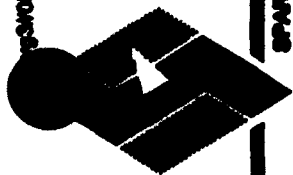


SUMMARY OF RAMAN CROSS SECTIONS FOR NITROGEN

EXCITING WAVELENGTH (nm)	DIFFERENTIAL RAMAN SCATTERING CROSS SECTION ($10^{-31} \text{ cm}^2 \text{ sr}^{-1}$)	UNCERTAINTY ($10^{-31} \text{ cm}^2 \text{ sr}^{-1}$)
337.1	35	
347	29 25	
351.1	24.3	± 3.0
363.8	20.4	± 2.5
435.8	9.2	± 1.0
457.9	7.6 7.4	± 0.5 ± 0.3
488	5.6 5.4 4.3	± 0.2 ± 0.3
514.5	4.4 4.3 4.2	± 1.7 ± 0.2 ± 0.2
632.8	2.1	± 0.3

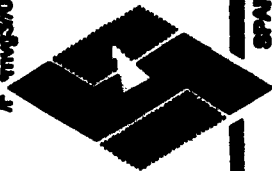
(Cross Sections Normalized With Respect to Nitrogen)

											λ_o (nm)
	Raman Shift										
Molecule	(cm ⁻¹)	337.1	347.0	351.1	363.8	435.8	457.9	488.0	514.5	632.8	
CO ₂	1,388	1.2 1.1 1.0	1.0		1.0			1.3 1.1	1.2 1.2	1.1	
H ₂ O	3,652	3.1 2.2	3.9 3.8					3.8 2.9 2.5	3.4		
O ₃	1,103								3.0		
O ₂	1,555	1.3 1.2 1.1	1.2 1.1 1.1	1.0	1.0	1.1	1.0	1.1 1.0	1.0 1.0 1.0	0.9	



RAMAN CROSS SECTION MODEL

- Raman Scattering Cross Sections are the Basic Data Required to Relate the Scattered Intensity to the Transmitted Wavelength and Specie Number Density
- Raman Cross Sections may be Determined from the Many Empirical Measurements Made at Discrete Excitation Wavelengths With Linear Extrapolation to the Desired Wavelength With Fairly Accurate Results
- A Better Method is to Formulate a Model that Calculates the Raman Scattering Cross Section of a Molecule at any Given Wavelength



RAMAN CROSS SECTION MODEL (Cont.)

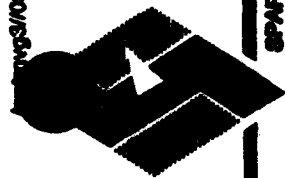
SPARTA INC.

- Model is Based on the Polarizability Theory of Placzek for Raman Scattering Observed Normal to the Polarization of Linearly Polarized Light

$$\frac{d\sigma}{d\Omega} = \left(\frac{2\pi}{c}\right)^4 \frac{b_j^2(\nu_0 - \nu_j)^4}{[1 - \exp(\frac{h\nu_j}{kT})]} g_j(45\alpha_j^2 + 7\gamma_j^2)$$

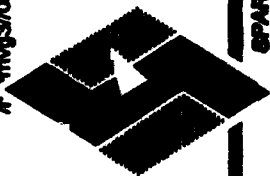
Where:

- ν_0 and ν_j are the Frequencies of Incident Radiation and of the j^{th} Vibrational Mode of the Molecule, Respectively
- $b_j = (h/8\pi^2\nu_j)^{1/2}$ is the Zero Point Amplitude of the Normal Vibrations of the j^{th} Vibrational Mode
- g_j is the Degree of Degeneracy of the j^{th} Vibrational Mode
- α_j and γ_j are the Isotropic and Anisotropic Parts of the Derived Polarizability Tensor
- h is Planck's Constant, k is Boltzmann's Constant, c is the Velocity of Light, and T is the Temperature



RAMAN CROSS SECTION MODEL (Cont.)

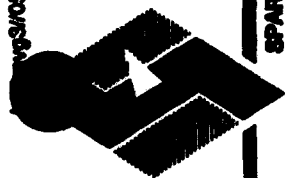
- $\frac{d\sigma}{d\Omega}$ is Dependent Upon Temperature Through the Exponential and is Negligible for $\nu_j < 1000 \text{ cm}^{-1}$
- α_j and γ_j Are Constant for Electronic or Vibrational Rotation Frequencies Located Far From Resonance of the Exciting Frequency
- $\frac{d\sigma}{d\Omega}$ is Dependant upon the Wavelength of the Exciting Radiation Through a Factor of $(\nu_o - \nu_j)^4$
- A Deviation from the $(\nu_o - \nu_j)^4$ Factor Indicates a Resonance Raman Effect Where α_j and γ_j are no Longer Constant
- $\frac{d\sigma}{d\Omega}$ is Independent of the Scattering Geometry



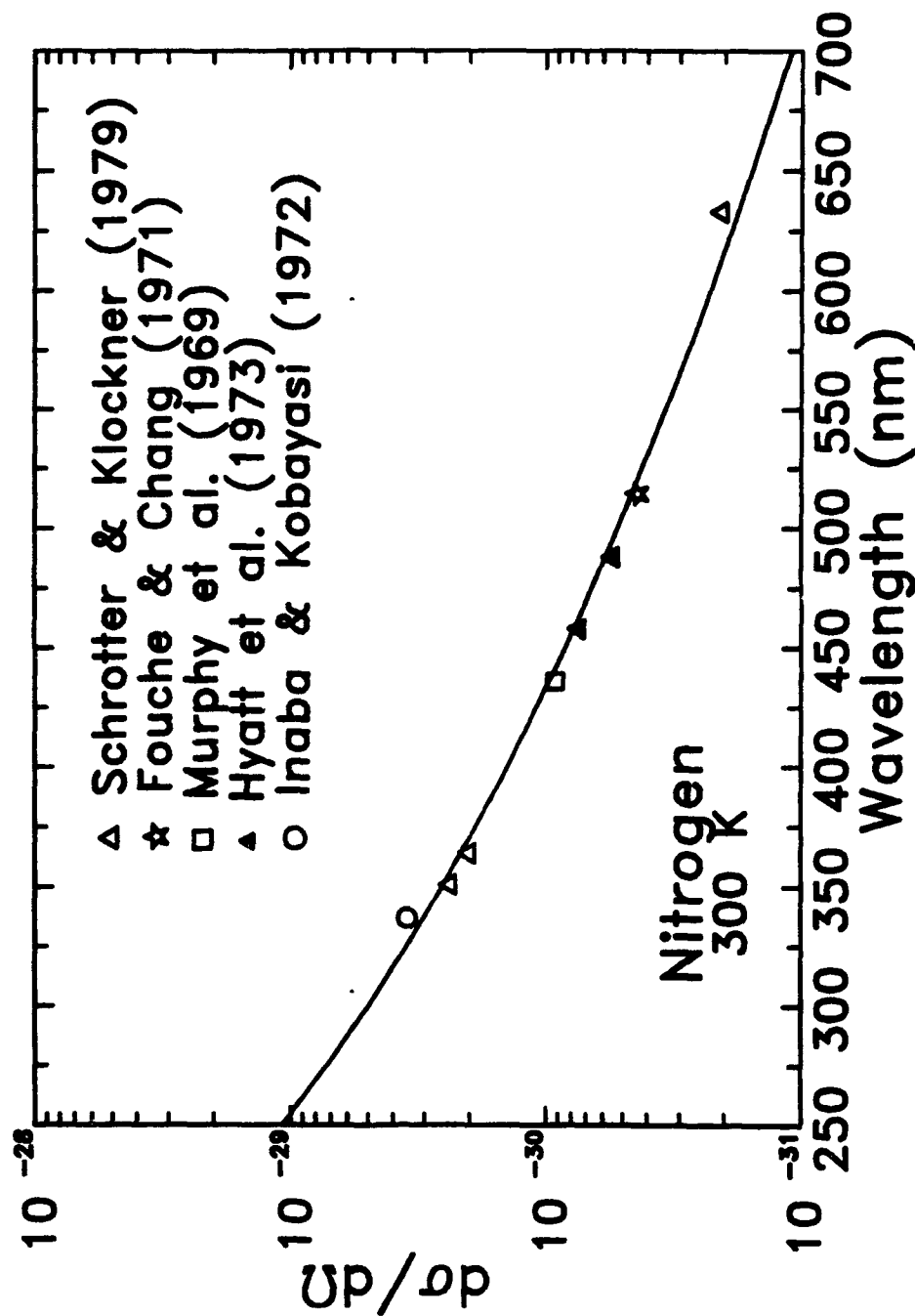
SPARTAN INC.

RAMAN CROSS SECTION MODEL (Cont.)

- $\frac{d\sigma}{d\Omega}$ May Be Calculated for any Molecule at any Excitation Wavelength Knowing the Values of ν_0 , ν_j , T , g_j , α_j , and γ_j
- Since g_j , α_j , and γ_j are Difficult and Time Consuming to Calculate, an Alternate Method has been Derived Which Gives Excellent Correlation to the Published Data
- Deriving $g_j(45\alpha_j^2 + 7\gamma_j^2)$ is Based Upon Taking the Average of the Sum of the Values for g_j , α_j , and γ_j for a Given Molecule
- For Molecules Where No Previous Raman Data Exists, $g_j(45\alpha_j^2 + 7\gamma_j^2)$ Would Have to be Calculated



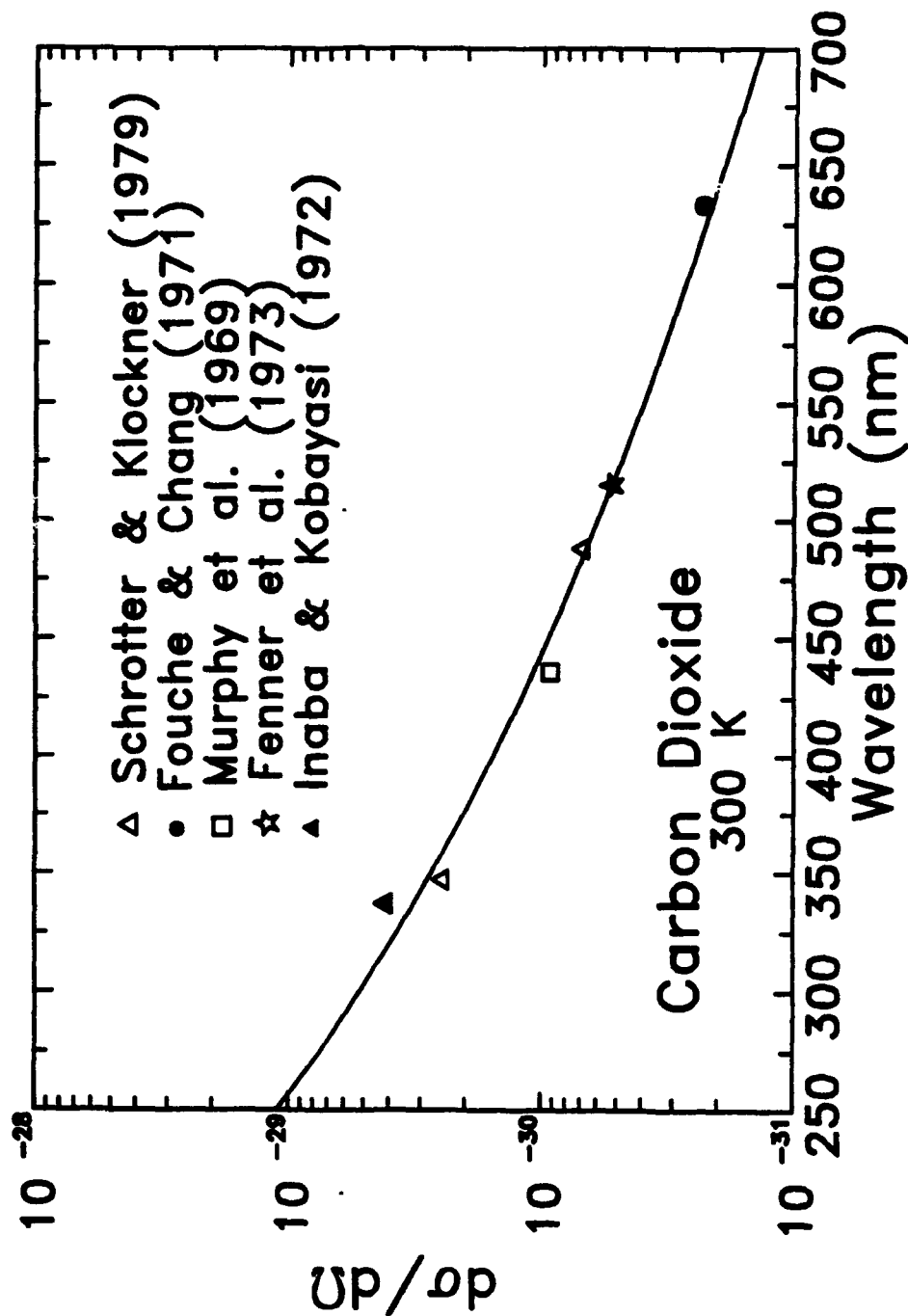
RESULTS FROM RAMAN CROSS SECTION MODEL - NITROGEN

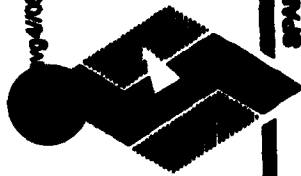




SPARTA INC.

RESULTS FROM RAMAN CROSS SECTION MODEL - CARBON DIOXIDE





SPARTA INC.

SUMMARY AND RECOMMENDATIONS FOR FUTURE WORK

SUMMARY

- Raman Simulation Capability Has Been Added to the Existing BACKSCAT Version 3.0 System
- New User Inputs:
 - Identification of Molecule Being Probed \Rightarrow Raman Shifted Wavelength
 - Total System Efficiency
- Provided Options:
 - Raman Cross Sections can be Calculated Using a Model for the Raman Cross Section or With User-Supplied Values
 - Available Molecules Include N_2 , O_2 , CO_2 , O_3 , and H_2O Vapor With Concentration Profiles Based on the AFGL Model Atmospheres or User Profiles



SPARTA INC.

SUMMARY AND RECOMMENDATIONS

(Cont.)

RECOMMENDATIONS FOR FUTURE WORK

- Add Hydrocarbons to List of Available Molecules
- Expand Capability to Perform Estimates of System Performance and to Invert Profiles From Measured Laser Returns

CALCULATION OF THE ANGULAR RADIANCE DISTRIBUTION FOR A COUPLED SYSTEM OF ATMOSPHERE AND CANOPY MEDIA USING AN IMPROVED GAUSS-SEIDEL ALGORITHM

S. Liang, A.H. Strahler

**Department of Geography and Center for Remote Sensing, Boston University,
725 Commonwealth Avenue, Boston, MA 02215**

The radiative transfer equations of coupled system of atmosphere and canopy media are solved numerically by an improved Gauss-Seidel iteration algorithm. The radiation field is decomposed into three components: uncollided sunlight, single scattering, and multiple scattering radiance for which the corresponding equations and boundary conditions are set up and their analytical or iterational solutions are explicitly derived. The hotspot effect of the canopy is accomplished by means of the modification of extinction coefficients of upward single scattering radiation and uncollided sunlight. To reduce the computation for the case of deep optical thickness, an improved iteration formula is derived to speed convergence. The formulation presented in this paper is well suited to analyze the relative magnitude of multiple scattering radiance and single scattering radiance in both the visible and near infrared regions.

CALCULATION OF THE ANGULAR RADIANCE DISTRIBUTION FOR A COUPLED ATMOSPHERE AND CANOPY

Shunlin Liang & Alan H. Strahler
Center for Remote Sensing, Boston University

1. Introduction

2. Radiative Transfer Models

- * atmospheric radiative transfer equation**
- * canopy radiative transfer equation**
- * canopy leaf model**

3. An Improved Gauss-Seidel Numerical Algorithm

4. Model Validation and Data Analysis

5. Conclusions

Introduction

- *. Limitations of the conventional remote sensing based on nadir observation**
- *. Space-borne multiple angle observations are possible in EOS era**
- *. Individual modeling efforts for the atmosphere and canopy**

Atmospheric radiative transfer equation

$$\mu \frac{\partial I(\tau, \Omega)}{\partial \tau} = I(\tau, \Omega) - \frac{\omega}{4\pi} \int_{4\pi} p(\Omega' \rightarrow \Omega) I(\tau, \Omega') d\Omega'$$

Canopy radiative transfer equation

$$-\mu \frac{\partial I(\tau, \Omega)}{\partial \tau} + h(\tau, \Omega) G(\Omega) I(\tau, \Omega) = \frac{1}{\pi} \int_{4\pi} \Gamma(\Omega' \rightarrow \Omega) I(\tau, \Omega') d\Omega'$$

subject to corresponding boundary conditions.

The function $G(\Omega)$ is the mean projection of a unit foliage area in the direction Ω , i. e.

$$G(\Omega) = \frac{1}{2\pi} \int_{2\pi} g_l(\Omega_l) |\Omega_l \cdot \Omega| d\Omega_l$$

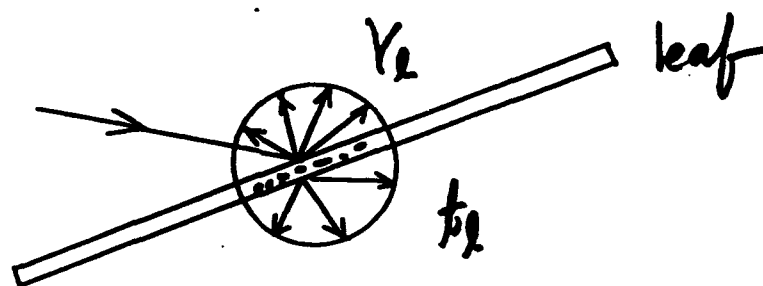
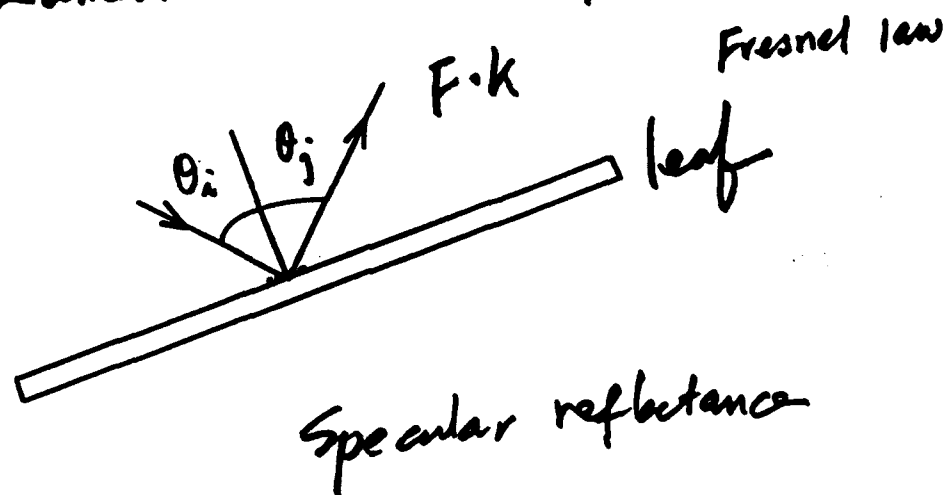
The correction function for hotspot effect is given by

$$h(\tau, \Omega) = 1 - \sqrt{\frac{G(\Omega_0)}{G(\Omega)} \frac{\mu}{|\mu_0|}} \exp \left[-\frac{\Delta(\Omega_0, \Omega)\tau}{kH} \right]$$

It can be observed that in the case of backscattering (i. e., $\Omega = -\Omega_0$), $\Delta(\Omega_0, \Omega) = 0$ and $h(\tau, \Omega) = 0$. The absence of extinction coefficient results in the local maximum of reflectance which is widely termed the hotspot peak.

leaf model:

bi-Lambertian reflectance + Specular reflectance



bi-Lambertian reflectance

The radiative transfer equations and their boundary conditions

are given by

$$\left\{ \begin{array}{l} -\mu \frac{\partial I^M(\tau, \Omega)}{\partial \tau} + I^M(\tau, \Omega) = \frac{\omega}{4\pi} \int_{4\pi} p(\Omega' \rightarrow \Omega) I^M(\tau, \Omega') d\Omega' + Q_1(\tau, \Omega) \quad \tau \leq \tau_a \\ -\mu \frac{\partial I^M(\tau, \Omega)}{\partial \tau} + G(\Omega) I^M(\tau, \Omega) = \frac{1}{\pi} \int_{2\pi} \Gamma(\Omega' \rightarrow \Omega) I^M(\tau, \Omega') d\Omega' + Q_2(\tau, \Omega) \quad \tau_a < \tau \leq \tau_1 \\ I^M(0, \Omega) = 0 \quad \mu < 0 \\ I^M(\tau_1, \Omega) = \int_{2\pi} f_s(\Omega, \Omega') |\mu'| I^M(\tau_1, \Omega') d\Omega' \quad \mu > 0 \end{array} \right.$$

here

$$\left\{ \begin{array}{l} Q_1(\tau, \Omega) = \frac{\omega}{4\pi} \int_{2\pi} p(\Omega' \rightarrow \Omega) I^0(\tau, \Omega') d\Omega' + \frac{\omega}{4\pi} \int_{4\pi} p(\Omega' \rightarrow \Omega) I^1(\tau, \Omega') d\Omega' \quad \tau \leq \tau_a \\ Q_2(\tau, \Omega) = \frac{1}{\pi} \int_{2\pi} \Gamma(\Omega' \rightarrow \Omega) I^0(\tau, \Omega') d\Omega' + \frac{1}{\pi} \int_{4\pi} \Gamma(\Omega' \rightarrow \Omega) I^1(\tau, \Omega') d\Omega' \quad \tau_a < \tau \leq \tau_1 \end{array} \right.$$

For simplicity of discussions, assume that we are faced with such a general equation

$$-\mu \frac{\partial I^M(\tau, \Omega)}{\partial \tau} + f(\Omega) I^M(\tau, \Omega) = J(\tau, \Omega)$$

where

$$f(\Omega) = \begin{cases} 1 & \tau \leq \tau_a \\ G(\Omega) & \tau_a < \tau \leq \tau_1 \end{cases}$$

and the source function is

$$J(\tau, \Omega) = \begin{cases} \frac{\omega}{4\pi} \int_{4\pi} p(\Omega' \rightarrow \Omega) [I^M(\tau, \Omega') + I^1(\tau, \Omega')] d\Omega' + \frac{\omega}{4\pi} \int_{2\pi} p(\Omega' \rightarrow \Omega) I^0(\tau, \Omega') d\Omega' & \tau \leq \tau_a \\ \frac{1}{\pi} \int_{4\pi} \Gamma(\Omega' \rightarrow \Omega) [I^M(\tau, \Omega') + I^1(\tau, \Omega')] d\Omega' + \frac{1}{\pi} \int_{2\pi} \Gamma(\Omega' \rightarrow \Omega) I^0(\tau, \Omega') d\Omega' & \tau_a < \tau \leq \tau_1 \end{cases}$$

Gauss-Seidel algorithm

From the spatial interval (τ_i, τ_{i+2}) , Herman and Browning assume that the source function $J(\tau, \Omega)$ may be taken to be independent of τ and equal to its value at the midpoint of the interval, letting $J(\tau, \Omega) = J(\tau_{i+1}, \Omega)$ for all τ in this interval.

The improved version is based on a linear variation of the source function. For three arbitrary layers $\tau_i \leq \tau \leq \tau_{i+2}$, the linear relation can be given by:

$$\begin{cases} J(\tau, \Omega) = J(\tau_i, \Omega) + \frac{J(\tau_{i+1}, \Omega) - J(\tau_i, \Omega)}{\Delta\tau}(\tau - \tau_i) & \mu < 0 \\ J(\tau, \Omega) = J(\tau_{i+2}, \Omega) + \frac{J(\tau_{i+2}, \Omega) - J(\tau_{i+1}, \Omega)}{\Delta\tau}(\tau - \tau_{i+2}) & \mu > 0 \end{cases}$$

For the downward radiance,

$$\begin{aligned} I^M(\tau_{i+2}, \Omega) = I^M(\tau_i, \Omega) \exp(-2\Delta\tau) + \frac{J(\tau_{i+1}, \Omega)}{f(\Omega)} \left[2 - \frac{1 - \exp(-2\Delta\tau)}{\Delta\tau} \right] \\ - \frac{J(\tau_i, \Omega)}{f(\Omega)} [1 - 1/\Delta\tau + (1 + \Delta\tau) \exp(-2\Delta\tau)] \quad \mu < 0 \end{aligned}$$

The same procedures will yield the formula for the upwelling direction

$$\begin{aligned} I^M(\tau_i, \Omega) = I^M(\tau_{i+2}, \Omega) \exp(-2\Delta\tau) + \frac{J(\tau_{i+1}, \Omega)}{f(\Omega)} \left[2 - \frac{1 - \exp(-2\Delta\tau)}{\Delta\tau} \right] \\ - \frac{J(\tau_{i+2}, \Omega)}{f(\Omega)} \left[1 - \frac{1}{\Delta\tau} + (1 + \Delta\tau) \exp(-2\Delta\tau) \right] \quad \mu > 0 . \end{aligned}$$

Table Validation of Gauss-Seidel Algorithm Using Discrete-Ordinate Algorithm

viewing angles $\mu = \cos\theta$	upwelling radiance					
	$\tau=0.1$		$\tau=1.0$		$\tau=3.0$	
	Gauss-Seidel	Discrete-Ordinate	Gauss-Seidel	Discrete-Ordinate	Gauss-Seidel	Discrete-Ordinate
0.067	0.43419	0.43408	0.59366	0.59400	0.62154	0.62237
0.283	0.25950	0.25955	0.47818	0.47954	0.52799	0.53298
0.574	0.22143	0.22146	0.32526	0.32689	0.39136	0.39783
0.840	0.21233	0.21234	0.24526	0.24652	0.29265	0.29904
0.987	0.20962	0.20963	0.21330	0.21441	0.24804	0.24803

incident net flux $i_0 = \pi$, soil reflectance $R_s = 0.3$, $\mu_0 = 0.70292$, $\phi = \phi_0$, $\omega = 0.96$, $g = 0.65$.

32-stream for discrete-ordinate algorithm, 20 by 20 for Gauss-Seidel algorithm.

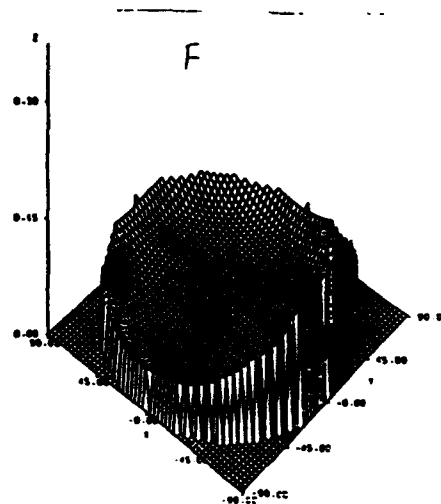
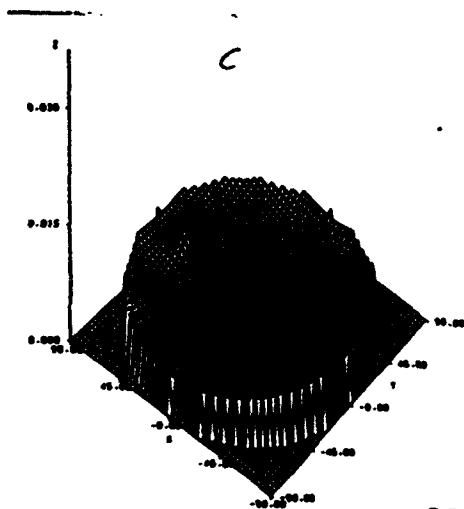
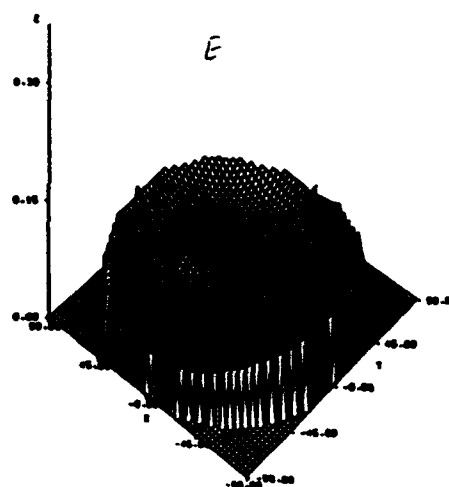
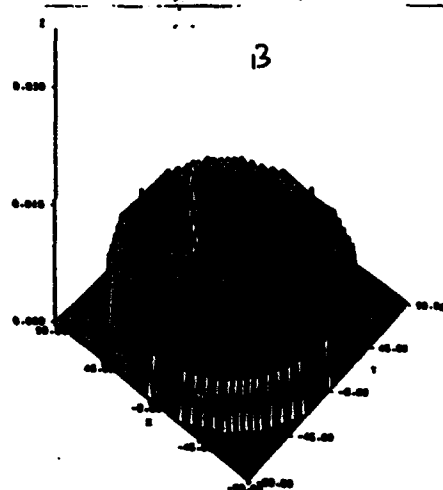
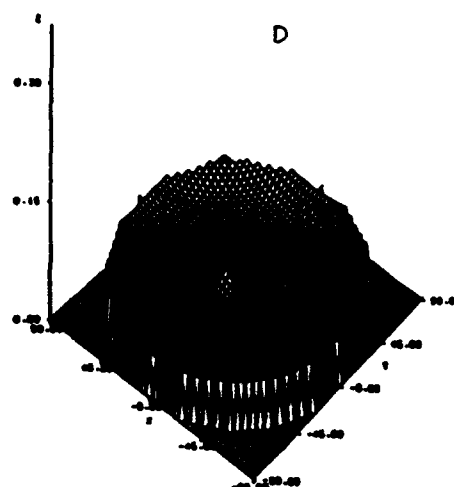
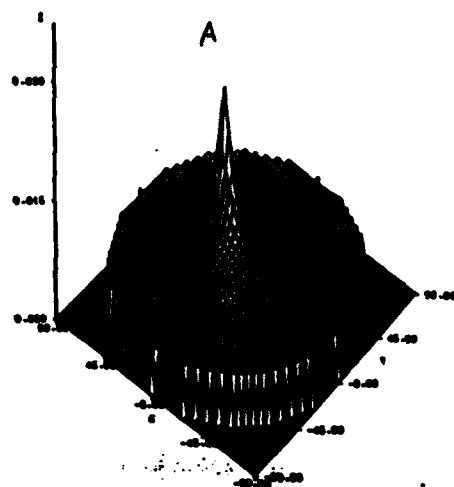


Fig. 3

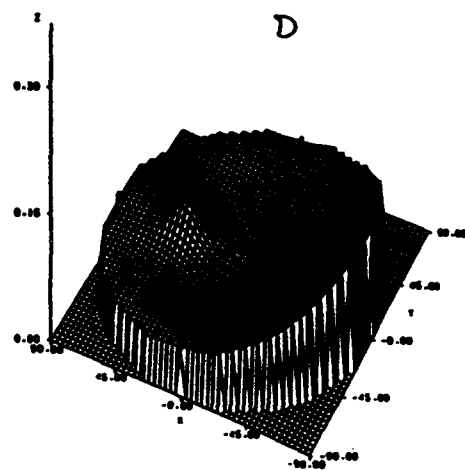
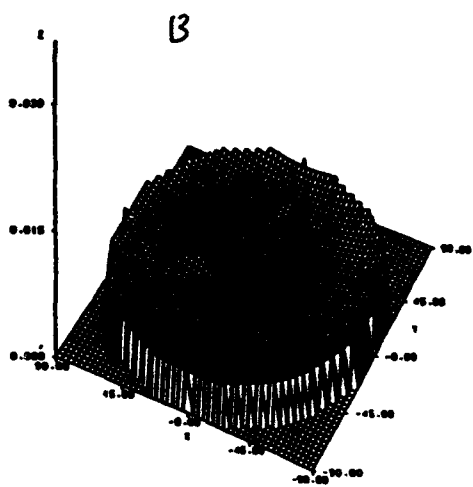
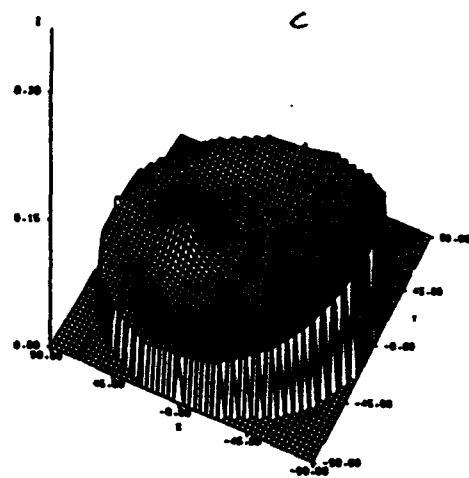
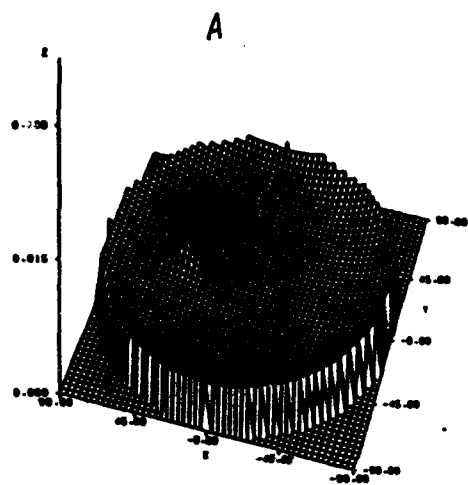


Fig. 4

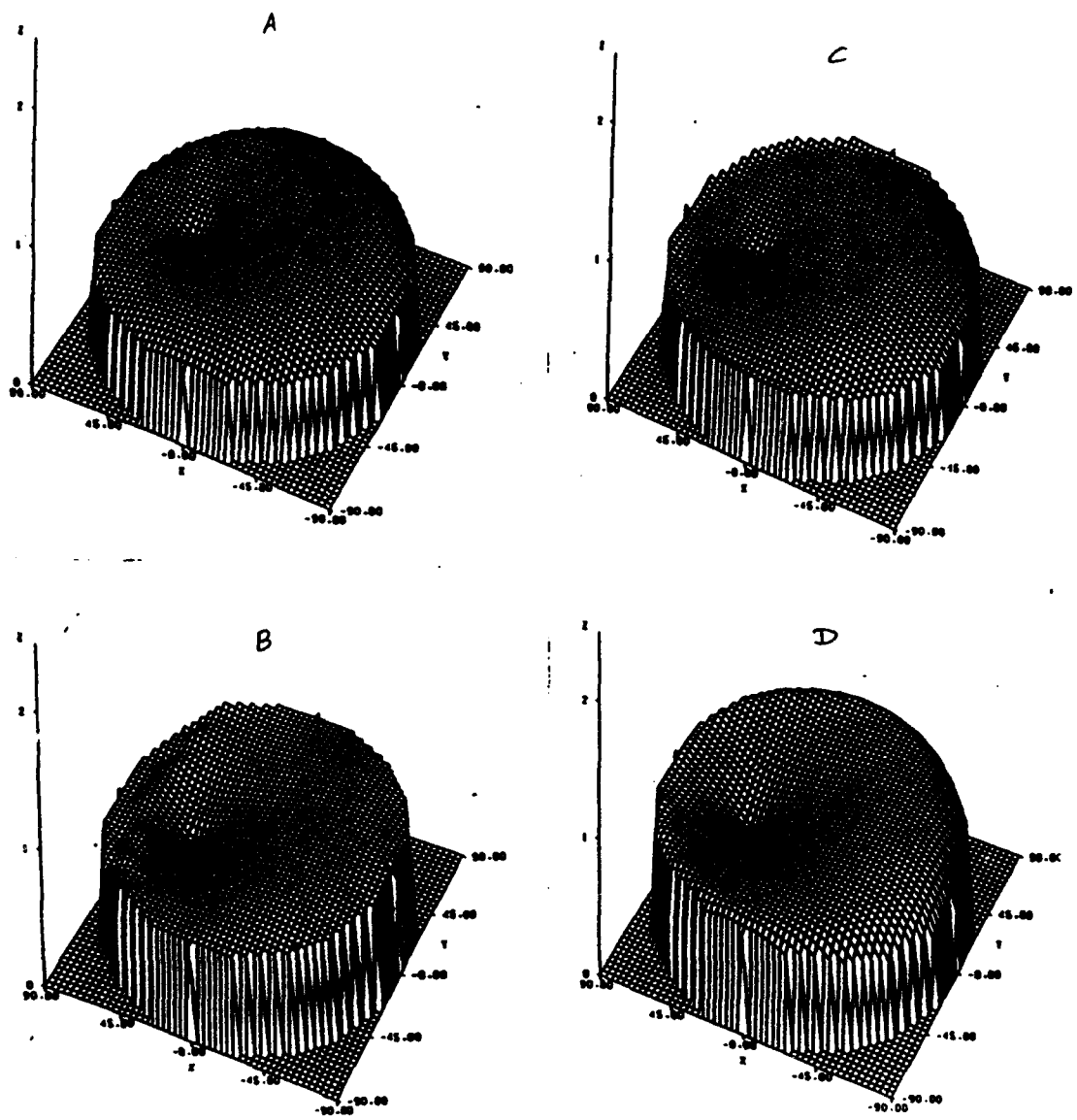


Fig. 9

Conclusion

- *. The improved Gauss-Seidel algorithm can be effectively used for the coupled medium
- *. We could not accurately retrieve canopy information in visible region without exact knowledge of atmospheric characteristics
- *. The near-IR region is of great significance for the remote sensing of vegetation

A PHYSICALLY REASONABLE ANALYTIC EXPRESSION FOR THE SINGLE SCATTERING PHASE FUNCTION

W.M. Cornette, J.G. Shanks

Photon Research Associates, Inc., 9393 Towne Centre Drive, Suite 2000, San Diego, CA 92121

An analytic phase function that reduces the Rayleigh phase function for the scattering of unpolarized light is presented and compared to the traditional Henyey-Greenstein phase function. Comparisons between the proposed phase function and the phase function for three of Deirmendjian's polydispersions are shown, and applications to radiative transfer are demonstrated.

A PHYSICALLY REASONABLE ANALYTIC EXPRESSION FOR THE SINGLE SCATTERING PHASE FUNCTION

June 1992

Presented at the 15th Annual Review Conference on Atmospheric Transmission Models;
2-4 June 1992, Geophysics Directorate, Phillips Laboratory, Hanscom AFB, Massachusetts

Presented By:

Dr. William M. Cornette
Dr. Joseph G. Shanks

PRA
Photon Research Associates, Inc.
9383 Towne Centre Drive, #200
San Diego, California 92121

MOTIVATION

- Henyey-Greenstein Phase Function Becomes Isotropic for Small Particles
- New Phase Function
 - Approximate Henyey-Greenstein Phase Function for Large Particles
 - Converge to Rayleigh Phase Function for Small Particles
 - Easily Incorporated into Radiative Transfer Calculations (e.g., APART, MOSART)

HENY-GREENSTEIN PHASE FUNCTION

$$P_{HG}(\mu, g) = \frac{1 - g^2}{(1 + g^2 - 2g\mu)^{3/2}}$$

$$\mu = \cos \theta$$

$$\langle \mu \rangle = g \text{ (the asymmetry factor)}$$

and the Legendre expansion is

$$P_{HG}(\mu, g) = \sum_{\ell=0}^{\infty} (2\ell + 1) g^{\ell} P_{\ell}(\mu)$$

RAYLEIGH PHASE FUNCTION

$$P_R(\mu) = 3 (1 + \mu^2)/4$$

for scattering of unpolarized light in the Rayleigh region

$$2\pi r/\lambda < 1$$

DOUBLE HENVEY-GREENSTEIN PHASE FUNCTION

$$P_{DHG}(\mu; f, g_1, g_2) = (1 - f) P_{HG}(\mu, g_1) + f P_{HG}(\mu, g_2)$$

Typically $g_1 > 0$
 $g_2 < 0$
 $0 \leq f \leq 1$

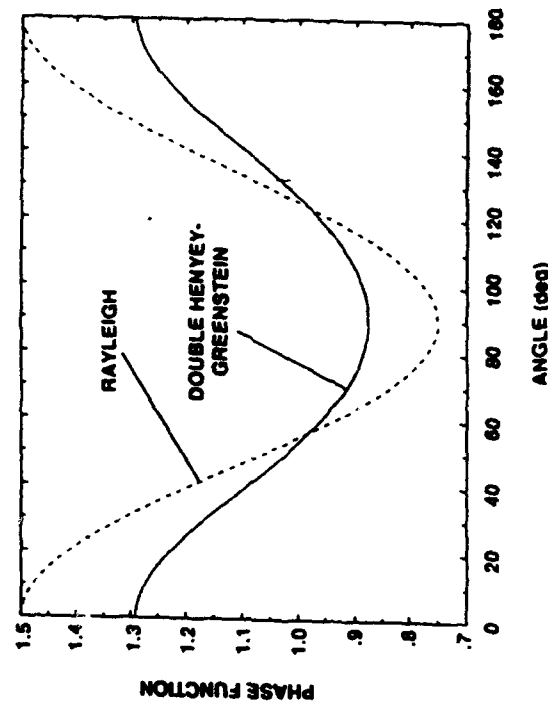
$$\text{so } \langle \mu \rangle = (1 - f) g_1 + f g_2$$

To approximate Rayleigh
 phase function,

$$g_1 = -g_2 = 0.230$$

$$f = 0.500$$

rms error = 0.15



R.000.011 BC/ALC

NEW PHASE FUNCTION

$$P(\mu, g) = \frac{3}{2} \frac{1 - g^2}{2 + g^2} \frac{1 + \mu^2}{(1 + g^2 - 2g\mu)^{3/2}}$$

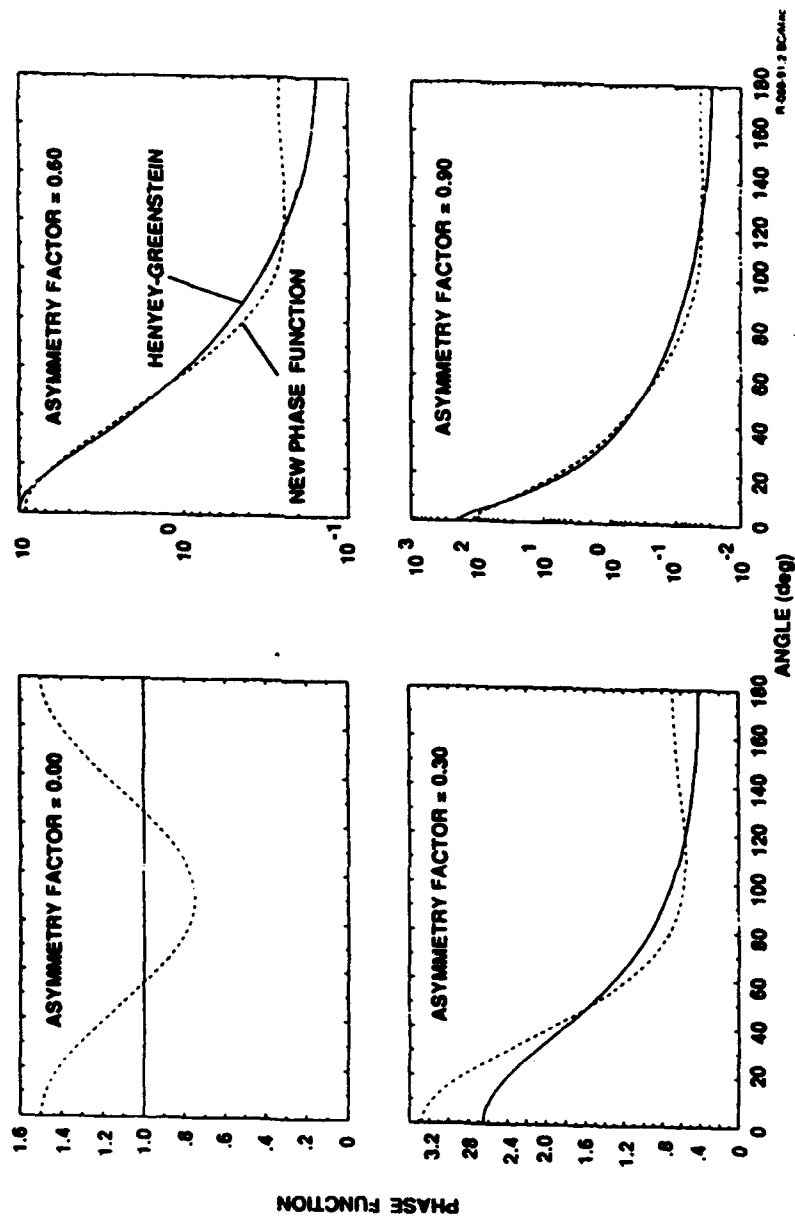
where

$$\langle \mu \rangle = g \frac{3(4 + g^2)}{5(2 + g^2)}$$

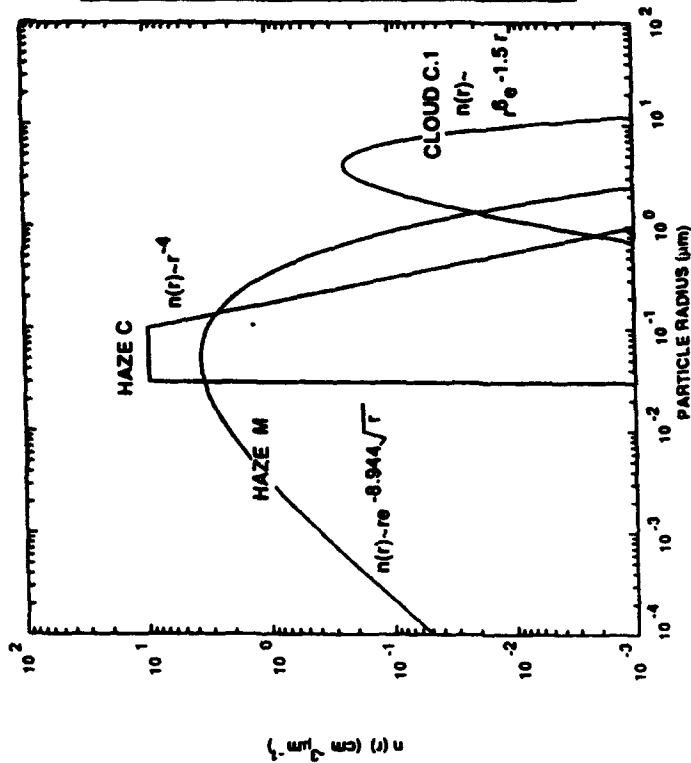
and

$$P(\mu, g) = \frac{3}{2} \frac{1}{2 + g^2} \sum_{l=0}^{\infty} \left\{ \frac{l(l-1)}{2l-1} g^{l-2} + \frac{5l^2-1}{2l-1} g^l + \frac{(l+1)^2}{2l+3} g^l + \frac{(l+1)(l+2)}{2l+3} g^{l+2} \right\} P_l(\mu)$$

NEW PHASE FUNCTION

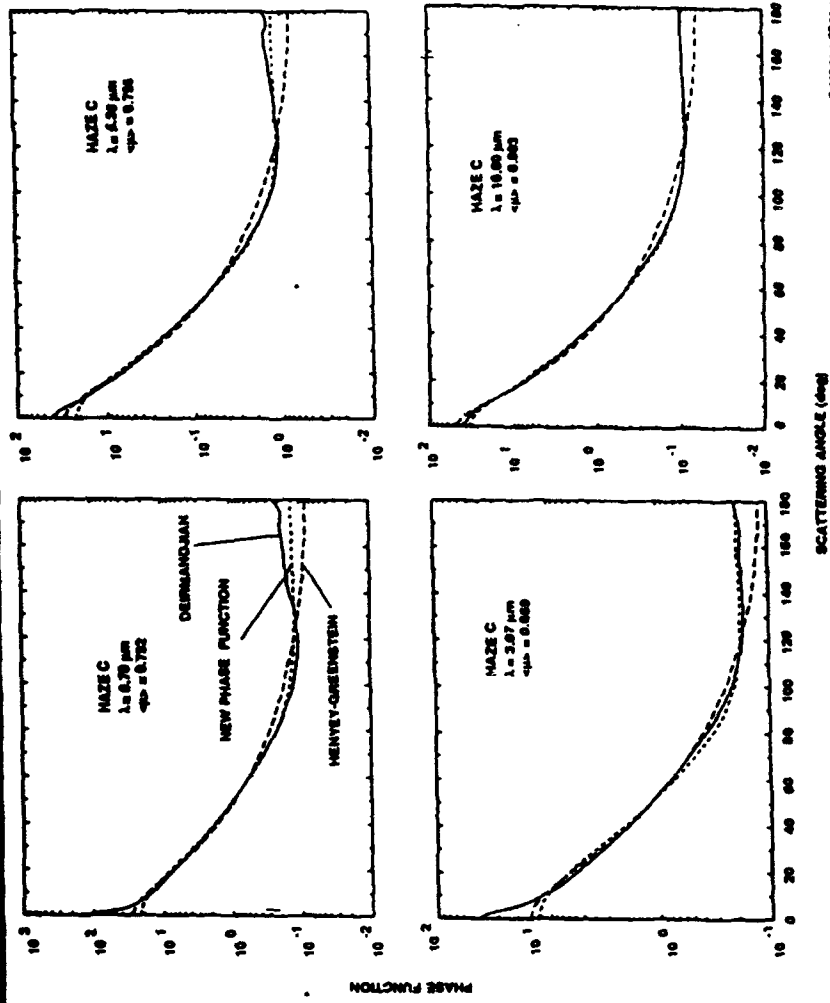


DEIRMANDJIAN HAZE AND CLOUD MODELS



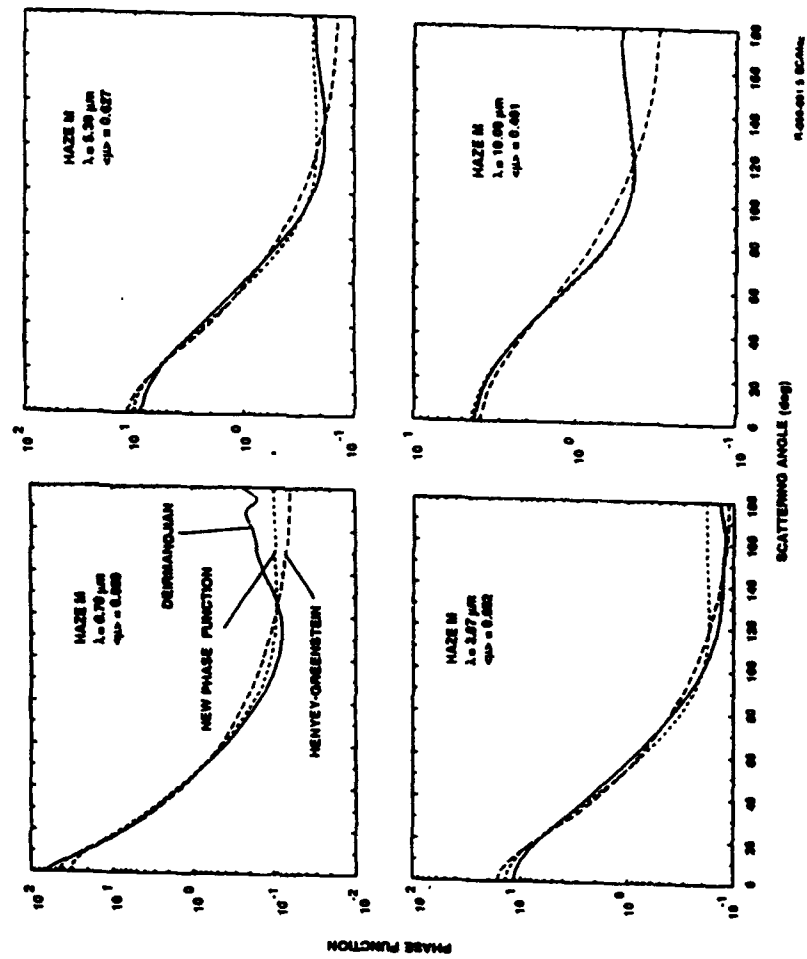
$\lambda(\mu\text{m})$	n	k	Albedo		
			Haze C	Haze M	Cloud C.1
0.45	1.34	0.0	1.000	1.000	1.000
0.70	1.33	0.0	1.000	1.000	1.000
1.61	1.315	0.0	1.000	1.000	1.000
3.07	1.525	0.0682	0.620	0.721	0.529
3.90	1.353	0.0059	0.930	0.948	0.914
5.30	1.315	0.0143	0.800	0.826	0.884
6.05	1.315	0.1370	0.260	0.297	0.543
10.00	1.212	0.0601	0.202	0.178	0.601
16.60	1.44	0.4000	0.104	0.075	0.395
100.00	1.957	0.5320	-	-	0.600

DEIRMANDJIAN HAZE C PHASE FUNCTIONS

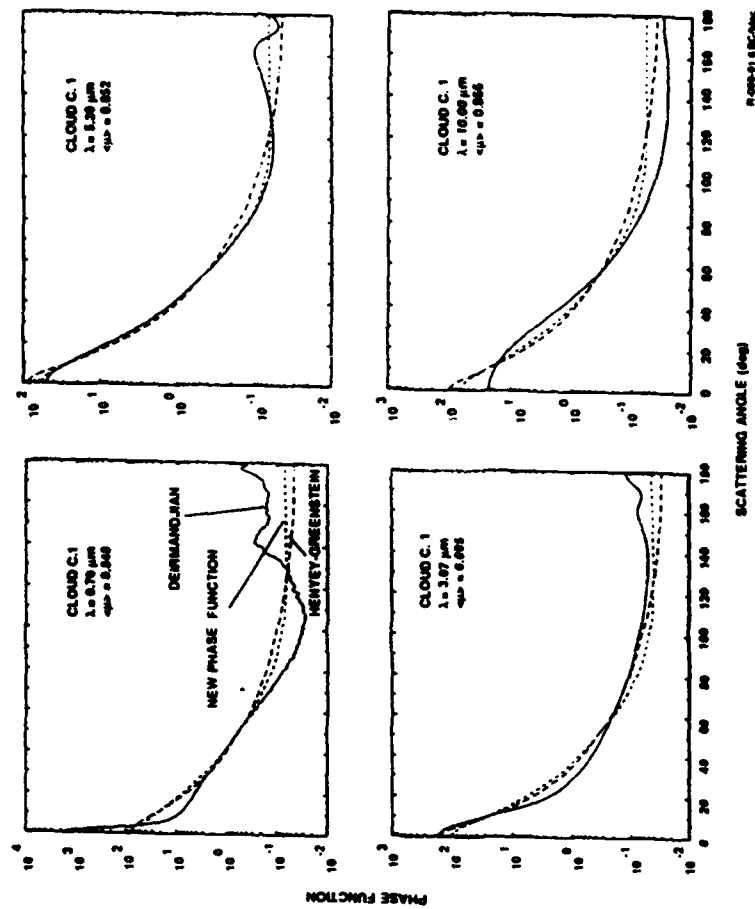


0-000-01 + 0-000-02

DEIRMANDJIAN HAZE M PHASE FUNCTIONS



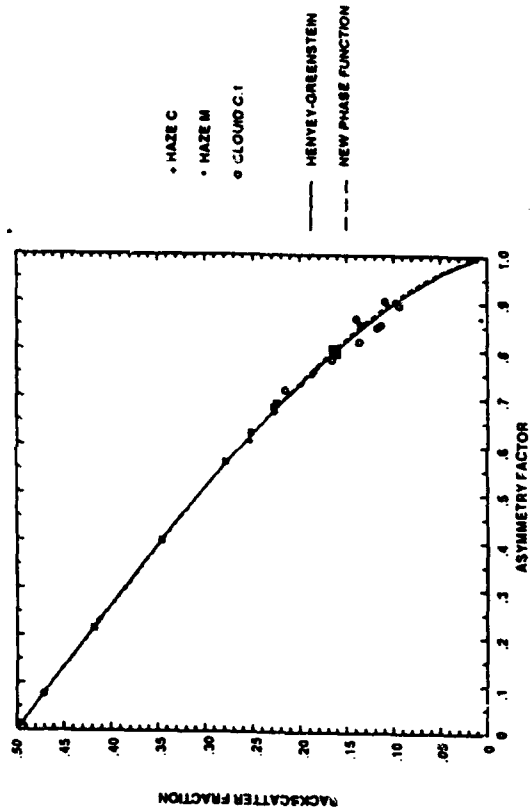
DEIRMANDJIAN CLOUD C.1 PHASE FUNCTIONS



AVERAGE BACKSCATTER FUNCTION

$$\beta(\mu_0) = \frac{1}{4\pi} \int_0^1 \int_0^{2\pi} \phi(\mu, \mu_0) d\theta d\mu$$

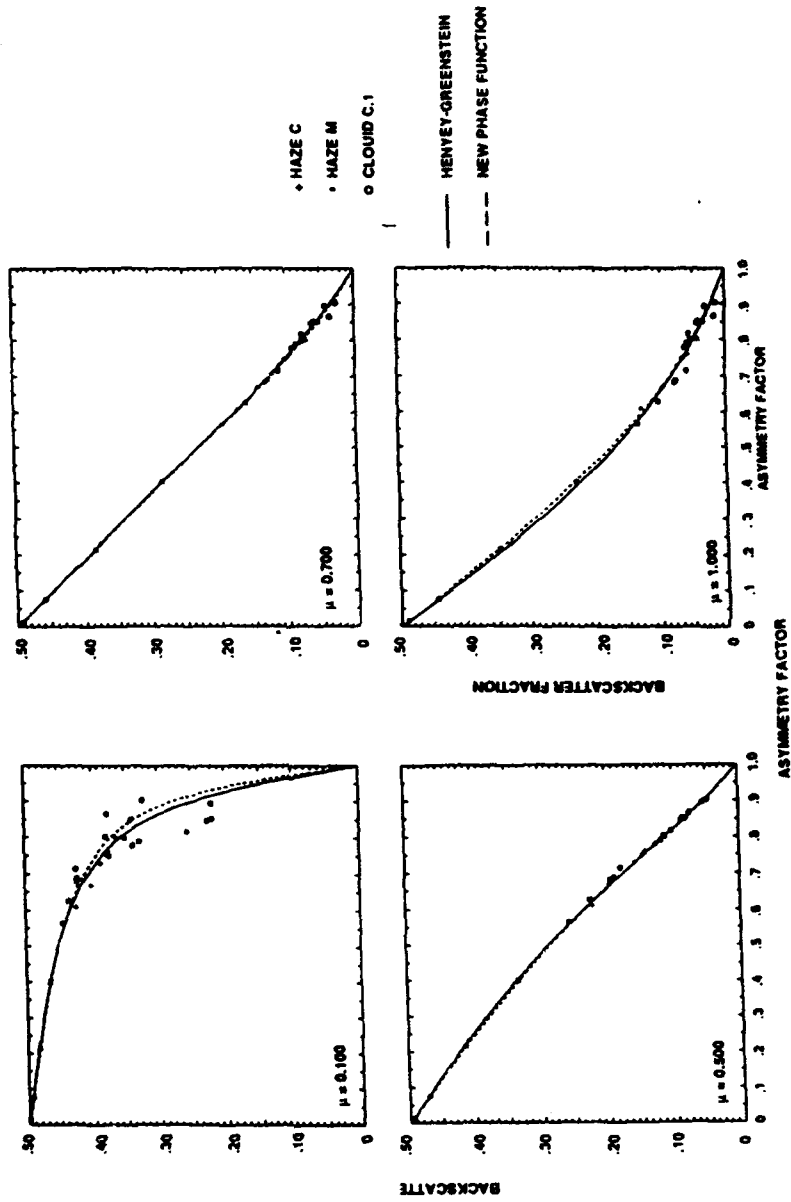
$$\bar{\beta} = \int_0^1 \beta(\mu_0) d\mu_0$$



W 000 01 000 000

0-002-01.12

ANGULAR BACKSCATTER FRACTION



SUMMARY

- New Phase Function is an Improvement Over Henyey-Greenstein Phase Function for Scattering of Natural Light, Especially for Particles with $X \lesssim 1$
- New Phase Function Easily Incorporated Into Radiative Transfer Algorithms
- TANSTAAFL: Convergence of Legendre Expansion is Slower Since New Phase Function Includes Higher Frequencies
- Paper to Appear in Applied Optics

ANALYSIS OF SOLAR TRANSMISSION DATA OVER THE SOUTH ATLANTIC OCEAN DURING SABLE 89

D. Longtin, J. Hummel
SPARTA, Inc., 24 Hartwell Avenue, Lexington, MA 02173

G.G. Koenig
PL/GDOPA, Hanscom AFB, MA 01731-5000

This paper discusses the analysis of solar transmissometer data that was taken during the South Atlantic Backscatter Lidar Experiment (SABLE). There were six days when the instrument was operated: 25 June, 28 June, 1 July, 2 July, 6 July, and 7 July 1989. The instrument was located on Ascension Island, and it measured solar transmission at 532 nm versus time and transmission across the solar spectrum.

In the analysis, the time series of solar transmissions at 532 nm are used to study the properties of cirrus and boundary layer stratocumulus that passed in front of the sun while the instrument was working. For 25 June 1989, a qualitative assessment shows the transmissions through cirrus to be between 0.4 and 0.8, and the cirrus thicknesses are estimated to be between 1.0 and 2.2 km. These estimates are consistent with cirrus observations from aircraft.

The remainder of the analysis focuses on the properties of stratocumulus cloud edges and thin spots. It is shown that stratocumulus have very similar edge characteristics from day-to-day: there is a uniform distribution of cloud transmission values between about 0.1 and 0.7, and the percentages increase significantly as cloud transmissions increase from 0.7 to 0.9. Also, the number of occurrences of stratocumulus thin spots and edges are compared against total number of stratocumulus occurrences. Although day-to-day variations exist, the comparisons clearly show that stratocumulus over Ascension Island often are not opaque, and they frequently transmit partial solar radiation. Since stratocumulus often cover broad regions of the marine environment, these findings could be of interest to climate modeling studies which often assume stratocumulus to be fully opaque.

Research Supported by Phillips Laboratory, Geophysics Directorate, Contract F19628-91-C-0093

ANALYSIS OF SOLAR TRANSMISSION DATA OVER THE SOUTH ATLANTIC OCEAN DURING SABLE 89

Presented At
The Annual Review Conference on Atmospheric Transmission Models

June 3, 1992

D.R. Longtin¹, LTC G.G. Koenig², and J.R. Hummel¹

¹SPARTA, Inc.

**24 Hartwell Avenue
Lexington, MA 02173**

² PL/GPOA

Hanscom AFB, MA 01731-5000

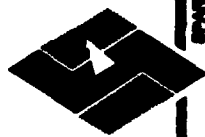
Contract F19628-91-C-0093



SPARTAN INC.

OUTLINE OF TALK

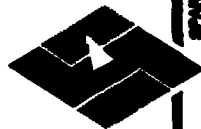
- Summary of Instrumentation
- Method of Analysis
 - Focus On Effects from Stratocumulus Clouds
- Results
 - Properties of Cloud Edges and Thin Spots
 - Estimates of Cloud Opacity
 - Time Duration of Cloud Edges and Thin Spots
- Conclusions



SPARTA INC.

SUMMARY OF SOLAR TRANSMISSOMETER DATA

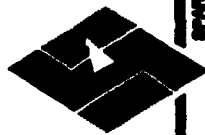
- Measurement Period: SABLE 89 (Local Time for Ascension Island)
 - 11:43-14:22 on 25 June
 - 13:31-17:38 on 28 June
 - 11:41-16:13 on 1 July
 - 10:21-18:01 on 2 July
 - 09:33-18:01 on 6 July
 - 10:31-18:11 on 7 July
- Measurements Taken Every Four Seconds
- Modes of Operation
 - Solar Transmissions at 532 nm Versus Time
 - Solar Scans Between 400 and 1200 nm (Not Used in This Analysis)



SPARTA INC.

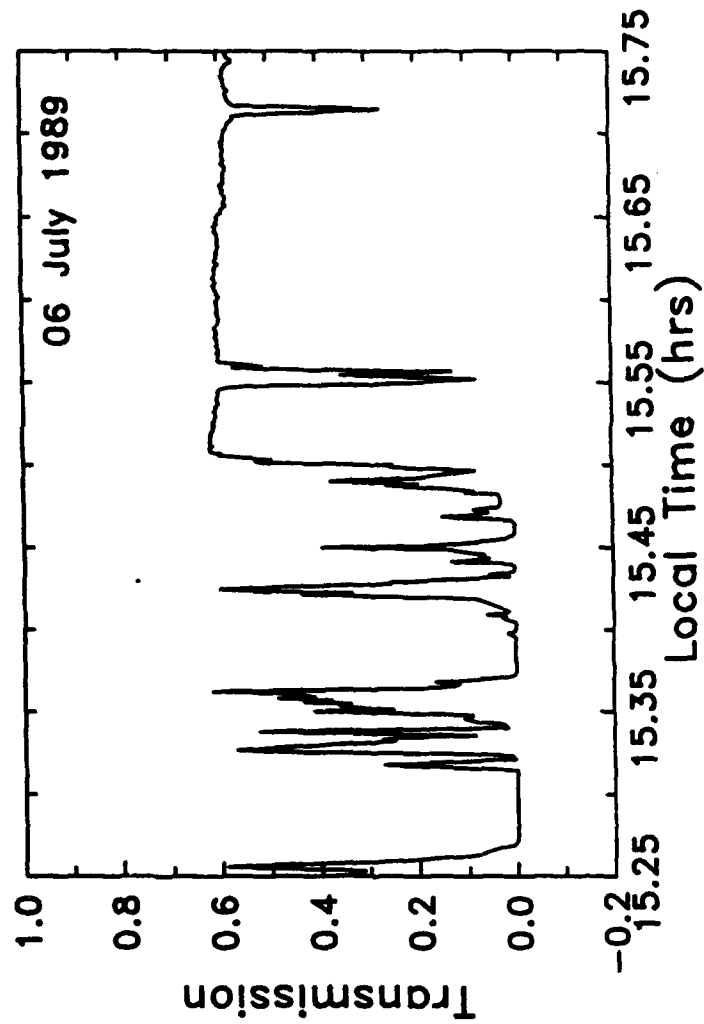
BOUNDARY LAYER CHARACTERISTICS AT ASCENSION ISLAND

- Typical Marine Trade Wind Environment
- Aerosols Show Horizontal Uniformity
- Subject to Frequent Boundary Layer Stratocumulus Clouds
 - Individual Clouds Often Small
 - Regular Horizontal Distribution



SPARTA INC.

SOLAR TRANSMISSION DEPICTING CLOUD EDGES AND THIN SPOTS





SPARTA INC.

PROCEDURE TO OBTAIN CLOUD TRANSMISSIONS

- Separate and Remove Atmospheric Transmissions From the Measured Transmissions

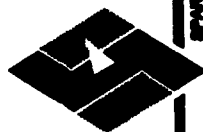
$$\tau_{mea} = \tau_{clr} \tau_{cld}$$

τ_{mea} = Measured Solar Transmission

τ_{clr} = Atmospheric Transmission (Aerosol, Molecular, and Zenith Effects)

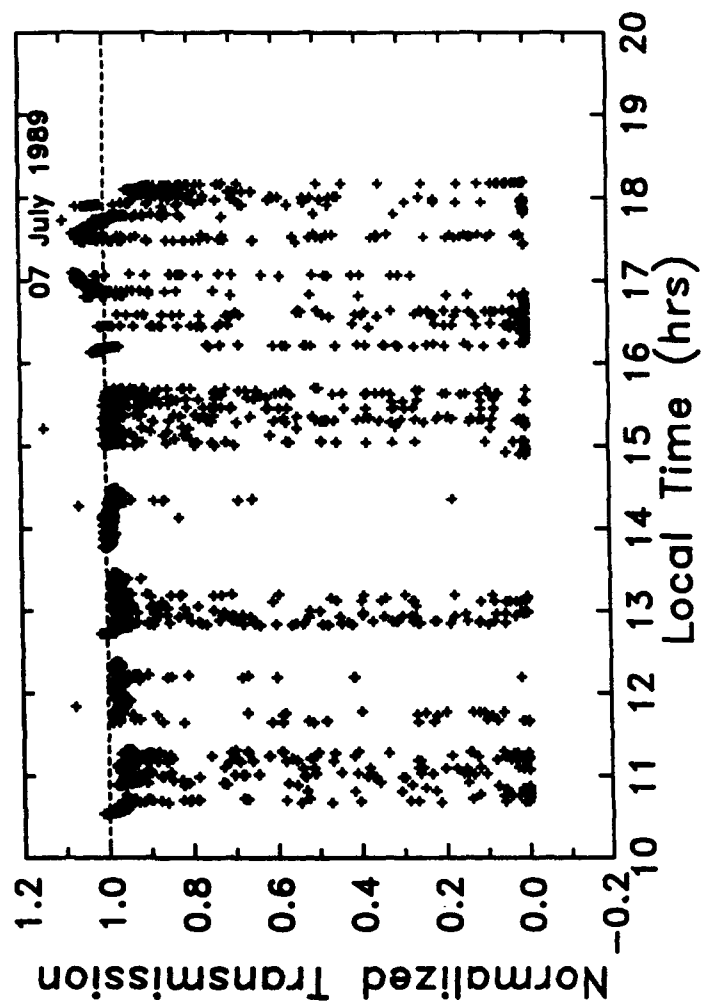
τ_{cld} = Cloud Transmission

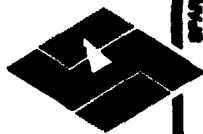
- LOWTRAN7 Used To Compute Values of τ_{clr}
- Adjust Surface Visibility Input in LOWTRAN7 Until The Resulting Envelope of τ_{cld} Is As Close To 1.0 As Possible
- No Corrections Needed for Forward Scattering Effects Through Stratocumulus Clouds



EXAMPLE OF CLOUD TRANSMISSIONS AFTER REMOVING ATMOSPHERIC TRANSMISSIONS

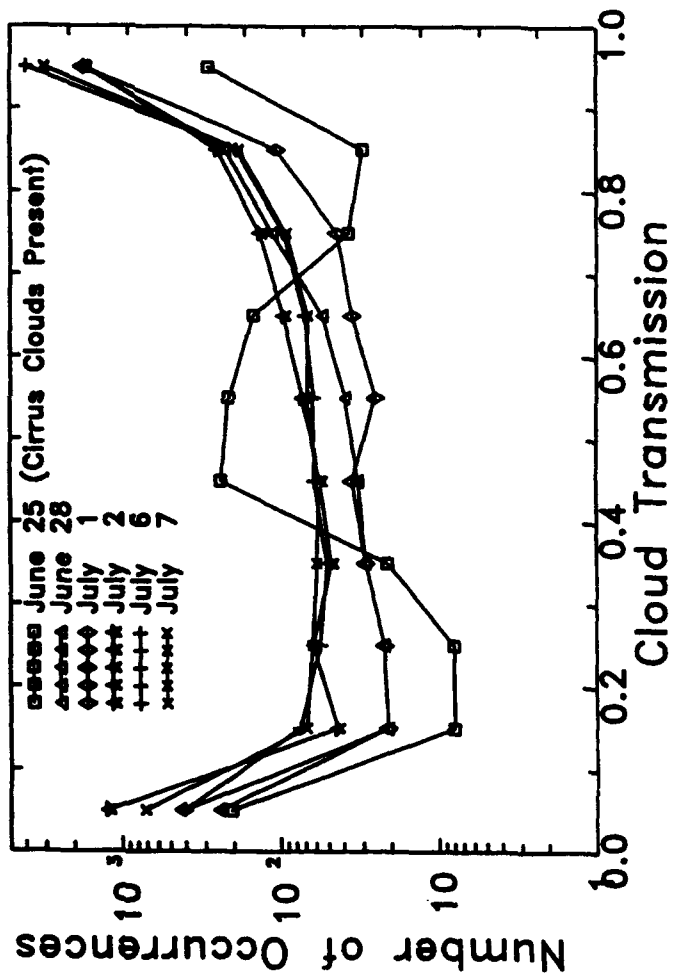
SPARTA INC.





SPARTA INC.

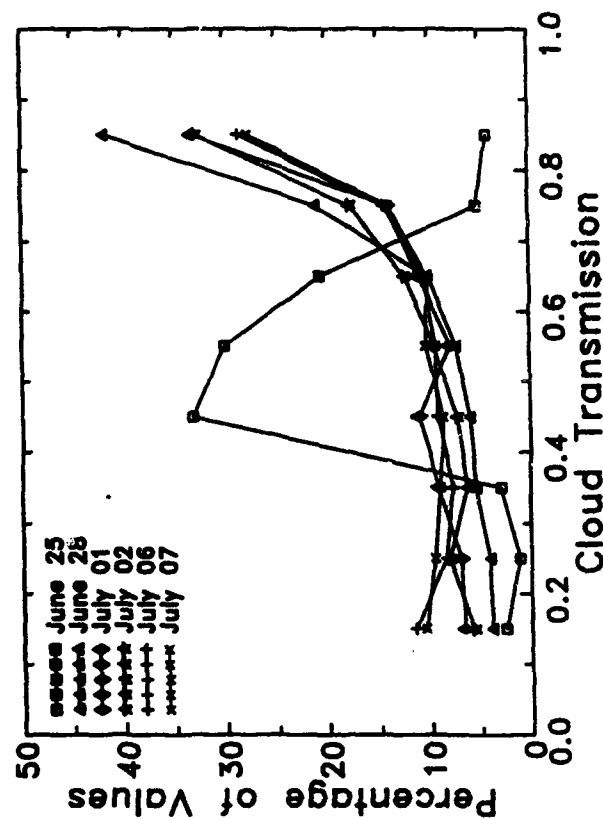
DAILY OCCURRENCES OF CLOUD TRANSMISSION





% DISTRIBUTION OF CLOUD TRANSMISSION FOR CLOUD EDGES AND THIN SPOTS ALONE

SPARTA INC.



DATE	AVERAGE	ST DEV
25 JUNE	0.544	0.130
28 JUNE	0.685	0.206
01 JULY	0.613	0.237
02 JULY	0.631	0.231
06 JULY	0.581	0.257
07 JULY	0.576	0.251



SPARTA INC.

ESTIMATES OF CLOUD OPACITY

- Estimate Overall Cloud Opacity As

$$\frac{N_{edge}}{N_{edge} + N_{cld}}$$

N_{cld} = Daily Opaque Occurrences ($\tau_{cld} \leq 0.1$)

N_{edge} = Daily Edge and Thin Spot Occurrences ($0.1 \leq \tau_{cld} \leq 0.9$)

- A Value Close To 1.0 Means That Clouds Possess Many Thin Spots
- A Value Close To 0.0 Means That Most Clouds Are Opaque

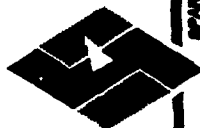
	28 JUNE	1 JULY	2 JULY	6 JULY	7 JULY
NO. OF EDGE PTS, N_{edge}	532	316	764	660	656
NO. OF OPAQUE PTS, N_{cld}	247	414	1229	407	716
$N_{edge}/(N_{edge} + N_{cld})$	0.683	0.433	0.383	0.618	0.478



SPARTA INC.

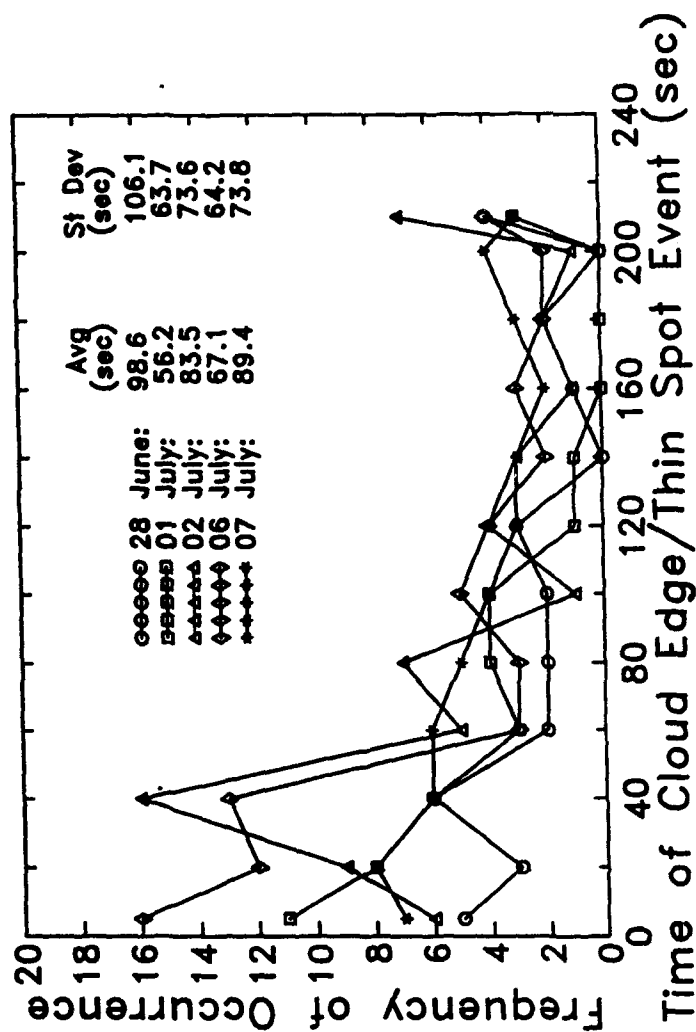
SCHEME TO ESTIMATE THE DURATION OF CLOUD EDGE AND THIN SPOT EVENTS

- Subdivide Daily Time Series of τ_{cd} Into Three Types of Continuously Distinct Time Periods
 - Skies Were Clear in the Direction of the Sun
 - Clouds Fully Blocked the Sun
 - Cloud Edges and Thin Spots Dominated
- "Clear" Periods Have τ_{cd} Exceed 0.9 For At Least 60 Seconds
- "Cloudy" Periods Have τ_{cd} Below 0.1 For At Least 60 Seconds
- Remaining Time Periods Classified as Cloud Edge and Thin Spot Events



SPARTA INC.

DURATION OF CLOUD EDGE AND THIN SPOT EVENTS





SPARTA INC.

CONCLUSIONS

- Stratocumulus Have Very Similar Edge Characteristics From Day-to-Day
 - Uniform Percent Distribution of τ_{cd} Between 0.1 and 0.7
 - Percentages Increase Significantly As τ_{cd} Increase From 0.7 to 0.9
- Stratocumulus Clouds Frequently Transmit Partial Direct Solar Radiation
- Time Durations of Most Cloud Edge and Thin Spot Events Are Less Than 200 Seconds
 - Events of Less Than 60 Seconds Occur Most Frequently
 - Gradual Falloff in the Number of Occurrences of Longer Time Duration
- These Findings Should Be Of Interest To
 - Cloud Modeling Studies That Treat Stratocumulus Clouds As Optically Thick
 - Ground-To-Space Systems Under Development in the DoD Community
 - Cloud-Free-Line-of-Sight (CFLOS) Studies

"Dr. Olga Lado-Bordowsky
Ecole Nationale Supérieure
de Sciences Appliquées et de
Technologie
Université de Rennes
6 Rue de Kerampont
22305 Lannion
FRANCE"
(33) 96912495

"Michael Abel, Lt. Col.
ESD/WE
Hanscom AFB, MA 01731"
(617) 377-3237

"Mr. Leonard Abreu
PL/GPOS
Hanscom AFB, MA 01731-5000"
(617) 377-2337

"Dr. Phabhat Acharya
Spectral Sciences, Inc.
99 S. Bedford Street
Burlington, MA 01803"
(617) 273-4770

"Ms. Gail Anderson
PL/OPS
Hanscom AFB, MA 01731-5000"
(617) 377-2335

"Stacy Angle
Loral IRIS
2 Forbes Road, Mail Stop 391
Lexington, MA 02173"
(617) 863-3918

"Col. Grant C. Aufderhaar
OUSDA (R&AT/E&LS)
The Pentagon/Room 3D129
Washington, DC 20301"
(703) 695-9604

"Dr. Alexander Berk
Spectral Sciences, Inc.
111 S. Bedford Street
Burlington, MA 01803"
(617) 273-4770

"Curt C. Betchley
Aerodyne Research, Inc.
45 Manning Road
Billerica, MA 01821"
(508) 663-9500

"Dr. W. A. M. Blumberg
PL/GPOS
Hanscom AFB, MA 01731"
(617) 377-3688

"Mr. James T. Bunting
PL/GPAS
Hanscom AFB, MA 01731-5000"
(617) 377-3495

"Dr. Ken Champion
PL/GPA
Hanscom AFB, MA 01731"
(617) 377-3033

"Dr. Kelly Chance
Harvard Smithsonian
Center for Astrophysics
60 Garden Street
Cambridge, MA 02138"
(617) 495-7389

"David T. Chang
AER Inc.
840 Memorial Drive
Cambridge, MA 02139"
(617) 547-6207

"Cynthia Cheng
MIT/Lincoln Lab - Group 35
244 Wood Street
Lexington, MA 02173"
(617) 981-0834

"Mr. James H. Chetwynd
PL/GPOS
Hanscom AFB, MA 01731-5000"
(617) 377-2337

"Dr. Vincent Chimelis
Phillips Lab / OL/AG
Patrick AFB, FL 32907"
(407) 723-3100

"Robert W. Cleary
USA-Materials Technology Lab Tecom
Watertown, MA 02172"
(617) 923-5440

"Mr. Shepard A. Clough
Atmospheric and Environmental
Research, Inc.
840 Memorial Drive
Cambridge, MA 02139"
(617) 547-6207

"Dr. William M. Cornette
Photon Research Associates, Inc.
9393 Town Center Drive
San Diego, CA 92121"
(619) 455-9741

"Dr. Gilbert Davidson
PhotoMetrics, Inc.
4 Arrow Drive
Woburn, MA 01801"
(617) 935-6500

"Dr. Edmond Dewan
PL/GPOS
Hanscom AFB, MA 01731-5000"
(617) 377-4401

"Vincent DiLeone
MIT Lincoln Laboratory
244 Wood Street
Lexington, MA 02173"
(617) 891-2333

"Susan Donner
Mission Research Corporation
1 Tara Blvd, #302
Nashua, NH 03062"
(603) 891-0070

"Dr. Robert G. Ellingson
Department of Meteorology
University of Maryland
College Park, MD 20742"
(301) 405-5386

"Mr. Vince Falcone
PL/GPAS
Hanscom AFB, MA 01731-5000"
(617) 377-4029

"Matthew Fetrow
Stewart Radiance Laboratory
139 Great Road
Bedford, MA 01730"
(617) 275-8273

"Ms. Joan-Marie Freni
Hughes STX Corporation
109 Massachusetts Avenue
Lexington, MA 02173"
(617) 863-0524

"Charlie Gallagher
PL/XPG
Hanscom AFB, MA 01731"
(617) 377-7463

"Mr. William O. Gallery
AER, Inc.
840 Memorial Drive
Cambridge, MA 02139"
(617) 547-6207

"Dr. Harold Gardiner
PL/GPOS
Hanscom AFB, MA 01731"
(617) 377-3672

"Margaret E. Gardner
Visidyne
10 Corporate Place
South Bedford Street
Burlington, MA 01803"
(617) 273-2820

"Allen S. Grossman
Lawrence Livermore National Laboratory
P.O. Box 808
Livermore, CA 94550"
(510) 423-6371

"Dr. L. A. Hall
PL/GPIU
Hanscom AFB, MA 01731"
(617) 377-3322

"Larrene Harada
WJSH
#901 N. Ft. Myer
Arlington, VA 22209"
(703) 558-7900

"Rebecca Healey
Yap Analytics
594 Marrett Road
Lexington, MA 02173"
(617) 377-3645

"Dr. Richard Hendl
PL/CA
Hanscom AFB, MA 01731-5000"
(617) 377-3601

"Dr. Mike Hoke
PL/GPOS
Hanscom AFB, MA 01731-5000"
(617) 377-3614

"Mr. Robert E. Huffman
PL/GPIM
Hanscom AFB, MA 01731-5000"
(617) 377-3311

"Dr. John R. Hummel
SPARTA, Inc.
24 Hartwell Avenue
Lexington, MA 02173"
(617) 863-1060

"Priscilla Ip
Mission Research Corporation
1 Tara Boulevard, Suite 302
Nashua, NH 03062-2801"
(603) 891-0070

"Ronald G. Isaacs
Atmospheric and Environmental
Research, Inc.
840 Memorial Drive
Cambridge, MA 02139"
(617) 547-6207

"Mr. Robert A. Joseph
ARCON Corporation
260 Bear Hill Road
Waltham, MA 02154"
(617) 890-3330

"Dennis Killinger
Univ. of South Florida
Department of Physics
Tampa, FL 33620"
(813) 974-3995

"Evelyn M. Kindler
Phillips Lab
Hanscom AFB, MA 01731"
(617) 377-7111

"Thomas Kleespies
PL/GPAS
Hanscom AFB, MA 01731"
(617) 377-3136

"William T. Kreiss
Horizons Technology Inc.
3990 Ruffin Road
San Diego, CA 92123"
(619) 292-8331

"Mr. Thomas H. Kyle
PL/XPG
Hanscom AFB, MA 01731-5000"
(617) 377-7443

"Pinchus M. Laufer
IDA
1801 N. Bauregard St.
Alexander, VA "
(703) 578-2857

"Shunlin Liang
Boston University
Dept. of Geography
675 Commonwealth Ave.
Boston, MA 02215"
(617) 353-2088

"Ruth P. Liebowitz
PL/TS
Hanscom AFB, MA 01731"
(617) 377-3643

"Dr. Jim Liljegen
Battelle Pacific Northwest Laboratory
PO Box 999
Richland, WA 99352"
(509) 375-2222

"Shu Lin
Hughes STX Corporation
109 Massachusetts Avenue
Lexington, MA 02173"
(617) 863-0716

"Qiancheng Ma
The Goddard Institute for Space Studies
2880 Broadway
New York, NY 10025"
(212) 678-5574

"Sam Maklauf
PL/GPOS
Hanscom AFB, MA 01731"
(617) 377-4203

"Steve Mazuk
Atmos. & Ionospheric Sciences Dept.
Aerospace Corporation
P.O. Box 92957/Mail Code M2-255
Los Angeles, CA 90009-2957"
(310) 336-5614

"Andrew K. McCann
Ontar
129 University Road
Brookline, MA 02146"
(617) 739-6607

"Chuck Molenkamp
Lawrence Livermore National Laboratory
P.O. Box 808
Livermore, CA 94550"
(510) 422-1827

"Meg Noah
Mission Research Corporation
1 Tara Blvd, #302
Nashua, NH 03062"
(603) 891-0070

"Paul Noah
Mission Research Corporation
1 Tara Blvd, #302
Nashua, NH 03062"
(603) 891-0070

"Valdar Oinas
Hughes STX
2880 Broadway
New York, NY 10025"
(212) 678-5528

"Armand J. Paboojian
ARCON Corp.
260 Bear Hill Rd.
Waltham, MA 02154"
(617) 377-2262

"Dee W. Pack
The Aerospace Corporation
P.O. Box 92957/Mail Code M2-255
Los Angeles, CA 90009-2957"
(310) 336-5645

"Cliff Paiva
Naval Surface Warfare Center
Code J-41, Bldg. 1450
Dahlgren, VA 22448"
(703) 663-1786

"Dr. W. H. Parkinson
Harvard Smithsonian Center for
Astrophysics
60 Garden Street
Cambridge, MA 02138"
(617) 495-4865

"Dr. Charles R. Philbrick
Penn State University
University Park, PA 16802"
(814) 865-2975

"Ms. Angela Phillips
E-O & Data Systems Group
Hughes Aircraft Company
P.O. Box 902
El Segundo, CA 90245"
(310) 616-0124

"Dr. Richard H. Picard
PL/GPOS
Hanscom AFB, MA 01731-5000"
(617) 377-2222

"Chuck Pritt
The Aerospace Corporation
P.O. Box 92957/Mail Code M2-255
Los Angeles, CA 90009-2957"
(310) 336-6701

"Rafael Quiroga
ITT-Federal Services Corp.
PO Box 5728
MS 830
Vandenberg AFB, CA 93437"
(805) 734-8232 X 5-7154

"Dr. Anthony Ratkowski
PL/GPO
Hanscom AFB, MA 01731-5000"
(617) 377-3655

"Dr. David C. Robertson
Spectral Sciences, Inc.
99 S. Bedford Street
Burlington, MA 01803"
(617) 273-4770

"Ian Robinson
Aerospace Corporation
P.O. Box 92957/Mail Code M2-255
Los Angeles, CA 90009-2957"
(310) 336-6142

"Dr. P.W. Rosenkranz
Massachusetts Institute of Technology
77 Massachusetts Avenue
Cambridge, MA 02139"
(617) 253-3073

"Dr. Laurence S. Rothman
PL/GPOS
Hanscom AFB, MA 01731-5000"
(617) 377-2336

"Ms. Crystal Schaaf
PL/GPA
Hanscom AFB, MA 01731-5000"
(617) 377-4178

"Dr. John Schroeder
Ontar Corporation
129 University Road
Brookline, MA 02146"
(617) 739-6607

"Dr. Bertram D. Schurin
MS E-55-MS/G-223
Hughes Aircraft Company
P.O. Box 902
El Segundo, CA 90245"
(310) 616-6978

"Dr. Lewis L. Smith
Mail Stop A01-26
Grumman Corporate Research Center
Bethpage, NY 11714-3580"
(516) 575-2196

"Dr. Knut Stamnes
Geophysical Institute
University of Alaska
Fairbanks, AK 99775-0800"
(907) 474-7368

"Jean-Marc. Theriault
PL/GPOA DREV
Hanscom AFB, MA 01731"
(617) 377-4854

"Clement Thomas
Boeing Defense & Space Div.
PO Box 3999
MS 8Y-17
Seattle, WA 98124-2499"
(206) 773-4622

"Dr. Richard H. Tipping
University of Alabama
Dept. of Physics & Astronomy
206 Gallalee
Box 870324
Tuscaloosa, AL 35487"
(205) 348-3799

"D.H. Tofsted
Atmospheric Sciences Laboratory
DELA-S-EO-S
White Sands Missile Range, NM 88002"
(505) 678-3039

"Dr. Chan N. Touart
Hughes STX Corporation
109 Massachusetts Avenue
Lexington, MA 02173"
(617) 863-0677

"Capt. Glenn E. Van Knowe
RL/WE
Griffiss AFB, NY 13441"
(315) 587-3085

"Ms. Sandra S. Weaver
WRDC/WE
WPAFB, OH 45433"
(513) 255-6697

"Dr. Alan E. Wetmore
Atmospheric Sciences Laboratory
White Sands Missile
Range, NM 88002-5501"
(505) 678-5563

"Mr. Peter P. Wintersteiner
ARCON Corporation
260 Bear Hill Road
Waltham, MA 02154"
(617) 890-3330

"Mr. Robert D. Worsham
Atmospheric and Environmental
Research, Inc.
840 Memorial Drive
Cambridge, MA 02139"
(617) 546-6207

"Julie A. Wyzywany, 1Lt.
RL/WE
Griffiss AFB, NY 13441"
(315) 330-3085

"Michael Yeh
Caelum Research Corporation
11229 Lockwood Drive
Silver Spring, MD 20901"
(301) 593-1748

"Dr. K. Yoshino
Harvard Smithsonian Center
for Astrophysics
60 Garden Street
Cambridge, MA 02138"
(617) 495-2796

"Dr. A. S. Zachor
Atmospheric Radiation Consultants
59 High Street
Acton, MA 01720"
(508) 263-1931

AUTHOR INDEX

Abreu, L.W.	57,75	Liang, S.	325
Acharya, P.K.	3	Liljegren, J.C.	204
Anderson, G.P. ...	57,75,82,221	Longtin, D.R.	288,353
Berk, A.	3,98	Ma, Q.	245
Bernstein, L.S.	98	Melfi, H.	203
Betchley, C.C.	82	Moncet, J.L.	286
Chetwynd, J.H.	57,75	Murcay, D.	203
Clark, F.O.	115	Parkinson, W.H.	189
Clough, S.A.	57,266,286	Robertson, D.C.	3,41,98
Conant, J.A.	82	Rothman, L.S.	58
Cornette, W.M.	338	Sandford, B.P.	41
DeLuisi, J.	203	Sawchuck, W.J.	221
Depiero, N.L.	288	Schroeder, J.	128
Downer, S.B.	115	Shanks, J.G.	338
Dummer, R.S.	149	Sharma, R.	98
Ellingson, R.G.	203	Shettle, E.P.	57
Esmond, J.R.	189	Smith, W.	203
Falcone, V.J.	140	Stannes, K.	2
Gallery, W.O.	140	Strahler, A.	325
Grant, K.	267	Summers, M.E.	221
Grasso, R.J.	288,307	Tipping, R.H.	245
Grossman, A.	267	Touart, C.N.	26
Hall, L.A.	82	Tsay, S.	2
Hoke, M.L.	57	Wiscombe, W.J.	203
Hummel, J.R.	288,307,353	Worsham, R.D.	57,140
Iacono, M.J.	286	Yen, M.	2
Ip, P.C.F.	115	Yoshino, K.	189
Isaacs, R.G.	140		
Kennealy, J.P.	115		
Kreiss, W.T.	149		
Kristl, J.A.	41		
Kneizys, F.X.	57,75		
Kunde, V.	203		
Knuteson, R.O.	204		
Koenig, G.G.	353		